INORGANIC/ORGANIC HYBRID POLYMERS

BY

ELENI KYRIAZI

B.Sc (Hons), M.Sc, MRSC

A thesis submitted in partial fulfilment of the requirements of the University of Greenwich for the Degree of Doctor of Philosophy in Chemistry

APRIL 2005

Medway School of Science

University of Greenwich, Medway Campus,

Chatham Maritime, Kent, ME4 4TB, UK

the UNIVERSITY of GREENWICH

ACKNOWLEDGEMENT

With many thanks to Dr Mike Thomas and Prof. Martin Snowden, my project supervisors, for all of the support and guidance that they gave during the course of this project.

I would also like to thank the staff and technicians for their assistance in the labs at the University of Greenwich.

I would also like to thank my family and all my friends for the help and support given during the preparation of this project report.

ABSTRACT

INORGANIC/ORGANIC HYBRID POLYMERS

The aims of this project were to synthesise and characterise a range of inorganic/organic hybrid polymers containing pendant vinyl groups and to study their uses as possible fire retardants. The work consisted of several parallel strands: the synthesis of organically modified silicas; the preparation of vinyl containing silsesquioxanes based on the hydrolysis of cyclohexyltrichlorosilane or propylmethacrylatepolysiloxane; the synthesis of latexes by co-polymerisation of either N-Isopropylacrylamide (NIPAM) or styrene with vinyltrimethoxysilane and the intercalation of styrene or NIPAM into montmorillonite.

All samples were characterised using a range of instrumental techniques including infrared spectroscopy (IR), nuclear magnetic resonance spectroscopy (NMR), X-ray diffraction (XRD), elemental analysis, thermal analysis, surface area analysis and electrokinetic analysis.

Vinyl modified silicas having large surface areas (about $400m^2g^{-1}$) were successfully obtained. On calcining at 540°C silicas having surface area in excess of $1000m^2g^{-1}$ were formed. Both the original organically modified silica and a sample after calcining were incorporated into poly(methylmethacrylate) and these samples were compared with pure poly(methymethacrylate) in a cone calorimeter to study their thermal properties. No significant enhancement to the thermal stability of the polymers was observed when the silica was incorporated.

Analysis of the co-polymer latexes were inconclusive, in the case of the products obtained from NIPAM but particles having a narrow size distribution were obtained using styrene. There was no apparent trend in the value of the zeta potential with composition.

Analysis of the intercalation of monomers into clays and the synthesis of silsesquioxanes were inconclusive.

ELENI KYRIAZI

B.Sc., M.Sc., MRSC

TABLE OF CONTENTS

TABLE OF TABLES

TABLE OF FIGURES

CHAPTER 1: - INTRODUCTION

1.1 AIMS OF PROJECT

The main aim of this work was to synthesise and characterise a range of inorganic/organic hybrid polymers containing pendant vinyl groups and to study their uses in a range of applications, such as fire retandancy.

A series of organically modified silicas were prepared via the sol-gel route by reacting tetraethoxysilane with vinyl-substituted alkoxysilanes. The final product has a silica core with pendant vinyl groups, which was further reacted with methyl methacrylate in order to incorporate the silica into the polymer backbone. The resulting products were tested for their fire retandant properties.

Further work included the preparation of silicon containing poly(N-isopropylacrylamide) microgels and latexes. Earlier work [1, 2] on both microgel and latexes was being followed and further studies will enable us to develop a detailed understanding of the structure-property relationships of these materials.

1.2 SILICA

1.2.1 STRUCTURE OF SILICA

Silica is a three dimensional network of silicon dioxide, most commonly encountered as sand **(Figure 1.2.1)**. Silica is found commonly in the crystalline state and rarely in an amorphous state. Silica has been more studied more than any other chemical compound except water.

Silica is found in nature in several forms, including quartz (hexagonal crystal structure made of trigonal crystallized silica) and opal (hydrated silicon dioxide). Infract silica has 17 crystalline forms [3].

Silica is manufactured in several forms including glass (in colourless high purity form called fused silica) and silica gel (used e.g. as desiccants in brand new clothes and leather goods). Silica is a major ingredient of Portland cement.

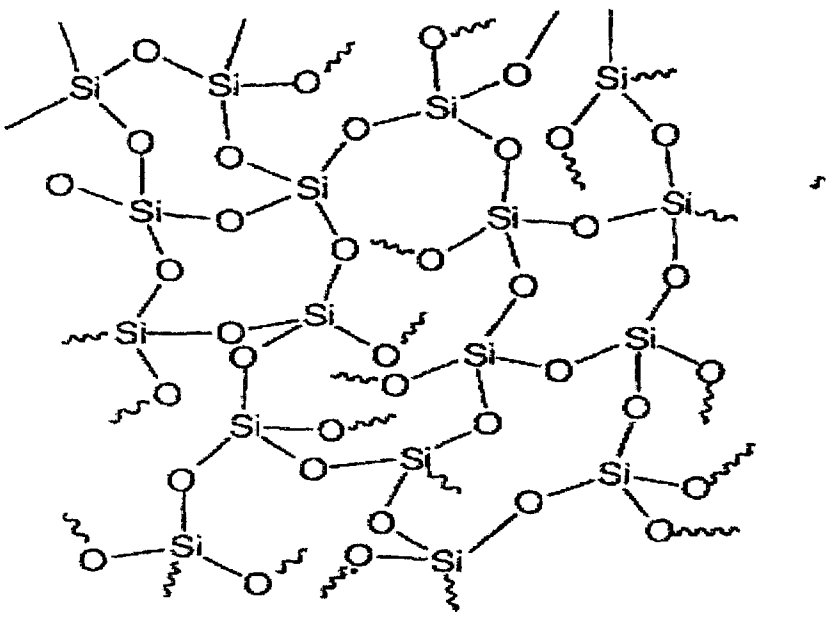

Figure 1.2.1: Structure of silica [3].

1.2.2 APPLICATIONS OF SILICA

Silica has played a continuous part in man's development and been one of the basic raw materials supporting the industrial revolution (as refractory, flux, and moulding sand) and today's information technology revolution (providing the raw material for silicon chips).

Industrial silica is used in a vast array of industries. The main ones are:

glass. Silica is the main ingredient of this vital material. The glass products containing silica include containers (bottles, jars, and drinking vessels), flat glass (for windows, automotive glass, mirrors, etc.), decorative glass (glasses, decanters, bowls, and figurines), fibreglass (reinforcing and insulating), technical glass (screens), and optical glass (spectacles and binoculars).

foundries. Quartz sand is a basic material for the production of moulds and cores in metal casting. It is also used for precision casting, dental applications and jewellery casting.

construction. The construction industry is by far the largest volume consumer of silica minerals. Industrial silica is used in construction aggregates, in concrete, dimension stone, masonry mortars, tile glues, floor screeds, cement manufacture, road line markings, and asphalt, in bridge and sewer refurbishment, in decorative bricks, not to mention in glass and steel structures.

ceramics. Industrial silica is a structural ingredient of clay bodies and a major constituent of ceramic glazes, ranging from refractory bricks to wall bricks and from sanitary ware to tableware and tiles.

chemical industry. Quartz derivatives are used in many areas, such as pesticides, fertilisers and pharmaceuticals preparations. Another derivative from industrial silica is silicon carbide, which is the raw materials for abrasives, anti-slip and polishing products.

Silica in its finest forms finds important usage as reinforcing filler for use in paint, plastics, rubber, and sealants. In paints, silica is used to render the paint more resistant to chemicals and for enhancing hardness and wear resistance and silica sand is used in water filtration and agriculture.

1.3 SOL-GEL PROCESS

The sol-gel process has been known for 150 years, but it is only in the last 15 years that it has been exploited for the formation of organic-inorganic hybrids, where in many cases the phases co-exist on a nanometre size scale. In recent years the sol-gel process has become an attractive and intensive area of research, for the preparation of highly homogenous glasses, ceramics and composites [5].

The term 'sol-gel' processing is broadly applied to describe fabrication of inorganic materials by preparing a sol, inducing gelation and then drying the gel. A sol is a colloidal suspension of solid particles in liquid.

The sol-gel process can be used to prepare both inorganic and hybrid organic-inorganic host structures. A suitable silicon alkoxide [for example, Si $(OR')_4$ where R' = CH_3 or C_2H_5] and/or an organosilicon precursor [for example, R - $Si(OR')_3$] is mixed with water in a mutual solvent such as methanol. During sol-gel formation, the viscosity of the solution gradually increases as the sol becomes interconnected to form a rigid three-dimensional, porous structure – the gel.

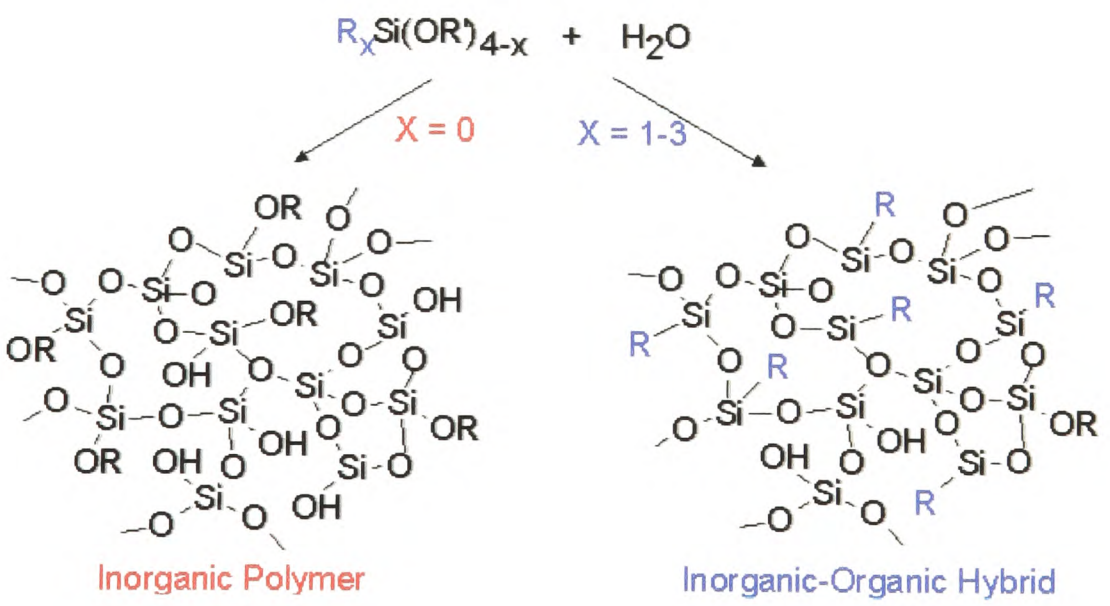

In the sol-gel process, the precursors for the preparation of a colloid consist of a metal or metalloid element surrounded by various ligands which do not include another metal or metalloid atom. For example, metal alkoxides have an organic ligand attached to a metal or metalloid atom. The most thoroughly studied example is tetraethoxysilane (TEOS). Metal alkoxides are very interesting and popular precursors because they react readily with water to give hydrolysed products which can condense to give disilanols and higher oligomers.

$$\equiv Si - OR + H_2O \longrightarrow \equiv Si - OH + ROH \qquad \textit{Hydrolysis}$$

$$\equiv Si - OH + HO - Si \equiv \longrightarrow \equiv Si - O - Si \equiv + H_2O \qquad \textit{Water Condensation}$$

$$\equiv Si - OR + HO - Si \equiv \longrightarrow \equiv Si - O - Si \equiv + ROH \qquad \textit{Alcohol Condensation}$$

where R is an alkyl group. Numerous investigations have shown that variations in the synthesis conditions such as the type of solvent, precursor(s), catalyst, temperature, pressure and concentration of solvent, cause modification in the structure and properties of the polysilicate products [5].

Under acidic conditions, it is likely that an alkoxide group is protonated in a rapid first step. Electron density is withdrawn from the silicon atom, making it more electrophilic and thus more susceptible to attack from water. The positive charge of the protonated alkoxide is reduced, making the alcohol a better leaving group **(Figure 1.3.1)**.

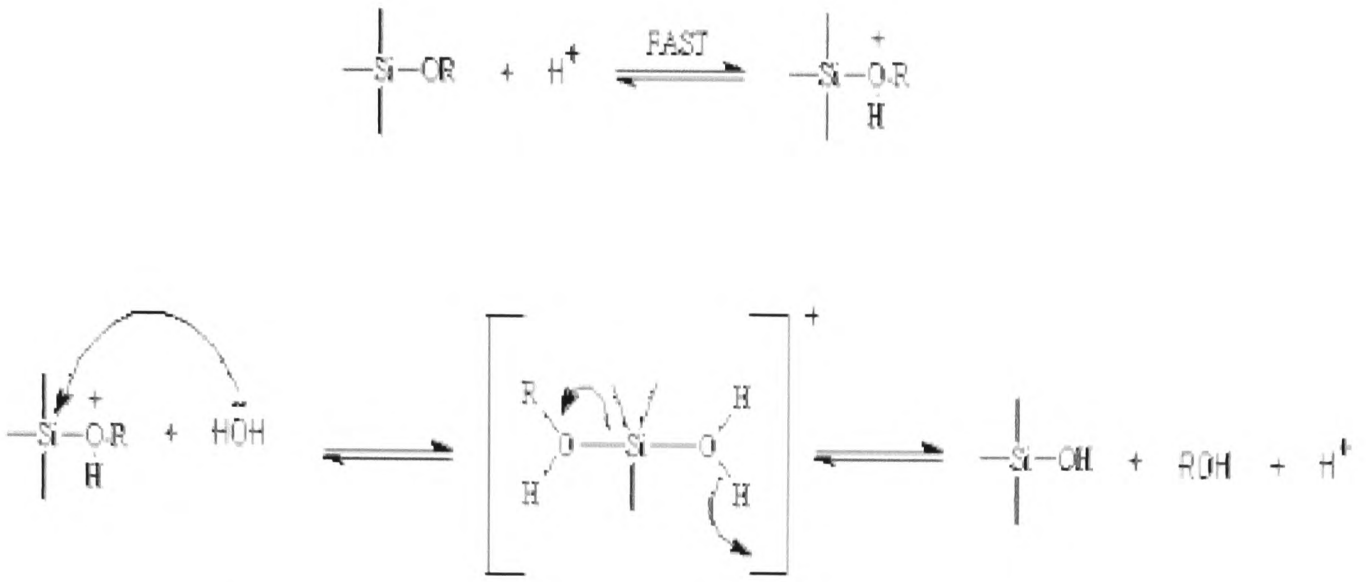

Figure 1.3.1: Acid-catalysed hydrolysis of alkoxy silianes.

Base-catalyzed hydrolysis of silicon alkoxides proceeds much more slowly than acid-catalyzed hydrolysis at an equivalent catalyst concentration. The water dissociates to produce hydroxyl anions which then attack the silicon atom. Then -OH displaces -OR with inversion of the silicon tetrahedron **(Figure 1.3.2)**.

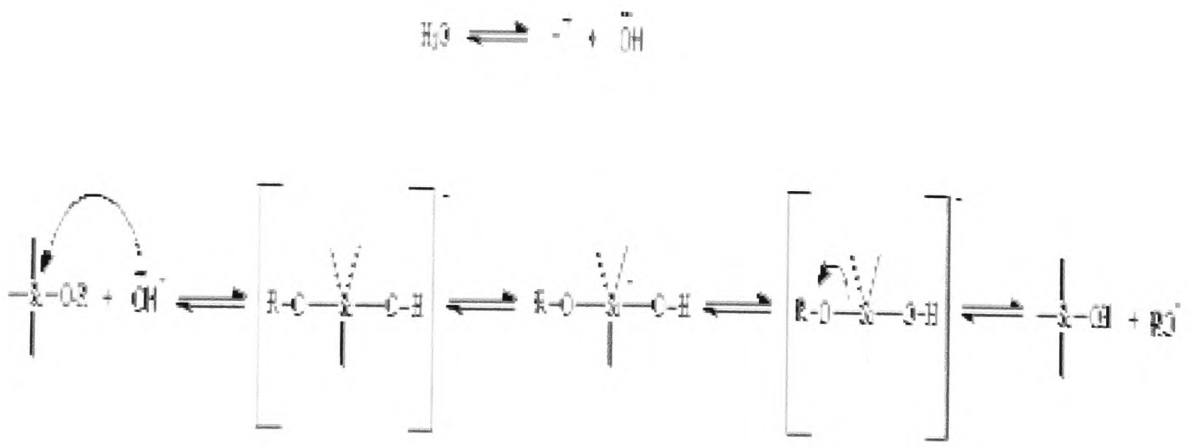

Figure 1.3.2: Base-catalysed hydrolysis of alkoxy silanes.

Under acidic conditions weakly branched polymeric networks are formed to give "crosslinked spaghetti", **Figure 1.3.3**. By contrast, under basic conditions, three dimensional clusters are initially formed which increase, forming large size, dense particles, **Figure 1.3.4**.

Figure 1.3.3: Acid-catalysed sol-gel preparation of silica [6].

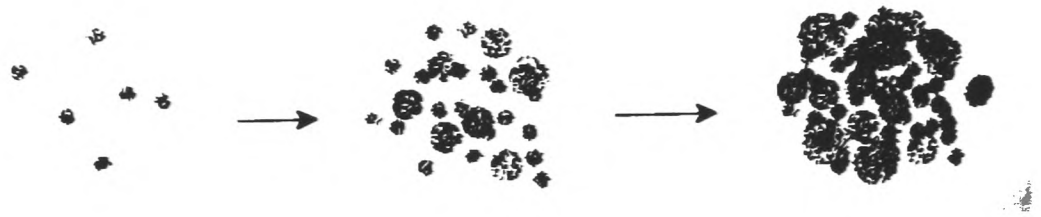

Figure 1.3.4: Base-catalysed sol-gel preparation of silica [6].

In recent years, much attention has focused on the novel combination of organic species with inorganic minerals and networks, because of the exciting range of properties demonstrated by these hybrids materials and the potential offer to mimic the vast array of structures on display in nature [7, 8]. The most common approach has involved the preparation of sol-gel hybrids, including the combination of inorganic oxides (particularly silica) with polymers and the formation of organically-modified silicates (ORMOSILs) from alkoxysilanes [9-11].

1.3.1 APPLICATIONS OF THE SOL GEL PROCESS

Applied sol-gel chemistry has offered scientists several potential advantages for material synthesis **(Figure 1.3.5)**. The huge interest in this technology reflects its potential for making thin films and coatings, active glasses, fibres, ceramics and porous gels and membranes [12].

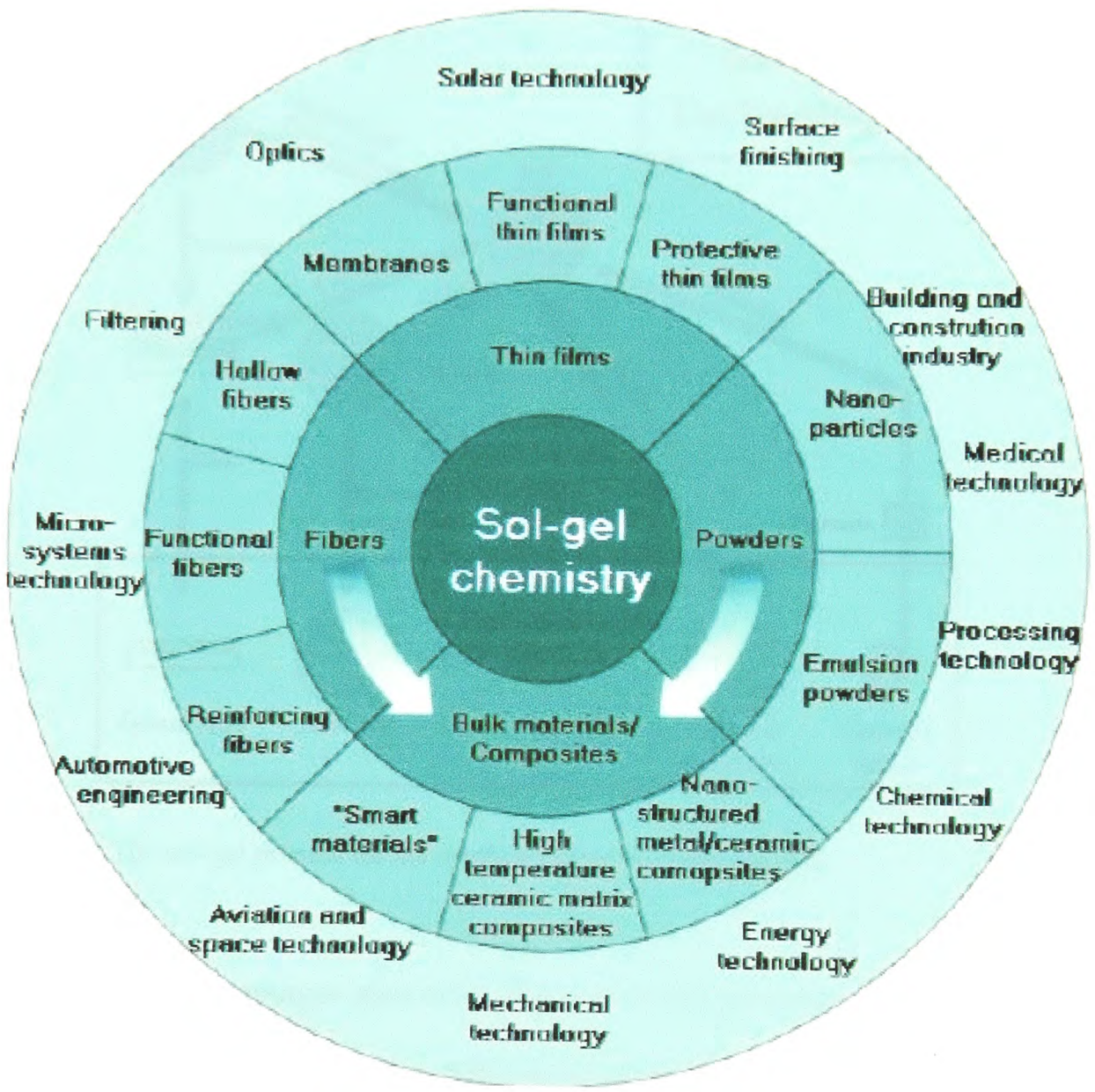

Figure 1.3.5: Applications of sol-gel chemistry [13].

The advantages of the sol-gel process in general are high purity, homogeneity, and low temperature. For a lower temperature process, there is a reduced loss of volatile components and thus the process is more environmental friendly. In addition, some materials that cannot be made by conventional means because of thermal and

thermodynamic instability can be made by this process. The sol-gel process has many applications in the synthesis of novel materials. Examples include aerogels (a porous solid formed by replacing the liquid of a gel with a gas), such as rigid plastic foam used in space crafts to capture stellar dust, xerogels (a gel containing little liquid) as matrices in biosensors, and high power laser materials **(Figure 1.3.6)**.

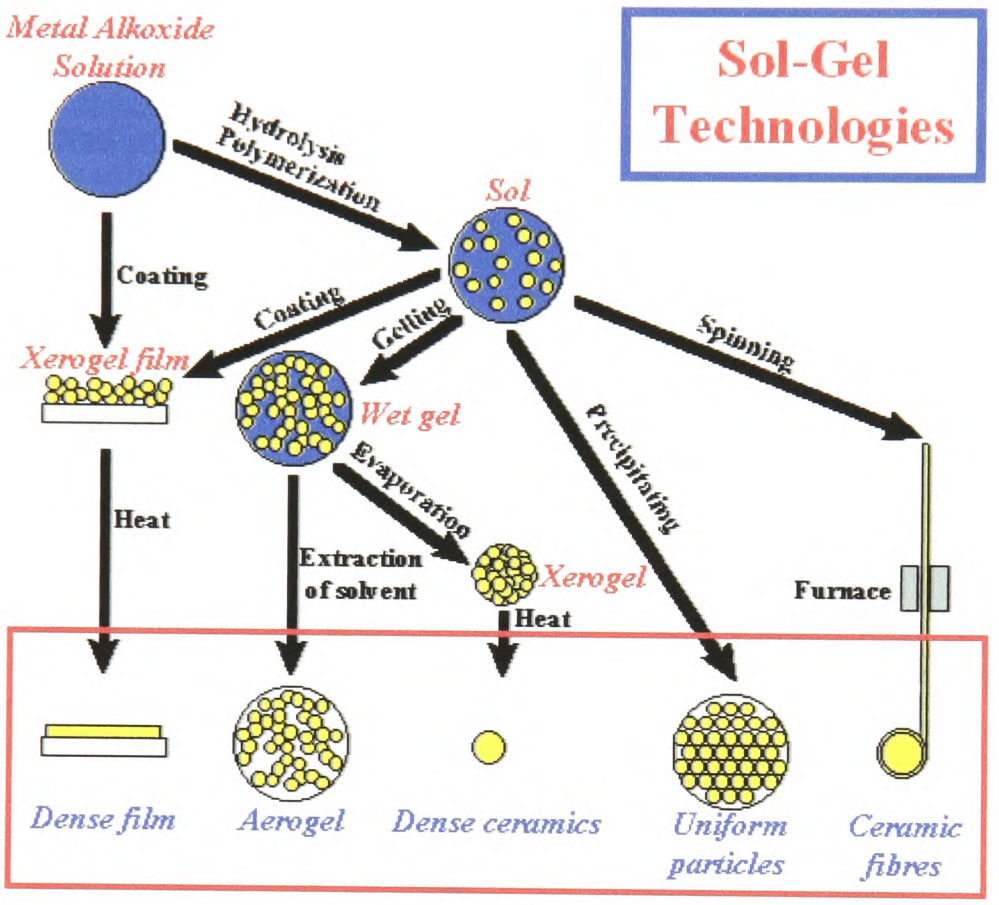

Figure 1.3.6: The sol-gel process for the synthesis of novel materials [14].

However, disadvantages also exist: the cost of the precursors, the difficulties in the synthesis of monoliths and the difficulties in the chemistry with respect to tailor properties. Disadvantages also include the shrinkage that accompanies drying and sintering as well as the processing times [15].

1.4 SILSESQUIOXANES

Silsesquioxanes, or T- resins, are a class of compounds with the empirical formula $RSiO_{1.5}$. These compounds derive their name from the one and one-half (1.5) or sesqui- stoichiometry of oxygen bound to silicon, with the alternate name "T- resin" derived from the presence of three oxygen subsistent on silicon (tri-substituted). Several structural representations of silsesquioxanes with the empirical formula $RSiO_{1.5}$ are possible, with the two most common representations being a ladder-type structure (A) and a cubic structure (B) containing eight silicon atoms placed at the vertices of the cube, **(Figure 1.4.1)**. The cubic structure is commonly called the T_8 cube, and is usually drawn incorrectly with O-Si-O bond angles of 90°. The actual structure of a T_8 "cube" is more a Si-O cage framework, as illustrated in (C). However, the cubic structure (B) is easier to visualize and will be used hereafter to denote the silsesquioxane backbone.

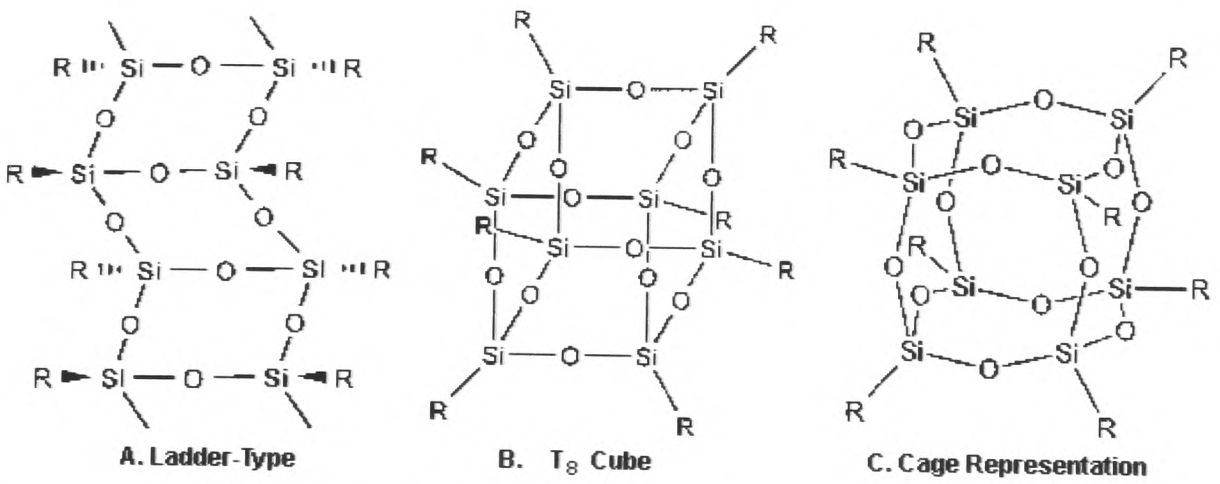

Figure 1.4.1: Structural presentations of silsesquioxanes [21].

Substituents on silicon can include hydrogen, alkyl, alkenyl, alkoxy and aryl groups. The octa-functional silsesquioxanes with R = vinyl or dimethylsilyloxy have found increased use as precursors to new inorganic/ organic hybrid polymers [22-24].

When the R group is polymerizable, a novel class of monomers called Polyhedral Oligomeric Silsesquioxanes, or POSS monomers result **(Figure 1.4.2)** [25, 26].

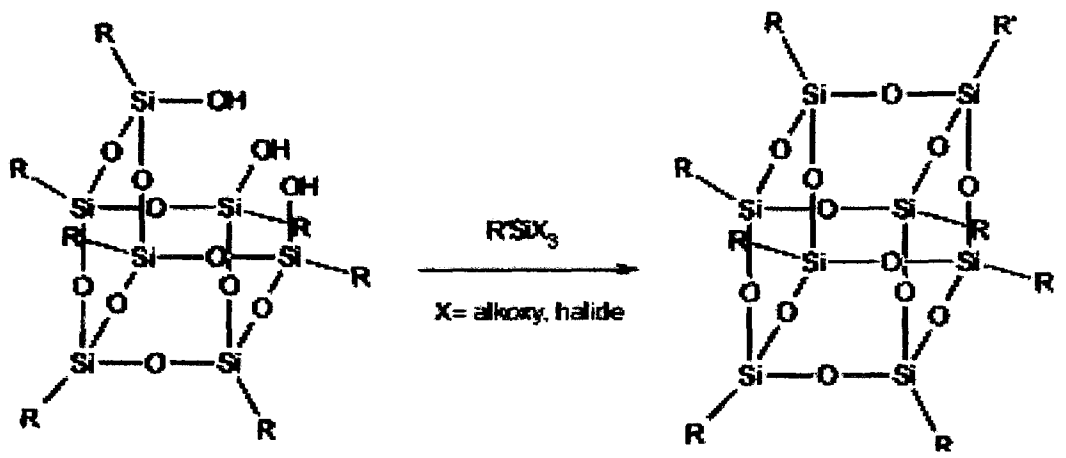

Figure 1.4.2: Synthesis of a POSS monomer where R' is a polymerisable group [27].

The POSS monomers can be polymerized using standard techniques to yield inorganic-organic hybrid polymers and copolymers [26, 28].

1.4.1 APPLICATIONS OF SILSESQUIOXANES

Silsesquioxanes play an important role in the development of heterogeneous silica-supported transition metal catalyst systems. Octameric silsesquioxanes resemble skeletal frameworks found in crystalline forms of silica and zeolites, and their rigid framework makes silsesquioxanes suitable models for silica surfaces [29, 30]. Particular interest is the incompletely condensed silsesquioxanes which have one silicon removed from a corner of the T_8 cube. This "T_7" structure, commonly referred

as trisilanol, possesses both structural and electronic similarities to hydroxylated silica surface sites [31].

There are numerous other applications of substituted silsesquioxanes, including their use as Wittig reagents [32] and precursors to silicon carbide (SiC) [33-35], nitrided glass (in combination with NH_3) [36], aluminosilicates [37 ,38] silica-reinforced composites [39] and a variety of microporous materials [40,41].

1.5 LATEXES

Latexes are liquids (typically water) in which microscopic polymer particles are dispersed. They are formed by the polymerisation of monomer emulsions. Solvent-based latexes do exist, but have limited applications. However, the use of organic solvents in latexes is discouraged for environmental reasons. In fact, the desire to discontinue the use of solvent-based polymer solutions has been a major driving force for the development of water-based latexes. The term latex covers emulsion polymers, polymer dispersions and polymer colloids [42].

The different methods of emulsion polymerisation have been reviewed [43]. Each technique has advantages and disadvantages in terms of cost, control over the polymerisation process and stability of the resulting emulsion. Monomer feed systems can also be used to control reactions and polymer composition. In some techniques very uniform polymers and latex particles can be produced. Particle structure is important and can be varied or maintained uniform during the process, depending on the system.

The product resulting from emulsion polymerisation is stable polymer dispersion with low residual monomer content and a solid content typically around 44 to 56% m/m. Polymer molecular weight varies with the polymerisation conditions but is

usually in the range of 100,000 to 1,000,000. The average particle size (Dw) of colloid-free latexes is usually around 100-170 nm and that of colloid-stabilised lattices about 200-500 nm. The process leading to latex formation from emulsions is summarised in **Figure 1.5.1**.

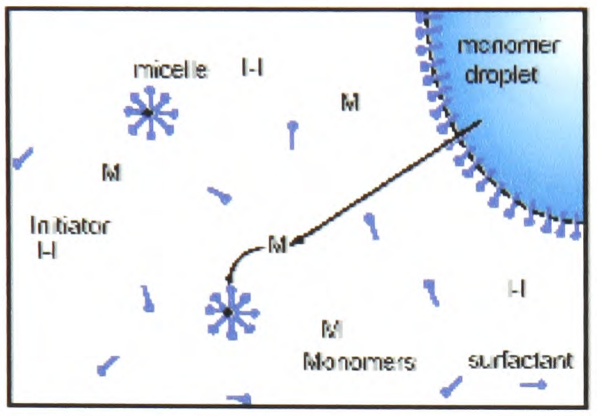

Figure 1: Initial situation

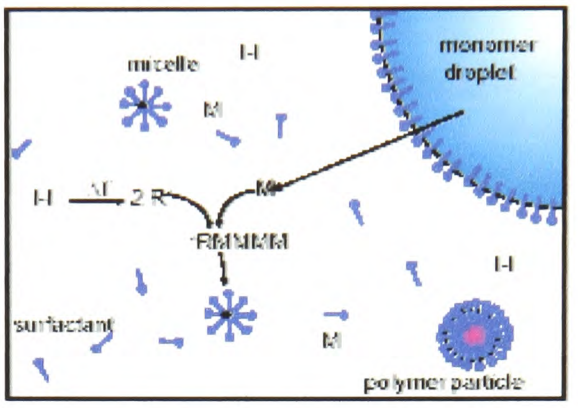

Figure 2: Stage I of the emulsion polymerisation process

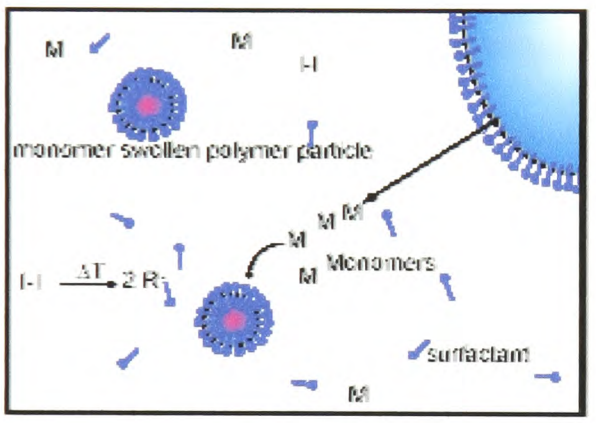

Figure 3: Stage II of the emulsion polymerisation process.

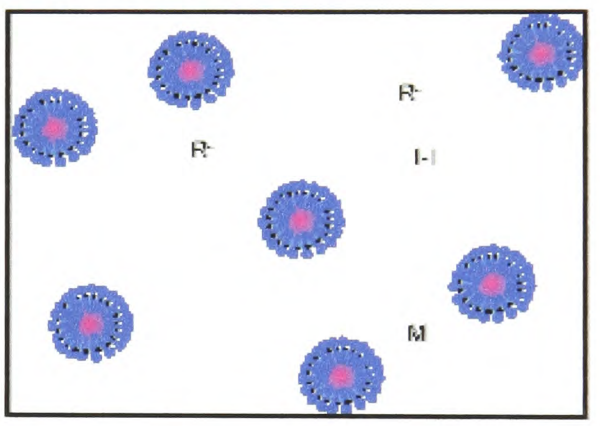

Figure 4: Stage III of the emulsion polymerisation process.

Figure 1.5.1: The different phases of the emulsion polymerisation process [44].

1.5.1 APPLICATIONS OF LATEXES

Latexes are currently undergoing extensive research and development as key replacement materials for many solvent-based systems.

They are being used in a broad range of fields from adhesives, inks, paints, coatings, drug delivery systems, medical assay kits, gloves, paper coatings, floor polish, films, carpet backing and foam mattresses to cosmetics. A latex is also used to

improve properties, for example as an impact modifier in polystyrene and to improve tensile properties in cement [45].

1.6 MICROGELS

One class of cross-linked polymers, often given the prefix of a "smart" or "intelligent" material, is a colloidal microgel . A microgel is an intramolecularly crosslinked macromolecule which is dispersed in normal or colloidal solutions, in which, depending on the degree of cross linking and on the nature of the solvent, it is more or less swollen. Besides linear and branched macromolecules and cross linked polymers, intramolecularly cross linked macromolecules may be considered as a fourth class of macromolecules. Though the term microgel has long been used and is well established, it is not quite satisfactory because it is only appropriate for the swollen state, i.e. if cross linked macromolecules are dissolved. Microgel particles have a high degree of sensitivity to their environment and they are capable of undergoing rapid changes in their physical properties, including changes in particle size and surface charge density. Microgels have similar properties to polymers and water-swollen gels (usually termed hydrogels or macrogels) but are discrete particles with characteristics that are dependent on the method of synthesis, cross-link density, monomer concentration, monomer composition, and solvency conditions. [46-47]

A number of techniques are commonly employed for the study of microgel dispersions. These include nuclear magnetic resonance spectroscopy (NMR), light scattering, differential scanning calorimetry (DSC) and electron microscopy (TEM and SEM). These techniques provide information on particle size, shape and size changes that take place as the microgels undergo their conformational transitions and fine detail regarding the polymer microstructure within the particle [49].

One common example of an aqueous-based colloidal microgel is poly (*N*-isopropylacrylamide) or poly (NIPAM). **Figure 1.6.1** shows the structure of poly (*N*-isopropylacrylamide). Microgels made from this material are thermosensitive when dispersed in water, shrinking and swelling reversibly with changing temperature. Poly (NIPAM) microgels are prepared by a single-step emulsion polymerisation reaction in the presence of a crosslinking agent and a free radical initiator.

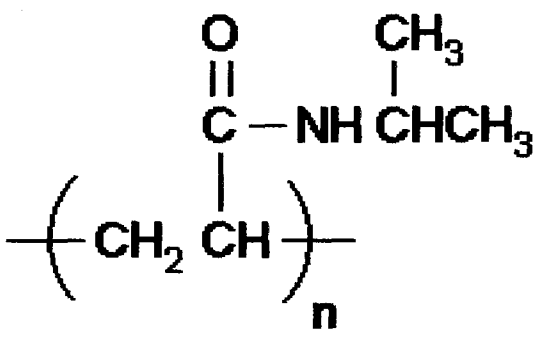

Figure 1.6.1: Structure of poly (NIPAM) [48].

1.6.1 APPLICATIONS OF MICROGELS

Microgels have found extensive use in the coatings industry because of their utility in improving the rheological properties of paints as well as the performance of films. Microgels may also impart shock-resistance to films as a consequence of their flexible 'sponge-like' structures [50].

Yet another application relates to the manufacture of fibre-containing cement plates resistant to freezing. It is claimed that the freeze resistance of fibre is improved by impregnating the plates with a microgel emulsion [50]. Also microgels have functionalised to perform as catalysts in reactions in aqueous and non-aqueous media. They are also useful models for studying polymer-polymer interactions and as starting materials for the synthesis of other porous materials.

The thermo sensitivity of poly (NIPAM) microgels has been exploited in a process designed for the crude oil recovery from petroleum reservoirs [50].

1.7 POLYMERS

Polymers are substances whose molecules have high molar masses and are composed of a large number of repeating units. There are both naturally occurring and synthetic polymers. Among naturally occurring polymers are proteins, starches, cellulose, and latex. Synthetic polymers are produced commercially on a very large scale and have a wide range of properties and uses. The materials commonly called plastics are all synthetic polymers. Vinyl polymers are polymers made from vinyl monomers; that is, small molecules containing carbon-carbon double bonds. They make up the largest family of polymers [51].

Polymers are formed by chemical reactions in which a large number of molecules called monomers are joined sequentially, forming a chain. In many polymers, only one monomer is used. In others, two or three different monomers may be combined. Polymers are classified by the characteristics of the reactions by which they are formed. If all atoms in the monomers are incorporated into the polymer, the polymer is called an *addition polymer*. Most addition polymers are made from monomers containing a double bond between carbon atoms. Such monomers are called olefins, and most commercial addition polymers are polyolefins.

If some of the atoms of the monomers are released as small molecules, such as water, the polymer is called a *condensation polymer*. Condensation polymers are made from monomers that have two different groups of atoms which can join together

to form, for example, ester or amide links. Polyesters are an important class of commercial polymers, as are polyamides (nylon).

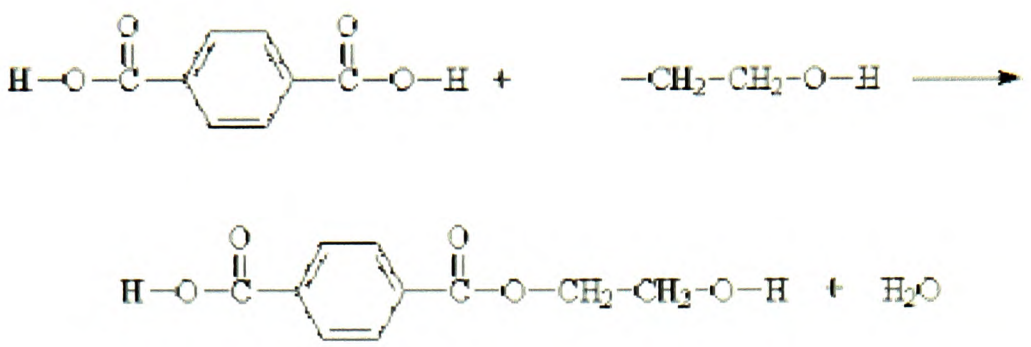

Two important polymer materials are elastomers and plastics. Elastomers, more commonly known as rubbers, can change shape elastically whenever a large force is applied to them and can later return to their original shape, or close enough to it, when the force is released. Plastics consist of a large group of synthetic materials that are made by forming or molding into their shape. Depending on their structure and chemical bond, plastics are either thermoplastics or thermosetting plastics. There are various different types of plastics such as nylon, polyethylene and polymethyl methacrylate (PMMA) [52].

1.7.1 POLY (METHYL METHACRYLATE)

Poly (methyl methacrylate) (PMMA) falls into the group of thermoplastic polymer materials. It is derived from the monomer methyl methacrylate.

Free radical vinyl polymerization is the usual process for making polymers from vinyl monomers **(Figure 1.7.1)**. PMMA is known to be hard and transparent, and an extremely good light conductor, which is better than normal glass. Because of its

strong optical qualities, PMMA is used in things such as lighting fixtures, furniture, household goods, shop signs, automotive parts, and laboratory equipment [52].

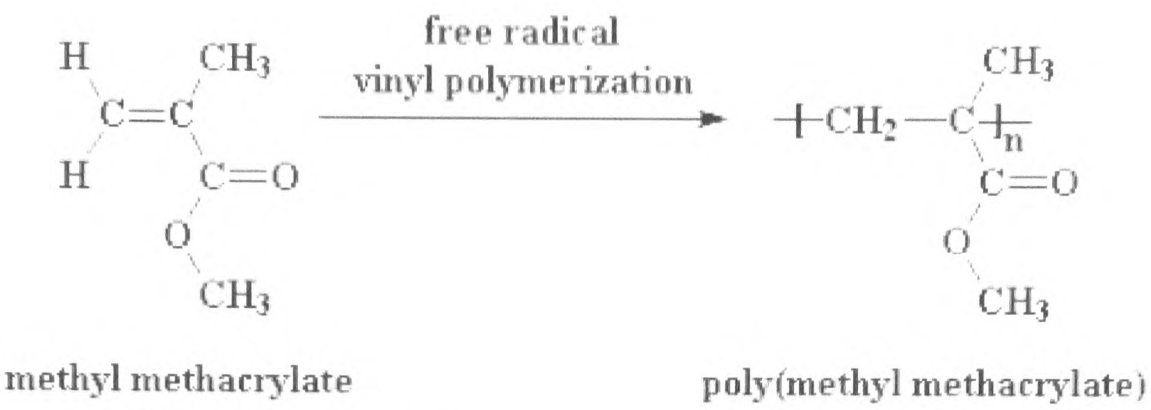

Figure 1.7.1: Polymerisation of PMMA [52].

1.8 FIRE RETARDANTS

In most cases polymers initiate or propagate fires because, being organic compounds, they decompose to volatile combustible products when they are exposed to heat. However, in many fields such as electrical, electronic, transport and building the use of polymers is restricted by their flammability, whatever the importance of the advantages their use may bring. The current use of synthetic polymers has greatly increased the "fire risk" and the "fire hazard", that is respectively the probability of fire occurrence and its consequence, either on humans or on structures. To fulfil the legal requirements flame retardants need to be added into the polymer. The role of these additives is to slow down polymer combustion and degradation (fire extinction), reduce smoke emission and avoid dripping in order to increase the escape time for people.

Fire safety is an important part of fire precautions. Fire precautions have the objective to minimise the number of and damage from fires by measures hindering their initiation, limiting their propagation and if possible excluding flash-over.

Preventing fires or delaying them makes escape possible over a longer period of time. As a result, life, health and property are efficiently protected.

There are many different flame retardants, and these work in a number of different ways. Some flame retardants are effective on their own; other products are used mainly or only as "synergists", acting to increase the effect of other types of flame retardant [53].

Additive flame retardants are used especially in thermoplastics. They are sometimes volatile and as a result their flame retardancy may be gradually lost. In contrast, reactive flame retardants serving are made chemically into the polymer molecule, together with the other starting components. This increases their volatility and their flame retardancy is thus retained. They are used mainly in thermosets (especially polymethyl methacrylates) in which they can be easily incorporated. They are, however, normally more expensive than additive flame retardants since their manufacture involves more expensive equipment.

To understand how flame retardants work it is first necessary to see how materials burn. Solid materials do not burn directly; they must be first decomposed by heat (pyrolysis) to release flammable gases. Visible flames appear when these flammable gases burn with the oxygen in the air. Materials such as wood do in fact burn vigorously, because once ignited the heat generated breaks down long-chain solid molecules into smaller molecules which evolve as gases. The gas flame itself is maintained by the action of high energy "radicals" which decompose molecules to give free carbon which can react with oxygen in air to "burn" to CO_2, generating heat energy **(Figure 1.8.1)**.

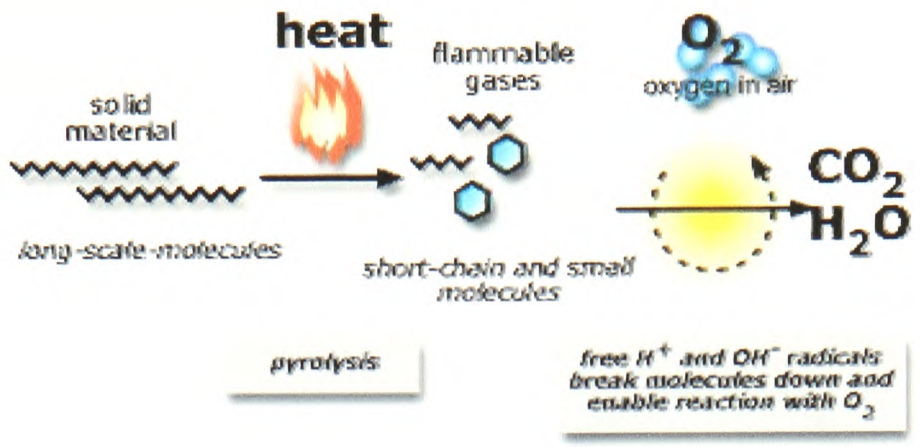

Figure 1.8.1: How fire works [54].

The objectives in flame retarding polymers is double; first, to increase ignition resistance and second, to reduce the rate of flame spread. Polyolefins such as polyethylene and polypropylene are flammable and will burn with a hot and clean flame, accompanied by melting and subsequent dripping or flowing of the molten polymer.

Fire retardants reduce the likelihood of ignition, and so may prevent a life-threatening fire from getting started. Once a fire starts, they slow the rate at which a fire develops, and this reduces the quantity of material involved in the fire, increasing escape time. In situations where smoke generation may be especially hazardous, materials can be formulated with combinations of smoke suppressants and selected fire retardants for increased protection.

The route of a fire can be divided into three phases, the initiating fire, the fully developed fire and the decreased fire **(Figure 1.8.2)**. The early stage of smouldering (Type I) is characterised by little heat output with smoke and irritant gases produced. The second phase, called flashover (Type II) occurs very rapidly, typically after a period of about two minutes in a typical room. The heat output in a domestic room fire can rise to a megawatt, and this well-ventilated fire is characterised by conversion of the organic fuel primarily to carbon dioxide and water, although some carbon

monoxide will also be produced. The later phase (Type III) of the fire is characterised by lower heat output, as either the fuel supply or oxygen supply is diminished.

Figure 1.8.2: Course of fire [54].

1.8.1 MOST IMPORTANT FIRE RETARDANTS

Manufacturers and specialist formulators offer a vast range of different flame retardant products, based on a number of very different types of chemicals. In many cases, several different types of flame retardants are combined to achieve optimal material performance and product safety (synergy). The main different chemical families of flame retardants are: [53]

inorganic chemicals (including antimony, aluminium and tin compounds),

halogen based fire retardants,

organophosphorus based fire retardants and

nitrogen based fire retardants.

The choice of a given flame retardant frequently depends on the type of application. Their suitability is subject to variables such as the material to be flame-retarded, the fire safety standards with which the product must comply, cost considerations and their recycle ability.

All flame retardants are manufactured, transported, used and tested in accordance with the strict standards and codes of practice lay down by national and international statutory, legislative and professional bodies.

Figure 1.8.3 shows the use of the different fire retardants in the world.

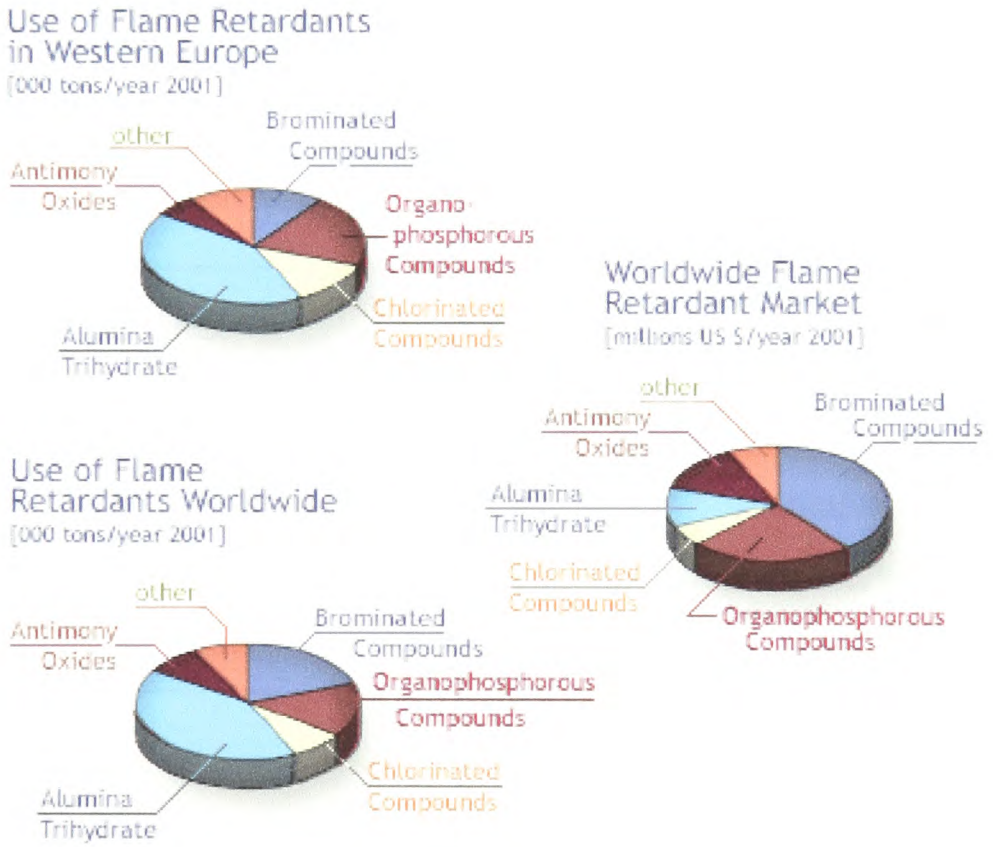

Figure 1.8.3: Use of fire retardants worldwide [54].

1.8.2 MAJOR FLAME RETARDANTS APPLICATIONS

The most important industry sectors where flame retardants are used are applications in electrical engineering and electrics, wire and cable and transportation [53]. Some of the major applications areas are summarised in **Table 1.8.1**, below.

Table 1.8.1: Major applications of flame retardants [53].

Industry sector.	Applications.
Electrical, Engineering and Electrics.	Wire and Cable. Consumer electronics housing and back plates. Office electronics housing and back plates. Printed circuit boards. Appliances.
Motor vehicles.	Wire and Cable. Seats.
Rail vehicles.	Compartment linings and coverings. Insulation. Compartment interior. Seats.
Aircraft.	Panels. Carpets, flooring.
Building.	Thermal insulation for roofs, facades, walls. Sheeting for roofs. Floor coverings. Ducting and conduit. Panels, linings and coverings.

1.9 BRIEF REVIEW OF ORGANICALLY MODIFIED SILICAS (ORMOSILS)

1.9.1 INTRODUCTION

Porous materials are used as adsorbents, catalysts and catalyst supports owing to their high surface areas and large pore volumes. Following the classification by IUPAC, they can be grouped by the size of their pores: *microporous* solids with pore diameters up to 2 nm, with zeolites as the most prominent example, *mesoporous* solids with pore sizes between 2 and 50 nm, for example aerogels [55-61], pillared clays and M41S materials [62], and *macroporous* solids such as glasses and foams. In addition these materials can be distinguished by the arrangement of the pores, periodic or random - and the pore radii distribution, which can be either narrow or quite broad [63-64].

Materials composed of both inorganic and organic entities are called hybrid materials. They combine, to some extent, the properties of both constituents in one material. The general idea behind these materials is similar to that of composites, where two or more materials are combined that differ in form and (mostly) chemical composition. While macroscopic constituents with defined phase boundaries are used for composite materials, molecular building blocks of different composition (inorganic and organic/organometallic/biological) are instead combined in hybrid materials. The combination of different building blocks allows the generation of materials with new properties or combinations of properties not accessible otherwise. In the case of porous materials, the goal is to achieve cooperation between the properties originating from the porous inorganic framework and the properties of the organic entities [65].

During the past decade, organic-inorganic hybrid materials [66-67] prepared by the sol-gel approach [68-70] have attracted a great deal of attention in materials science. The synthesis of hybrid mesoporous silica materials with controlled functionality and hydrophobicity could open up new avenues for organometallic chemistry, catalysis, and organic-inorganic host-guest chemistry [71-72]. The major driving forces behind the intense activities in this area are the new and different properties of the nanocomposites which the traditional macroscale composites and traditional materials do not have. For example, unlike the traditional composite materials which have macroscale domain sizes of millimetres and even micrometer scale, most of the organic/inorganic hybrid materials are nanometres, typically 1-100 nm, as the minimum size of the components or phases. Therefore, they are often still optically transparent materials although microphase separation may exist.

Based on the structural distinction, Sanchez and Ribot classified the organic-inorganic hybrid materials into two classes [63]:

Class I corresponds to hybrid systems in which weak interactions such as van der Waals forces and hydrogen bonds or electrostatic interactions are created between organic and inorganic phases.

Class II corresponds to hybrid organic-inorganic compounds where both organic and inorganic components are bonded through strong covalent chemical bonds. Hybrid materials made in this way are termed CREAMERS (ceramic polymers), ORMOSILS (organically modified silicates) or ORMOCERS (organically modified ceramics) **(Figure 1.9.1)** [73].

Through the combinations of different inorganic and organic components in conjunction with appropriate processing methods, various types of primary and

secondary bonding can be developed leading to materials with unique combination of properties which cannot be achieved by other materials.

Hybrid organic-inorganic materials prepared by the sol-gel process hold considerable promise in the development of chemical sensors, catalysts, photochromic and nonlinear optical devices, and chromatographic stationary phases. Silicate-based inorganic–organic hybrid materials in which strong covalent bonding is established between the organic–inorganic phases are called organically modified silicate (ORMOSIL). Organically modified silicates (ORMOSILs), for example, are made by hydrolyzing and condensing organoalkoxysilanes with either tetraethoxysilane (TEOS) or tetramethoxysilane (TMOS). The blending of the inorganic precursors [$Si(OR)_4$] with the organoalkoxysilanes [R'-$Si(OR)_3$] can lead to materials with better properties than those derived from the individual precursors alone [74]. Of greatest importance to many ORMOSIL applications is the distribution of organic groups throughout the inorganic framework.

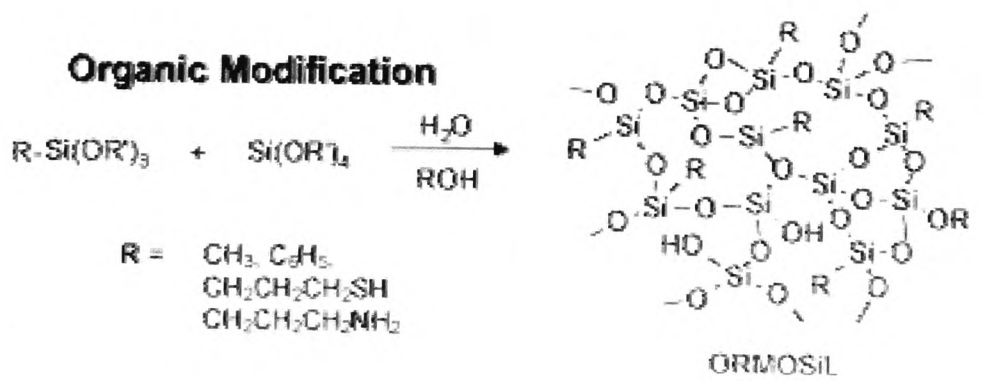

Figure 1.9.1: Example of organically modified silicate formation [73].

1.9.2 SYNTHESIS METHODS

The favourable physical and derived materials properties of porous materials are a consequence of their highly porous structure. Therefore, any chemical modification of the materials must retain this structure. In the case of mesostructured porous materials, the periodicity of the structure must also be retained. The purpose of modifying porous materials by organic groups is to extend the variety of properties without affecting the existing positive properties. These properties can be improved by organic groups. The incorporation of functional organic groups introduces new properties and makes the materials viable for a broader field of applications, for example in catalysis, for sensors or even sieving and separations.

Chemical modification of porous materials via covalent bonding of organic molecules has been achieved using two general strategies: the post-synthesis procedure was the first to be used and later co-condensation procedures were introduced by Burkett et al. [75], Macquarrie [76] and others [77-78].

1.9.2.1 Post-synthesis Modification

In the post-synthesis grafting method **(Figure 1.9.2)**, the surface of the inorganic mesoporous material is reacted with organic reagents through the surface silanol groups. The original structure of the mesoporous matrix is usually maintained intact. Grafting procedures are more common in the modification of periodic mesoporous materials, since this can be done via the gas phase but also easily via the liquid phase [78-82].

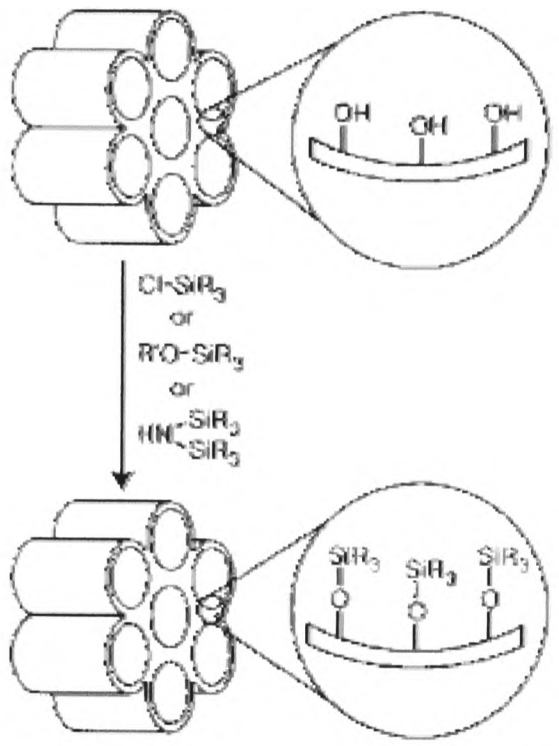

Figure 1.9.2: Functionalization of mesoporous silicates by grafting [84].

As reported by Maschmeyer [77] and others [83] there have been three main approaches for post synthesis modification of mesoporous compounds:

i. primary modification: direct grafting which involves reaction of a suitable organosilane reagent with the silica surface using an appropriate solvent under reflux conditions [84-87],

ii. secondary modification which involves further grafting onto a previously grafted species to create new functionalised surfaces.

iii. transformation of the materials prepared under procedure (i) or (ii) by additional treatments such as heating, evacuation, calcinations.

Research on post-synthesis grafting is mostly focused on MCM-41, with its simple hexagonal arrangement of parallel, one-dimensional channels [87-89].

Instead of grafting organic functions through Si-O-Si bridges using silicon-bearing species, Yamamoto and Tatsumi [88] developed an interesting strategy leading to methyl groups covalently bonded to surface silicon atoms. Other types of mesoporous

silicas such as SBA-15 and FSM-16 were also surface modified using different silylating agents [90-93]. Post synthesis surface modification of mesoporous silica with basic functional groups was achieved via primary or secondary modification [94]. In contrast, only a few investigations were devoted to the preparation of similar hybrid materials with acidic functions [95].

1.9.2.2 Co-condensation method

The co-condensation method **(Figure 1.9.3)**, also called "one-pot" synthesis, is currently the most common and direct synthesis route to the introduction of the organic groups into the silica network. It provides better control over the amount of organic groups incorporated into the matrix and ensures the uniform surface coverage with organic groups under mild conditions.

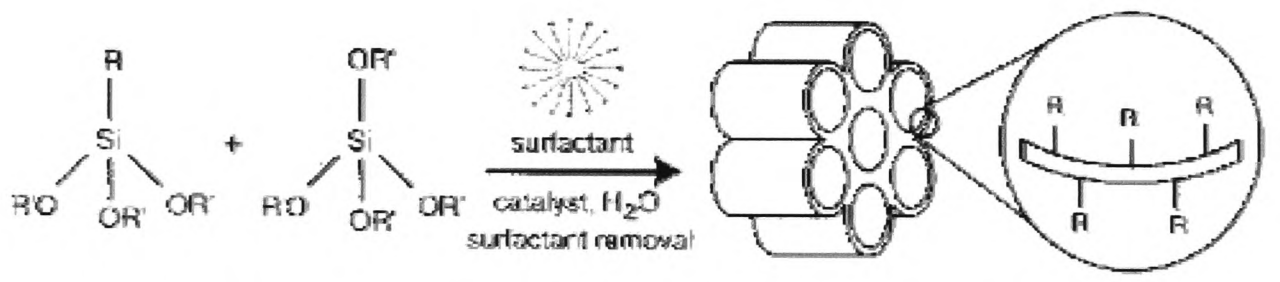

Figure 1.9.3: Organic modification of the mesoporous silicate under co-condensation [84].

Co-condensation of siloxane and organosiloxane precursors via the sol-gel technique to produce functionalized amorphous silica has been extensively investigated [96-98]. In these materials, an organic moiety is covalently linked via a non-hydrolysable Si-C bond to a siloxane species, which hydrolyzes to form a silica network. Burkett et al. [75] and Macquarrie [76] were the first to combine this approach with the technique to generate, in a single step, ordered mesoporous silica-

based nanocomposites with covalently linked organic functionalities protruding from the inorganic walls into the pores.

The co-condensation approach can also be used in the synthesis of organically modified M41S materials [99-100]. Co-condensation of a tetraalkoxysilane and one or more organoalkoxysilanes with Si-C bonds is an alternative method of producing inorganic-organic hybrid networks by sol-gel chemistry. Since the early work by the research groups of Mann [100], Macquarrie [76], and Stein [79] co-condensation reactions have been used to prepare hybrid mesoporous silicates under a wide range of reaction conditions. Some common criteria in the choice of the co-condensation reaction system include the need to avoid phase separation of the precursors to obtain uniform distributions of functional groups and the need to avoid Si-C bond cleavage during the sol-gel reaction and during surfactant removal.

1.9.3 Comparison between Grafting and Co-condensation Methods

Lim and Stein compared the relative distribution of surface groups in vinyl-functionalized MCM-41 samples prepared by either a post-synthesis grafting process or a direct co-condensation synthesis [106-108]. Based on their results, the vinyl groups appeared to be non-uniformly distributed in samples prepared by the grafting process, with a large proportion of vinyl groups on the external surface of the crystallites or inside channels but near the channel openings. In products from a direct co-condensation reaction, the vinyl groups appeared to be more uniformly distributed throughout the channels.

Each of the two functionalization methods has certain advantages. If uniform surface coverage with organic groups is desired in a single step synthesis, the direct method may be the first choice. It also provides better control over the amount of

organic groups incorporated in the structure. However, products obtained by post-synthesis grafting are often structurally better defined and hydrolytically more stable than samples from the direct synthesis method. Although pore sizes can be controlled to some extent by both methods, pore size control is more easily achieved by grafting.

1.9.4 CHARACTERISATION

The analysis and characterisation of sol-gel derived materials is important for two main reasons: the starting materials are very different from the final products (both chemically and physically) and secondly, due to the enormous versatility of the sol-gel method, the resulting materials (and their precursors) can cover a vast range of both physical and chemical properties. For example, the precursors are monomers and their reaction products polymers, the former generally are soluble, the latter insoluble. Furthermore, they may be hydrophobic vs. hydrophilic, liquid vs. solid, and during the process many intermediate stages are generated. The final products, however, may also be very different: they can be hydrophilic or hydrophobic, gels or glasses, films or bulk materials, inorganic or hybrid materials, dense or porous, tough or brittle. They can have various degrees of cross-linking and may be based on different metals such as silicon, titanium, vanadium and niobium or mixtures of them. For these reasons a variety of chemical and physical characterisation techniques have been used to analyse the different aspects of these materials.

1.9.4.1 Nuclear Magnetic Resonance Spectroscopy

Solid-state ^{29}Si NMR [109-110], ^{13}C NMR [111] and ^{1}H NMR [112-114] spectroscopic measurements were used to gain insights into the silicon, carbon and hydrogen environments and observe the way the surface of mesoporous silica functions. Using ^{29}Si NMR spectroscopy the chemical environments of silicon atoms in silicates can be analysed. For this both liquid and solid state NMR techniques are used, to probe the local chemistry of silicon before and after the sol-gel transition, respectively.

The signals in NMR spectra are characterised by three main parameters: chemical shift, peak intensity and line width. The chemical shifts found in the ^{29}Si NMR spectra of silicates range from -60 to -120 ppm. These signals shifts up-field by approximately 10 ppm for every Si-O-Si connection made to the central Si atom. The chemical shifts observed in the solid state associate well with the chemical shifts observed in solution spectra for the same silicate structures.

In solid state NMR spectroscopy line broadening tends to increase reflecting the variety in the possible chemical environments of the different silicon atoms. Solid state NMR spectroscopy generally is not able to differentiate between species with different OR-groups (R = alkyl or hydrogen) on silicon. These differences can often be resolved using solution NMR, also due to the generally lower molecular weight of the material present before gelation [115].

1.9.4.2 Nitrogen Adsorption

Adsorption isotherms are plots of the amounts of gas adsorbed at equilibrium as a function of the partial pressure P/P_O at constant temperature, usually nitrogen at its boiling point (77.4 K). The isotherms obtained generally can be grouped in to 5

classes, the characteristic features of which are depicted in **Figure 1.9.4** [84]. Isotherm type I is typical for adsorption by microporous materials (pore sizes < 2 nm) where the BET equation is not valid. Type II isotherms are characteristic for non-porous materials and types III and V are obtained for very weak adsorption interactions of which the fundamentals are not very well understood. For mesoporous materials isotherms of type IV are generally obtained.

Nitrogen adsorption measurements revealed a systematic decrease in the BET surface area and the pore volume for hybrid materials prepared by post synthesis procedures [116-118]. Generally, the type IV adsorption isotherm characteristic of mesoporous materials was preserved upon post synthesis modification but the capillary nitrogen condensation step shifted gradually to lower relative pressures indicative of decreasing pore sizes. This decrease was dependent on the size of the grafted ligand [119] and the surface coverage [120-123]. In contrast, Anwander and Roesky [119] observed that the characteristic type IV isotherm for pure MCM-41 silica was replaced by the type I isotherm after anchoring silylamide species on the internal surface. As for mesoporous silica prepared by co-condensation procedures, they often exhibit high surface areas [124-125] and pore sizes of 1.8-3.5 nm for modified MCM-41 and 6 nm for functionalized SBA-15 [126]. Moreover, it appears that the hybrid mesoporous silica prepared via co-condensation exhibit thicker pore walls compared to their corresponding pure silica derivatives [128].

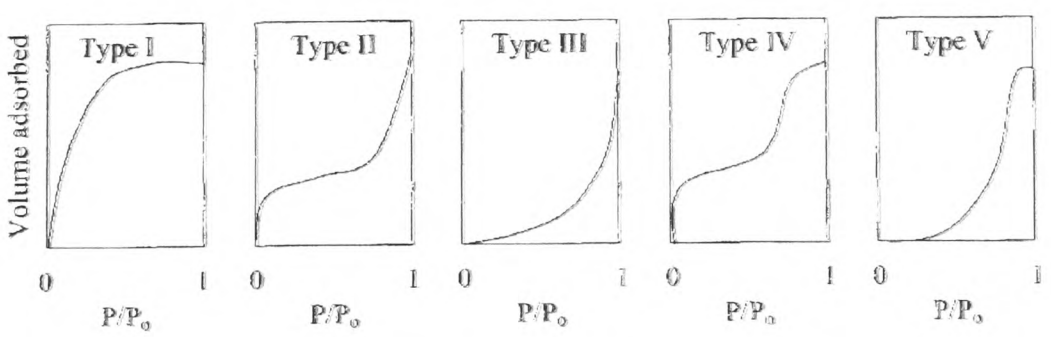

Figure 1.9.4: Characteristic shapes of the five classes of BET (Brunauer, Emmett and Teller) adsorption isotherms [84].

1.9.4.3 Infrared Spectroscopy

For the study of the products of the sol-gel process infrared spectroscopy is very useful. Using infrared spectroscopy the hydrolysis and condensation of silicates can be easily monitored. Wood and Rabinovich showed that particularly the 700-1800 cm^{-1} range is useful to study the hydrolysis of TEOS [127]. Acid catalysis of the reaction leads to the disappearance of the specific bands at the ranges of 966 cm^{-1} and 792 cm^{-1} as well as the 1650 cm^{-1} vibration of water and the simultaneous appearance of the molecular backbone vibration of ethanol (880 cm^{-1}). At the same time Si-O-Si vibrations appear at 1160 cm^{-1} and 1200 cm cm^{-1} indicating the early stages of formation of a gel network. The development of the network can also be monitored by following the Si-O-H vibration at 950-980 cm^{-1} which decreases in intensity but also shifts to higher wave numbers as the condensation of the polymer proceeds [129].

The wavelength at which the Si-O-Si band appears in the spectrum depends on the degree of cross-linking of the silica network [130]. For highly cross-linked, base catalysed gels Si-O-Si vibrations have been observed at high frequency (1100 cm^{-1}) whereas for poorly cross-linked acid catalysed gels these vibrations were found at 1030 cm^{-1}.

1.9.4.4 X-ray Diffraction

Functional mesoporous materials exhibit XRD patterns dominated by low-angle peaks. Generally, post-synthesis surface functionalization does not dramatically affect their structural ordering [131-137]. In the case of hybrid mesoporous materials synthesised in single step via co-condensation, the structural ordering was strongly dependent on the relative amount of the organic precursor present in the synthesis mixtures. Several research groups observed a progressive decrease in the mesoporous

size order as the relative amount of organosilane in the synthesis mixture increased [128, 130].

1.9.5 Applications of ORMOSILs

Several reviews have been written recently on the design and applications of ORMOSILS. For example, Wilkes and Wen [130] and Sanchez and Ribot [131] have presented detailed accounts of the synthesis, structure, and application of hybrid networks that have been prepared via the incorporation of *predominately* polymeric/oligomeric species within inorganic networks. Corriu and Leclercq [132] have focused on the chemistry of sol-gel processing and have described the synthesis and preparation of gels from new precursors, new sol-gel routes, and inorganic-organic precursors. Schubert and co-workers [133] have written a well-documented account about the sol-gel formation of hybrid materials that includes brief descriptions of their applications as composite polymers, solid electrolytes and hosts for dye molecules, catalysts, sensors, and membranes.

Hybrid mesoporous materials have also been employed in environmental issues either for the generation of desired products without formation of waste, or for waste clean-up, including sorption of toxic heavy metal cations [138-141] and anions, and organic solvents [141]. The characteristics of suitable mesoporous sieves for environmental remediation include their high adsorption capacity and specificity for certain contaminants.

CHAPTER 2: - EXPERIMENTAL

2.1 STARTING MATERIALS

2.1.1 GENERAL CHEMICALS

3-(Trimethoxysilyl) propyl methacrylate, ammonium persulphate, benzoyl peroxide, cetyltrimethylammonium bromide (CTAB), cyclohexyltrichlorosilane ($CySiCl_3$), hexadecacyltrimethylammonium chloride (C_{16}), poly(N-isopropylacrylamide) (NIPAM), potassium persulphate, styrene, toluene, tetraethylorthosilicate (TEOS), vinyltrichlorosilane, 2, 2'-azobisisobutylronitrile (AIBN), vinyltrimethoxysilane, and lauryl peroxide were supplied by Aldrich and were used without further purification. The acetone, chloroform, concentrated hydrochloric acid, triethylamine and hexane were general purpose reagents from Aldrich. Methyl methacrylate was also supplied by Aldrich but it was purified before use. [142]

The water used in all cases was deionised.

2.1.2 CLAY MINERALS

The source of montmorillonites used for the experiments reported, was K10 and Bentonite supplied by Aldrich. Physical analysis and measurements of the cation exchange capacity (CEC) of the clays were reported by Aldrich and are shown in **Table 2.1.1**.

Table 2.1.1: Physical analysis of clays used in this work.

Products	CEC (meq/100g)	BET (m^2/g)	Bulk Density (g/L)
K10	30	220-270	300-370
Bentonite	80 - 100	<100	800 - 900

2.2 INSTRUMENTAL ANALYSIS

2.2.1 CARBON AND HYDROGEN ELEMENTAL ANALYSIS

Carbon and hydrogen were analyzed using a Carlo Erba Elemental Analyses (model 1106) at the University of Greenwich.

2.2.2 INFRARED SPECTROSCOPY (IR)

Infrared spectra were obtained on a Perkin-Elmer Paragon 1000 Fourier Transform infrared spectrometer at wavenumber range of 4000cm^{-1} to 500cm^{-1}. Solid samples were incorporated with potassium bromide to form discs wherever possible. Partially gummy solids were smeared between potassium bromide plates. Liquid samples were run as thin films between sodium chloride plates.

2.2.3 NUCLEAR MAGNETIC RESONANCE SPECTROSCOPY (NMR)

Nuclear Magnetic Resonance was performed on a JEOL 270 MHz FTNMR instrument. Samples were run with an internal standard of tetramethylsilane (TMS) or trimethylborate (TMB) using deuterated chloroform ($CDCl_3$) as the solvent. Samples were examined using ^{29}Si, ^{1}H, and ^{13}C isotopes.

2.2.4 SOLID STATE NUCLEAR MAGNETIC RESONANCE SPECTROSCOPY

The apparatus used was a JOEL 300 spectrometer with a magnetic field strength of 7.0463 T. The spectra were recorded at 59.627 MHz using a magic angle spinning probe, containing a 4 mm (outside diameter) zirconium rotor. The spinning speed of the sample was between 8 KHz and 9.5 KHz. The contact time of the

excitation pulse was 1 microsecond, with a recycle delay time of 1 second. The minimum number of scans for any sample was 4,096. All samples were referenced with respect to tetramethylsilane.

2.2.5 X-RAY DIFFRACTION

The samples were analysed using a Philips X-ray diffractometer. The radiation used was Cu-Kα radiation (λ = 1.5418Å). The d-spacings were calculated from Bragg's law (nλ= 2d sin θ). The region of scan was 2θ = 4°- 84°.

2.2.6 GEL PERMEATION CHROMATOGRAPHY (GPC)

Polyorganosiloxane products soluble in toluene were analysed using high performance liquid chromatography, comprising a Waters HPLC system. Ultrastyragel gel permeation columns of specified pore sizes were used with toluene as elution solvent at a flow rate of 1.5 cm^3/min. The polyorganosiloxanes samples as approximately 10% v/v solutions in tertbutylbenzene were filtered through a 0.5μm Millipore filter prior to injection (5 μl).

2.2.7 THERMAL ANALYSIS (TGA)

Differential thermal analysis (DTA) and thermogravimetric analysis (TGA) were performed on a Dupont TA instrument model number 910 and 951 respectively. The samples were recorded under the following conditions: temperature heating rate of 10 °C/min under static air and a temperature range of 30–1000 °C.

2.2.8 Surface Area Analysis

Surface area measurements were carried out using a Micromeritics Gemini 2375 V4.01 surface area analyzer, by nitrogen adsorption at 77K. Surface area and pore size were obtained.

2.2.9 Electrokinetic Analysis

Particle size and zeta potential measurements were carried out on a Malvern Instruments, Zetasizer 3000.

2.2.10 Freeze Drying

Freeze drying was carried out on a Freeze Dryer 3-5, Birchover Instruments Ltd.

2.2.11 Cone Calorimetry

Cone Calorimeter evaluations were carried out on a Fire Testing Technology Cone Calorimeter. The specimens, measuring 100 mm x 100 mm x 12 mm were stored in the warm laboratory before testing. Each specimen was wrapped in aluminium foil, and placed on a mineral blanket with the surface level with the holder, such that only the upper face was exposed to the radiant heater. An edge-guard was used with all specimens. Samples were tested at 50 kW/m^2. The quoted data are from one test at each heat flux.

2.3 PREPARATION OF ORGANOPHILIC CLAY

The montmorillonite K10 and Bentonite clay (10 g) were stirred in distilled water (100 ml) at room temperature until complete dispersion occurred. Hexadecyltrimethylammonium chloride (C_{16}, 40 g) was added and the mixtures were stirred for a further 60 min. The organomontmorillonites were recovered by filtering the solution, followed by repeated washings of the filtered cake with water. The final products were left to dry overnight.

2.4 PREPARATION OF ORGANOCLAY COMPOSITES WITH STYRENE OR NIPAM

The montmorillonites or their equivalent organoclays were suspended in toluene and added to a mixture of styrene and toluene. The mixture was stirred for 2 hours at room temperature. The products were collected after filtration and washed with distilled water. The styrene-organoclay complexes were left to dry overnight. The above procedure was repeated with NIPAM, which was substituted for the styrene.

Different weight ratios of organoclays to polymer were prepared (2:2, 2:1.5, 2:1, and 2:0.5).

2.5 SYNTHESIS OF A POLY (NIPAM) MICROGEL CONTAINING ORGANOPHILIC CLAY

The NIPAM -organoclay complexes (0.52 g) and ammonium persulphate (0.24 g) were added to 200 ml of H_2O in a round-bottomed flask. 3 - (trimethoxysilyl) propyl methacrylate (2.5 g), dissolved in 100 ml of H_2O was added to the above mixture.

The solution was stirred for 6 hours at 70°C under nitrogen, after this time the solution was filtered through glass wool and placed in a bottle in the fridge for two days.

After repeated centrifugation and washing with water, to remove unreacted monomer and initiator, the sample was freeze dried.

The above procedure was repeated for 4 hours at the same temperature.

2.6 GENERAL PROCEDURE FOR THE HYDROLYTIC CONDENSATION OF CYCLOHEXYLTRICHLOROSILANE (CyC_6SiCl_4)

To a solution of CyC_6SiCl_4 (25 ml) and technical-grade acetone (460 ml), distilled water (120 ml) was carefully added with stirring. The solution was placed in a large glass bottle and stoppered well to allow standing for 6 months, with frequent mixing. The precipitates were collected in a large sintered glass Buchner funnel and washed with water. The material was dried overnight at 70 °C.

The hydrolytic condensation of cyclohexyltrichlorosilane affords three different products [27]: $Cy_7Si_7O_9(OH)_3$ - **1**,

$Cy_6Si_6O_9$ - **2**, **and**

$Cy_8Si_8O_{11}(OH)_2$ – **3**

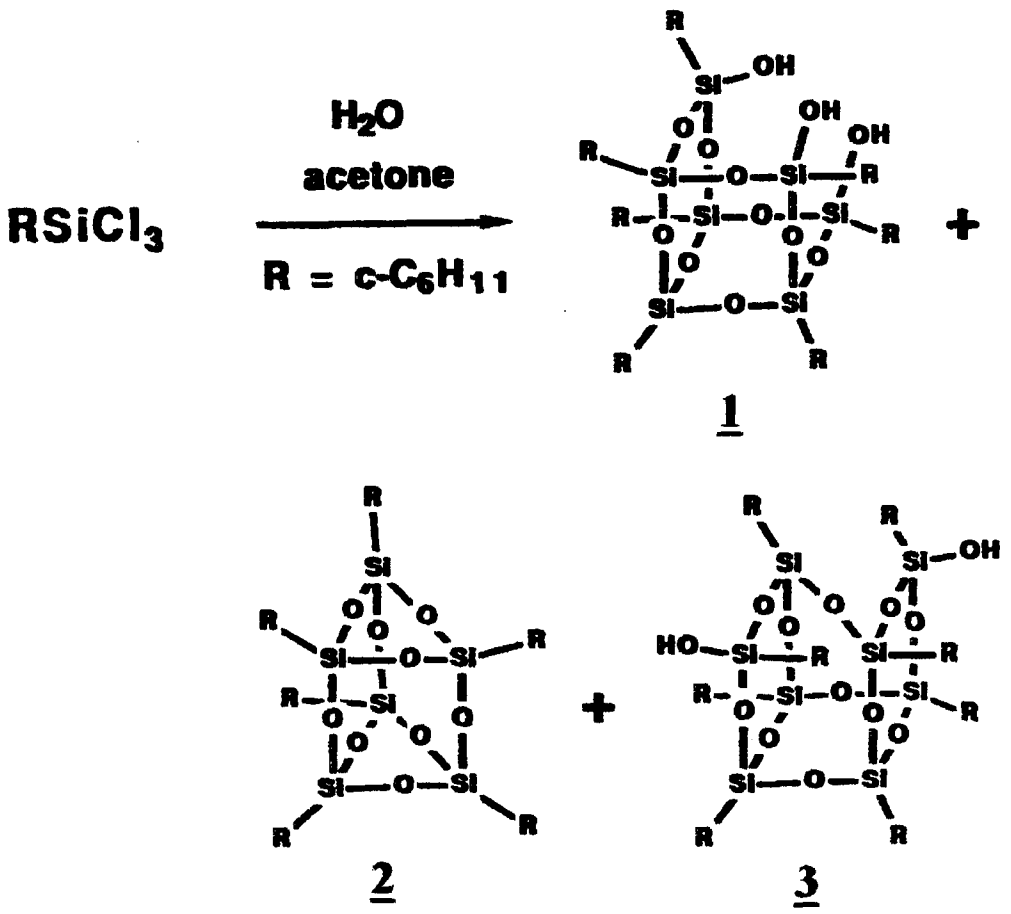

Isolation of 2: -the crude product mixture was stirred with 5 times its weight of pyridine for approximately 30 min. Hexamer 2 was collected in a medium sintered glass Buchner funnel, washed with a small amount of pyridine, and dried overnight at 25 °C in a fume cupboard. Re-crystallization from boiling chloroform affords pure material.

Isolation of 1: -the pyridine extract form the solution of 2 was carefully poured into 5 times its volume of ice cold aqueous HCl (1 ml of concentrated HCl / ml of pyridine). Any large clumps of precipitated product were broken up as finely as possible and then collected on a large Buchner funnel, washed with large amounts of water for 1 hour. Crystallization from the minimum amount of hot diethyl ether yields a pure product.

Isolation of 3: -the mother liquors from the crystallization of 1 from ether were further concentrated to approximately 10 ml of ether / g of 3 in the original crude product mixture to precipitate additional 1 (which was collected by filtration). The

remaining solution was evaporated to dryness and then re-crystallized from a minimum amount of hot chloroform (10 ml/g of 3).

The course of the reaction does not appear to be affected by periodic product isolations and the filtrate will continue to precipitate 1 for approximately 3 years. The eventual yield of crystalline products is typically 60-70%, based on $CySiCl_3$.

Filtration of a typical reaction mixture after 12 weeks affords 70 g of crude product, which contains 45% of heptameric 1, 40% of hexameric 2, and 15% of octameric 3. Subsequent filtrations of the reaction mixture yield crude product mixtures with progressively lower percentages of 2. For example, a second filtration after an additional 12 weeks typically yields 40 g of material containing 1, 2, and 3 in a 62:12:26 ratios. A third filtration after 12 months more typically gives 70 g of the three products in a 77:7:16 ratios. Crystalline material precipitating after 1.5 years is almost entirely 1.

The three products of the reaction exhibit very different solubility properties and can be easily separated. Pyridine extraction of the crude product mixture quantitatively separates the insoluble 2 from the two silanol-containing products. Separation of 1 from 3 can be effected by fractional crystallization from ethanol: 1 is approximately 5 times less soluble in ether than 3 and precipitates as analytically pure microcrystals upon concentration of hot ether solutions. Compound 3 can be isolated in pure form by recrystallization from $CHCl_3$, in which it is 5 times less soluble than both 1 and 2.

2.7 REACTION OF $CyC_6Si_7O_9$ (1) WITH VINYLTRICHLOROSILANE

A toluene (10 ml) solution of vinyltrichlorosilane (2.05 g) was rapidly added to a solution of 1 (0.97 g) in 10 ml of 4:1 (v/v) $C_6H_5CH_3/Et_3N$ and stirred for 2 hours at 25°C. The product was extracted with toluene and solvent removal in vacuo gave a solid product.

2.8 POLYMERISATION OF VINYLTRICHLOSILANE IN DIOXANE IN THE PRESENCE OF 2, 2'-AZOBISISOBUTYLRONITRILE

A mixture of vinyltrichlorosilane (0.05 mol) and 2, 2'-azobisisobutylronitrile (AIBN) ($2.5x10^{-3}$ mol) was poured into a 200 ml round flask followed by the addition of 50 ml of dioxane. The mixture was stirred for 2 hours at 60 °C under nitrogen. The precipitate was filtered and left to dry overnight.

The above procedure was repeated with vinyltrimethoxysilane and styrene instead of vinyltrichlorosilane.

2.9 SYNTHESIS OF PROPYLMETHACRYLATEPOLYSILOXANE

Ethanol (50.00 g), water (10.00 g) and hydrochloric acid (150 ml, 0.10 mol dm^{-3}) were mixed in a 400 ml beaker. 3- (Trimethoxysilyl) propyl methacrylate (50.00 g) was added and the mixture was stirred at 50 °C for 2.5 h. The mixture was transferred to a separating funnel for solvent extraction using toluene (250 ml). The aqueous layer was removed; the toluene was dried using anhydrous calcium chloride and then removed under vacuum to yield a viscous oil (21.30 g).

2.10 EXTRACTION OF PROPYLMETHACRYLATEPOLYSILOXANE WITH PYRIDINE

Propylmethacrylatepolysiloxane was first stirred with 5 times its weight of pyridine for approximately 30 min. The product was collected in a medium sintered-glass Buchner funnel, washed with a small amount of pyridine and dried overnight at room temperature in a fume hood.

The pyridine extract was carefully poured into 5 times its volume of ice-cold aqueous HCl (1ml of concentrated HCl / ml of pyridine). Any large lumps of precipitated product were broken up as finely as possible and then collected on a large Buchner funnel and first washed with 100 ml of toluene and then washed with large amounts of water for 1 hour. The product was then placed in a desiccator to remove any excess of toluene.

Elemental analysis, infrared analysis and ^{13}C, ^{1}H, ^{29}Si NMR analysis were performed on the product.

2.11 SYNTHESIS OF CROSSLINKED POLY PROPYLMETHACRYLATEPOLYSILOXANE

Propylmethacrylatepolysiloxane (9.0 g) was dissolved in toluene (360 ml) in a 500 ml beaker. The solution was transferred to a 1 litre photoreactor vessel and benzoyl peroxide (1.23 g) was added as an initiator. The mixture was then irradiated with ultraviolet light (λ = 254, 265, 297, 313, 366 nm) and magnetically stirred under nitrogen for 24 hours.

The resulting gel was filtered off under vacuum, washed with toluene and dried under vacuum at 50 °C overnight to give a white powder (8.93 g).

2.12 REACTION OF PROPYLMETHACRYLATEPOLYSILOXANE WITH VINYLTRIMETHOXYSILANE

A toluene (20 ml) solution of vinyltrimethoxysilane (0.25 g) was rapidly added to a solution of propylmethacrylatepolysiloxane (0.97 g) in 25 ml of 4:1 (v/v) $C_6H_5CH_3/Et_3N$ and stirred for 2 hours at 25°C.

The product was cooled down, evaporation with pentane and solvent removal in vacuo gave a solid product.

2.13 COPOLYMERIZATION OF NIPAM AND 3- (TRIMETHOXYSILYL) PROPYL METHACRYLATE

NIPAM (10.00 g), 3 - (Trimethoxysilyl) propyl methacrylate (3.00 g) and benzoyl peroxide (0.50 g) were dissolved in toluene (65 ml) in a flask. The mixture was stirred for 6 h under nitrogen.

The resulting copolymers were purified by repeated precipitation from hexane and re-dissolution in toluene and then dried at room temperature.

2.14 PREPARATION OF CO-POLYMER LATEXES

Deionised water (20 ml) was added to a 100 ml round bottomed flask immersed in a thermostatic bath set at 90 °C. Styrene (1.2 g) and vinyltrimethoxysilane (0.8 g) were added and stirred for 15 min under nitrogen. Potassium persulphate (0.02 g) was added to the mixture to initiate the reaction. A water-cooled condenser was also attached to the system also. The mixture was allowed to react at 90 °C for 9 hours.

Washing and centrifugation removed any unreacted styrene, vinyltrimethoxysilane and potassium persulphate.

Other syntheses were carried out with different proportions of vinyltrimethoxysilane, as shown in **Table 2.1.2**, below.

Table 2.14.1: Composition of co-polymer latexes.

Composition of vinyltrimethoxysilane (wt%)	styrene	vinyltrimethoxysilane
10%	1.8g	0.2g
20%	1.6g	0.4g
30%	1.4g	0.6g
40%	1.2g	0.8g
50%	1.0g	1.0g
60%	0.8g	1.2g
70%	0.6g	1.4g
80%	0.4g	1.6g
90%	0.2g	1.8g

2.15 PREPARATION OF MESOSTRUCTURED ORGANO-MODIFIED SILICA

Cetyltrimethylammoniumbromide (CTAB) (2.68 g) was dissolved with stirring in a mixture of distilled water (88.3 g) and concentrated hydrochloric acid (49.2 g, 37% wt HCl). Tetraethoxysilane (TEOS) (3.06 g) was added rapidly with vigorous stirring until a clear solution had formed. For syntheses including vinyltrimethoxysilane, this was first mixed with TEOS. The mixture was left at room temperature overnight. Precipitated solids were filtered off, washed with distilled water (500 ml) and allowed to dry at room temperature. Calcination was carried out

in a tube furnace, under flowing nitrogen. Samples were heated from 1°C min^{-1} to 540°C maintaining that flowing nitrogen for 6 hours.

Other syntheses were carried out with different proportions of the reagents and with the inclusion of vinyltrimethoxysilane. **Table 2.1.3** summarises the mole ratio of the organic-modified silicas.

Table 2.15.1: Summary of the mole ratio of TEOS:Vinyltrimethoxysilane:CTAB:HCl:H_2O.

Mole ratio TEOS:Vinyltrimethoxysilane :CTAB:HCl:H_20	**Vinyltrimethoxysilane**	**TEOS**	**CTAB**	**HCl conc**
2.2: 0.0: 1.1: 75: 1000	0.0g	15.3g	13.4g	246g
2.2: 0.09: 1.1: 75: 1000	0.44g	15.3g	13.4g	246g
2.2: 0.16: 1.1: 75: 1000	0.8g	15.3g	13.4g	246g
2.0: 0.25: 1.1: 75: 1000	1.35g	13.9g	13.4g	246g
2.0: 0.09: 1.1: 75: 1000	0.45g	13.9g	13.4g	246g
2.0: 0.09: 1.1: 45: 1000	0.45g	13.9g	13.4g	147.5g
2.1: 0.32: 1.2: 75: 1000	1.65g	14.6g	14.4g	246g
2.0: 0.29: 1.1: 45: 1000	1.60g	13.9g	13.4g	147.5g
2.0: 0.31: 1.2: 66: 1000	1.70g	13.9g	14.4g	216.5g

In a second series of experiments the water was removed from the solid products by azeotropic distillation using toluene and a Dean and Stark apparatus. The solids were filtered and dried in vacuum desiccator over paraffin wax to remove any residue toluene.

2.16 PURIFICATION OF METHYL METHACRYLATE

Methyl methacrylate (400ml) was washed twice with 5% NaOH, to remove inhibitors such as hydroquinone and twice with water. The solution was dried over $MgSO_4$ and then filtered. The purified methyl methacrylate was used immediately for the following experiment. [2]

2.17 SYNTHESIS OF FLAME RETARDING POLY (METHYL METHACRYLATE) WITH SILICA CONTAINING COMPOUNDS

A mixture of methyl methacrylate (MMA) (350 ml), benzoyl peroxide (1.0 g) and lauryl peroxide (0.5 g) was purged under nitrogen for 10 minutes and then heated at 70 °C, under nitrogen. When the mixture became sufficiently viscous (typically 1 hour) it was poured into a glass pyrex covered with a glass lid and left in the fume cupboard till set.

For the silica containing samples, the same procedure was followed but a silica polymer was added to the viscous mixture when taken out from the reaction, before starting to set. Two different polymers were used, which were prepared by the above procedure (Experiment 15) and showed the highest surface area. One of them was a sample calcinated and the other one was a sample treated using Dean and Stark extraction.

Two sets of each experiment were performed.

CHAPTER 3: - RESULTS

3.1 ANALYSIS OF CLAYS

Two clays, K10 and bentonite were used for this experiment. Both clays were used for a series of experiments, including their intercalation with C_{16} to prepare their equivalent organophilic clays followed by reaction with NIPAM or styrene to prepare of a poly (NIPAM) microgel containing an organoclay.

All clays, organoclays, and intercalated composites were characterised by X-ray diffraction and infrared spectroscopy and elemental analysis.

3.1.1 ELEMENTAL ANALYSIS

Elemental analysis for nitrogen (N), carbon (C) and hydrogen (H) was performed on each of the clays used for the purpose of this work. **Table 3.1.1** lists the results from the analysis.

Table 3.1.1: Elemental analysis of montmorillonites.

	Elements		
Montmorillonite	**Nitrogen**	**Carbon**	**Hydrogen**
K10	0.00	0.08	1.49
Bentonite	0.00	0.24	1.10

Elemental analysis was also performed for K10 organo-montmorillonite. The results clearly show the successful intercalation of the C_{16} in the K10 organoclay (**Table 3.1.2**). The small increase in nitrogen value compare with the result of the K10 montmorillonite is without a doubt due to the addition of C_{16} in the clay as well

as the big increase of the carbon atoms in the organoclay. The raise of the number of hydrogen atoms can be as a result of the water still existing in the compound even after the drying process. Further analysis for the bentonite organoclay could not be performed.

Table 3.1.2: Elemental analysis of intercalation species of montmorillonites.

	Elements		
Montmorillonite	**Nitrogen**	**Carbon**	**Hydrogen**
K10	0.45	8.10	2.10

3.1.2 INFRARED (IR) ANALYSIS

3.1.2.1 Study of the montmorillonites

Montmorillonites are particularly suited for infrared studies because of their high surface area, which gives rise to favourably strong spectra. **Figures 3.1.1-3.1.2** shows the IR spectra at room temperature in the region 4000-500 cm^{-1} for each of the two clays. The adsorption peak appearing in each of the clays at ~3500 cm^{-1} is due to hydroxyl groups. The weak band appeared in the K10 and bentonite clays spectra at ~3600 cm^{-1} could arise from the hydroxyl groups shared between aluminium (Al^{3+}) and iron (Fe^{3+}) since the octahedral layer may contain a small proportion of iron (Fe^{3+}) [143-144]. The samples exhibited Si-O-Si stretching vibrations at 1120 cm^{-1} as a shoulder to the main peak at 1050 cm^{-1}. The Si-O-Si stretching vibrations should give a single band near to 1050 cm^{-1}. This peak is split into two components in the dioctahedral series of layer silicates because of distortion of the tetrahedral layer. This distortion causes the shoulder to appear near to 1120 cm^{-1}.

3.1.2.2 Study of their organoclays

The infrared spectra of the two organoclays **(Figure 3.1.3-3.1.4)** show that structural changes occurred after the exchange of the cations in the interlayer space of the clays by the alkyl ammonium ions. The characteristic bands of the minerals appear in the infrared spectra without any changes, while new bands, due to the presence of aliphatic chains, appear. The two intense bands in the region 3000-2800 cm^{-1} are attributed to the symmetric and asymmetric stretches of the methyl and methylene groups. Bands between 1520-1400cm^{-1} are generally due to the bending of the CH bond in the CH_3 and CH_2 groups.

Only by looking at the infrareds of both clays, K10 and bentonite and their equivalent organoclays there is a clear indication that the intercalation has been successful. The appearance of new bands on the infrared spectrum of the organoclays has confirmed that the reaction between the clays and the organic intermediate used, in this occasion C_{16}, worked. The above statement can be verified by the elemental analysis results.

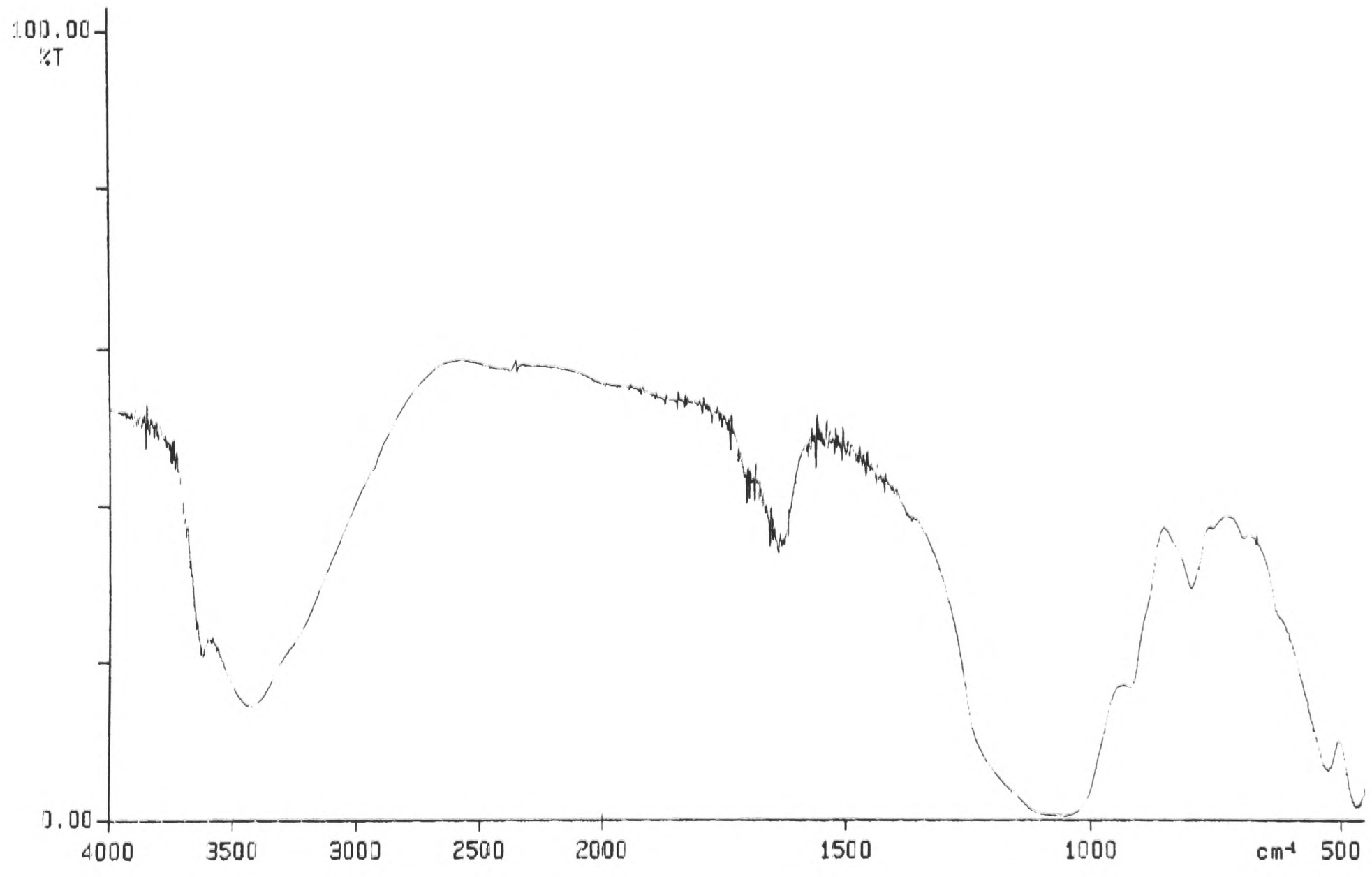

Figure 3.1.1: Infrared spectrum of K10 montmorillonite.

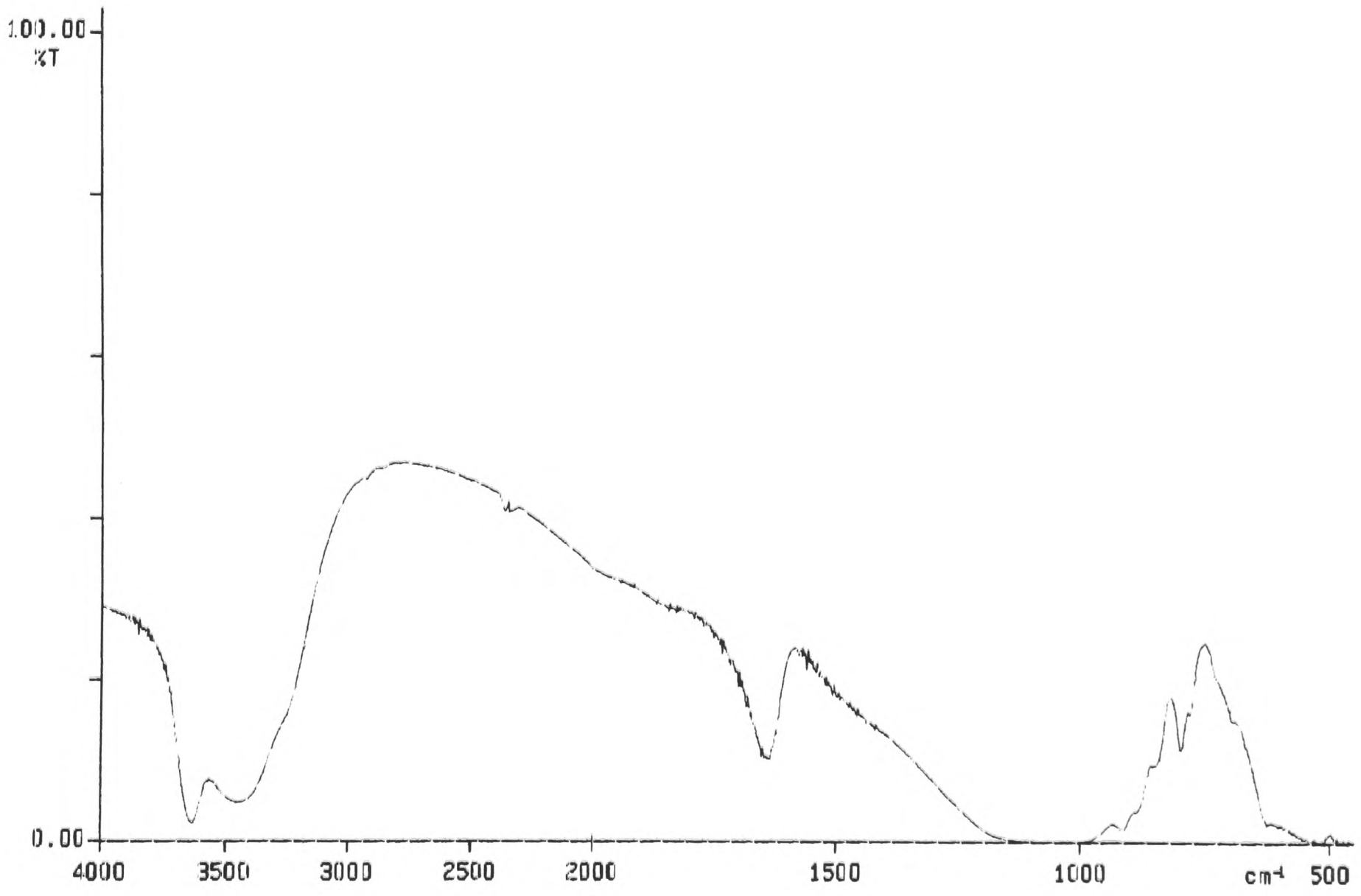

Figure 3.1.2: Infrared spectrum of bentonite montmorillonite.

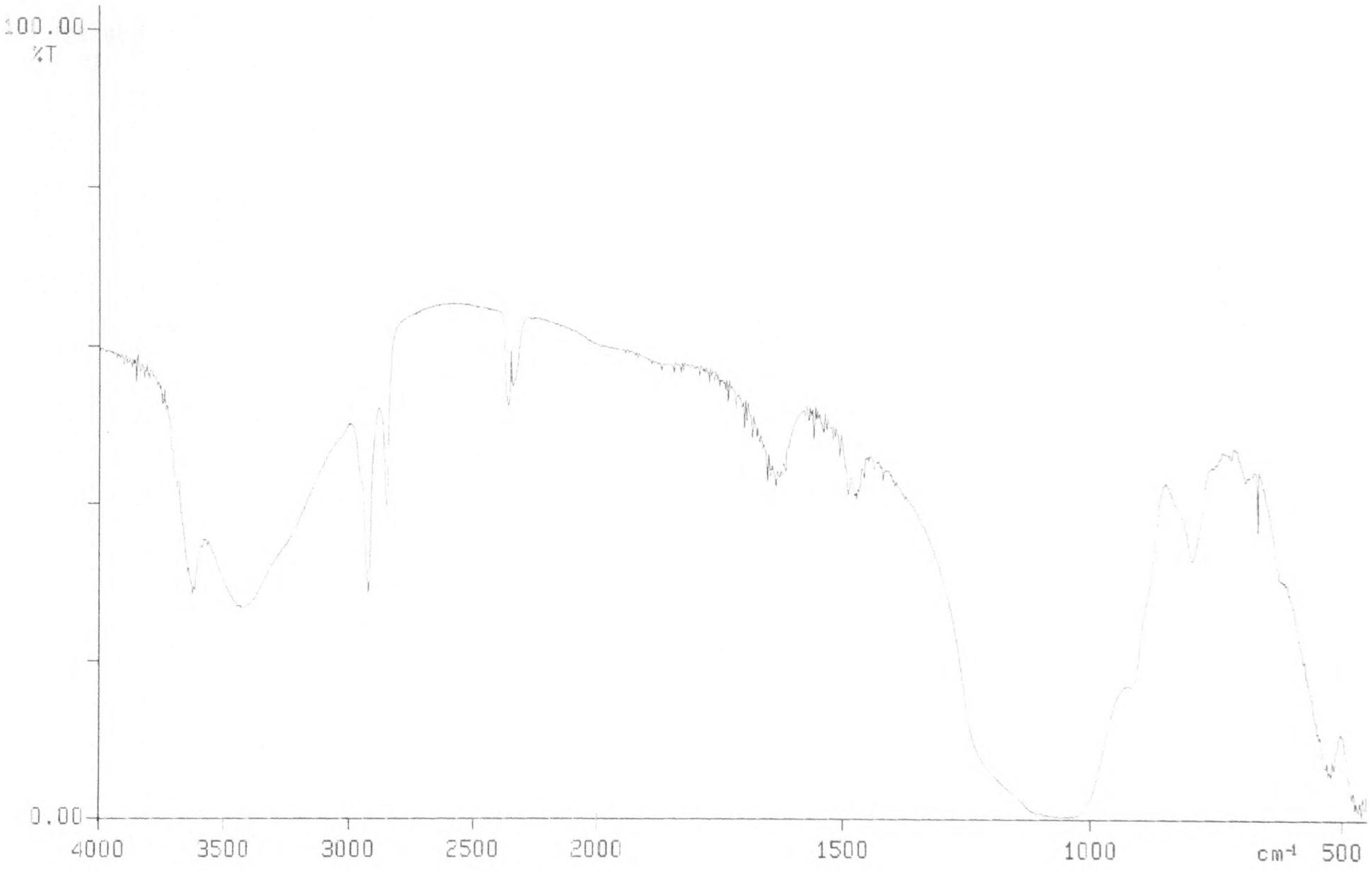

Figure 3.1.3: Infrared spectrum of K10 organoclay.

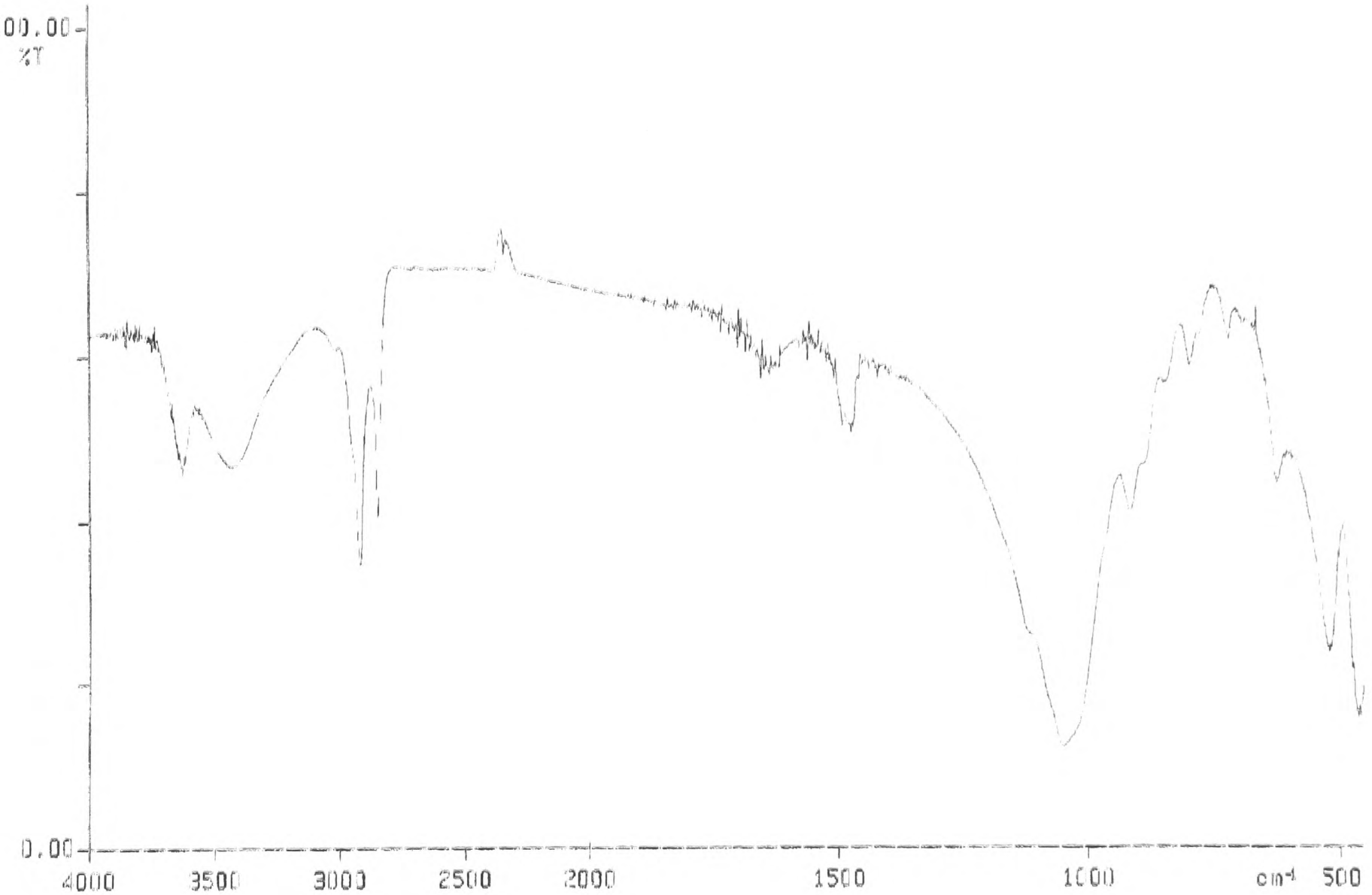

Figure 3.1.4: -Infrared spectrum of bentonite organoclay.

3.1.2.3 Study of intercalated clays

Two different compounds have been used for the intercalation of clays. The clays, K10 and bentonite, and also their equivalent organoclays were treated with styrene and NIPAM at different ratios.

Infrared studies provide an insight into the interlayer of the styrene-intercalated clay complexes. Comparing the starting clay with its equivalent final product there are clearly great differences. Looking at Figure **3.1.1** and **Figure 3.1.5**, a comparison between K10 montmorillonite and its reacted compound with NIPAM a group of peaks appear in the region of 1400-1000 cm^{-1}, a characteristic group confirming the appearance of NIPAM as well as the two, medium peaks at 2850-2800cm^{-1} which represent a =C-O bond. On the other hand a comparison between K10 and its intercalated species with styrene **(Figure 3.1.6)** does not give any result.

The spectrum of the K10-C_{16}-styrene compound **(Figure 3.1.7)** shows a broad absorption band in the 1100-1000cm^{-1} region due to Si-O-Si. A comparison with its equivalent organoclay compound **(Figure 3.1.3)** shows no differences on the spectra. On the other hand the intercalation of the organophilic K10 with NIPAM seems to be more successful. **Figure 3.1.8** is the infrared spectra of the K10-C_{16}-NIPAM complex showing a group of peaks at the range of 1500cm^{-1} up to 100cm^{-1}, characteristic of the NIPAM. The sharp peak at 3200cm^{-1} verifies the appearance of C_{16}.

By looking at the spectrum of bentonite **(Figure 3.1.2)** and its equivalent intercalation with styrene **(Figure 3.1.9)** there are no great variations between the two. In contrast, the bentonite-NIPAM **(Figure 3.1.10)** compound appears to have successfully being formed as the infrared spectrum clearly indicates the appearance of NIPAM specified by the group of peaks at the range of 1500cm^{-1} up to 100cm^{-1}.

Similar behavior can be seen with bentonite and its intercalated compound. By comparison of **Figure 3.1.4** with **Figure 3.1.11** and **Figure 3.1.12** it can be concluded that the reaction of NIPAM was more successful than the corresponding reaction with styrene.

The infrared spectra of all the compounds prepared at different ratios gave similar results. From these results we can conclude that both clays and their organophilic compounds actually reacted better with NIPAM than with styrene. In fact observing the infrared spectra of all the styrene reacted compounds there are no great alterations between the starting and final compound. All the infrared spectra can be found in Appendix.

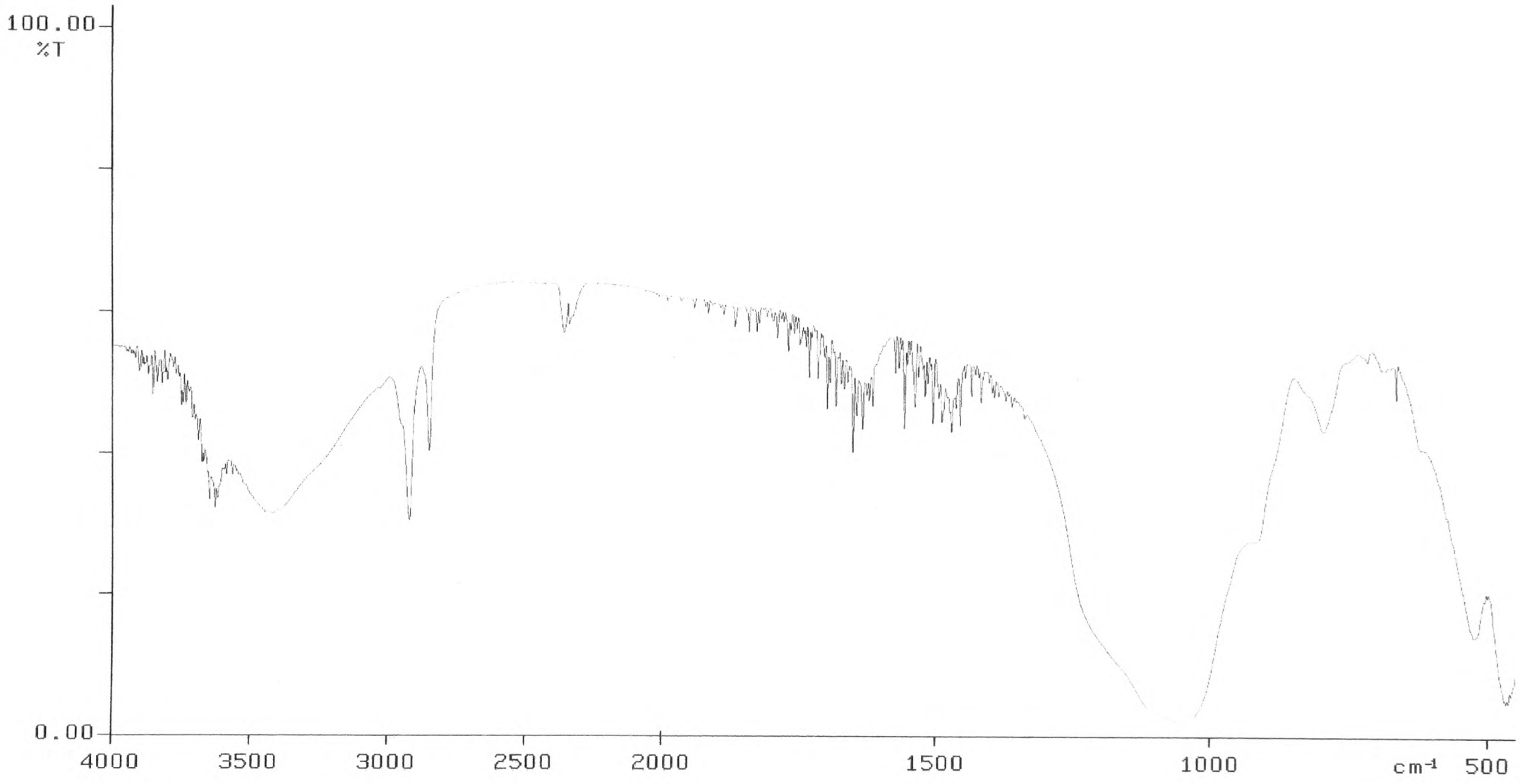

Figure 3.1.7: Infrared spectrum of K10 organophilic compound with styrene (2:2).

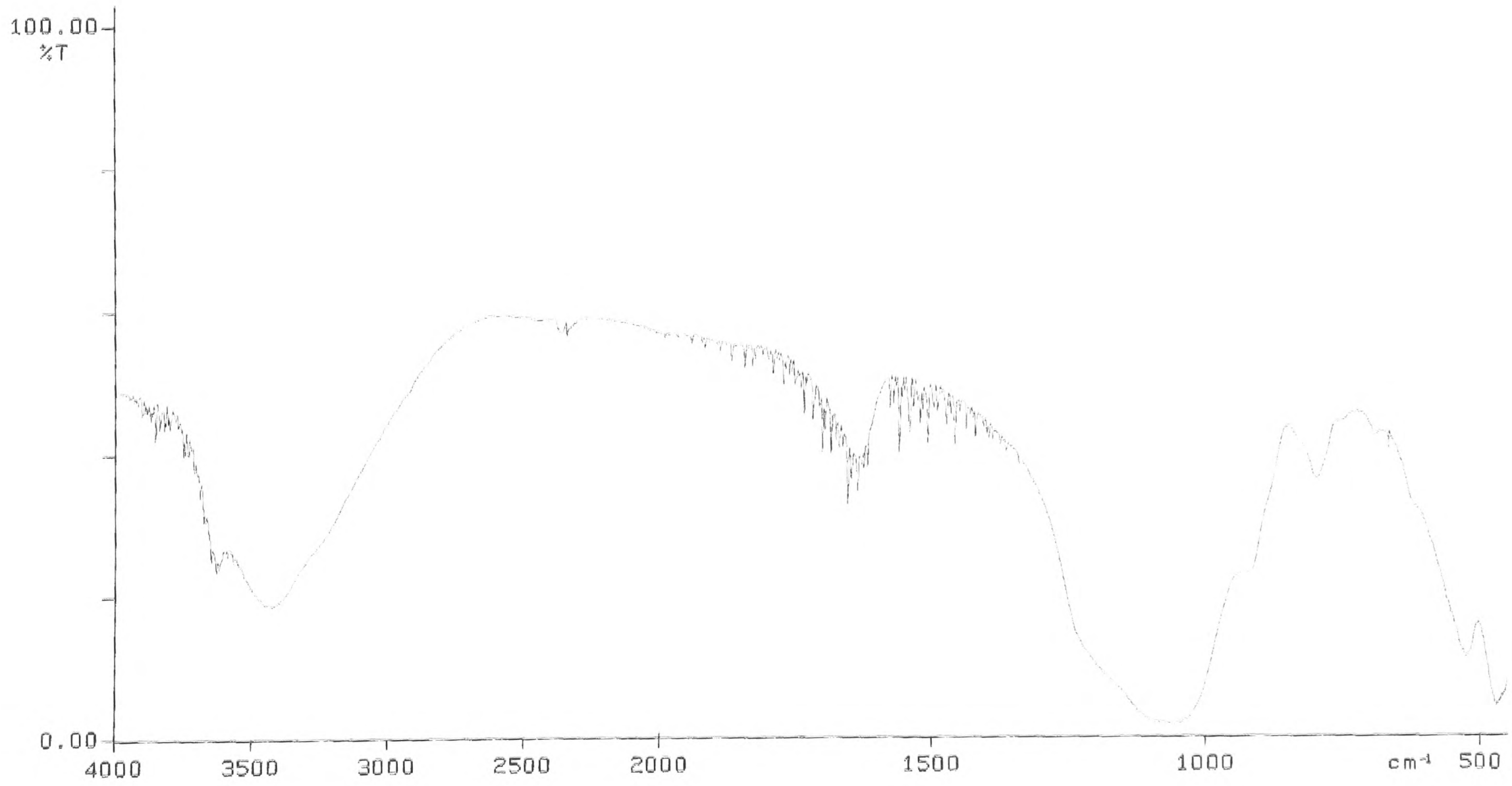

Figure 3.1.6: Infrared spectrum of K10 with styrene (2:2).

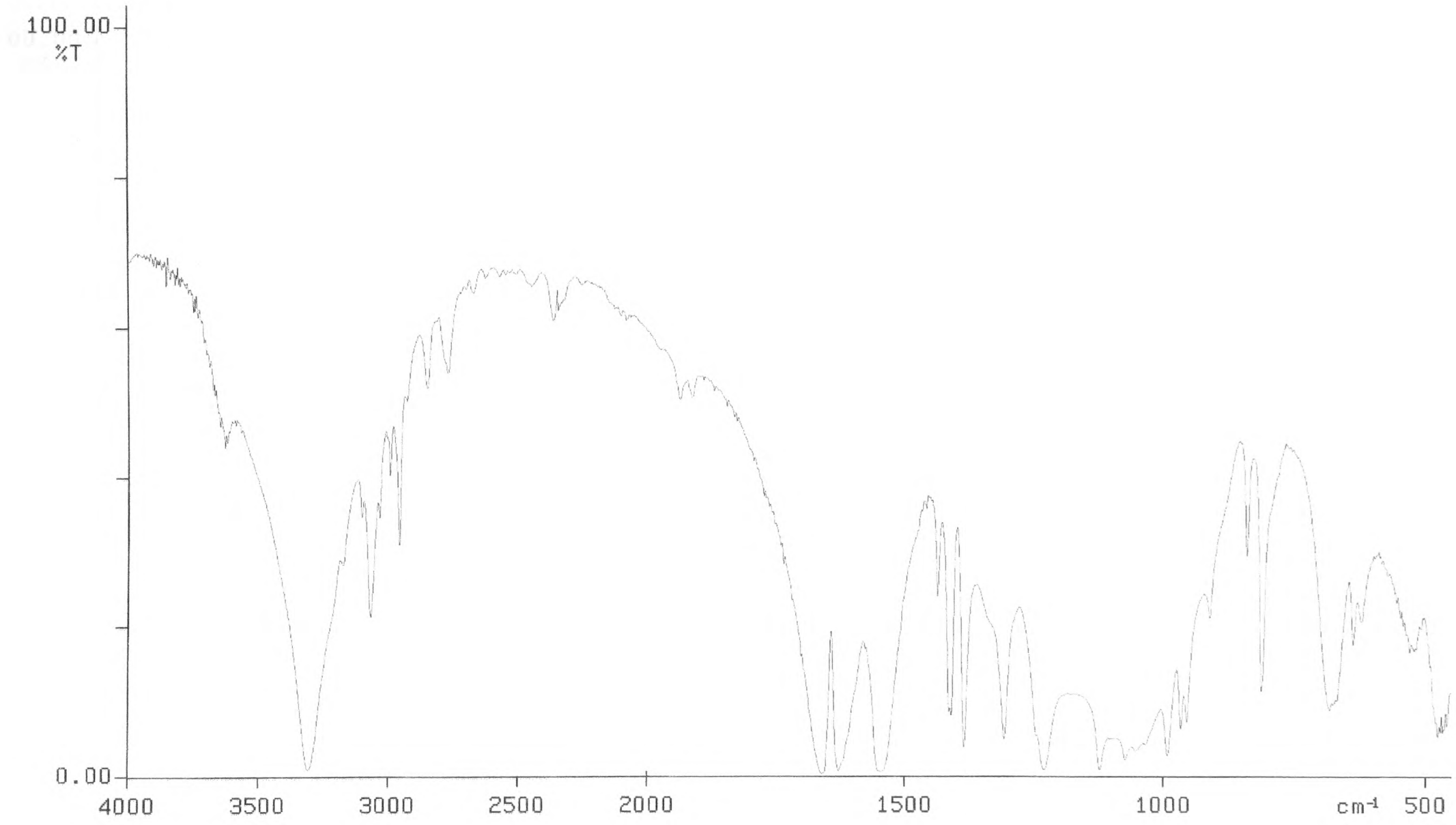

Figure 3.1.5: Infrared spectrum of K10 clay with NIPAM (2:2).

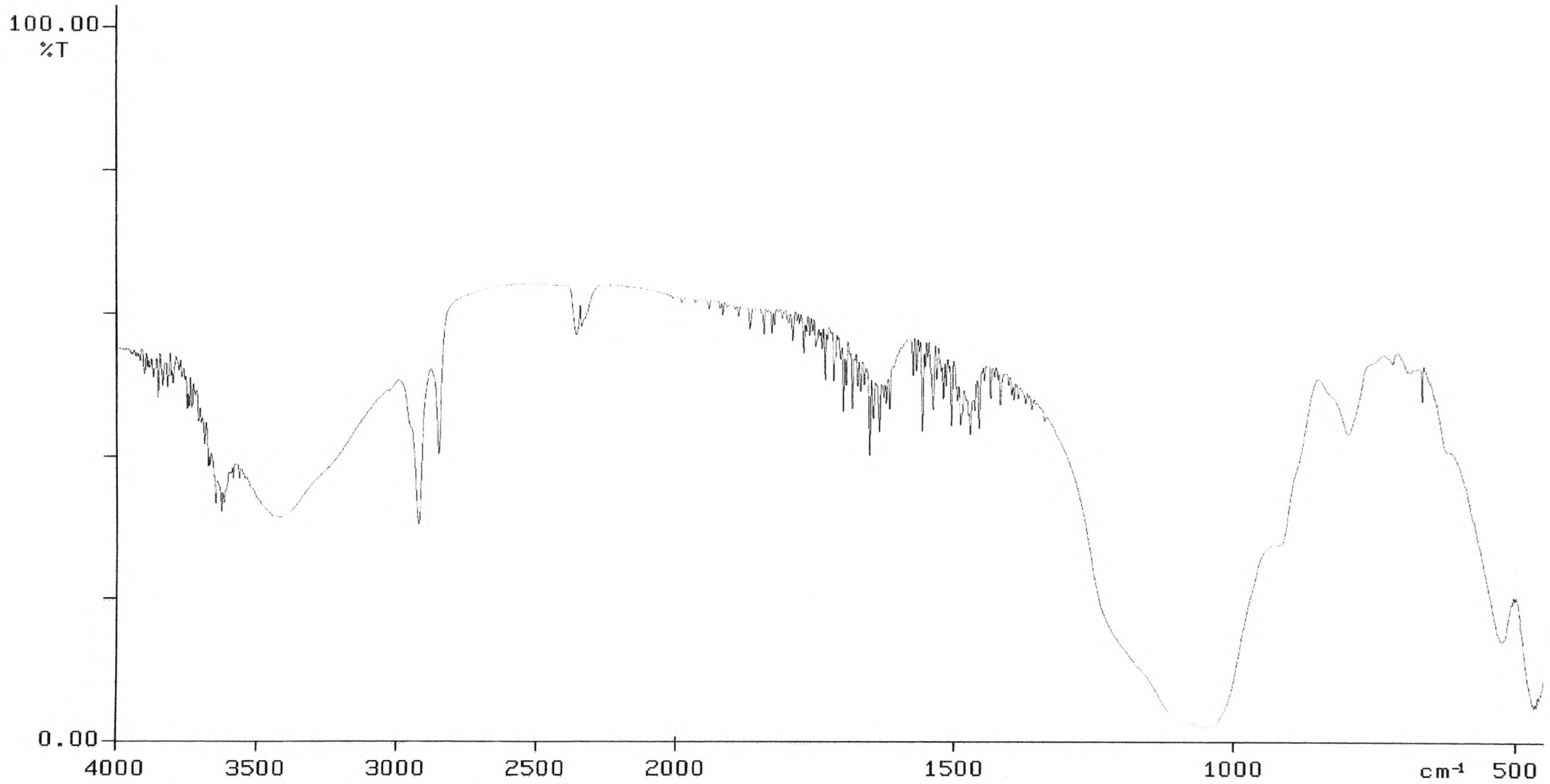

Figure 3.1.8: Infrared spectrum of K10 organophilic compound with NIPAM (2:2).

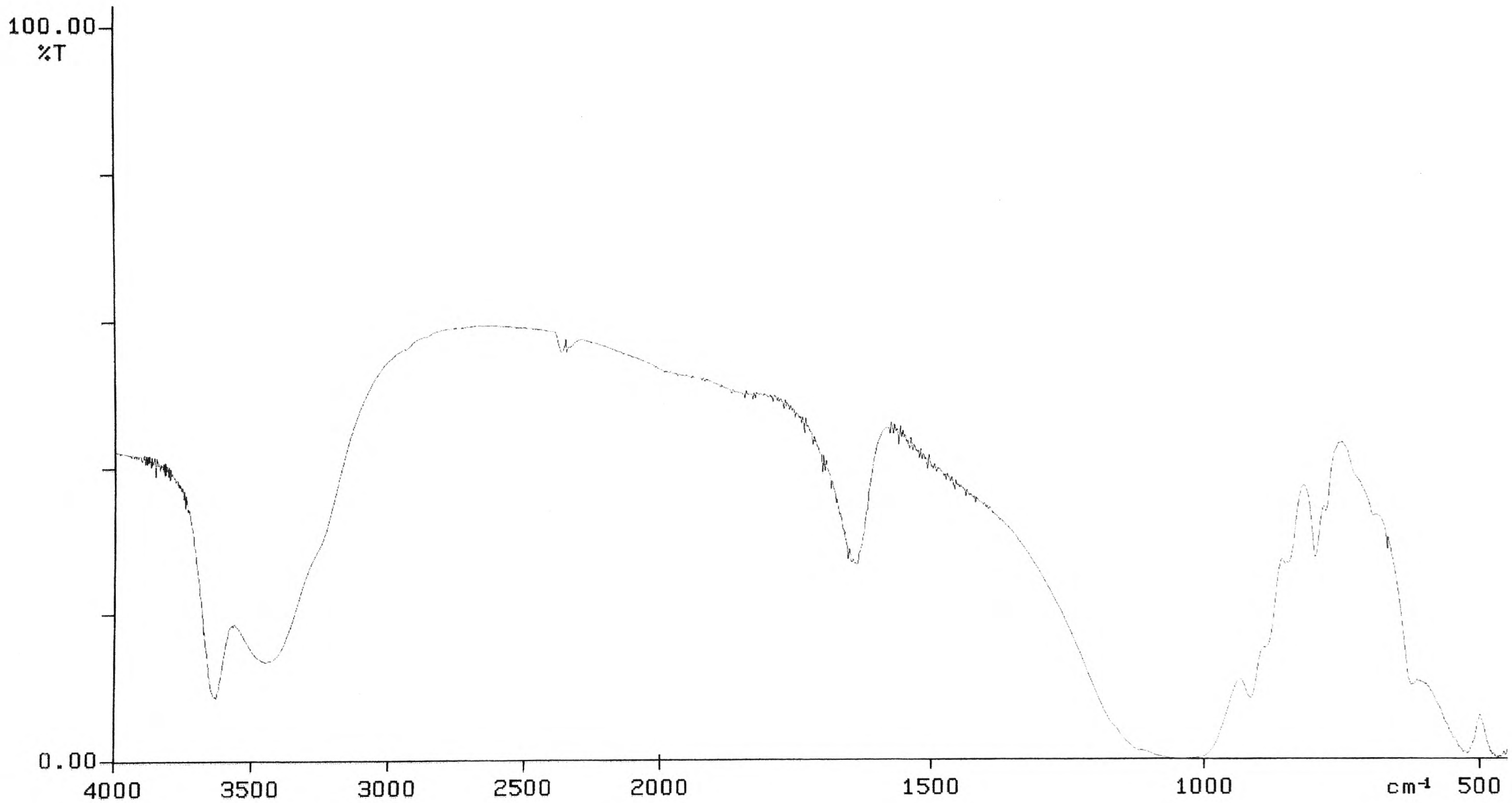

Figure 3.1.9: Infrared spectrum of bentonite-styrene compound (2:2).

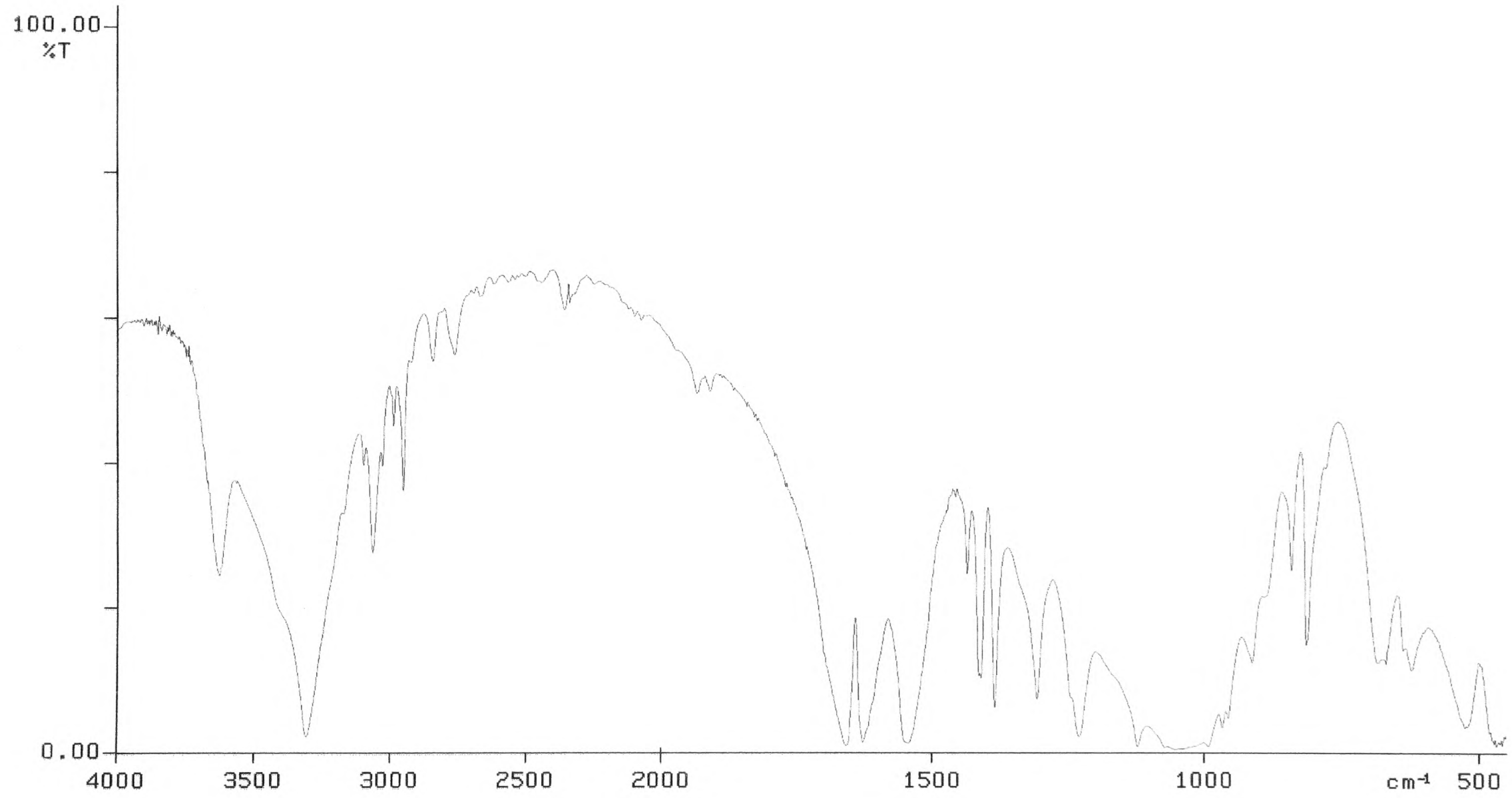

Figure 3.1.10: Infrared spectrum of bentonite-NIPAM compound (2:2).

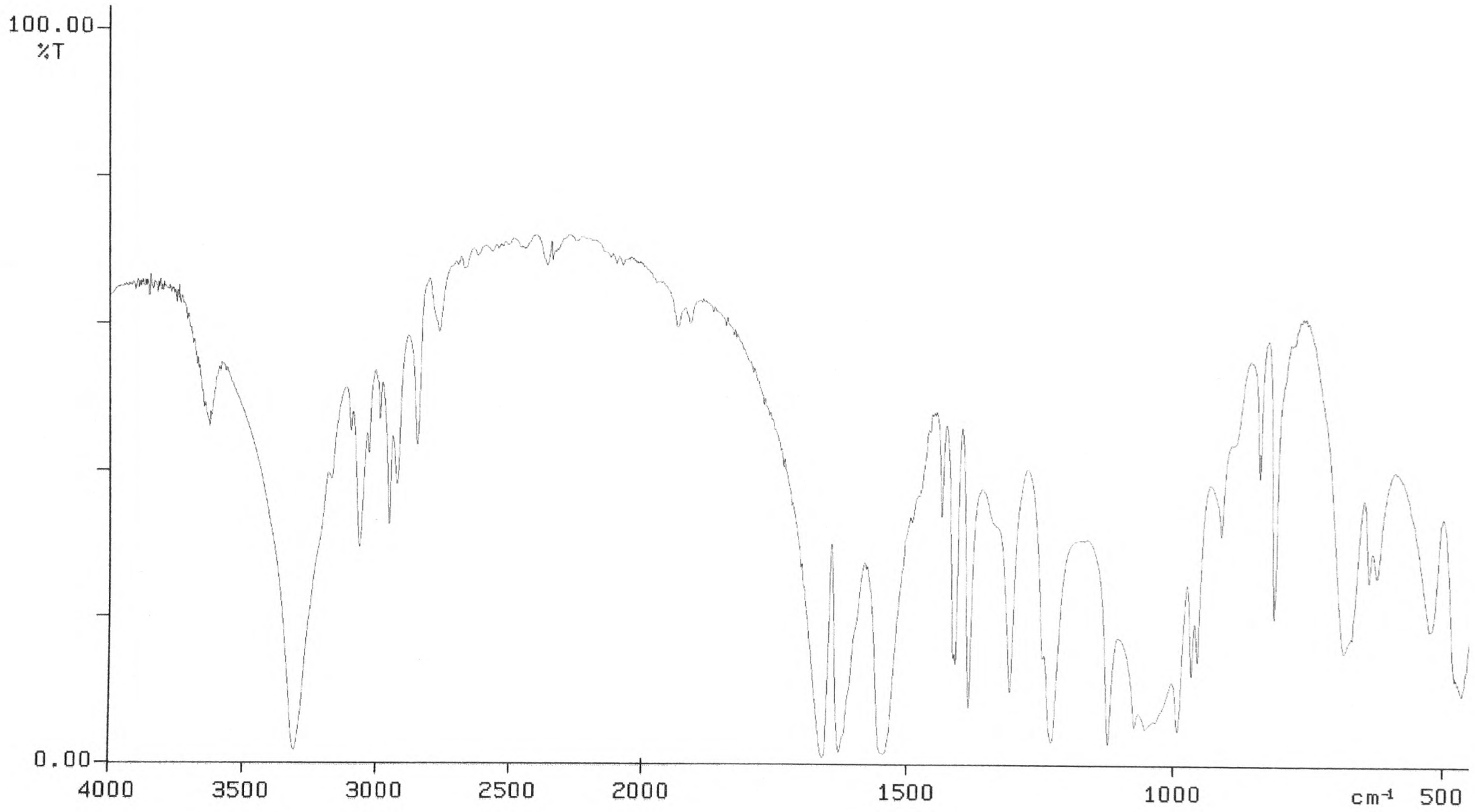

Figure 3.1.11: Infrared spectrum of bentonite organophilic compound with NIPAM (2:2).

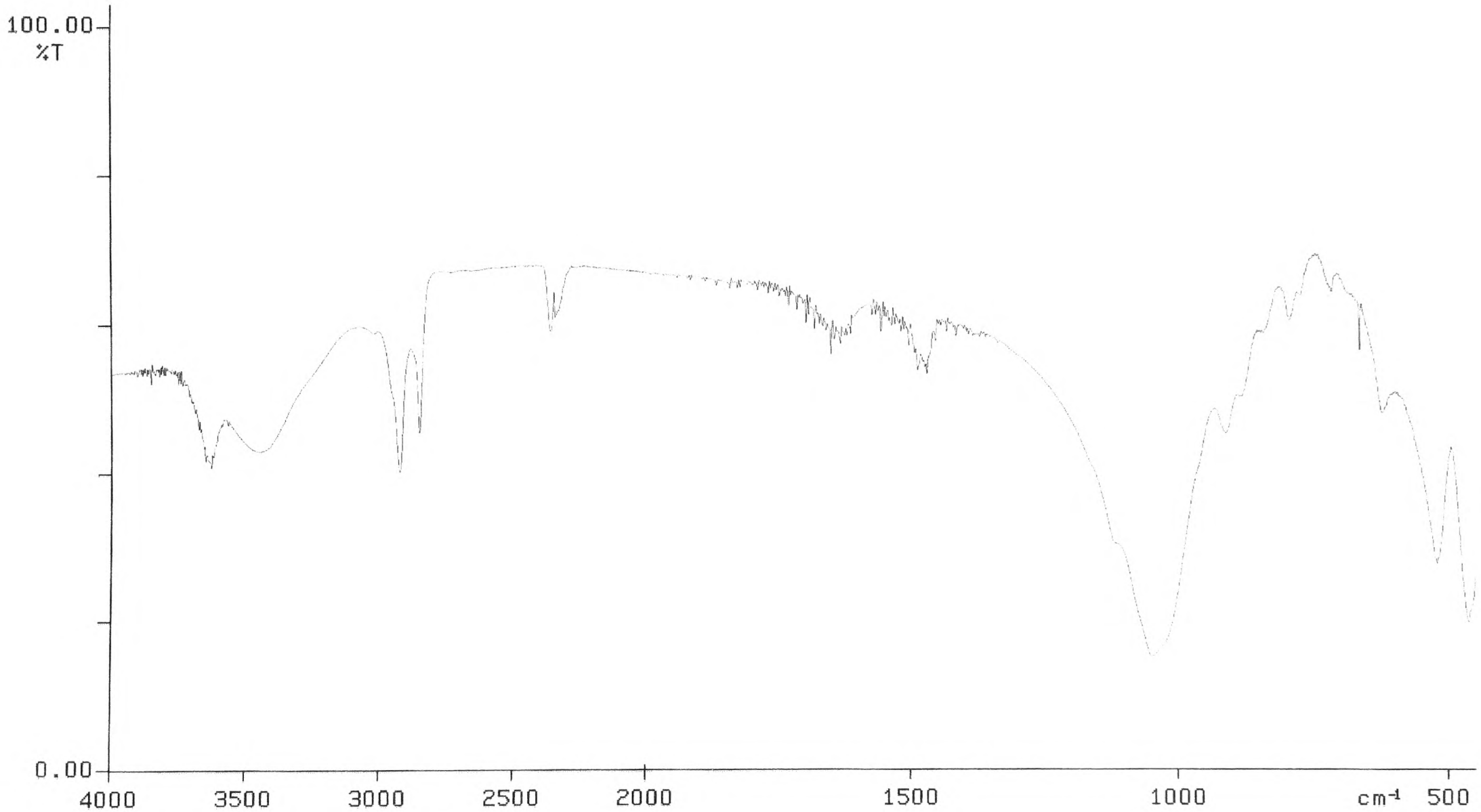

Figure 3.1.12: Infrared spectrum of bentonite organophilic compound with styrene (2:2).

3.1.3 X-RAY POWDER DIFFRACTION ANALYSIS

3.1.3.1 Study of montmorillonites

The X-ray diffraction patterns of the two montmorillonites used in this study are shown in **Figure 3.2.1** and **Figure 3.2.2**. Both K10 and bentonite gave a peak in the diffraction pattern, which can be assigned to the basal spacing in the clay minerals, although the peak for the bentonite is significantly broader, and at a higher d-spacing than the corresponding peak for K10. Bentonite is an unrefined, impure form of montmorillonite but the X-ray diffraction results seem to indicate that it was the most crystalline.

The calculated d-spacing for the two clays are given in **Table 3.1.3**.

Table 3.1.3: d-spacing (Å) and relative intensity for the two clays.

K10		**Bentonite**	
d-spacing (Å)	**Relative Intensity**	**d-spacing (Å)**	**Relative Intensity**
14.73	32.16	14.56	100.0
9.76	82.99	12.61	77.53
4.92	23.56	4.45	61.39
4.45	39.58	4.23	26.54
4.22	26.70	3.33	65.00
3.33	100.0	3.10	29.61
2.55	23.64		

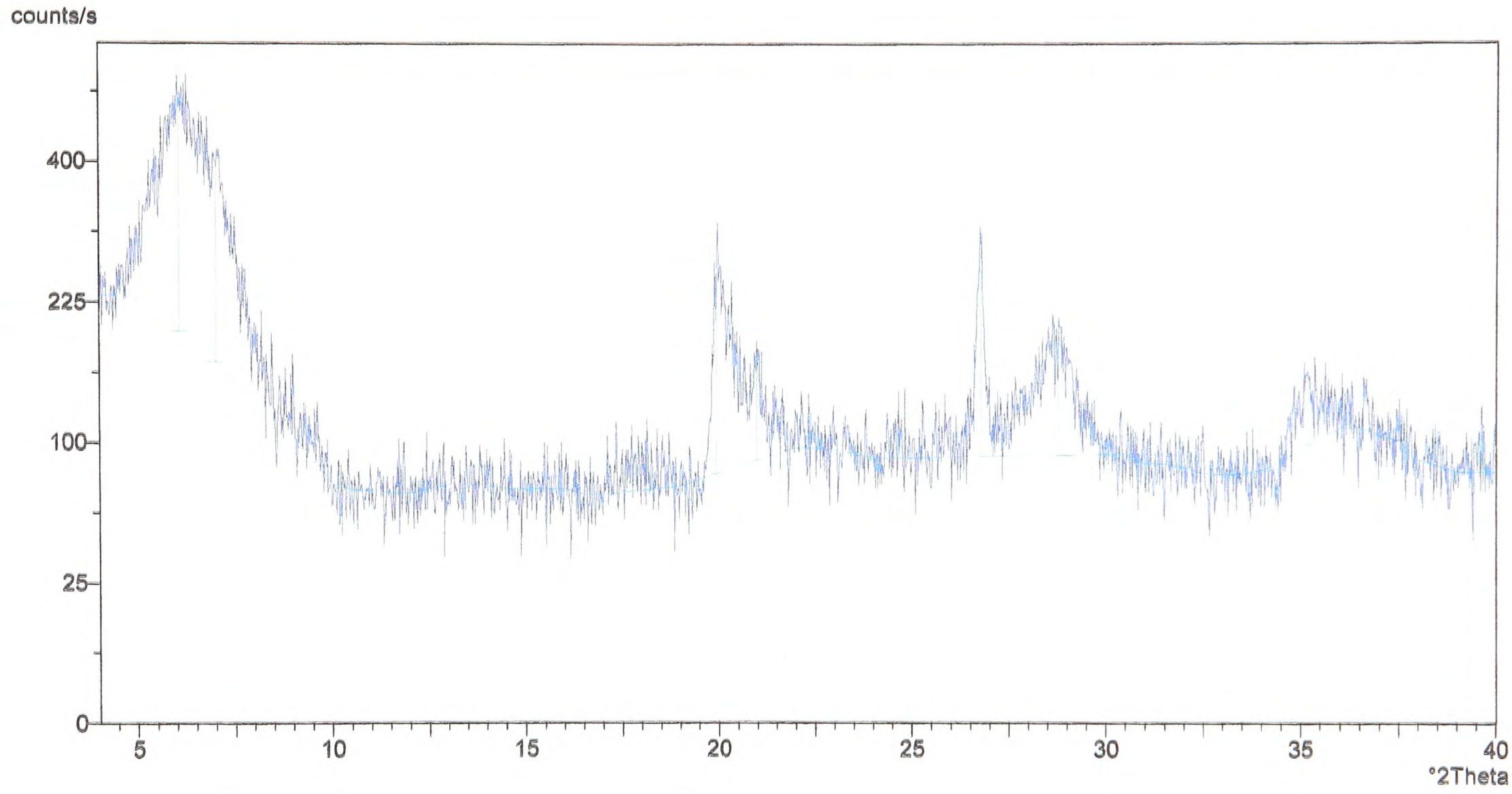

Figure 3.1.13: - X-ray diffraction pattern of bentonite.

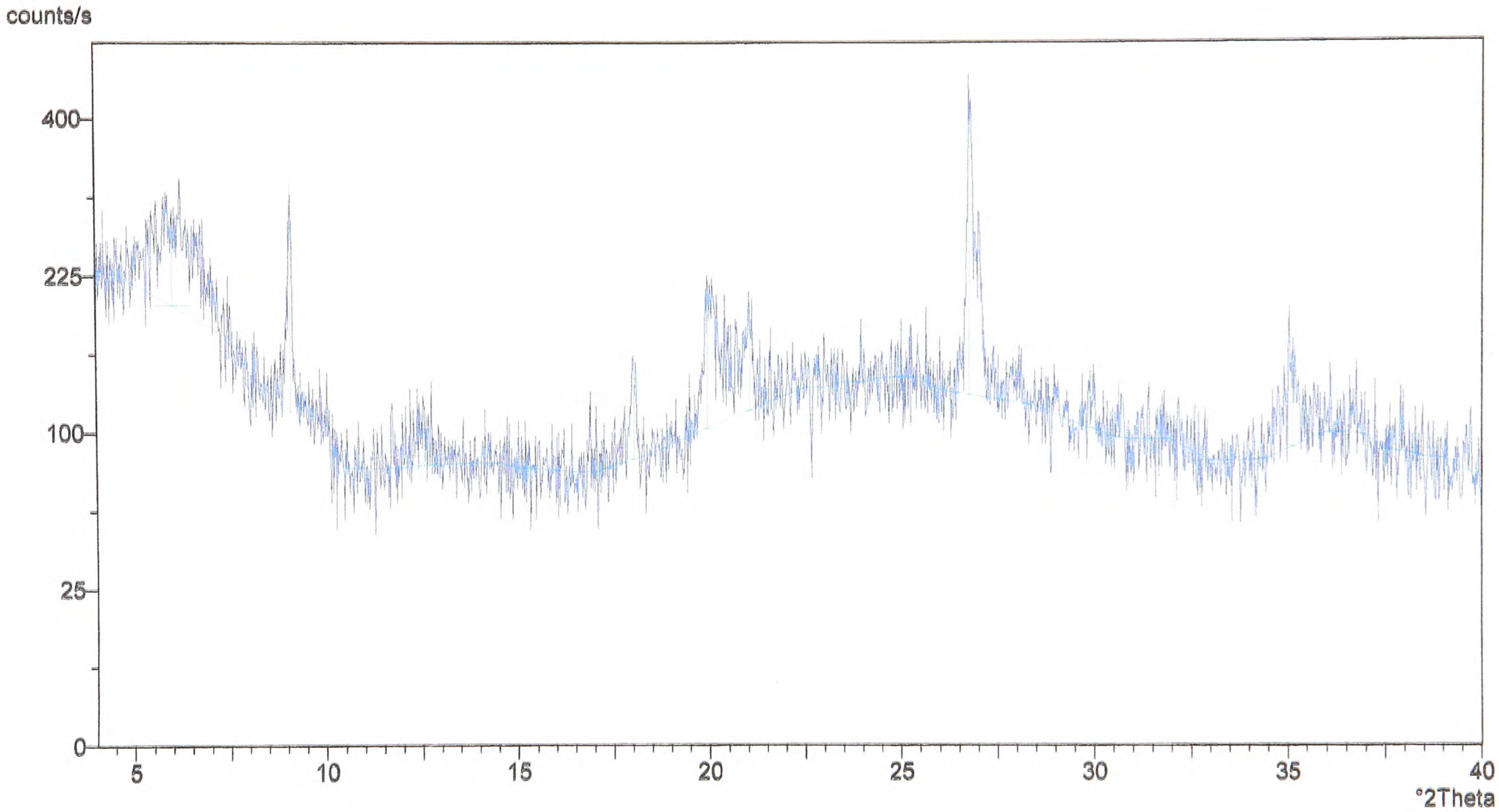

Figure 3.1.14: - X-ray diffraction pattern K10 clay.

3.1.3.2 Study of organophilic clays

The organophilic clays all undergo ion exchange with cetyltrimethylammonium chloride (C_{16}) to give the organophilic clay. It would be expected that if exchange had occurred the basal spacing would increase since the tetraalkylammonium ion is significantly bigger than the sodium and calcium ions usually found in montmorillonite.

The diffraction patterns for the two ion-exchange clays are shown in **Figure 3.2.15** and **Figure 3.2.16**. It can be seen that in both cases a new peak seems to be forming at low values of 2θ implying an increase in d-spacing. For K10 the original peak at 9.8Å was observed and a new peak having a significantly larger d-spacing was also present. Unfortunately this peak was very close to the smallest value of 2θ for the instrument used and so it was not possible to say for certain whether this peak was real. Similarly, there appears to be a peak at the instrument cut off for the bentonite sample.

These results seem to confirm the evidence from infrared spectroscopy, elemental and thermal analysis that ion exchange had been successful.

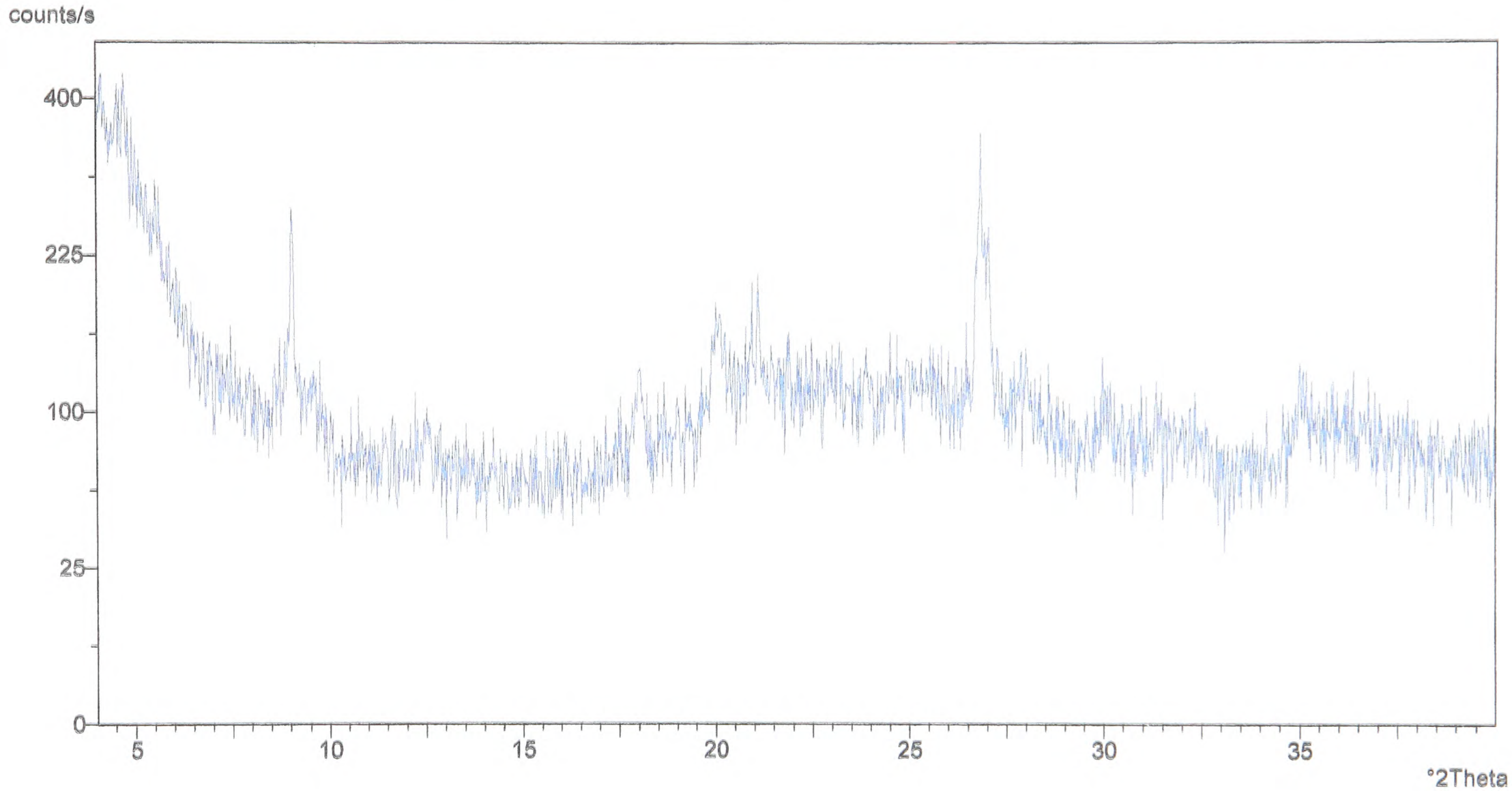

Figure 3.1.15: - X-ray diffraction pattern of organophilic K10 clay.

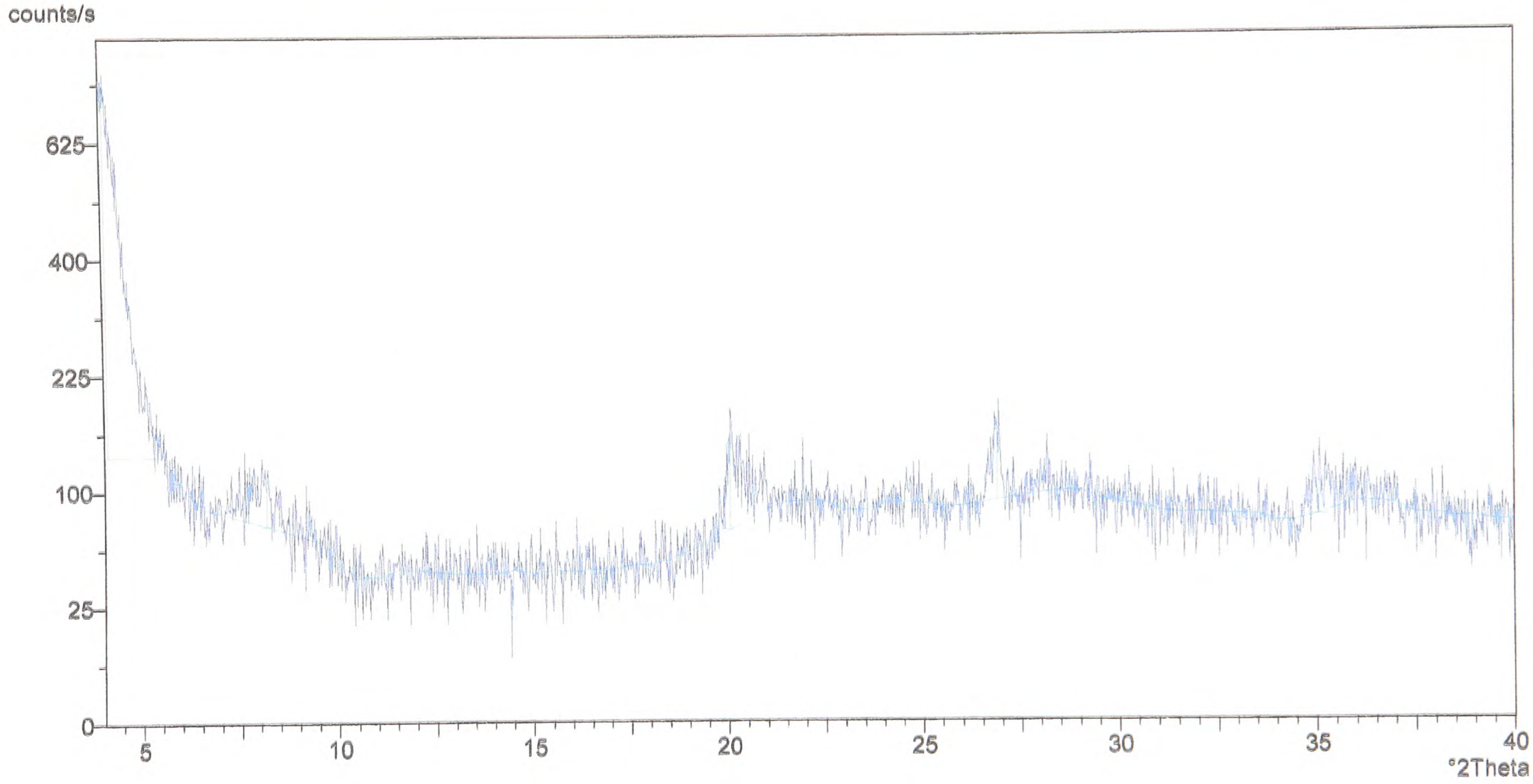

Figure 3.1.16: - X-ray diffraction pattern of organophilic bentonite.

3.1.3.3 Study of intercalated clays

The clays, which had undergone ion exchange with the cetyltrimethylammonium ion, were then reacted in various ratios with two different compounds, styrene and NIPAM. Comparing the diffraction patterns of K10-C_{16}-NIPAM **(Figure 3.2.17)** with the NIPAM **(Figure 3.2.18)** diffraction pattern we can clearly see the success of the intercalation. Unfortunately there are no conclusive results for the successful exchange of the ions with C_{16} but as mentioned before the peak seems to be close to the smallest value of 2θ for the instrument used and so it was not possible to say for certain whether this peak was real. The same behaviour can be seen with K10-NIPAM complex at different ratios. Example can be seen in **Figure 3.1.19**.

Looking at the bentonite intercalated complexes, the same pattern of results can be seen. All the X-ray patterns can be found in the Appendix.

On the other hand, looking at the both K10-styrene and bentonite-styrene X-ray patterns and their equivalent organoclays the results are inconclusive as no differences can be found between the patterns.

The most significant outcome is that the samples become much more crystalline. **Table 3.1.4** and **Table 3.1.5** show the results of all the compounds from the X-Ray analysis.

Table 3.1.4: X-Ray Diffraction results of NIPAM compared with K10 and bentonite and their equivalent organoclays.

NIPAM		K10 + NIPAM		K10 + C_{16} + NIPAM		Bentonite + NIPAM		Bentonite + C_{16} + NIPAM	
d-spacing (Å)	Relative Intensity	d-spacing (Å)	Relative Intensity	d-spacing (Å)	Relative Intensity	d-spacing (Å)	Relative Intensity	d-spacing (Å)	Relative Intensity
8.78	11.58	8.77	20.94	9.76	8.46	17.69	12.60	8.77	36.01
7.34	38.08	7.37	59.33	8.78	19.46	7.38	100.0	7.34	100.0
5.90	7.98	4.87	21.33	7.34	100.00	4.53	14.16	4.51	22.81
4.37	14.09	4.35	32.89	4.87	12.39	4.38	79.02	4.38	46.51
3.90	12.40	3.90	15.32	4.34	38.93	3.91	32.92	4.36	55.65
3.70	31.00	3.70	32.08	3.90	13.41	3.71	29.55	4.35	49.13
3.66	22.54	3.66	51.27	3.70	31.57	3.66	60.97	3.69	31.33
2.95	49.97	2.94	100.0	3.66	47.55	3.37	13.75	3.66	67.41
2.94	100.0	2.91	31.85	2.94	48.78	2.95	74.85	2.94	28.62
2.91	8.49	2.84	9.69	2.91	24.20	2.91	67.63	2.91	28.54

K10 + Styrene		K10 + C_{16} + Styrene		Bentonite + Styrene		Bentonite + C_{16} + Styrene	
d-spacing (Å)	**Relative Intensity**	**d-spacing (Å)**	**Relative Intensity**	**d-spacing (Å)**	**Relative Intensity**	**d-spacing (Å)**	**Relative Intensity**
23.73	23.91	19.19	18.42	13.36	58.79	23.54	100.0
17.67	35.24	10.07	57.14	6.25	1.50	11.42	9.62
10.05	81.06	4.99	24.27	4.54	100	4.54	59.57
5.00	45.04	4.50	44.91	4.30	42.01	3.67	12.27
4.52	26.29	4.27	55.72	4.08	8.41	3.37	52.50
3.35	100	3.79	23.64	3.37	75.29	3.21	12.34
3.33	87.02	3.57	17.20	3.16	29.87	3.05	7.85
3.23	30.30	3.35	100.0	2.59	22.70	2.60	10.95
3.20	36.28	3.20	15.59	2.23	5.44	2.29	8.04
1.99	31.86	2.56	17.73			1.99	5.61

Table 3.1.5: X-Ray Diffraction results of both clays and their equivalent organoclays intercalated with styrene.

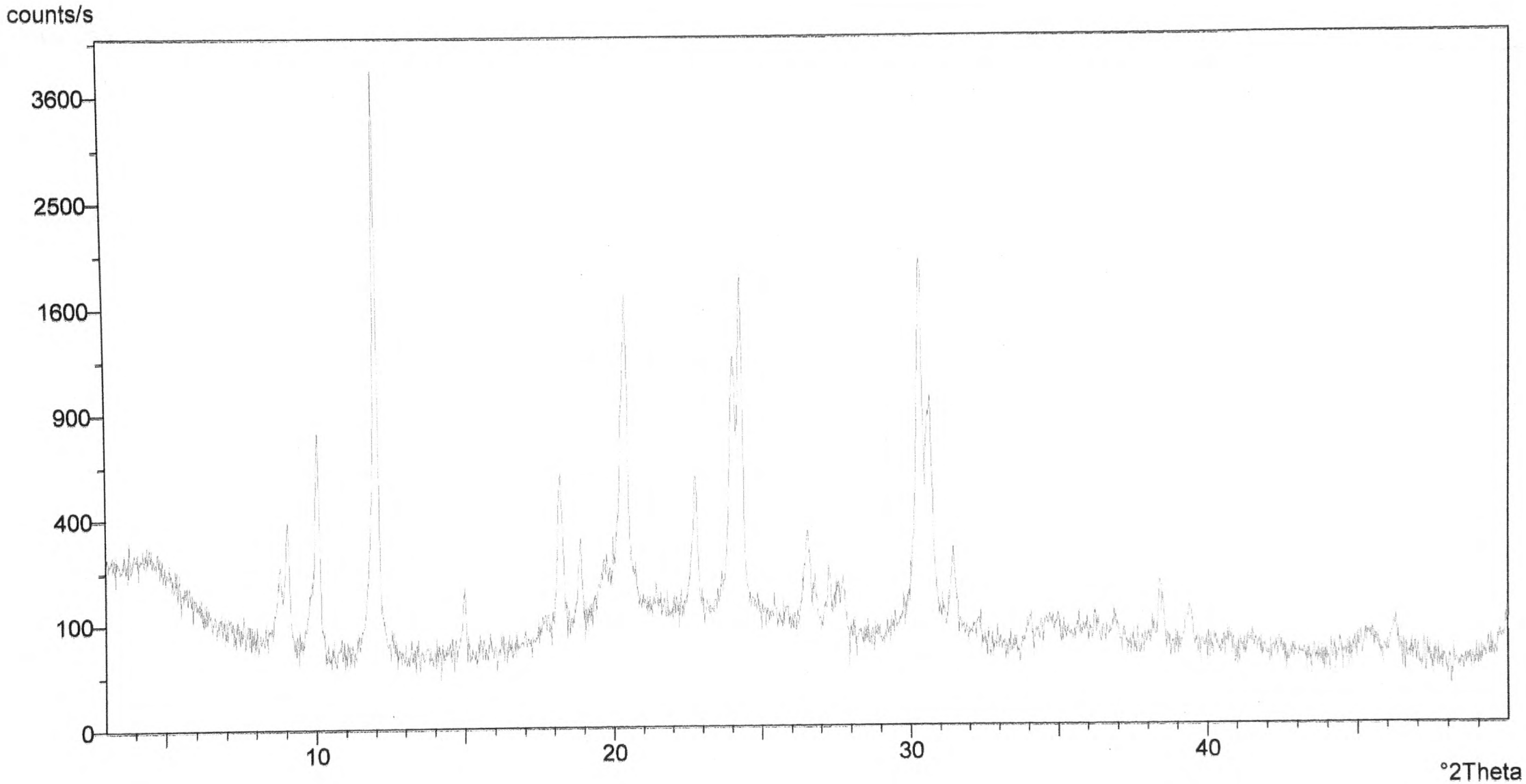

Figure 3.1.17: X-ray diffraction pattern of K10-C_{16}-NIPAM (2:2).

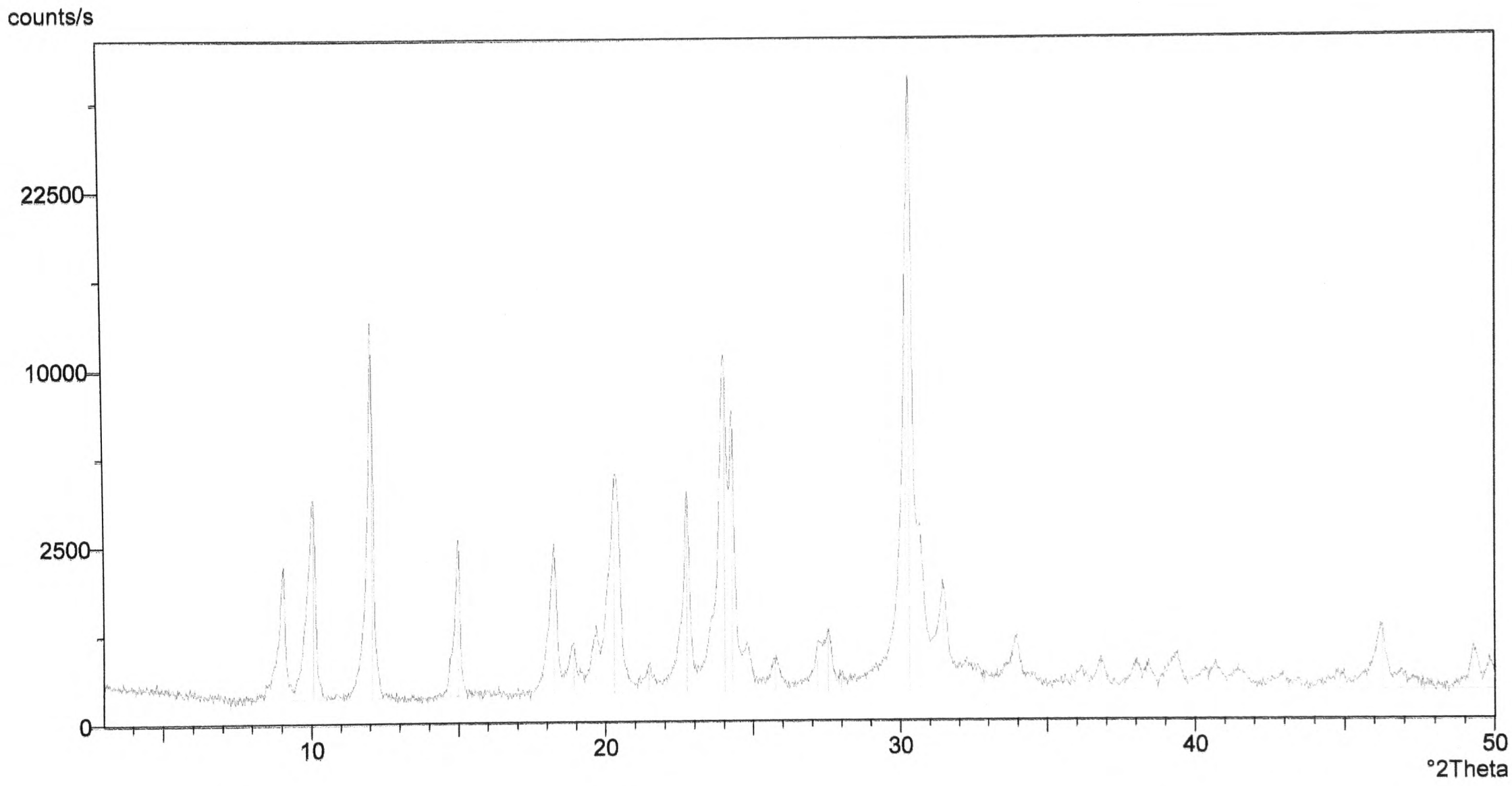

Figure 3.1.18: X-ray diffraction pattern of poly (NIPAM).

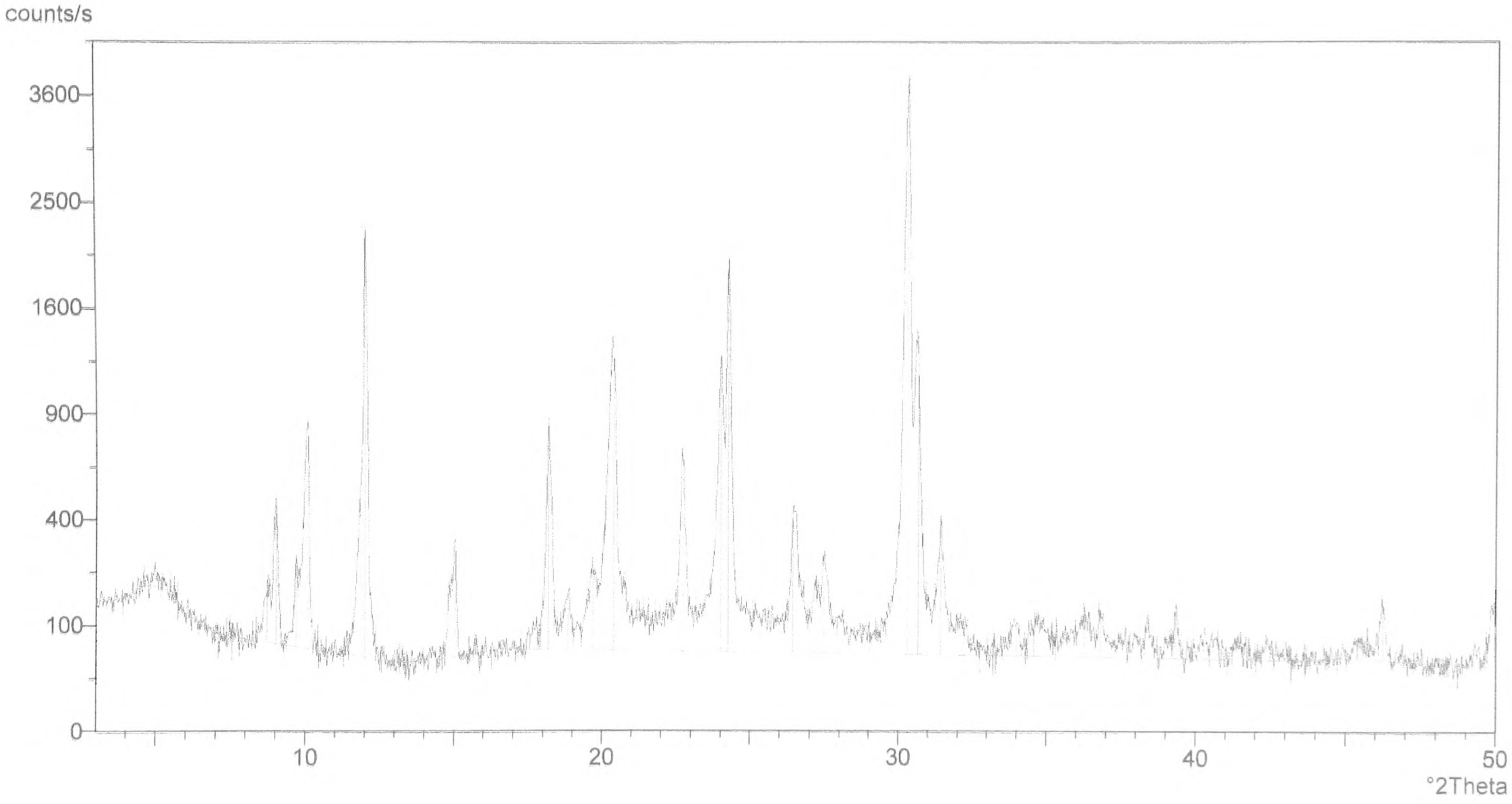

Figure 3.1.19: X-ray diffraction pattern of K10-NIPAM (2:2).

3.2 SYNTHESIS OF POLY(NIPAM) MICROGEL CONTAINING ORGANOPHILIC CLAY

The bentonite organoclay (bentonite + C_{16}) intercalated with NIPAM was used for the preparation of a microgel with the addition of ammonium persulfate to initiate the polymerisation. The reaction for the preparation of the microgel was repeated at two different time lengths, one for 6 hours and the other one for 4 hours, to observe any alteration on the final products caused by the time. Studying the infrared spectra of the microgels prepared at two different time periods **(Figure 3.2.1** and **Figure 3.2.2)** there is a change to the sharpness of the peaks as the time of reaction increased. Firstly, the sharp peaks of the microgel reacted for 6 hours, at 3000cm^{-1} and ~1500cm^{-1} have become less distinct on the infrared spectrum of the microgel reacting for 4 hours. Another important difference is in the region of 1000 cm^{-1}, where the 4 hour treated microgel appears to have sharper peak whereas in the 6 hour treated microgel the peak is broad. In addition there is a distinctive peak at ~700cm^{-1} which corresponds to strong =C-H bending.

The most important adsorption peaks can be found at ~3400cm^{-1} showing the presence of NIPAM **(Figure 3.2.3)** and at 1000cm^{-1}, a broad peak, characteristic for bentonite organoclay due to the Si-O-Si bond in the clay **(Figure 3.1.4)**. Also, peaks can be seen at ~3000cm^{-1} and ~1500cm^{-1} corresponding to alkane, C-H bond.

X-ray analysis of both products showed that they were amorphous.

The results conclude that there was a reaction between the organophilic clay and NIPAM and that the reaction time has actually affected the structure of the final product at some degree.

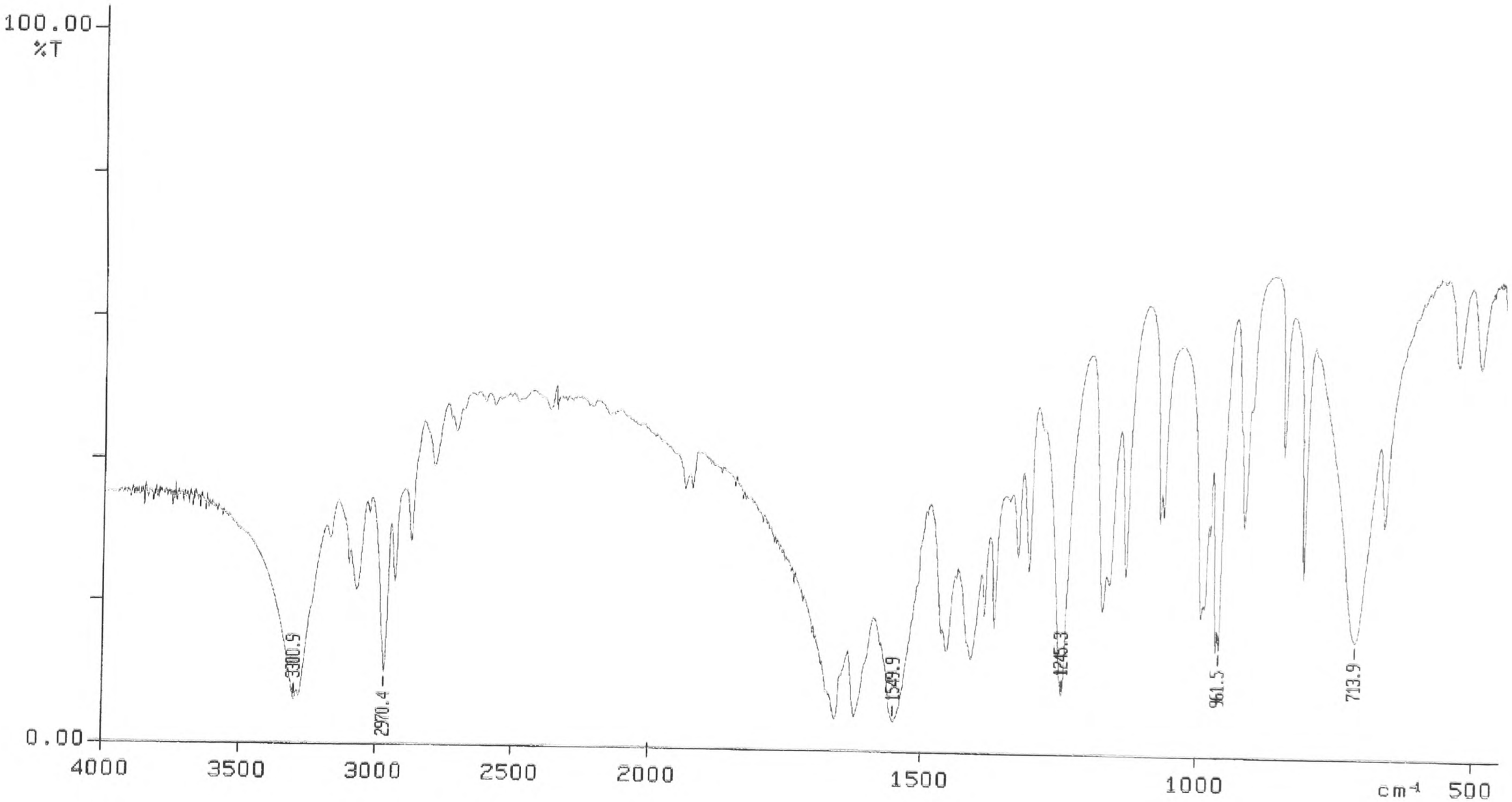

Figure 3.2.3: Infrared spectrum of NIPAM.

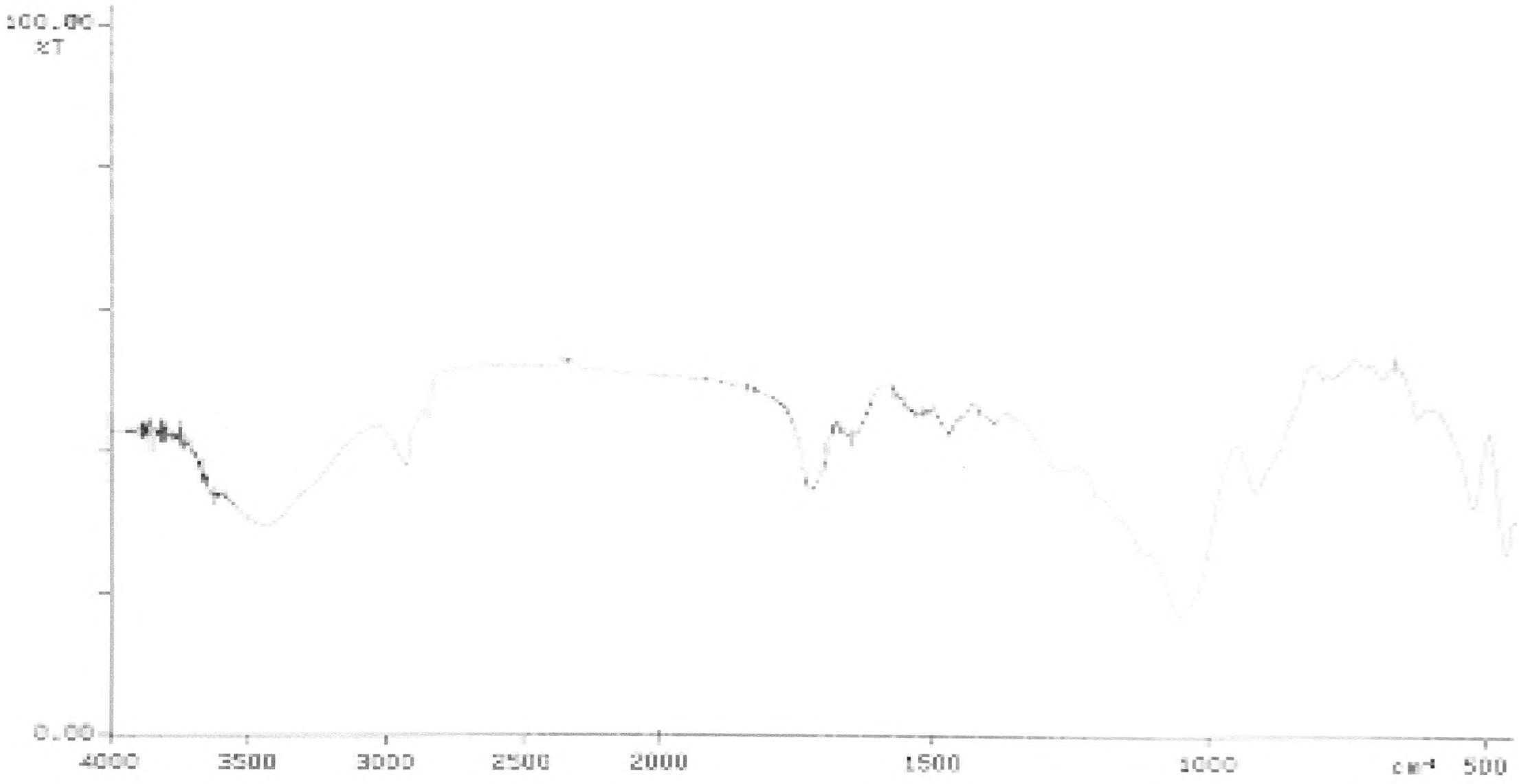

Figure 3.2.2: Infrared spectrum of bentonite-C_{16}-NIPAM microgel (4 hours).

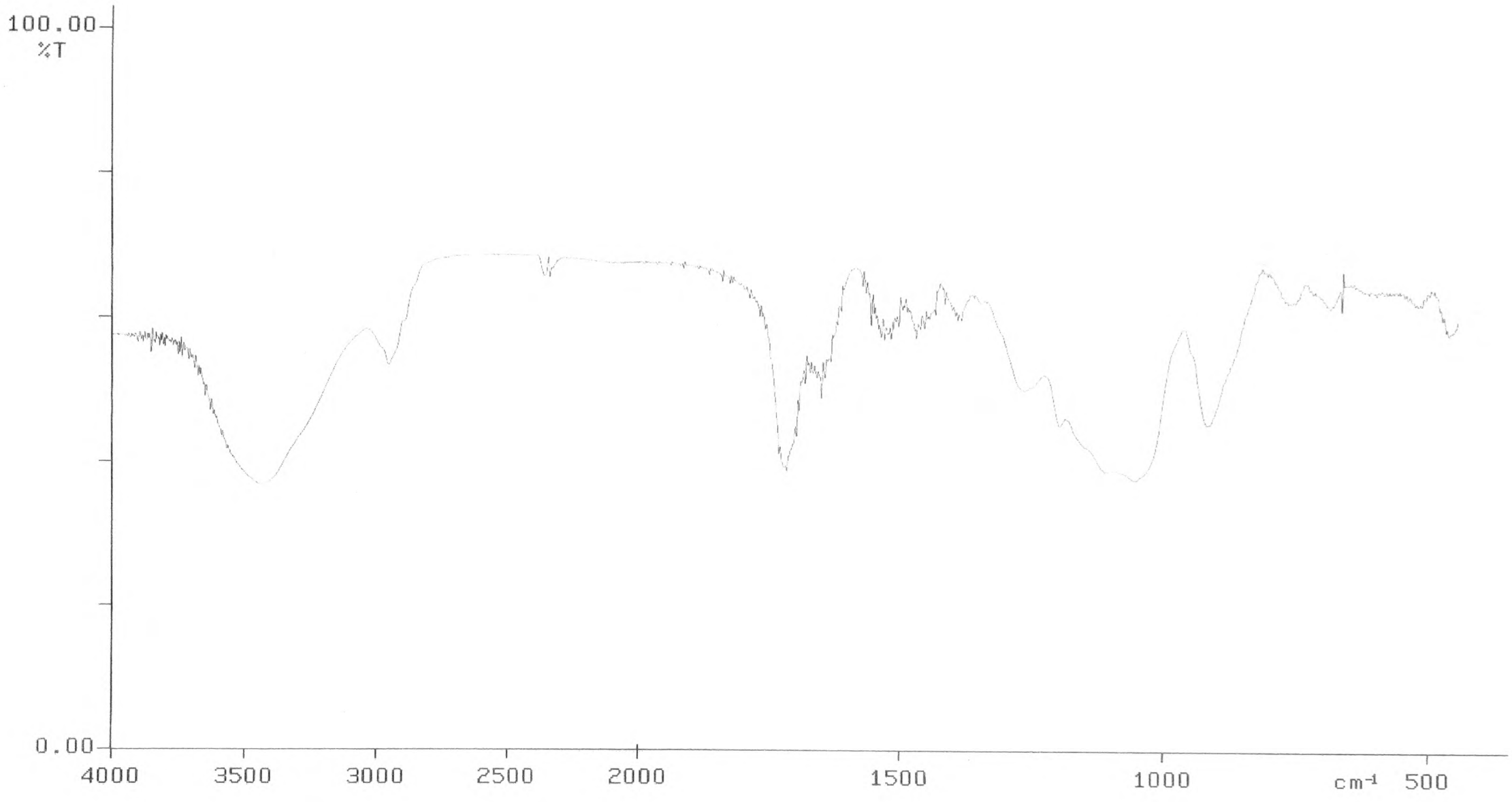

Figure 3.2.1: Infrared spectrum of bentonite-C_{16}-NIPAM microgel (6 hours).

3.3 HYDROLYTIC CONDENSATION OF CYCLOHEXYLTRICHLOROSILANE

Feher [27] has reported in his papers the reaction of the hydrolytic condensation of cyclohexyltrichlorosilane ($CySiCl_3$) in aqueous acetone **(Scheme 3.3.1)**. The remarkable thing about that reaction is that it produces three different compounds and that the course of the reaction does not appear to be affected by periodic product isolations and the filtrate will continue to precipitate 1 for approximately 3 years. With time the percentage ratio of 2 and 3 products decreases, favouring the creation of 1. After 1.5 years the crystalline material is almost entire 1.

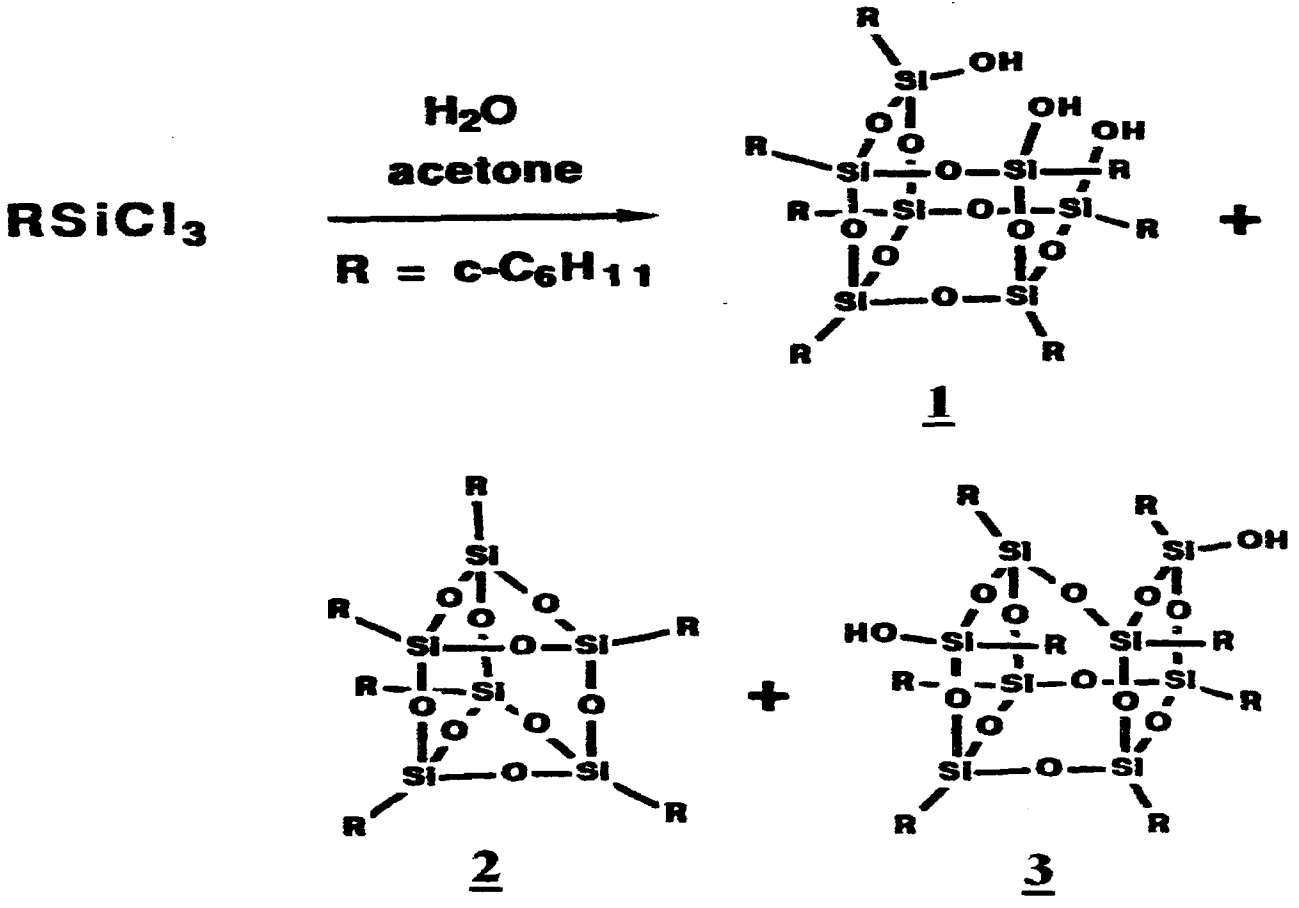

Scheme 3.3.1: The hydrolytic condensation of $CySiCl_3$ [2].

Infrared analysis of all three final compounds was performed **(Figure 3.3.1, Figure 3.3.2** and **Figure 3.3.3)**. Comparison of those three for any significant difference was inconclusive. All three had peaks in similar areas and are listed below **(Table 3.3.1)**.

Table 3.3.1: Infrared vibrational band assignments of all 1, 2 and 3.

Wavelength/cm^{-1}	Assignment
3400-3500	symmetric Si-OH stretching
2900-2910	symmetric -CH-stretch in $-CH_3$
1450-1460	asymmetric $-CH_3$ deformation
1410-1420	symmetric $-CH_3$ deformation
1100-1040(1060,centre)	asymmetric Si-O-Si stretch
690	symmetric –Si-C stretch
640	asymmetric –Si-C stretch

Elemental analysis was performed for 1 and Table 3.3.2 reports the results as well as the theoretical values of the compound.

Table 3.3.2: Elemental analysis of $Cy_7Si_7O_9(OH)_3$.

	Carbon (C)	Hydrogen (H)
Value Found %	52.46	8.67
Theoretical Value %	51.48	8.17

Comparing the values found from the elemental analysis and the values **calculated for compound 1, we can conclude that the compound prepared was the one** expected.

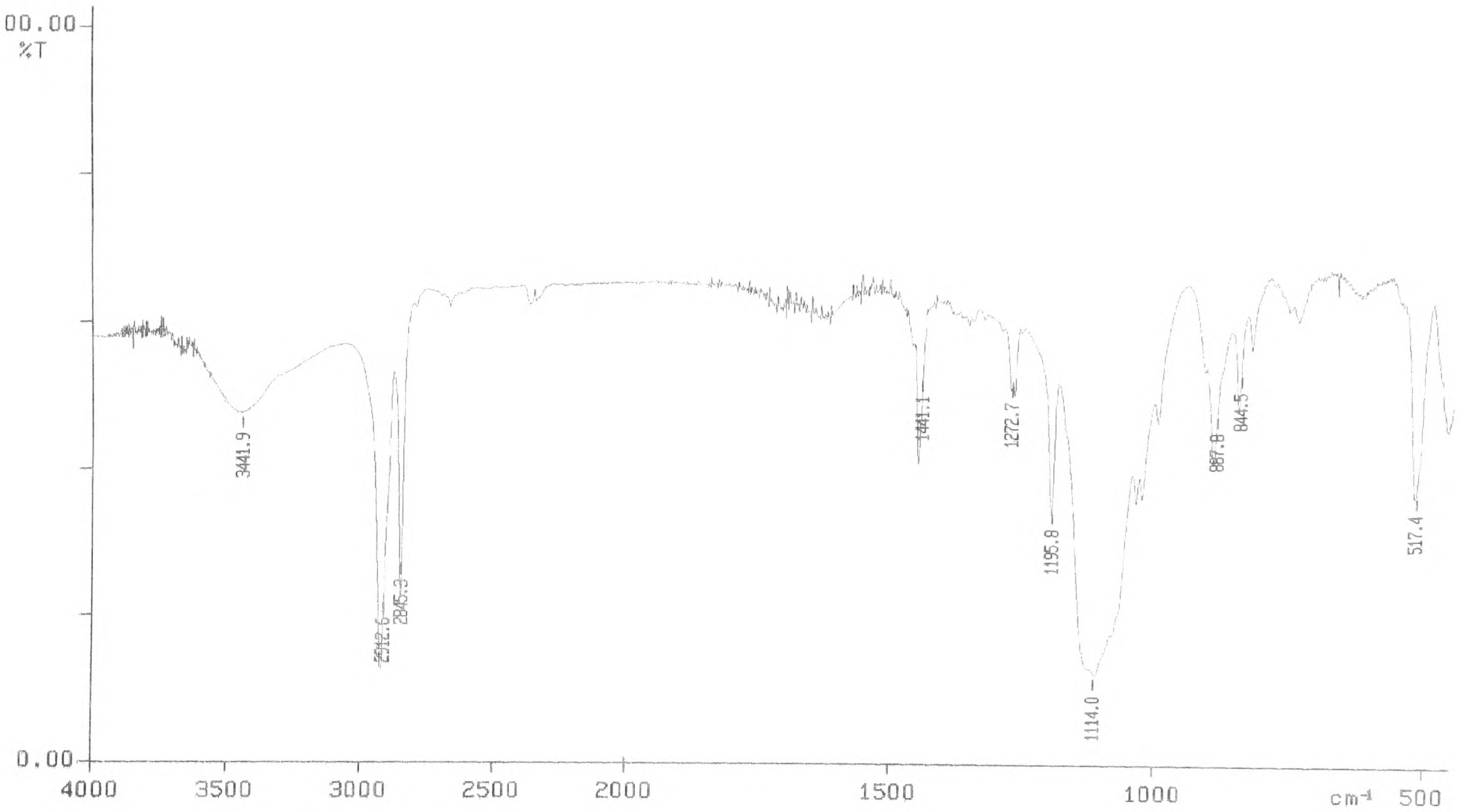

Figure 3.3.1: Infrared spectrum of the product mixture from cyclohexyltrichlorosilane ($CySiCl_3$) in aqueous acetone.

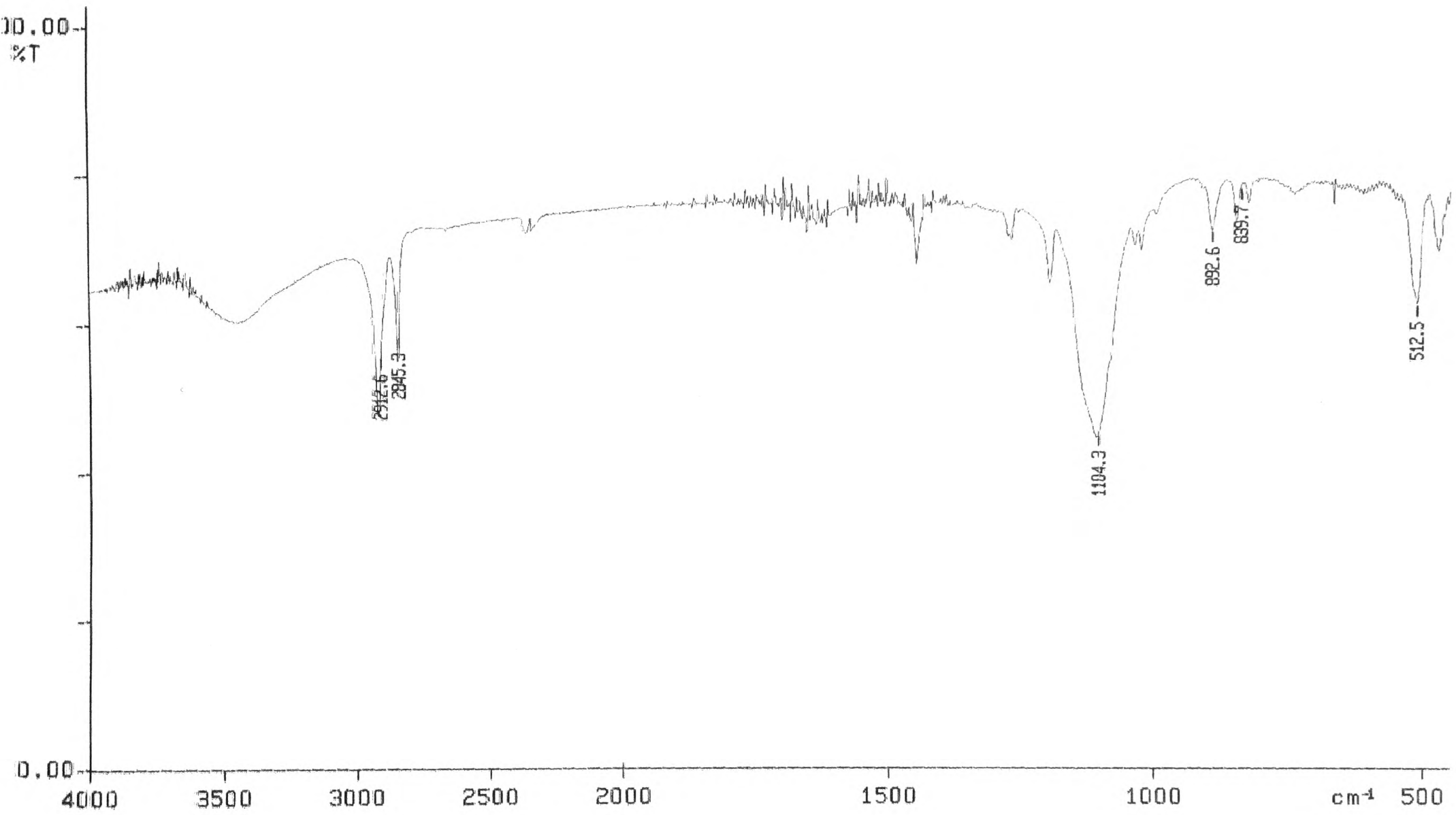

Figure 3.3.2: Infrared spectrum of **2**.

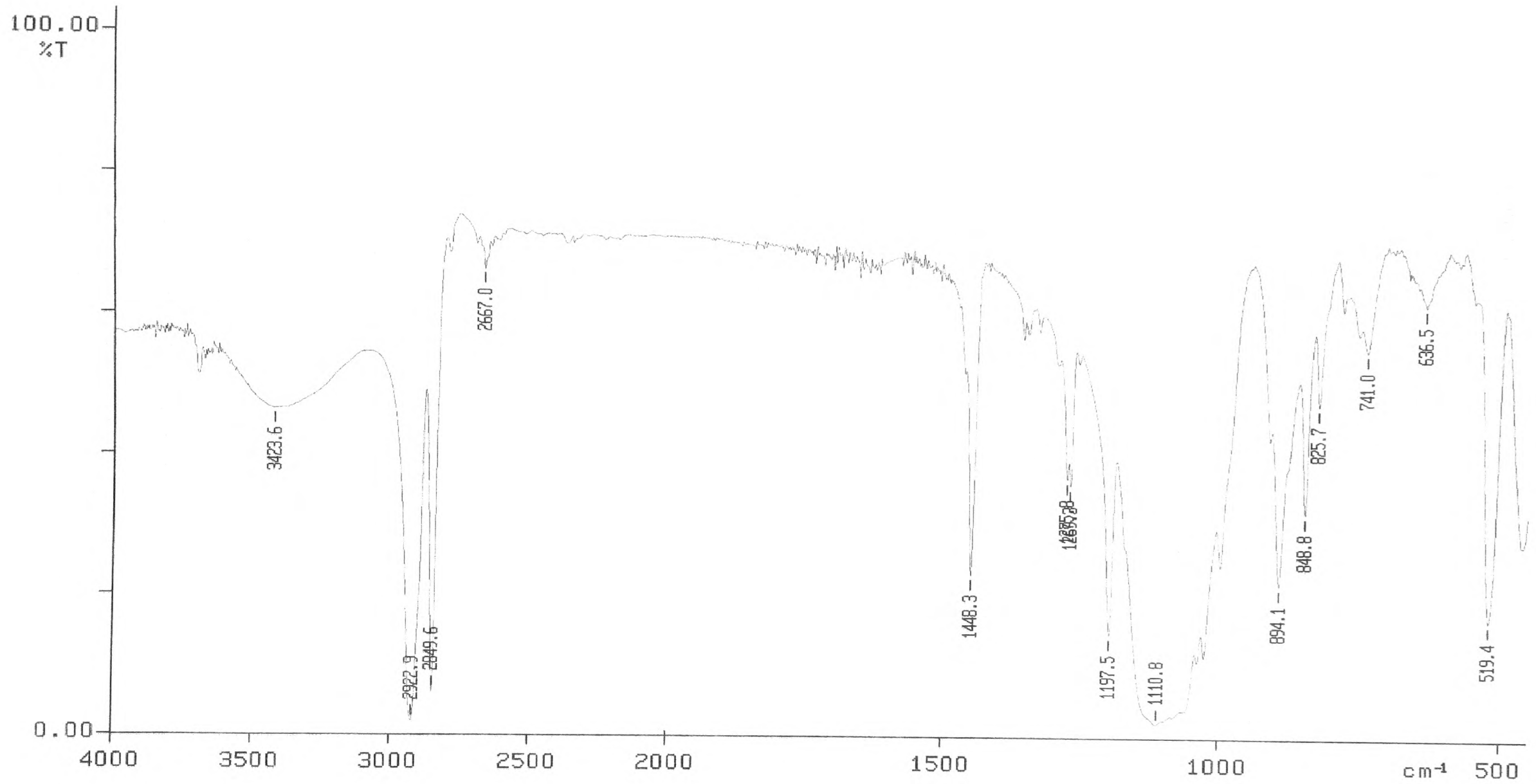

Figure 3.3.3: Infrared spectrum of **1**.

3.4 REACTION OF $(C_6H_{11})_7Si_7O_9(OH)_3$ -1 WITH VINYLTRICHLOROSILANE

The proposed reaction of 1 with vinytrichlorosilane giving 4, a vinyl silsesquioxane is shown below.

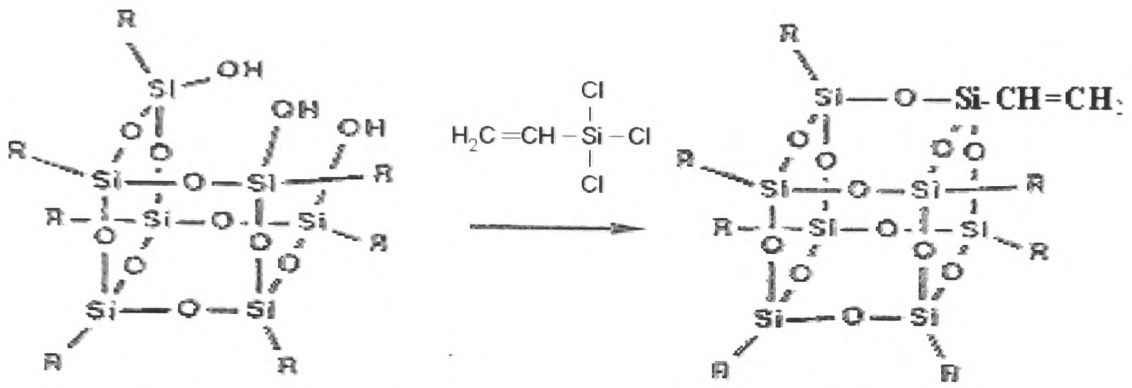

1 (R = c-C_6H_{11}) 4

The elemental analysis of 4 is summarized in Table 3.4.1 including also the theoretical values of the product.

Table 3.4.1: Elemental analysis of 4.

	Carbon (C)	Hydrogen (H)
Value Found %	44.05	9.65
Theoretical Value %	53.01	8.03

The calculated values of 4 compared with the values taken from the elemental analysis are different, showing big increase on the carbon contents and a decrease on

the hydrogen. That suggests that there was a possible reaction between the silsesquioxane and the vinyltrichlorosilane.

The infrared spectrum of 4 can be seen below (Figure 3.4.1). Characteristic adsorption peaks are at 3421 cm^{-1} is due to Si-OH bond and at the region of 1400 cm^{-1} there is a range of peaks caused by a Si-C stretching. The peaks around 1000-1200cm^{-1} are because of the strong stretching of -Si-O-Si bond of the silsesquioxane. Finally a weak peak at around 3100cm^{-1} can be attributed to =C-H bond of the vinyl group. Other characteristic peaks can be seen in **Table 2.2**.

Table 3.4.2: Characteristic peaks of 4.

Wavelength/cm^{-1}	Assignment
2900-2910	symmetric -CH-stretch in $-CH_3$
1600	weak C=C bond stretching
1470-1430 & 1380-1370	C-H bending, strong, alkane
<900	C-H bending, strong

The elemental analysis and the infrared analysis performed on the final **product indicate that there was a reaction between 4** and vinyltrichlorosilane but unfortunately we can not state if the vinyltrichlorosilane was actually attached to the open -OH groups of the silsesquioxane.

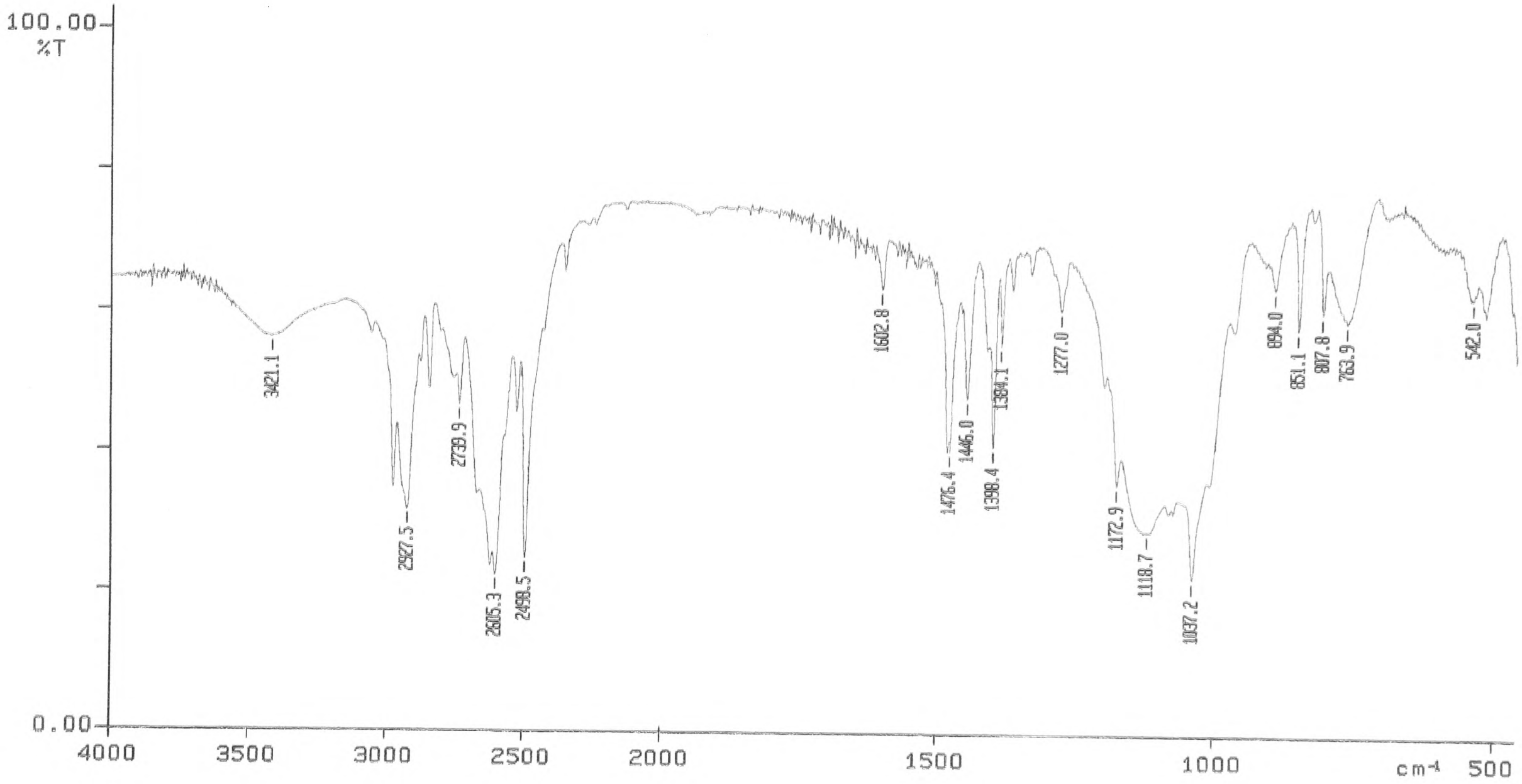

Figure 3.4.1: Infrared spectrum of **4**.

3.5 POLYMERISATION OF VINYL-CONTAINIG MONOMERS IN DIOXANE IN THE PRESENCE OF 2, 2-AZOBISISOBUTYLRONITRILE

For this experiment three different vinyl-containing monomers where used and their results were compared to observe their behavior under polymerization. First, vinyltrichlorosilane was reacted with dioxane, in the presence of 2, 2-azobisisobutyronitrile (AIBN) as an initiator.

Elemental analysis of the sample was performed and the results are shown in **Table 3.5.1** as well as the theoretical values observed. Nitrogen values are as a result of residual 2, 2-azobisisobutyronitrile (AIBN).

Table 3.5.1: Elemental analysis of the vinyltrichlorosilane polymer.

	Nitrogen (N)	**Carbon (C)**	**Hydrogen (H)**
Value Found %	2.89	31.36	4.63
Theoretical Value %	0	28.73	4.79

Infrared analysis of the vinyltrichlorosilane polymer **(Figure 3.5.1)** showed a peak at 3447cm^{-1} representing -OH stretching due to hydrolysis of the Si-Cl bond. Also peaks at around 1110-1050 cm^{-1} appear which corresponds to a Si-O-Si bond. The interesting thing about that is the fact that actually the Si-Cl groups from the vinyltrichlorosilane have been hydrolyzed creating siloxane bonds. Other evidence for the reaction having lead to the hydrolysis can be seen by the absence of the Si-Cl bond at around 625cm^{-1}. The peaks around 2950cm^{-1} confirm that polymerization has occurred.

X-ray analysis of the polymer showed that it was amorphous.

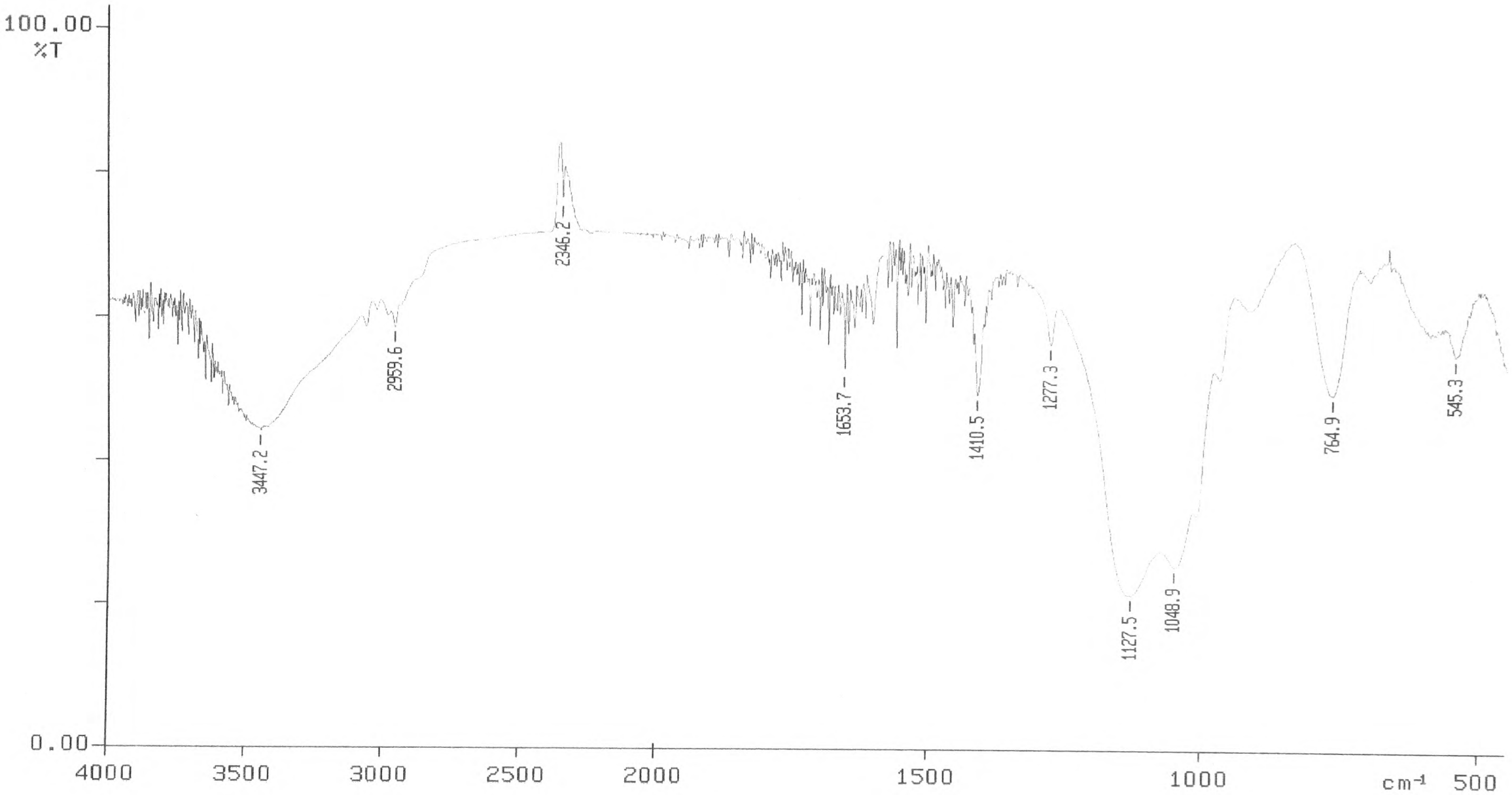

Figure 3.5.1: Infrared spectrum of the vinyltrichlorosilane polymer.

The second monomer used for the experiment was vinyltrimethoxysilane. Elemental analysis of the polymer was repeated several times to obtain consistent results but the sample was clearly non-homogenous. A similar infrared spectrum was obtained **(Figure 3.5.2)** as the one previously giving no conclusions to the success of the polymerization.

The X-ray analysis of this polymer gave a few, none distinguishing peaks, showing that the product was again amorphous.

It seems like the polymerization of the vinyl group was successful but there is no evidence of hydrolysis of either the Si-Cl or the Si-O-Me groups. This was expected since it is known that the Si-Cl and Si-O-C groups are hydrolytically unstable [2].

Finally, styrene was reacted with dioxane, using AIBN as an inhibitor. Infrared analysis, elemental and X-ray analysis was performed on the styrene polymer.

Table 3.5.2 reports the results from the elemental analysis of the polymer plus the theoretical values calculated. Nitrogen values are as a result of residual 2, 2-azobisisobutyronitrile (AIBN).

Table 3.5.2: Elemental analysis of the styrene polymer

	Nitrogen (N)	**Carbon (C)**	**Hydrogen (H)**
Value Found %	0.37	88.33	7.86
Theoretical Value %	0	75.29	7.84

The infrared spectrum of the styrene polymer can be seen in **Figure 3.5.3**. The peak at 1601cm^{-1} correspond to a -N=N- stretching bond since AIBN was used as an initiator. The spectrum is consistent with the successful preparation of polystyrene.

X-ray analysis of the styrene polymer gave peaks in the diffraction pattern **(Figure 3.5.6)**. Their positions are summarized in **Table 3.5.3**.

Table 3.5.3: d-spacing (Å) and relative intensity for the styrene polymer.

d-spacing (Å)	Relative Intensity
9.04	40.03
8.83	41.99
7.38	100.0
4.39	72.41
4.38	65.16

These results show that the polystyrene has some degree of crystallinity.

The results confirm that the vinyl groups attached to silicon behave in the same way as those attached to carbon in styrene. Although this was likely it was decided that confirmation was required.

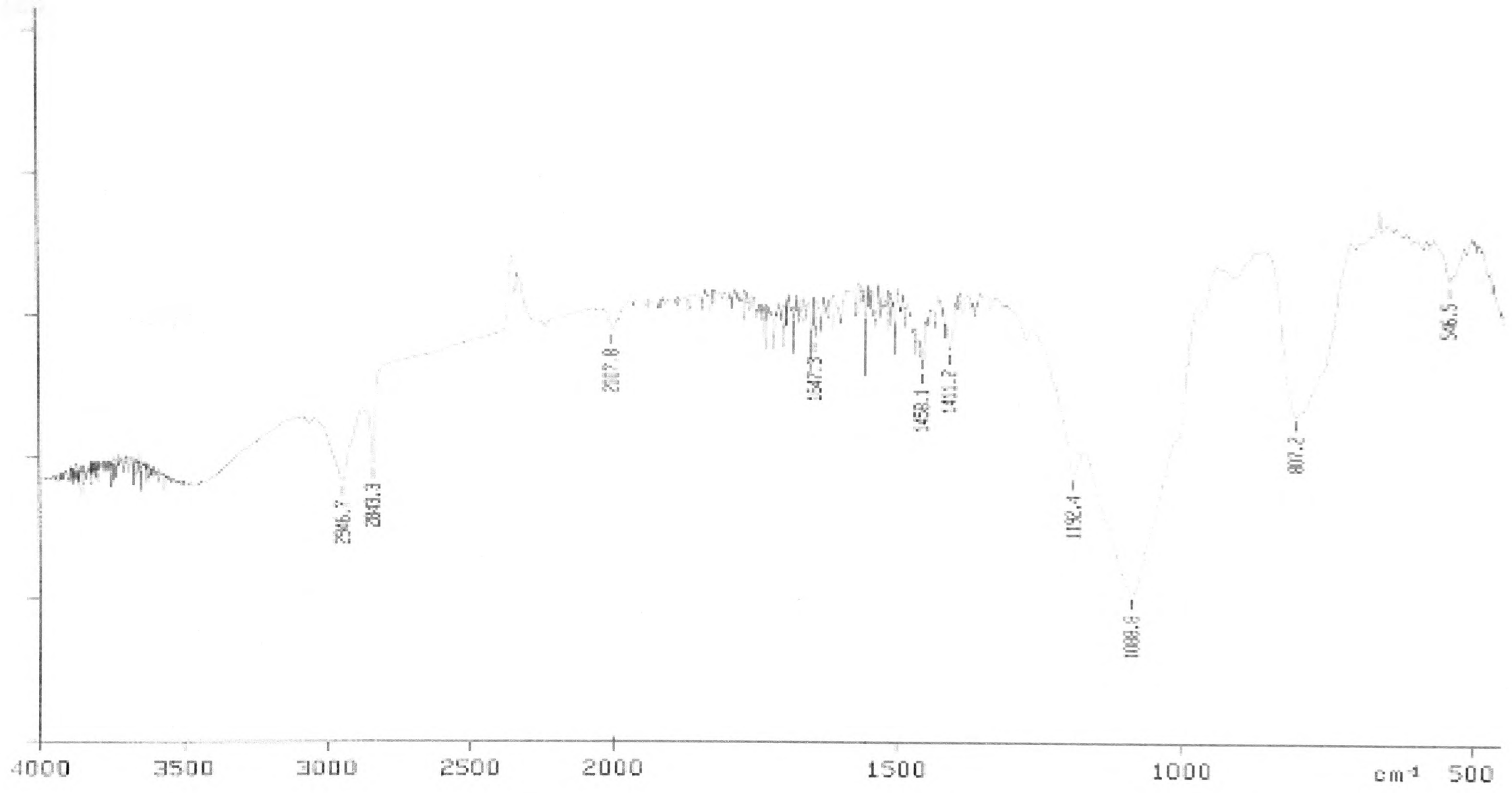

Figure 3.5.2: Infrared spectrum of vinyltrimethoxysilane polymer.

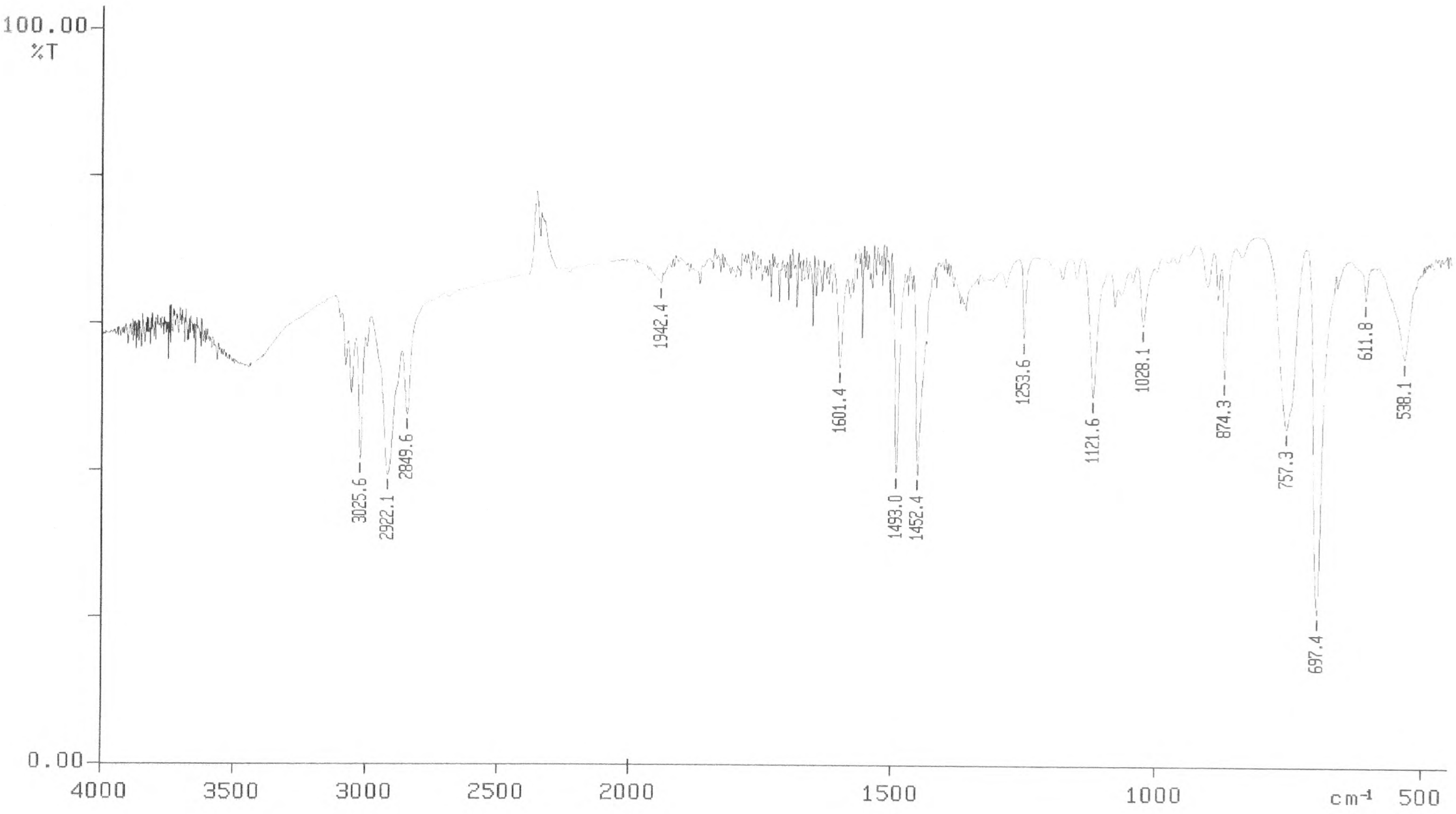

Figure 3.5.3: Infrared of the styrene polymer.

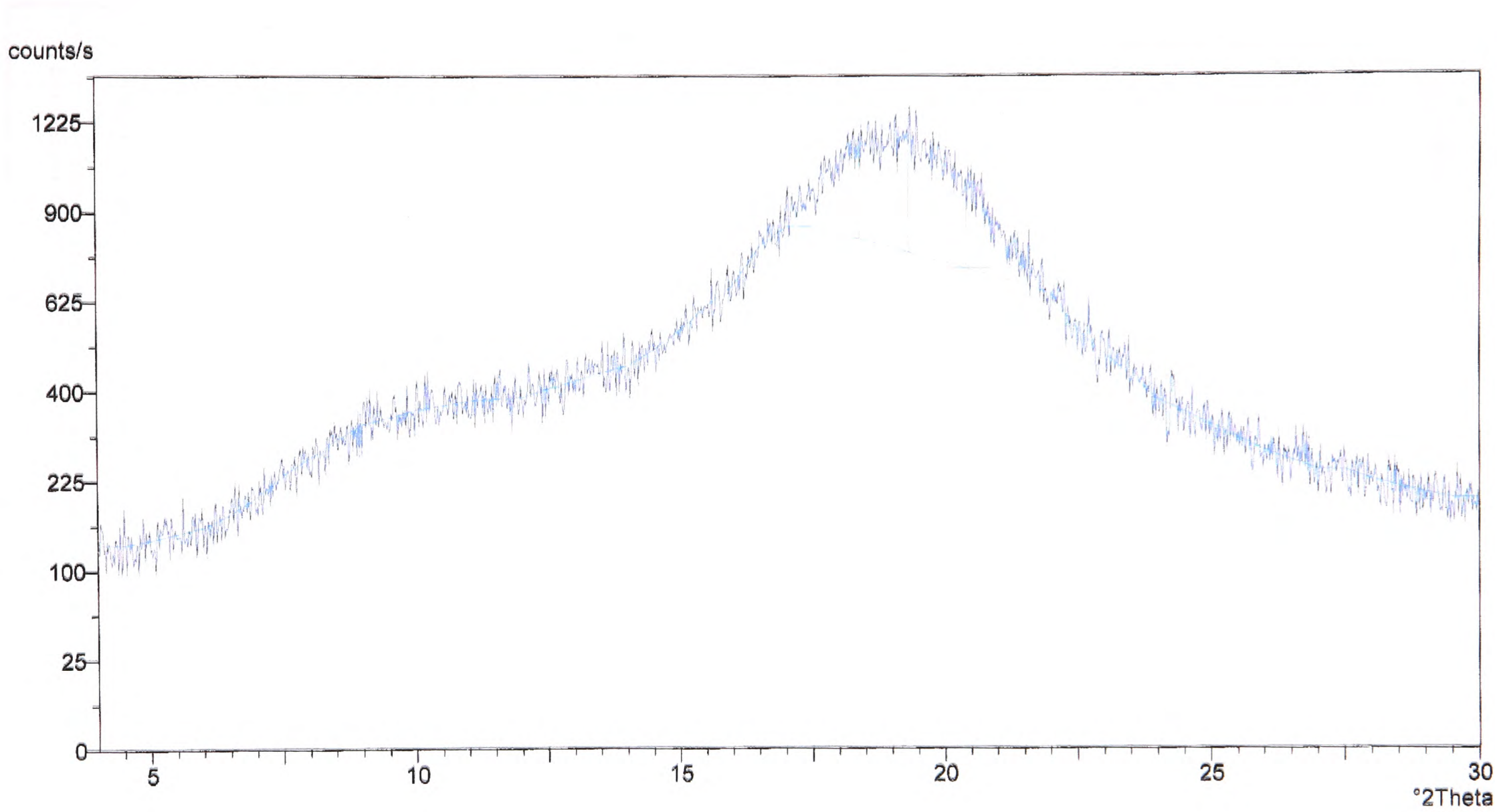

Figure 3.5.4: X-ray diffraction of the styrene polymer.

3.6 HYDROLYSIS OF 3-(TRIMETHOXYSILYL) PROPYL METHACRYLATE TO GIVE PROPYLMETHACRYLATEPOLYSILOXANE

The aim of this experiment was to create a methacrylate polysiloxane by hydrolysis of 3-(Trimethoxysilyl) propyl methacrylate. The end product from the synthesis of propylmethacrylatepolysiloxane was a viscous oil. Infrared analysis, elemental analysis and ^{1}H, ^{13}C and ^{29}Si NMR were performed. The following reaction probably occurred:

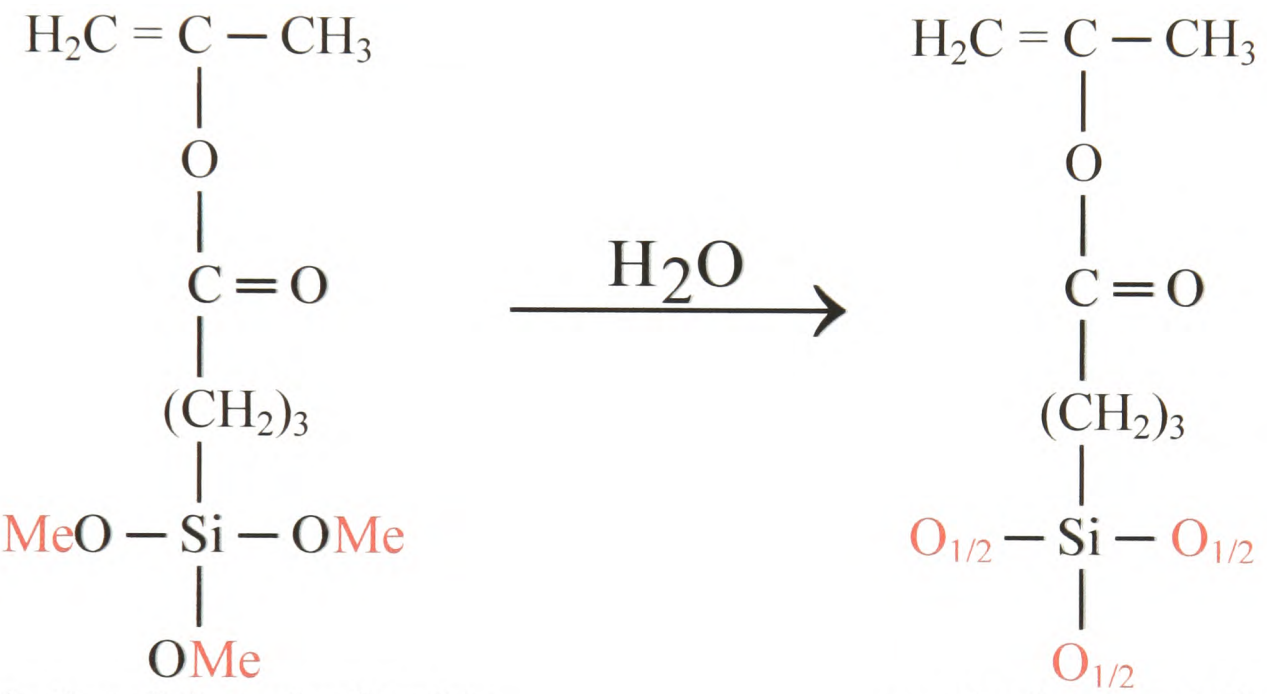

3-(Trimethoxysilyl) propyl methacrylate **propylmethacrylatepolysiloxane**

Elemental analysis of the final compound was performed and **Table 3.6.1** lists the results with the calculated theoretical results.

Table 3.6.1: Elemental analysis of $C_7H_{11}O_2SiO_{3/2}$

	Carbon (C)	**Hydrogen (H)**
Value Found %	49.93	6.56
Theoretical Value %	46.67	6.11

It can be seen that the percentage of each element from the results of the elemental analysis are not consistent probably because the compound did not fully hydrolyse or fully cross-link to give the polysiloxane.

This is confirmed by infrared analysis of the product, which showed a peak at 3500cm^{-1} due to Si-OH bond. Evidence for the formation of the siloxane bond (Si-C) can be seen in the spectrum as a broad peak at around 1100cm^{-1}.

Analysis by ^{13}C **(Figure 3.6.2)** and ^{1}H NMR **(Figure 3.6.3)** was carried out. In the ^{13}C NMR spectrum the first chemical shift at 20ppm relates to a -CH_2 environment followed by a chemical shift at 30ppm corresponding to a -CH alkane. The chemical shift at 65ppm is consistent to an alcohol or ether (-C-O-). The set of chemical shifts at the range of 120ppm to 140ppm are due to toluene residue. Finally the chemical shift at 170ppm appears as a result of the carboxylic ester present in propylmethacrylatepolysiloxane.

The ^{1}H NMR spectrum shows a chemical shift at 0.8-1.0ppm corresponding to a -CH_3 chemical environment and two peaks around 2.00ppm, from which the sharp peak is probably due to the methyl groups of the toluene and the broader peak is due to a -(CH_2) environment. The peaks at 4.2ppm and 5.4ppm are more likely due to the Si-OH bond and the peak at 6.1ppm confirms the presence of an alkene. The set of chemical shifts at the region of 7.0ppm are as a result of the residue toluene. The intergration of the spectrum gives us inconclusive results because different environments arise in the spectrum, for example the presence of toluene residue still in the sample.

The ^{29}Si NMR spectrum **(Figure 3.6.4)** gave a clear indication of a T unit (around -50ppm to -60ppm) with the presence of different environments.

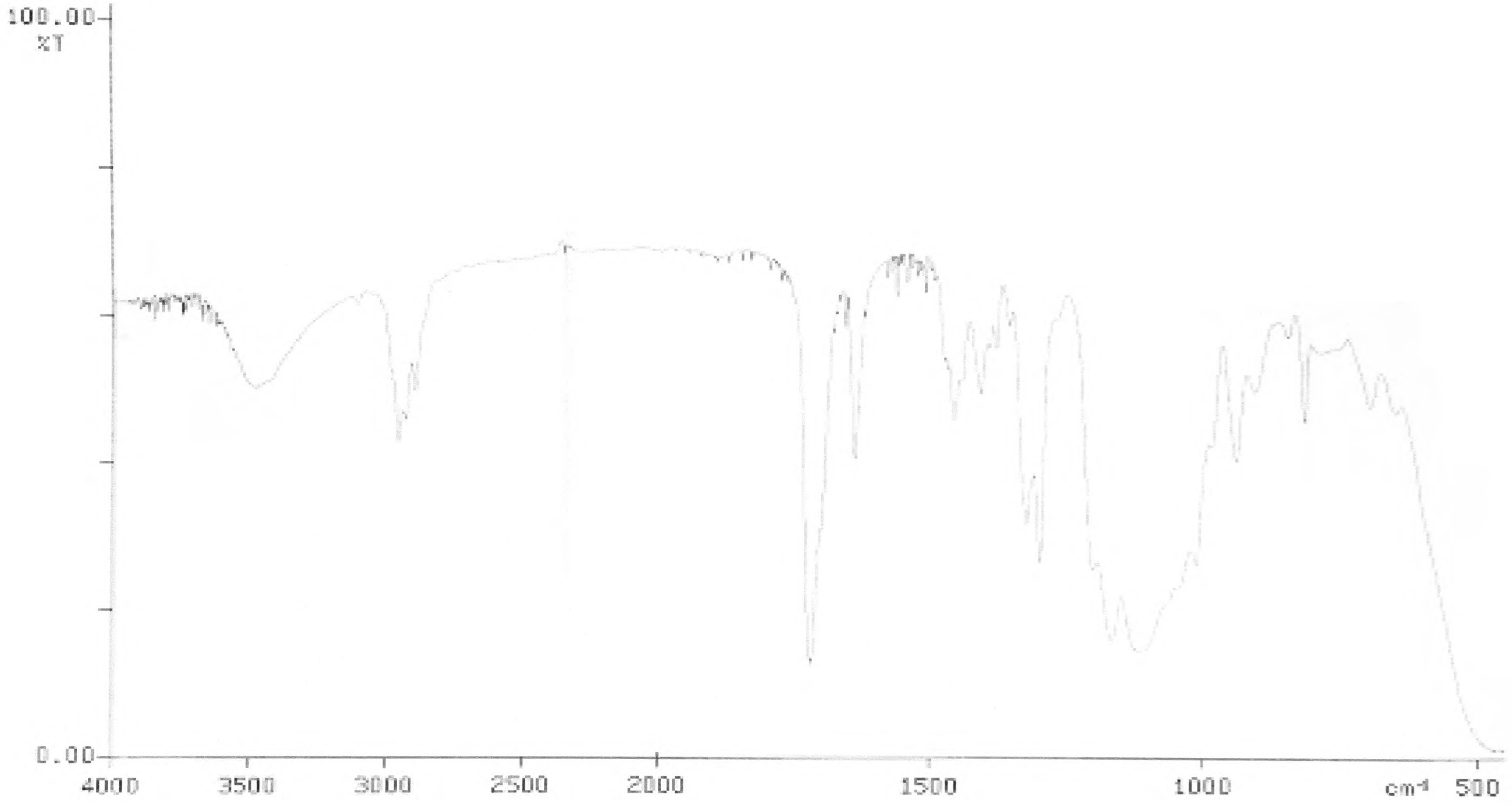

Figure 3.6.1: Infrared spectrum for propylmethacrylatepolysiloxane.

Figure 3.6.2: ^{13}C NMR spectra for $C_7H_{11}O_2SiO_{3/2}$.

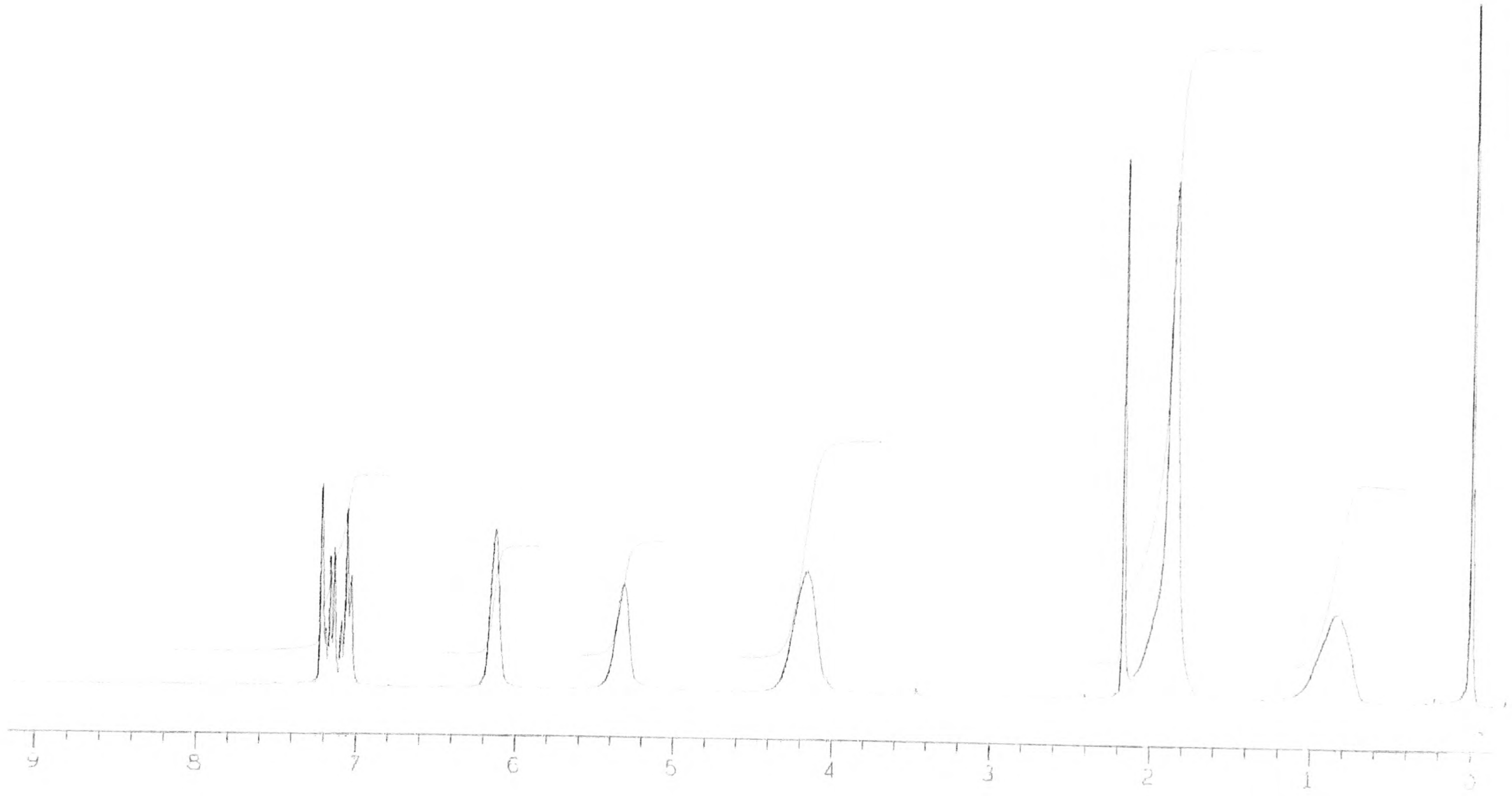

Figure 3.6.3: ^{1}H NMR spectra for $C_7H_{11}O_2SiO_{3/2}$.

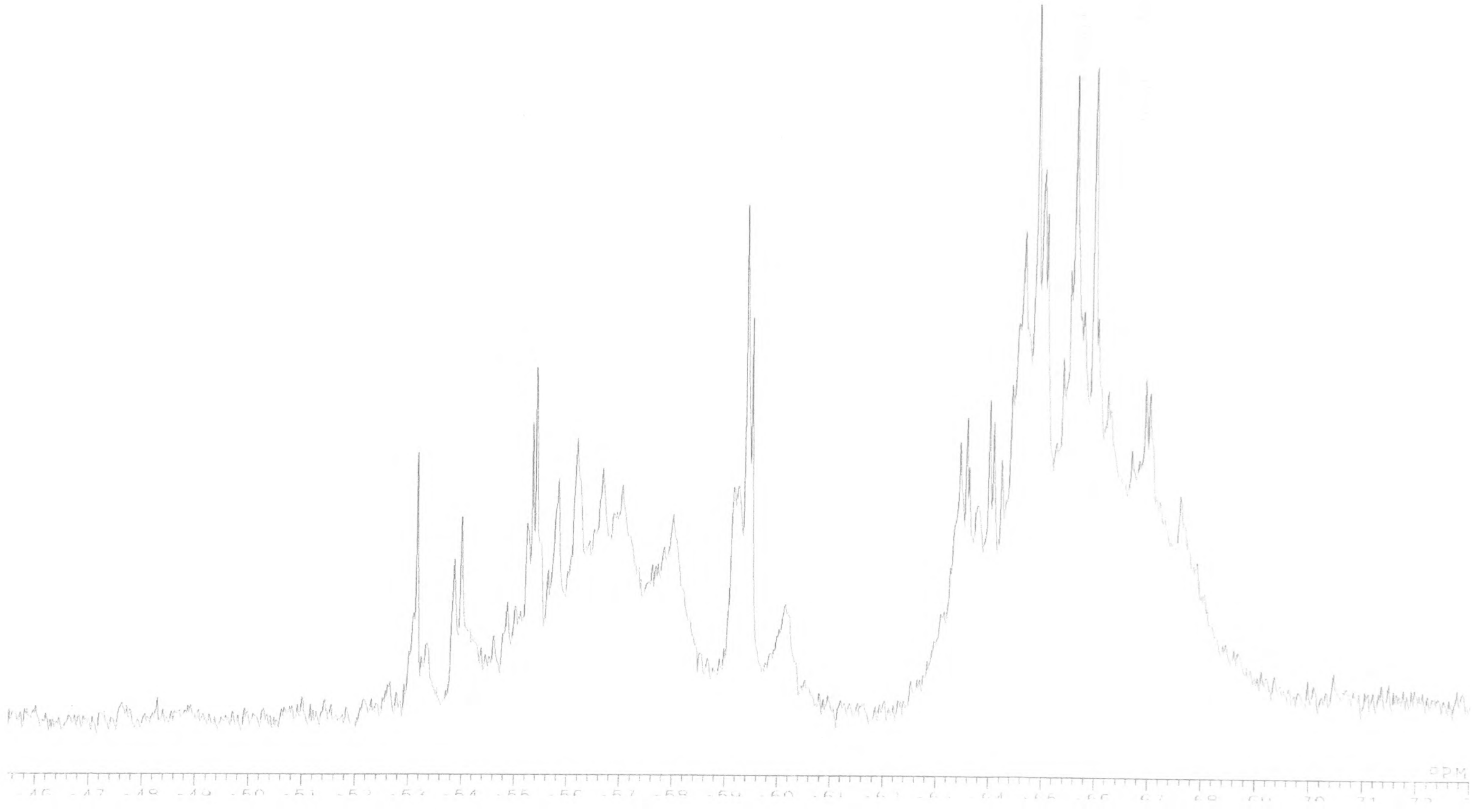

Figure 3.6.4: ^{29}Si NMR spectra for $C_7H_{11}O_2SiO_{3/2}$.

The methacrylate group of the viscous oil was then crosslinked via peroxide cure using a photoreactor vessel. The aim was to form a three-dimensional polymer by means of inter-chain reactions resulting in changes in physical properties. Benzoyl peroxide was used for this purpose to initiate the high-temperature radical cure of the oil. The final product was a fine white powder. The infrared spectrum of this white powder **(Figure 3.6.5)** showed only minor differences with that of the original starting material and there are small differences from the elemental analysis **(Table 3.6.2)**. These may be due, however, to residual solvent in both materials and so it would appear that this reaction has not occurred.

Table 3.6.2: Elemental analysis of crosslinked $C_7H_{11}O_2SiO_{3/2}$.

	Carbon (C)	**Hydrogen (H)**
White powder	51.23	5.71
Starting material	49.93	6.56

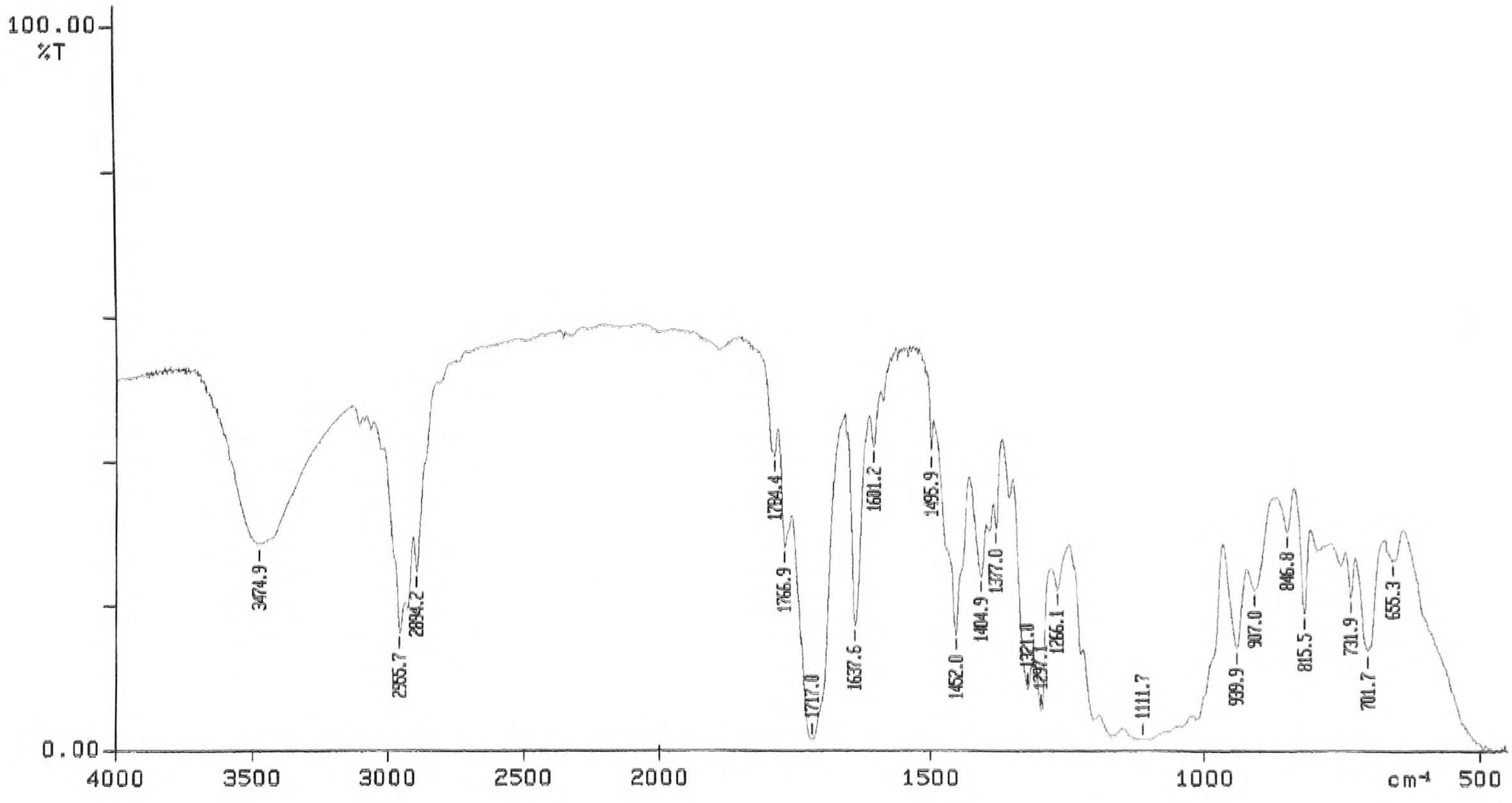

Figure 3.6.5: Infrared spectrum for crosslinked propylmethacrylatepolysiloxane.

3.7 EXTRACTION OF PROPYLMETHACRYLATEPOLYSILOXANE WITH PYRIDINE

Feher [27] in his work on the hydrolysis products of cyclohexyl trichlorosilane showed that three main products were formed which he called 1, 2 and 3 (Figure 3.7.1). In this experiment we were attempting to find out whether similar types of products were formed with the propylmethacrylatepolysiloxane. Trimethoxysilane was hydrolysed since, in principle, similar reactions might have occurred. It is probable; however, that the structures formed will depend on the relative rates of hydrolysis of the two starting materials.

Figure 3.7.1: The hydrolytic condensation of $CySiCl_3$ [2]

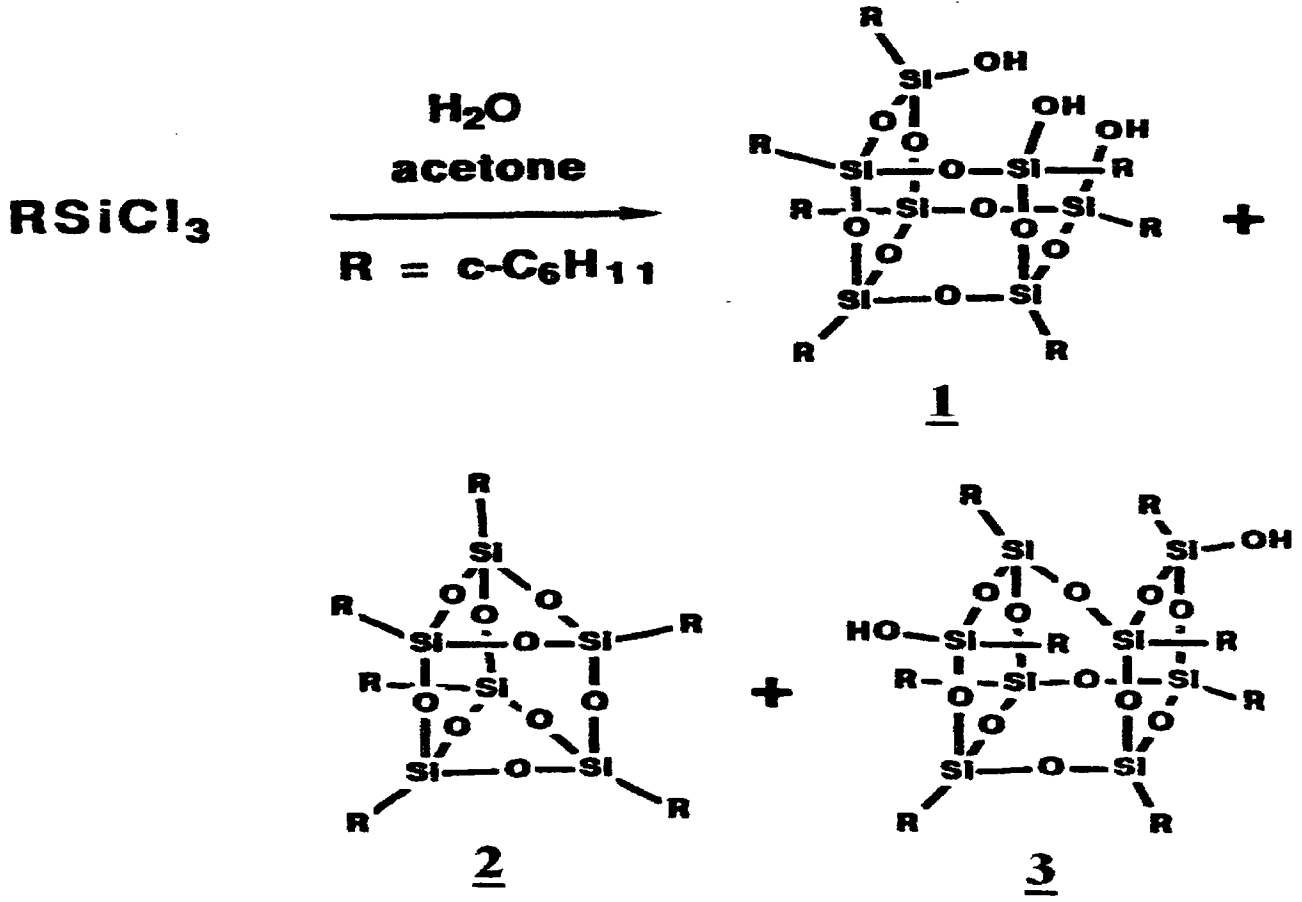

Elemental analysis was performed on the final product of the reaction, shown in **Table 3.7.1**. Nitrogen values are clearly due to the presence of residue pyridine (C_5H_5N) in the product.

Table 3.7.1: Elemental analysis of the product of the extraction of propylmethacrylatepolysiloxane with pyridine

	Nitrogen (N)	**Carbon (C)**	**Hydrogen (H)**
Value Found %	0.25	50.13	6.60

Infrared analysis of the polymer **(Figure 3.7.2)** gave sharp peaks including vibrations at around 1250cm^{-1} and 910-715cm^{-1} confirming the presence of Si-CH_3 bond. The broad peak at 1100-1000cm^{-1} is due to a Si-C stretching and another broad peak at 3500cm^{-1} possibly due to existence of water (-OH stretching) still in the final compound.

The infrared analysis did not give any conclusion whether or not there was any hydrolysis of the trimethoxysilane groups.

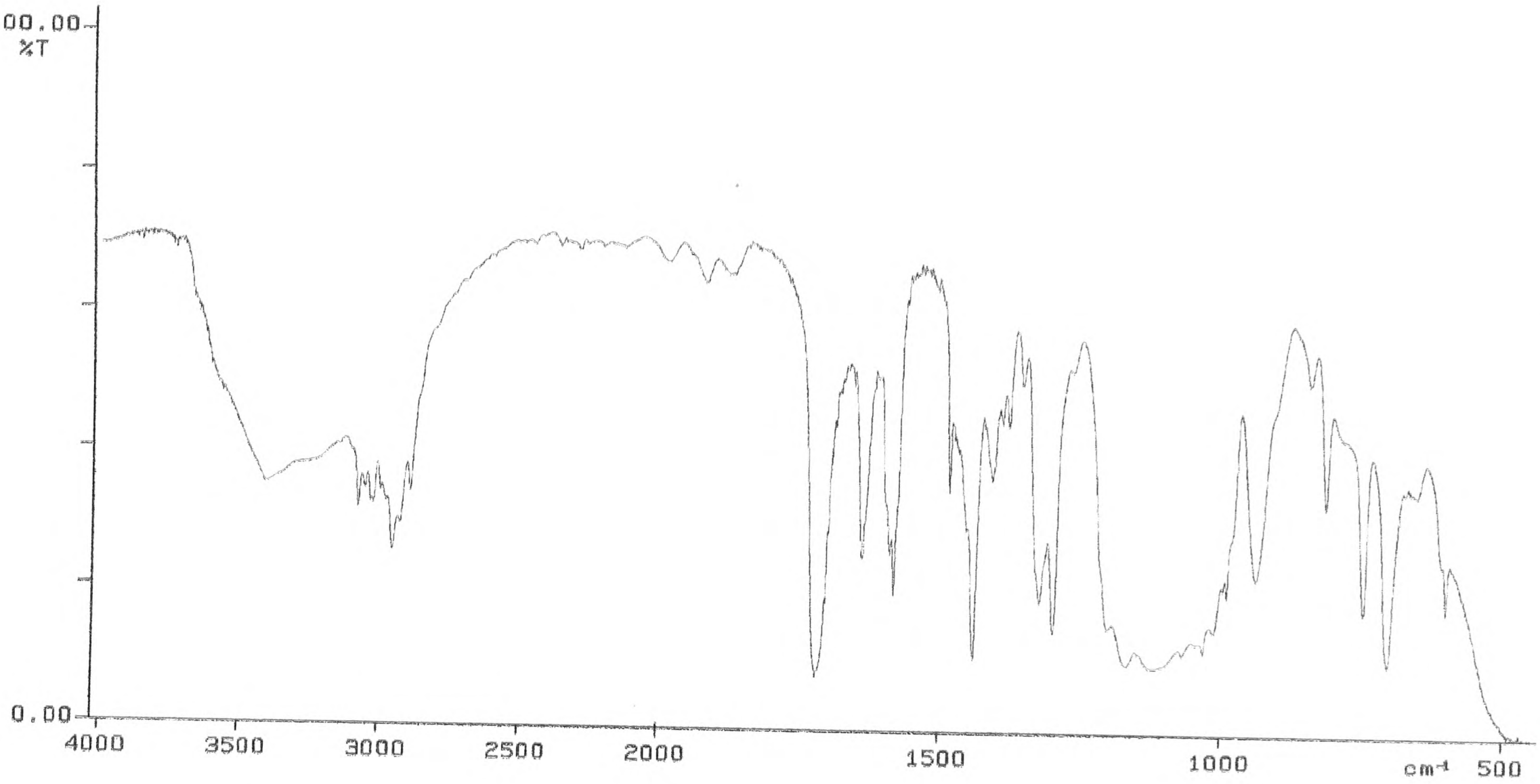

Figure 3.7.2: Infrared analysis of the product from the reaction of propylmethacrylatepolysiloxane with pyridine.

Analysis of ^{13}C **(Figure 3.7.3)** and ^{1}H **(Figure 3.7.4)** NMR was carried out. Studying the ^{13}C NMR spectrum, the first peaks at 10ppm, 20ppm and 30ppm indicate the presence of alkanes, CH_3-, -CH_2- and -CH-. The two peaks at 65ppm and 80ppm can be either from the pyridine residue or from the presence of an alcohol or ether. The set of chemical shifts at the range of 130ppm up to 150ppm are clearly due to residue pyridine in the sample. The last peak at 170ppm is probably due to the ester (O-C=O) into the compound.

Analyzing the ^{1}H NMR spectrum the conclusions are similar as above. The chemical shifts at 4ppm and 5.5ppm are most probably due to -OH environments while the peaks at 7ppm and after are clearly because of the pyridine residue. The pyridine residue does not allow us to have a clear number of the proton NMR environments in the product.

^{29}Si NMR **(Figure 3.7.5)** was also carried out showing a variety of similar environments at the range of -70 ppm to -50 ppm which are due to T type silicone centers.

In the case of cyclohexyl trichlorosilane aqueous propanone was used and the reaction is very slow (up to 3 months to get solid product) whereas in the case of the trimethoxysilane the reaction is much quicker and the product was a viscous oil. It should be noted, however, that the hydrolysis of cyclohexyl trichlorosilane initially gives an oil. It is possible therefore that in the early stages of both reactions similar products are formed and that the final solid products in the case of cyclohexyl trichlorosilane form after further reaction of the oil initially observed. No solid products were produced even after prolonged reaction times in the case of the propylmethacrylatepolysiloxane.

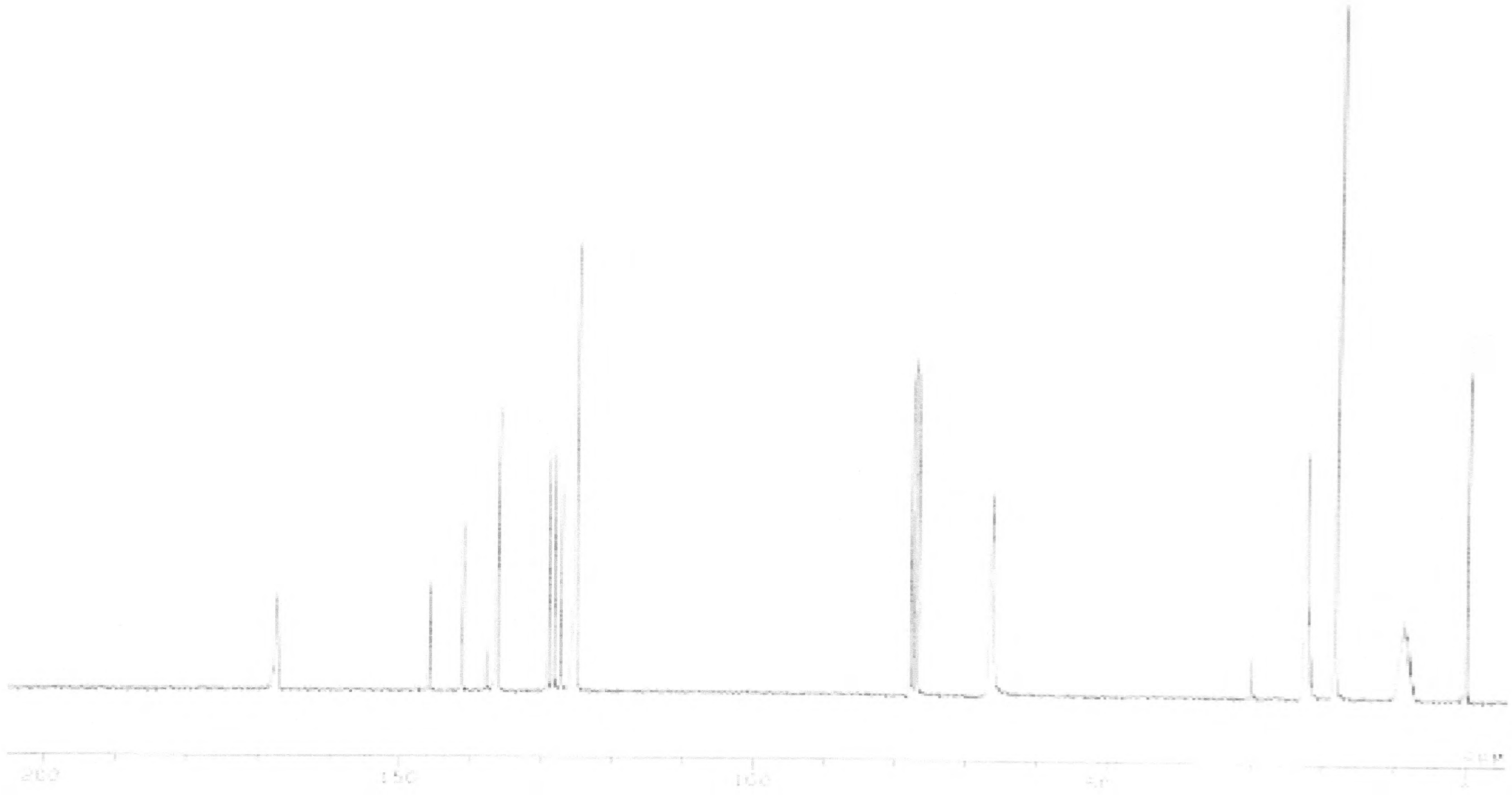

Figure 3.7.3: ^{13}C NMR spectra for $C_7H_{11}O_2SiO_{3/2}$ and pyridine.

Figure 3.7.4: ^{1}H NMR spectra for $C_7H_{11}O_2SiO_{3/2}$ and pyridine.

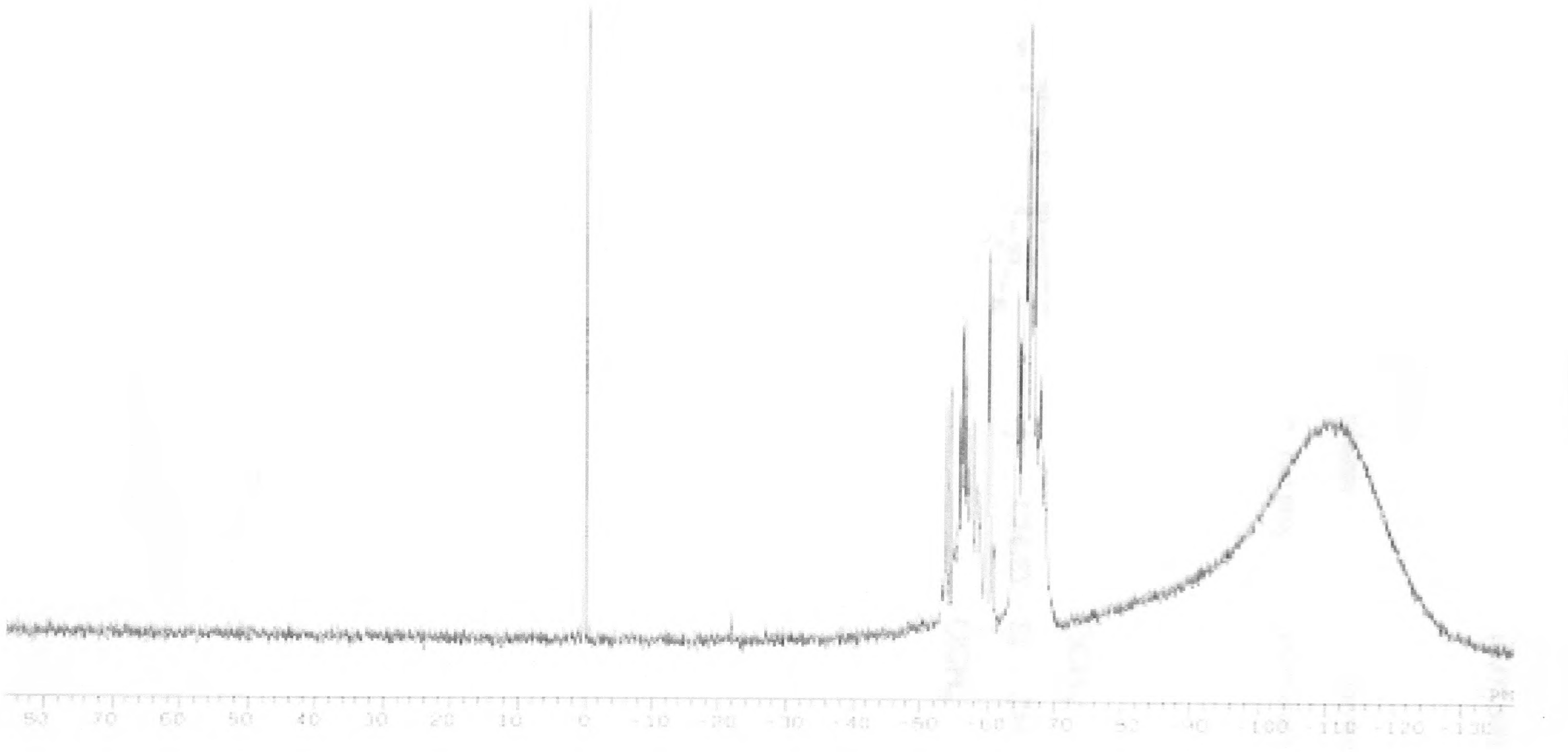

Figure 3.7.5: ^{29}Si NMR spectra for $C_7H_{11}O_2SiO_{3/2}$ and pyridine.

3.8 REACTION OF PROPYLMETHACRYLATEPOLYSILOXANE WITH VINYLTRIMETHOXYSILANE

The polymerization of propylmethacrylatepolysiloxane with vinytrimethoxysilane is another chain growing polymer reaction. The proposed reaction can be seen below

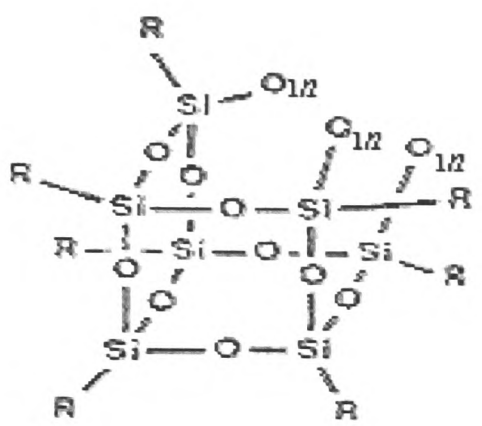

$R=C_7H_{11}O_2$

+

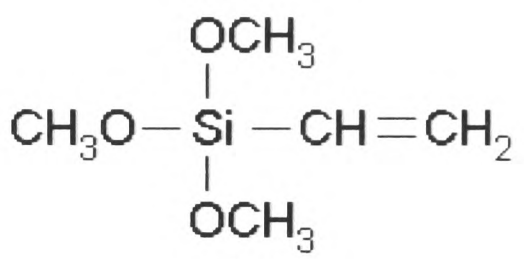

↓

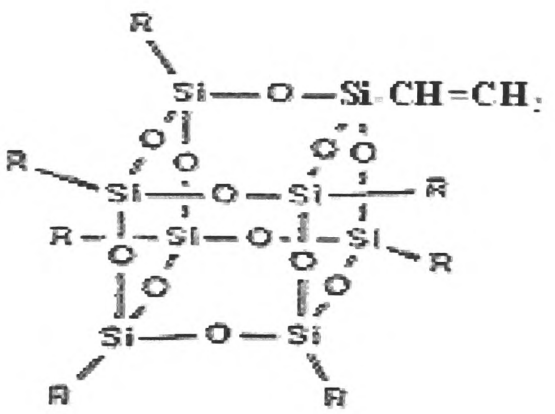

$R=C_7H_{11}O_2$

Elemental analysis of the above compound can be seen in **Table 3.8.1**. The analysis showed a small increase in the carbon percentage of the compound suggesting that there was a possible reaction between the two compounds.

Table 3.8.1: Elemental analysis of the final product of the reaction of propylmethacrylatepolysiloxane with vinytrimethoxysilane

	Carbon (C)	**Hydrogen (H)**
Values Found %	45.17	6.16
Theoretical Values of the starting material %	46.67	6.11

Figure 3.8.1 shows the infrared spectrum of the final product of the reaction highlighting the peaks at 3000cm^{-1} (asymmetric -CH stretching in -CH_3), ~1600cm^{-1} (C-C multiple bond stretching frequency) as well as at 1100cm^{-1} (Si-C asymmetric stretching frequency) and at ~760cm^{-1} (Si-CH_3 stretching frequency)

Comparing this infrared spectrum with the spectrum of the starting compound **(Figure 3.6.1)** we can notice great similarities. Except the appearance of a peak at 3500cm^{-1} which correspondents to a Si-OH stretching bond, meaning the starting material wasn't fully hydrolyzed, as mentioned before.

The same experiment was performed but without the presence of vinyltrimethoxysilane and **Figure 3.8.2** shows the infrared spectra. Comparing it with the spectrum of the starting material **(Figure 3.8.1)** we can clearly see some similarities. However, the peak that appears at 3500cm^{-1}, an -OH stretching suggests the presence of water or the Si-OH bond. Remarkably that peak does not appear in the spectrum of the final product **(Figure 3.8.1)** suggesting a reaction between the two compounds.

The X-ray analysis of the product showed that it was amorphous **(Figure 3.8.3)**.

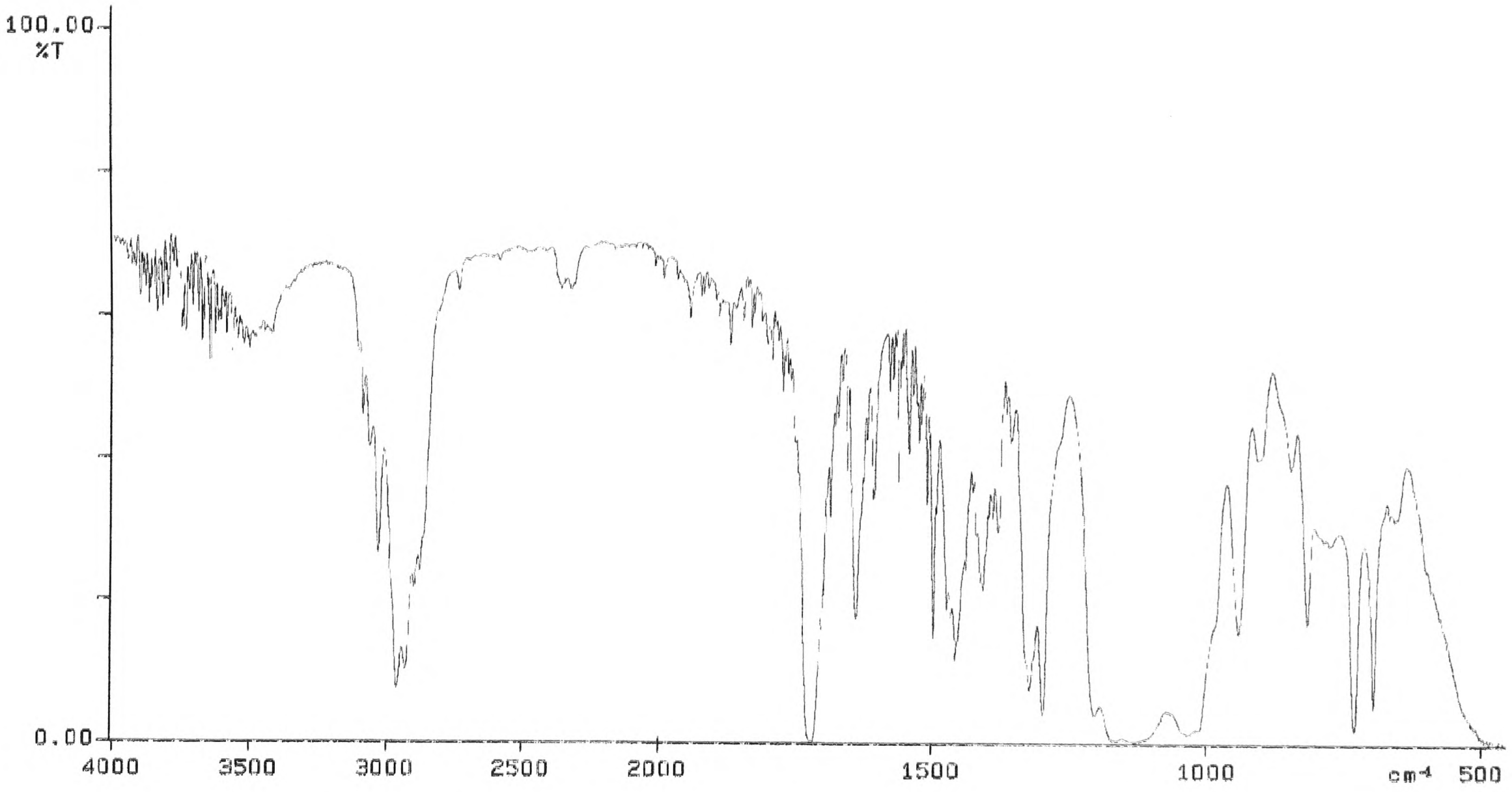

Figure 3.8.1: Infrared spectrum of the final product of the reaction of propylmethacrylatepolysiloxane with vinytrimethoxysilane.

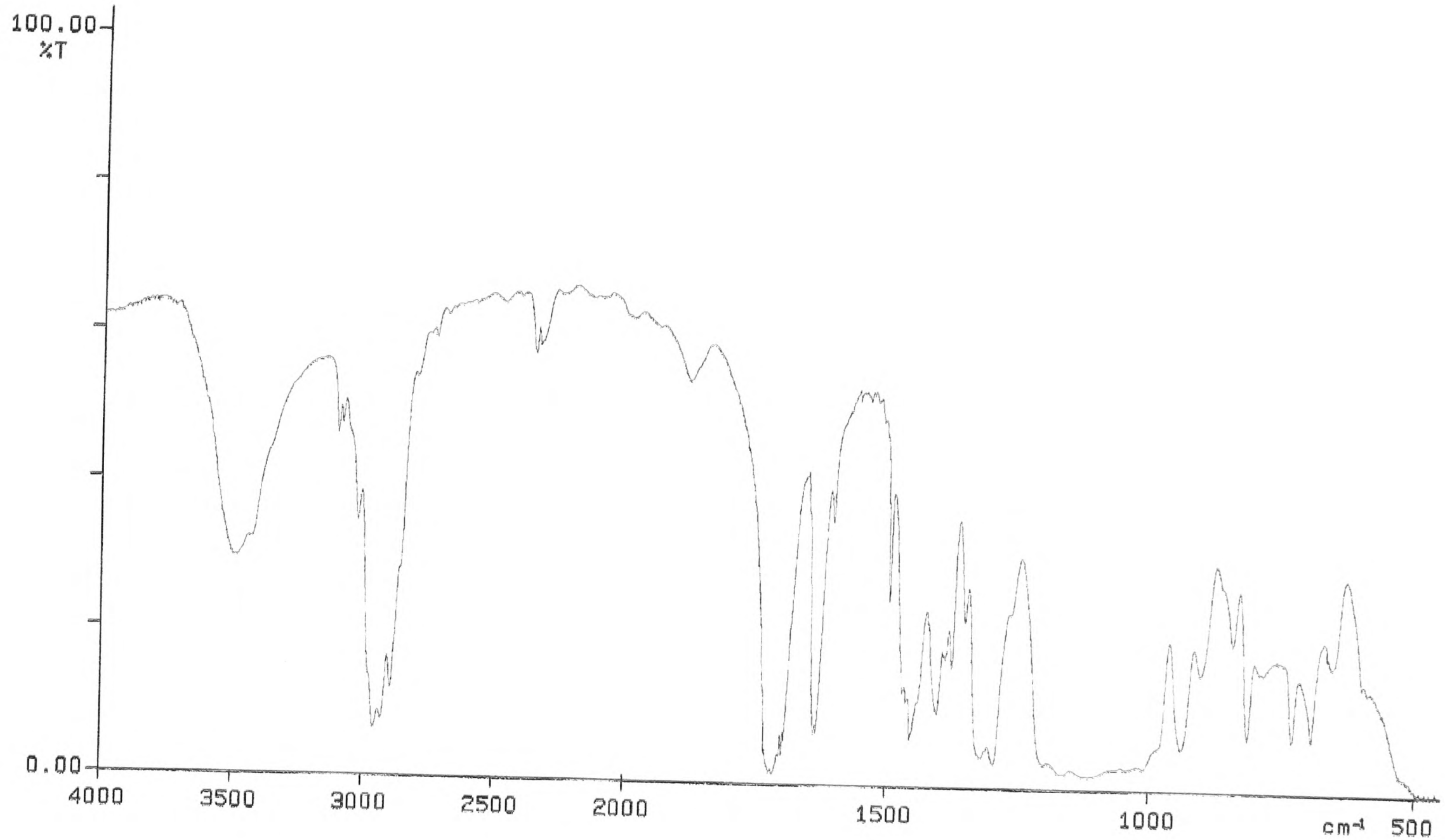

Figure 3.8.2: Infrared spectrum of the final product of the reaction of propylmethacrylatepolysiloxane without the presence of vinytrimethoxysilane.

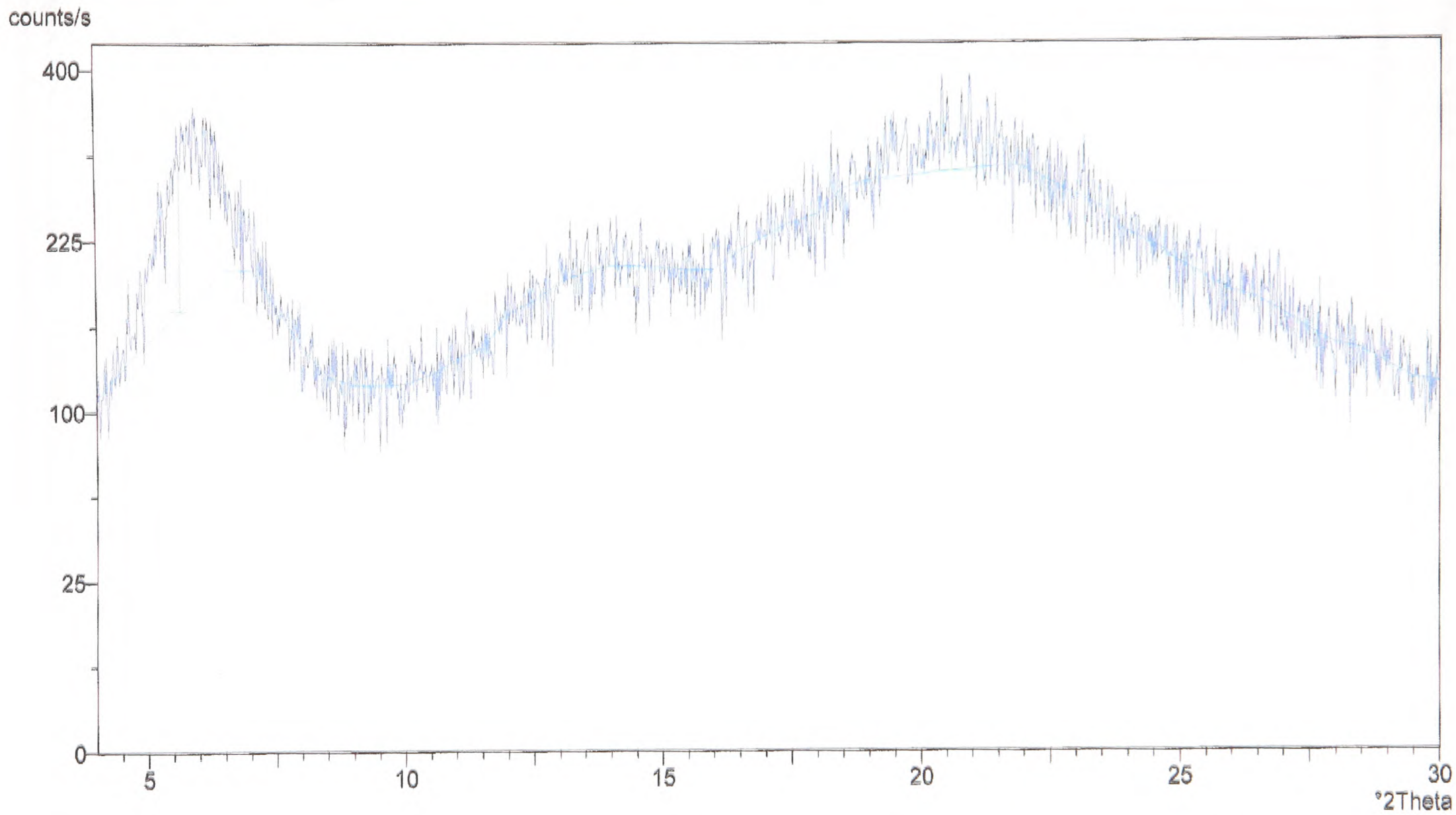

Figure 3.8.3: X-ray diffraction pattern of the final polymer of the reaction of propylmethacrylatepolysiloxane with the presence of vinytrimethoxysilane.

The production of high molecular species was revealed by GPC analysis **(Figure 3.8.4)**. The reaction led to the production of high molecular weight product, illustrated by a small peak on the GPC chromatogram.

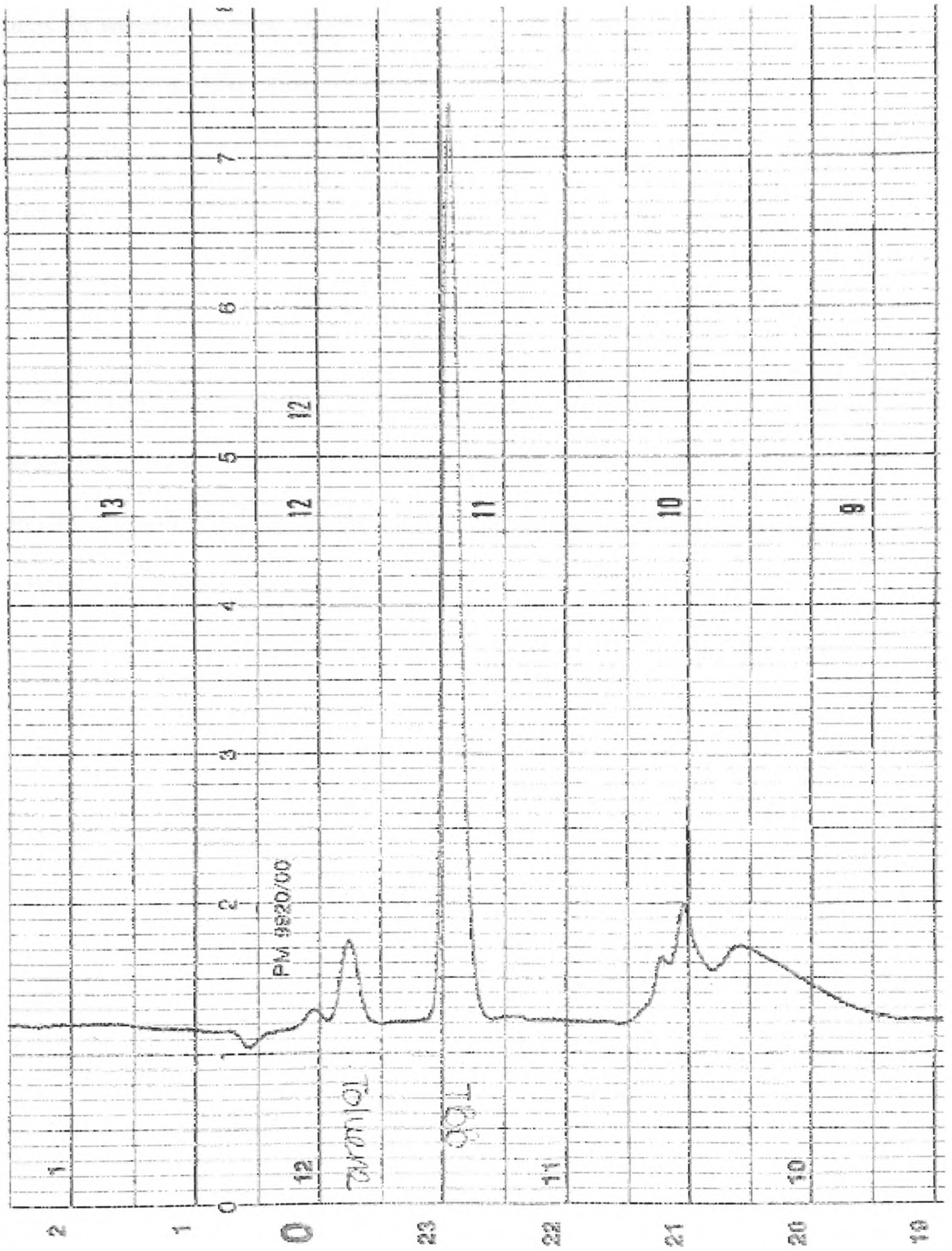

Figure 3.8.4: GPC chromatogram of the final polymer of the reaction of propylmethacrylatepolysiloxane with vinytrimethoxysilane.

Two thermal techniques were also performed on the product. Thermogravimetric analysis (TGA) is a method for determining the weight loss as a sample is heated. **Figure 3.8.5** shows the thermogram of the polymer. Four major steps for weight loss were observed in the TG curve. The first occurs at around 200°C. This is the loss of any water retained in the compound. Next step occurs between 400°C and 600°C probably due to the loss of hydrocarbons. Final weight loss after 600°C is most likely to be further oxidation of the hydrocarbons and breakage of silicones.

Differential Thermal Analysis (DTA) is a method monitoring the temperature between a sample and an inert reference as they are heated uniformly. **Figure 3.8.6** shows the chromatograph of the polymer. We can clearly see the endothermic process and the exothermic process of the product while burning. The decomposition temperature of the product is at around 330°C as the diagram indicates.

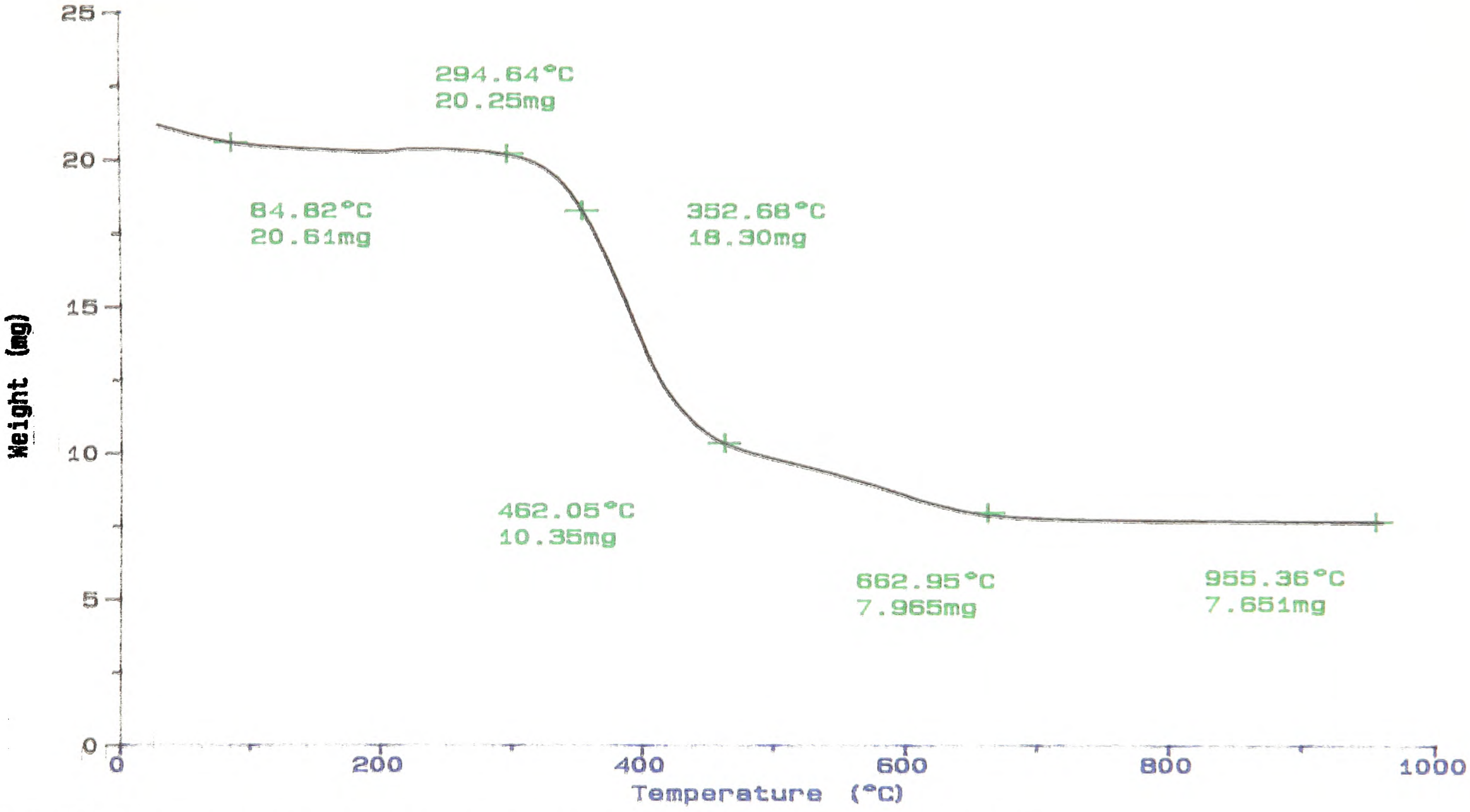

Figure 3.8.5: TGA trace of the final polymer of the reaction of propylmethacrylatepolysiloxane with vinytrimethoxysilane.

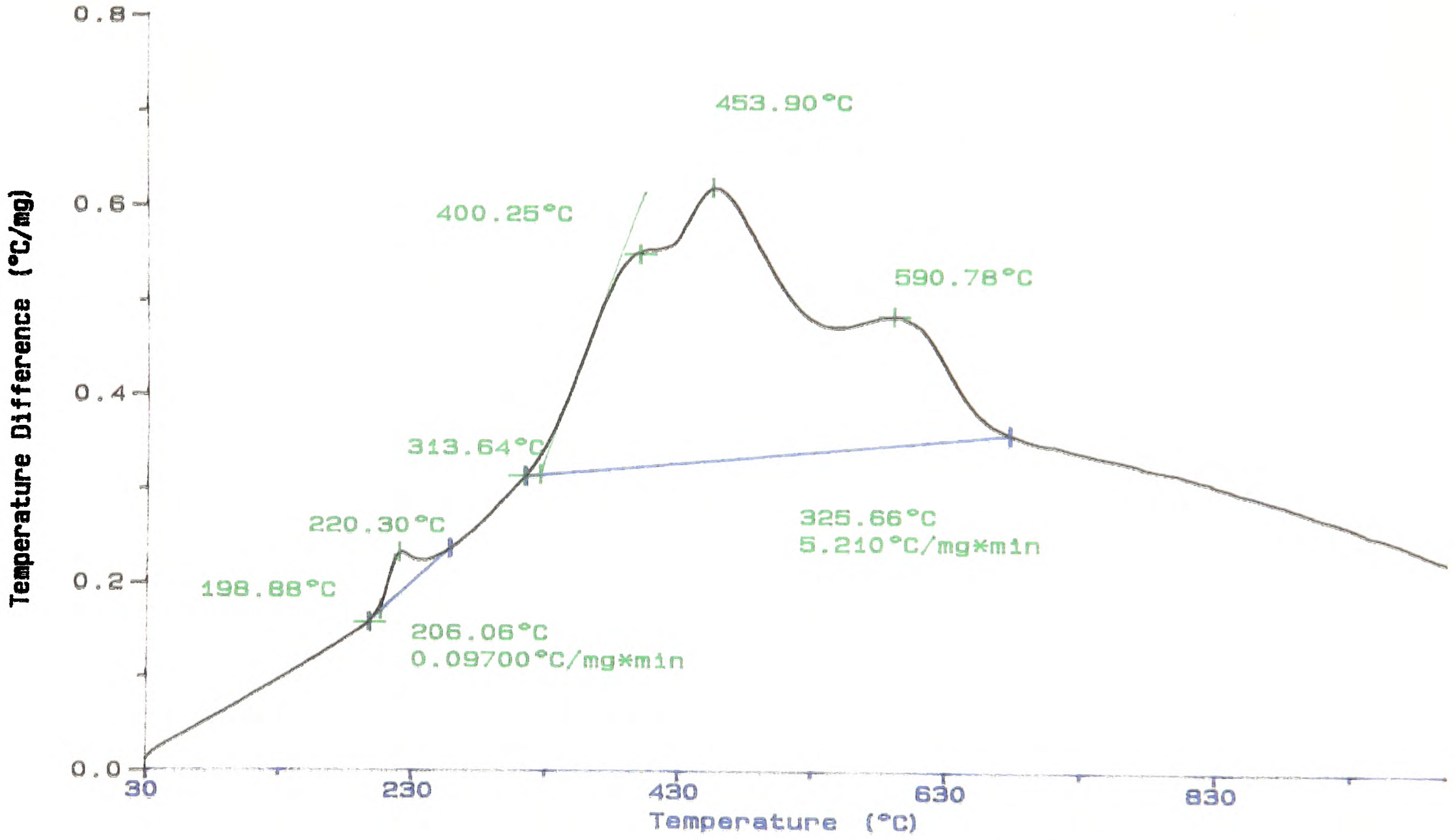

Figure 3.8.6: DTA chromatograph of the final polymer of the reaction of propylmethacrylatepolysiloxane with vinytrimethoxysilane.

3.9 COPOLYMERIZATION OF NIPAM AND 3- (TRIMETHOXYSILYL) PROPYL METHACRYLATE

3-(trimethoxysilyl) propyl methacrylate was copolymerized with NIPAM **(Figure 3.9.1)**. The silica produced was a powder and infrared analysis, CHN, X-ray and ^{13}C, ^{1}H, ^{29}Si NMR analysis was performed.

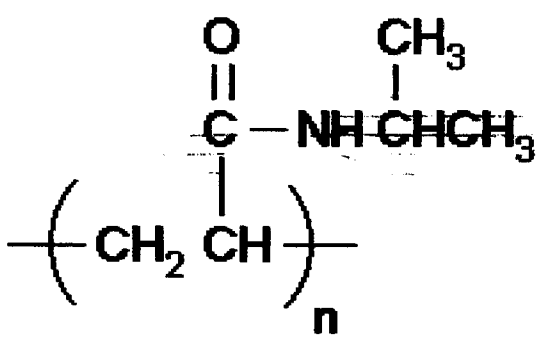

Figure 3.9.1: Structure of poly (*N*-isopropylacrylamide) (NIPAM).

A suggested structure produced by this reaction is a high molecular weight polymer with an unknown number of chains.

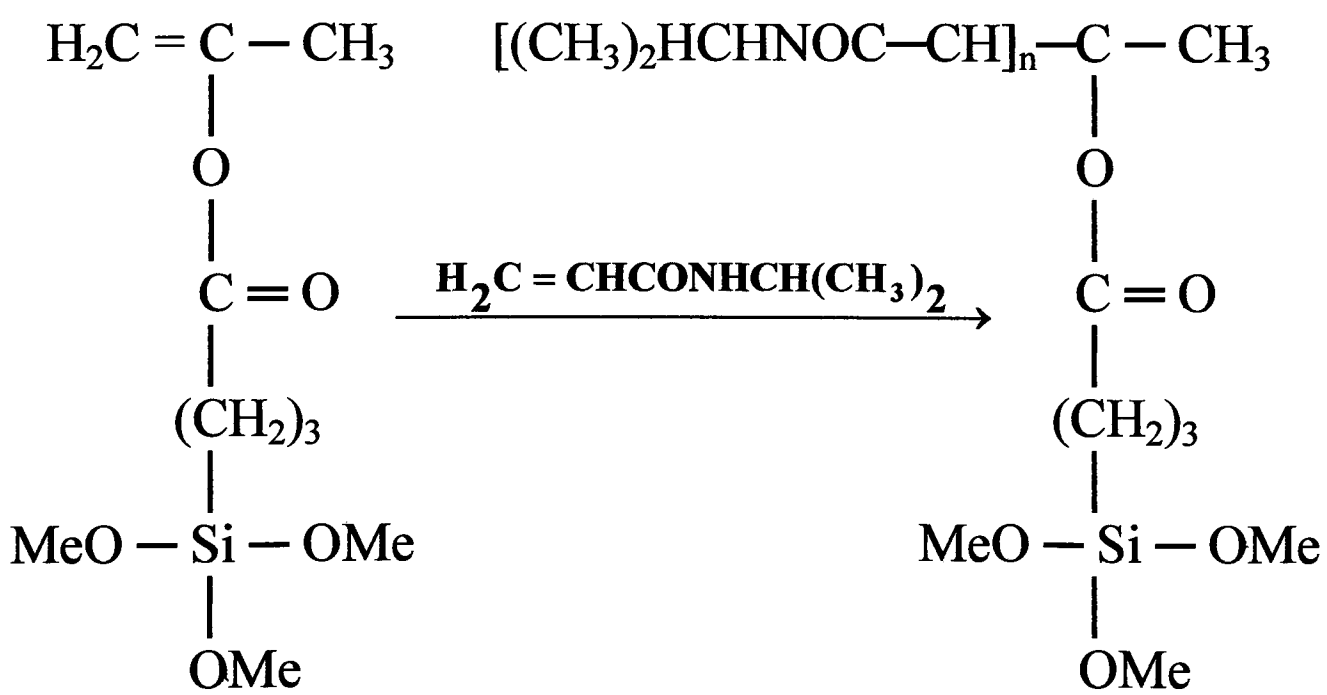

Elemental analysis of the polymer showed the presence of NIPAM in the sample. **Table 3.9.1** shows the results of the CHN analysis.

Table 3.9.1: Elemental analysis of the polymer of the copolymerisation of 3-(trimethoxysilyl) propyl methacrylate with NIPAM.

	Nitrogen (N)	**Carbon (C)**	**Hydrogen (H)**
Value Found %	16.65	53.61	6.73
Theoretical value of the starting material %	0	48.32	8.05

The nitrogen value found is obviously as a result of the NIPAM reaction and the increase on the carbon and hydrogen percentage suggests the possible creation of the final compound as shown above.

Infrared analysis of the polymer **(Figure 3.9.2)** gave sharp peaks and are summarised on the table below **(Table 3.9.2)**.

Table 3.9.2: Infrared adsorption peaks of the polymer of the copolymerisation of 3-(trimethoxysilyl) propyl methacrylate with NIPAM.

Wavelength/cm^{-1}	**Assignment**
~3300cm^{-1}	N-H stretching
~3000 cm^{-1}	asymmetric -CH stretching in -CH_3
~1600 cm^{-1}	C-C multiple bond stretching
~1100 cm^{-1}	Si-O-Si asymmetric stretching
~760 cm^{-1}	Si-C stretching

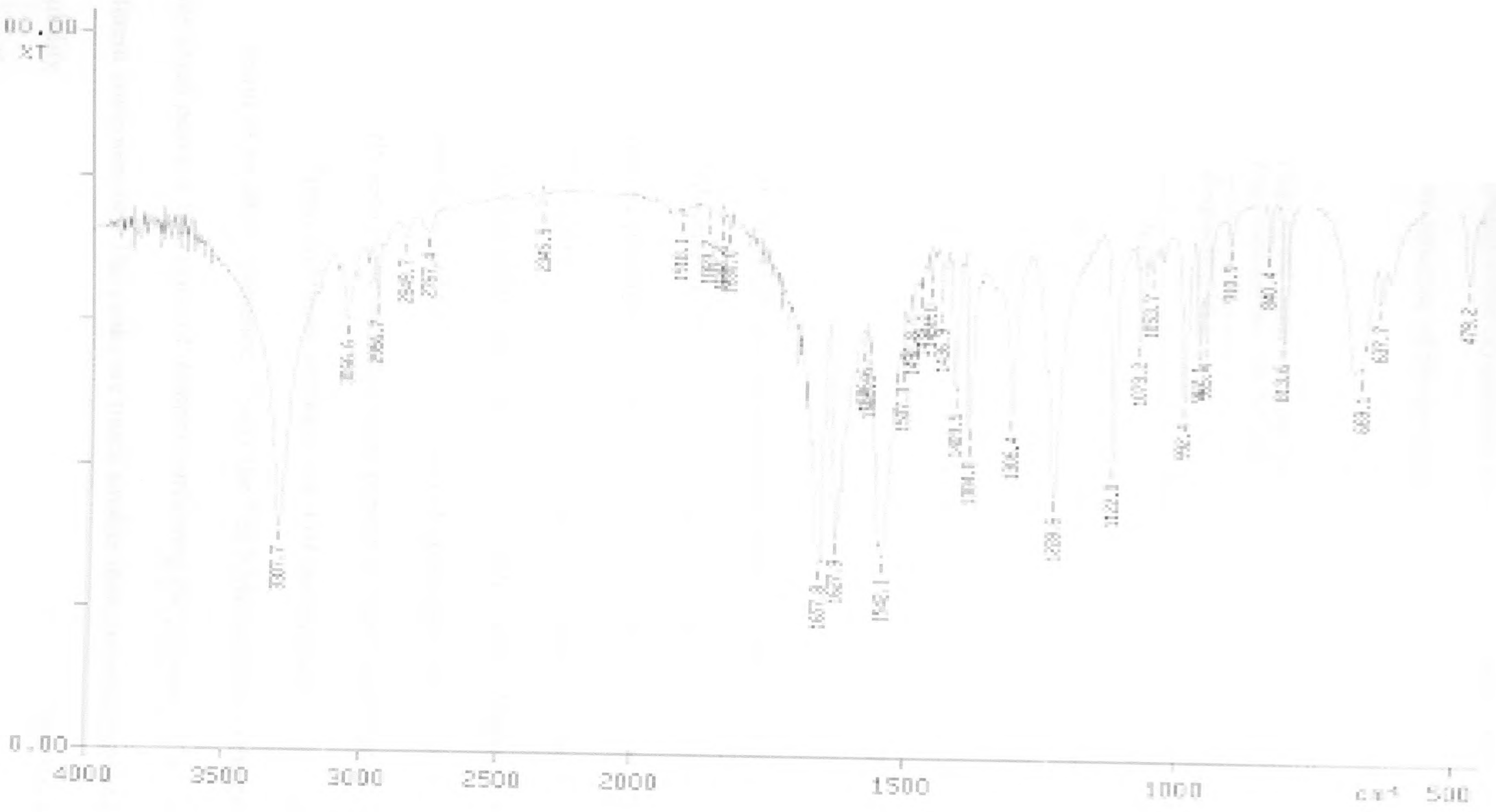

Figure 3.9.2: Infrared spectrum of polymer of the copolymerisation of 3-(trimethoxysilyl) propyl methacrylate with NIPAM.

The X-ray diffraction pattern of the polymer **(Figure 3.9.3)** shows broad, distinct peaks, showing some crystallinity of the sample. **Table 3.9.3** shows the d-spacing and relative intensity of the polymer.

Table 3.9.3: d-spacing (Å) and relative intensity for the polymer of the copolymerisation of 3-(trimethoxysilyl) propyl methacrylate with NIPAM.

d-spacing (Å)	Relative Intensity
9.04	40.03
8.83	41.99
7.38	100.0
4.38	65.16
4.39	72.41

^{13}C, ^{1}H and ^{29}Si NMR analysis was performed for the polymer. **Figure 3.9.4** shows the ^{13}C NMR analysis performed including peaks at 125ppmn and at the region of 128ppm which are present as a result of the benzoyl peroxide residue used for the completion of the reaction. The other small peaks at 134ppm, 137ppm and 138ppm are because of the presence of an alkene. The ^{1}H NMR spectra **(Figure 3.9.5)** indicates the presence of alkanes at the region of 1ppm and 2ppm. The benzene residue is clearly seen at the chemical shifts present at 7ppm and 8ppm. The small, broad peaks at 4.5ppm and 6ppm are due to an -OH environment as the peak at 6ppm is as a result of an alkene presence. Finally the ^{29}Si NMR spectrum **(Figure 3.9.6)** gives small peaks at the region of -60ppm confirming the presence of a T unit with different environments. The peaks are much smaller than expected probably due to the solubility of the product. The very big, broad peak at -100ppm is clear because of the glass effect when the sample was analyzed.

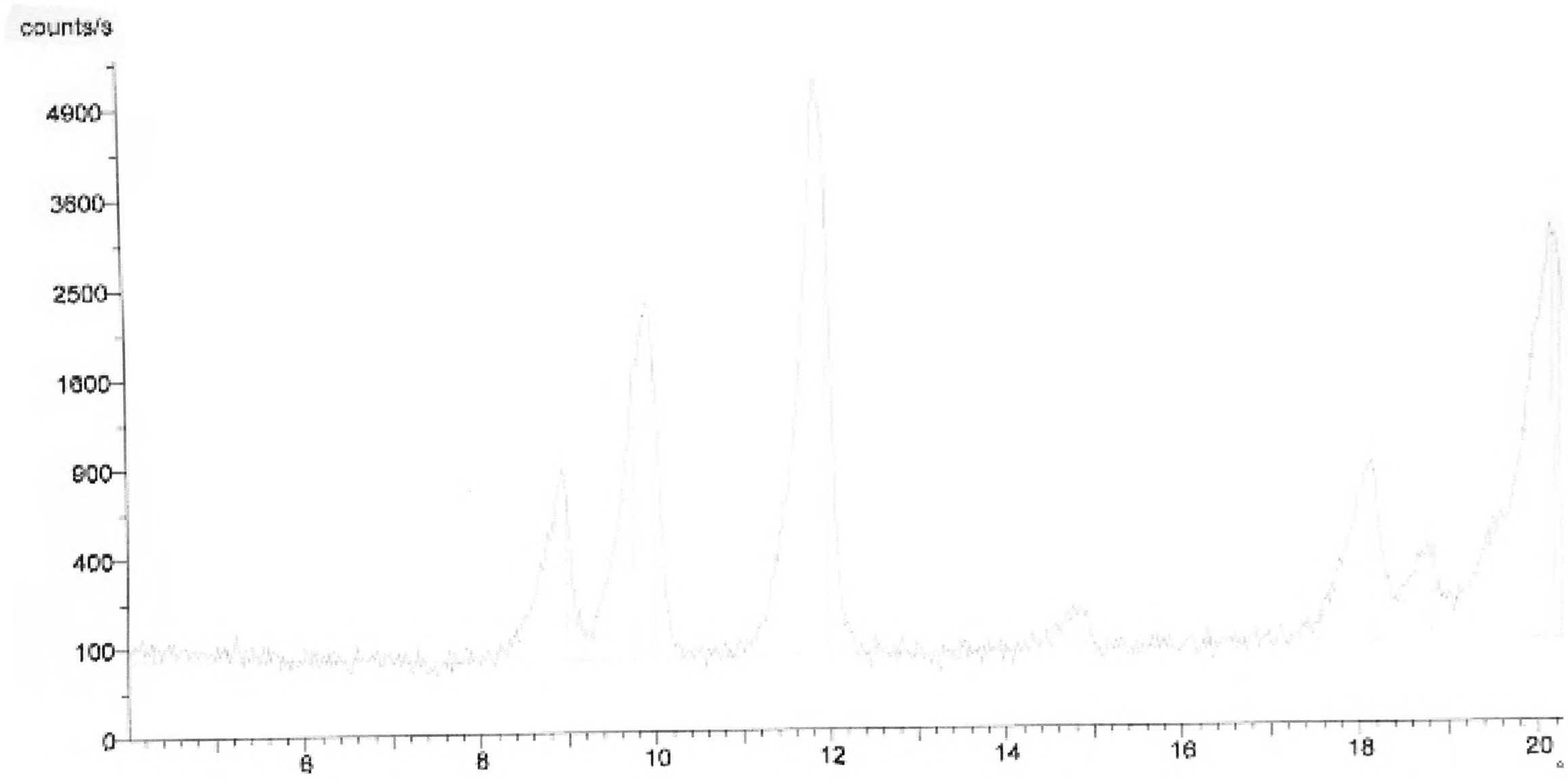

Figure 3.9.3: X-ray diffraction pattern of polymer of the copolymerisation of 3-(trimethoxysilyl) propyl methacrylate with NIPAM.

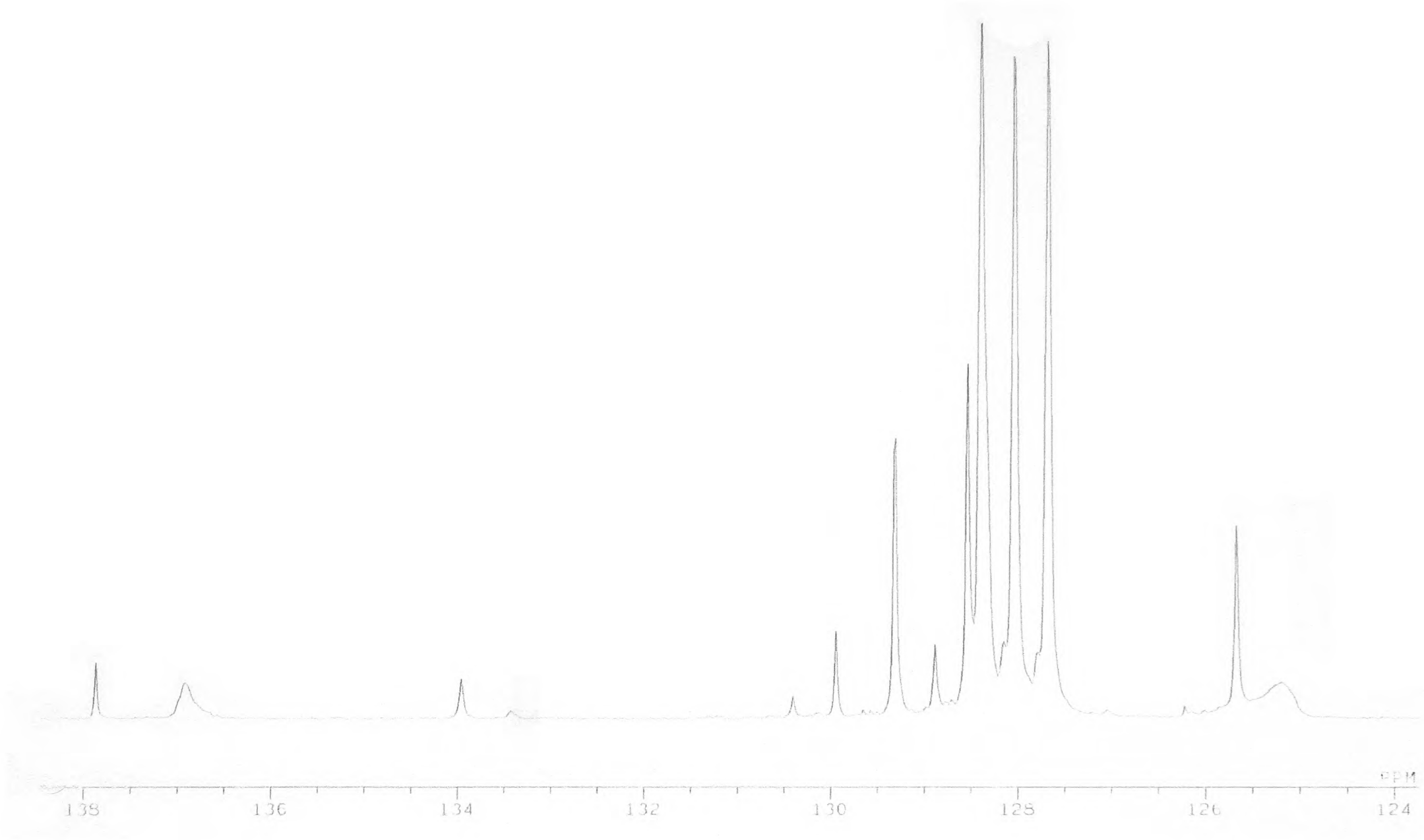

Figure 3.9.4: ^{13}C NMR spectrum of the polymer of the copolymerisation of 3-(trimethoxysilyl) propyl methacrylate with NIPAM.

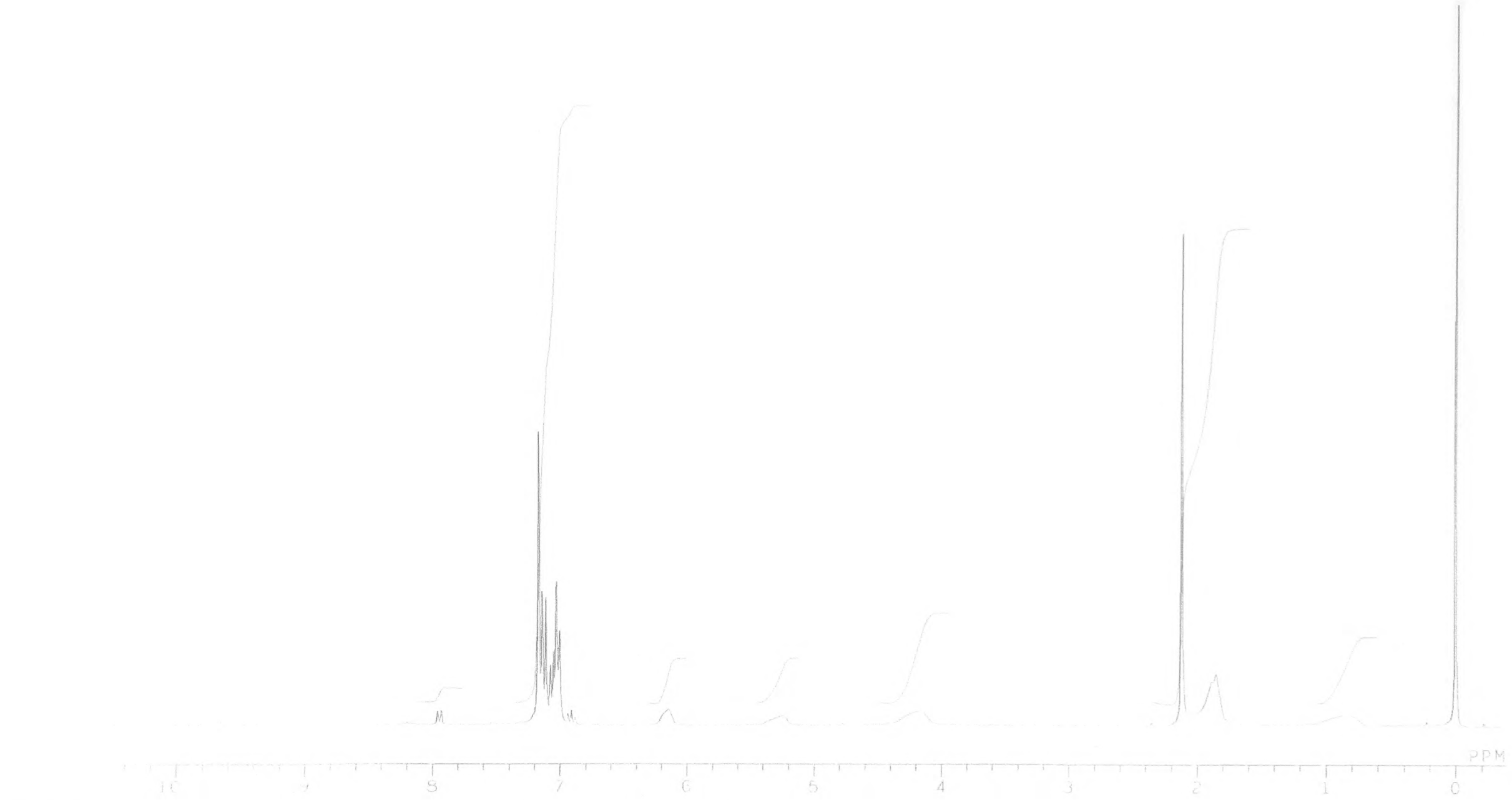

Figure 3.9.5: ^{1}H NMR spectrum of the polymer of the copolymerisation of 3-(trimethoxysilyl) propyl methacrylate with NIPAM.

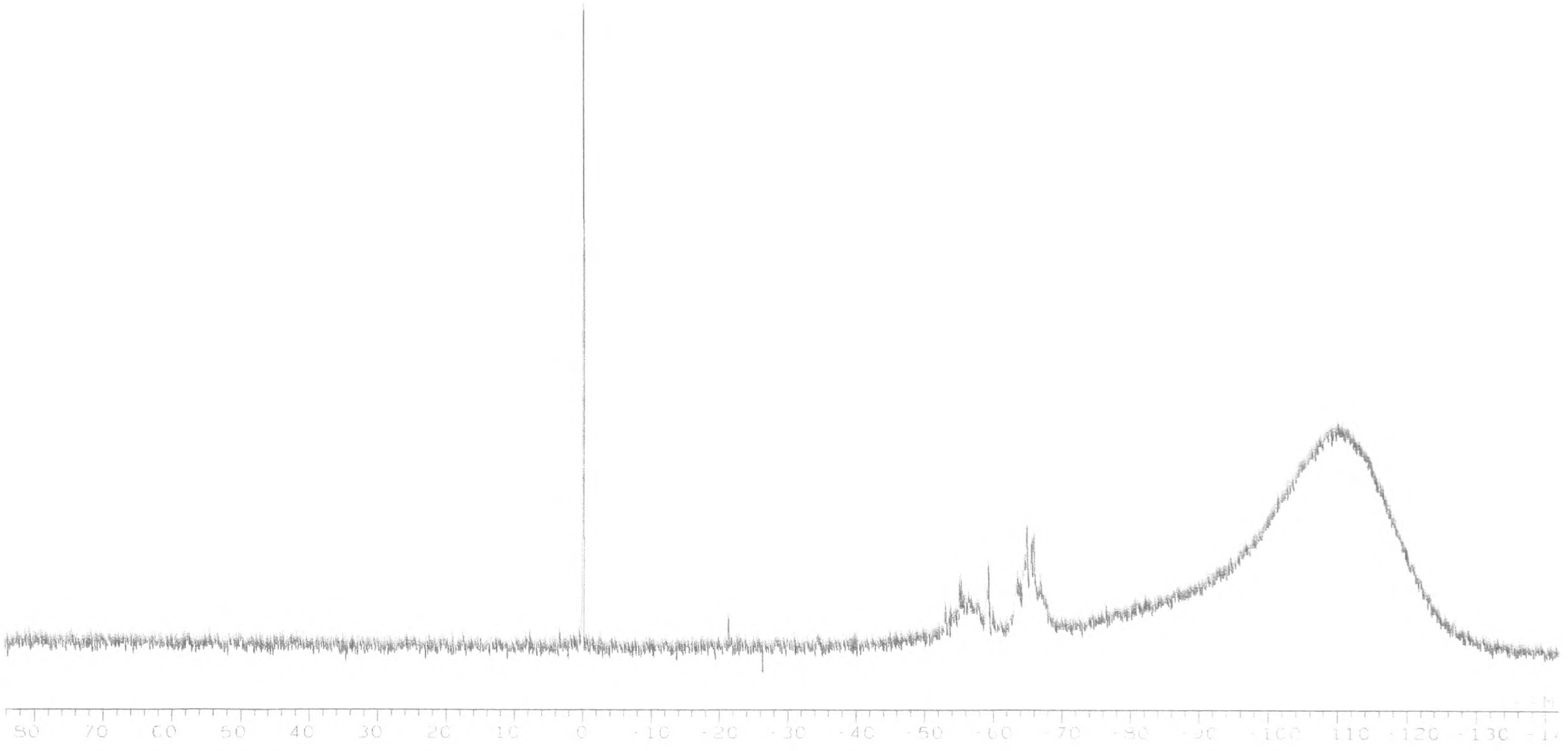

Figure 3.9.6: ^{29}Si NMR spectrum of the polymer of the copolymerisation of 3-(trimethoxysilyl) propyl methacrylate with NIPAM.

3.10 VINYL CONTAINING LATEXES

A series of vinyltrimethoxysilane-styrene co-polymer latexes having vinyltrimethoxysilane to styrene ratios of 10-90 wt% were prepared via a free radical

The reaction of vinyltrimethoxysilane with styrene under the reaction conditions employed could give three different types of product:

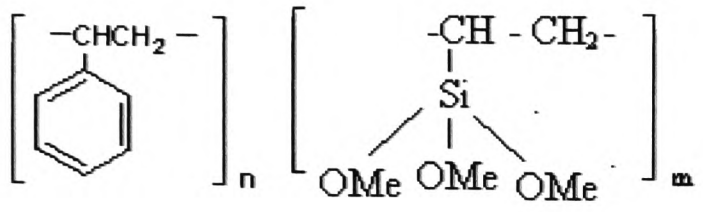

[1]

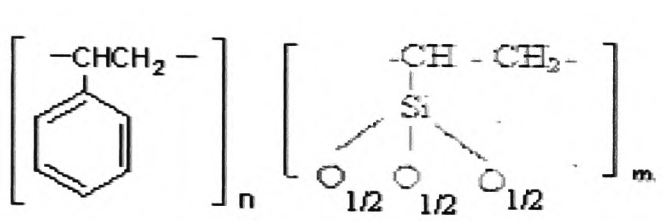

[2]

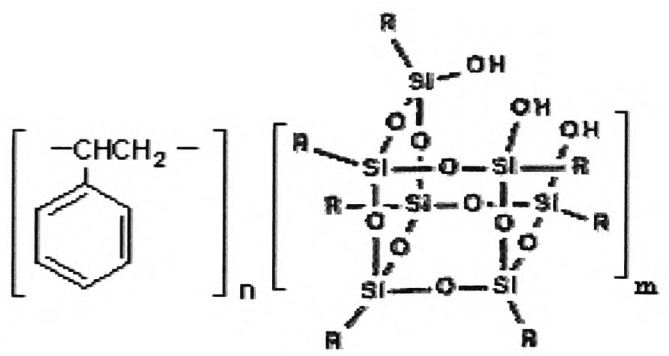

[3]

where R = -CH-CH_2-

Elemental analysis, infrared analysis, X-ray analysis, ^{13}C, ^{1}H, ^{29}Si NMR analysis, light scattering and transmission electron microscopy (TEM) were performed.

3.10.1 ELEMENTAL ANALYSIS

To confirm which of these structures, **[1]**, **[2]** or **[3]** was formed in the experiment, CHN analysis was performed. The results from the analysis of all the samples are summarized in **Table 3.10.1** as well as the calculated values assuming that **[1]**, **[2]** and **[3]** had been formed.

It is clear from looking at the **Table 3.10.1** the results are inconclusive. It is most likely to have created one compound, probably **[2]** or we can have a combination of two or three different compounds at different ratios. From the elemental analysis we can see that the 10%, 20%, 40% and 50% compositions give favor to the **[2]** structure unlike the 30%, 60%, 80% and 90% compositions which support **[1]** structure. Only the 70% composition give preferentiality to the **[3]** structure. As Feher explained in his paper [2] there can be a ratio of different compounds but as the time goes there can be only one predominant compound, and that can be **[3]** because of the open OH groups which can react easily and create a chain of new polymers.

Table 3.10.1: CHN results of all the different vinytrimethoxysilane:styrene compositions (%) and the expected values of **[1]**, **[2]** and **[3]**.

Samples			**10%**	**20%**	**30%**	**40%**	**50%**	**60%**	**70%**	**80%**	**90%**
Carbon	Value Found %		88.45	83.67	72.97	75.12	72.90	56.86	53.98	43.27	31.72
	Calculated %	**[1]**	86.12	79.92	73.73	67.54	61.35	55.15	48.96	42.77	36.57
		[2]	87.13	83.67	76.78	71.60	66.42	61.25	56.07	50.89	45.72
		[3]	86.56	80.82	75.07	69.32	63.58	57.83	52.08	46.33	40.59
Hydrogen	Value Found %		7.55	7.27	6.73	6.99	6.82	5.69	5.79	5.00	4.29
	Calculated %	**[1]**	7.30	6.91	6.52	6.13	5.74	5.36	4.97	4.58	4.19
		[2]	7.73	7.77	7.82	7.86	7.90	7.94	7.98	8.03	8.07
		[3]	7.29	6.90	6.50	6.10	5.71	5.31	4.92	4.59	4.13

3.10.2 INFRARED ANALYSIS

Infrared analysis was performed on the latexes prepared with different vinyltrimethoxysilane:styrene ratios and changes in the spectra can be seen. As the percentage of vinyltrimethoxysilane increases for the preparation of the samples and the amount of styrene decreases, in the infrared spectra we can notice the appearance of an adsorption peak at 3400 cm^{-1}. This peak indicates a Si-OH bond has been created from the reaction as the vinyltrimethoxysilane increases over styrene. Also a peak at 3650 cm^{-1} has slowly disappear explaining that the free OH has reacted with something, most possibly the Si giving the adsorption peak at 3400cm^{-1}. Another difference is at the range of around 1030 cm^{-1}. Looking the infrared spectrum of 10% composition latex, the peak at 1029 cm^{-1} is a sharp peak indicating the appearance of a Si-O-R bond. Slowly, as the vinyltrimethoxysilane:styrene ratio widens, we see that peak broadens and becomes less distinct. It seems there is a bond breaking down but is not completed perhaps because the time of the reaction was very short.

Other important peaks appear in the spectra can be seen in **Table 3.10.2**.

Figure 3.10.1 and **Figure 3.10.2** gives two examples of the vinyl containing latex at 10% composition and 80% composition. The rest of the infrared spectra can be seen in Appendix.

Table 3.10.2: Important infrared frequencies of the vinyl containing latexes.

Frequency (cm^{-1})	Assignments
~3000	C-H stretching
2400	Si-H (strong)
1600	C=C stretching
1450-1490	Si-C (strong & sharp)
1215-1070	=C-O-C stretching
960-815	$CH=CH_2$
750-630	C-H bending

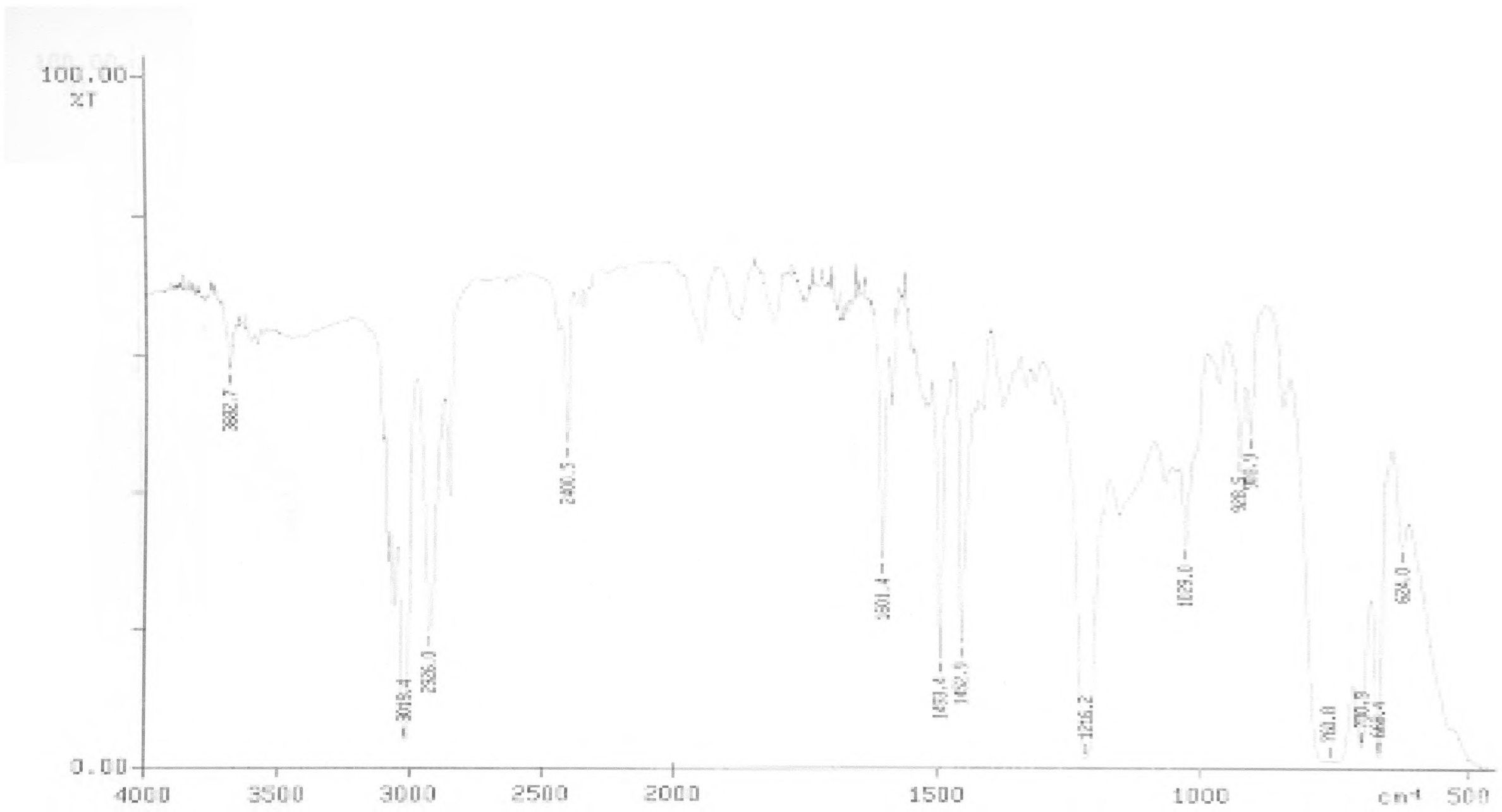

Figure 3.10.1: Infrared spectrum of the 10% composition of the vinyl-containing latex.

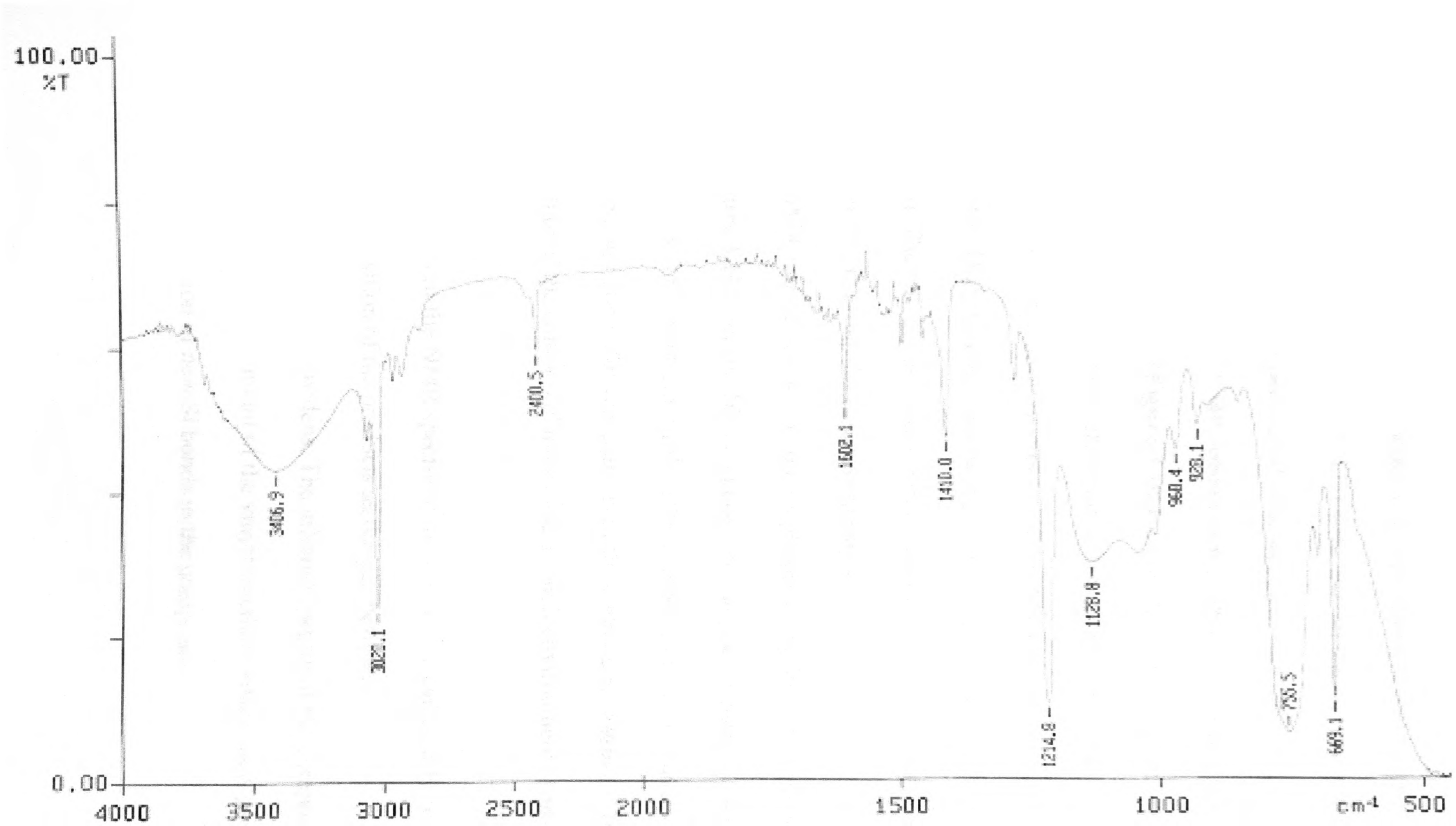

Figure 3.10.2: Infrared spectrum of the 80% composition of the vinyl-containing latex.

3.10.3 NUCLEAR MAGNETIC RESONANCE: ^{13}C AND ^{29}Si NMR

Nuclear magnetic resonance spectroscopy is a very effective tool for the study of polymer structure, both in solution and in solid state. For all the samples prepared a solid state ^{13}C and ^{29}Si NMR was performed. The samples were white, very powdery.

From the two examples of ^{13}C NMR spectra of the 10% composition **(Figure 3.10.3)** and the 90% composition **(Figure 3.10.4)** of the latexes we can clearly see the differences between the two spectra. A chemical shift at 50ppm has almost disappeared on the 90% composition whereas in the 10% composition is one of the major chemical shifts. That chemical shift at that point corresponds to a C-O bond (area of 40-80ppm). The two big chemical shifts at around 150 ppm on both spectra are because of an aromatic group for example the styrene.

Also ^{29}Si NMR was performed on the vinyl containing latexes. Two examples can be seen in **Figure 3.10.5** for the 10% composition latex and **Figure 3.10.6** for the 90% composition latex. The spectrum for the 10% composition is obvious a very poor spectrum due to the glass effect due the analysis of the compound. **Figure 3.10.6** gives a clearer picture of the compound indicating a T unit environment at around -60ppm.

From the analysis of the NMR spectra of the latexes we can clearly see the difference on the composition of the products as the gap between vinytrimethoxysilane:styrene ratio widens. The infrared spectra of the compounds conclude that as we increase the amount of the vinyltriinethoxysilane, new peaks appear indicating the creation of new Si bonds in the compound.

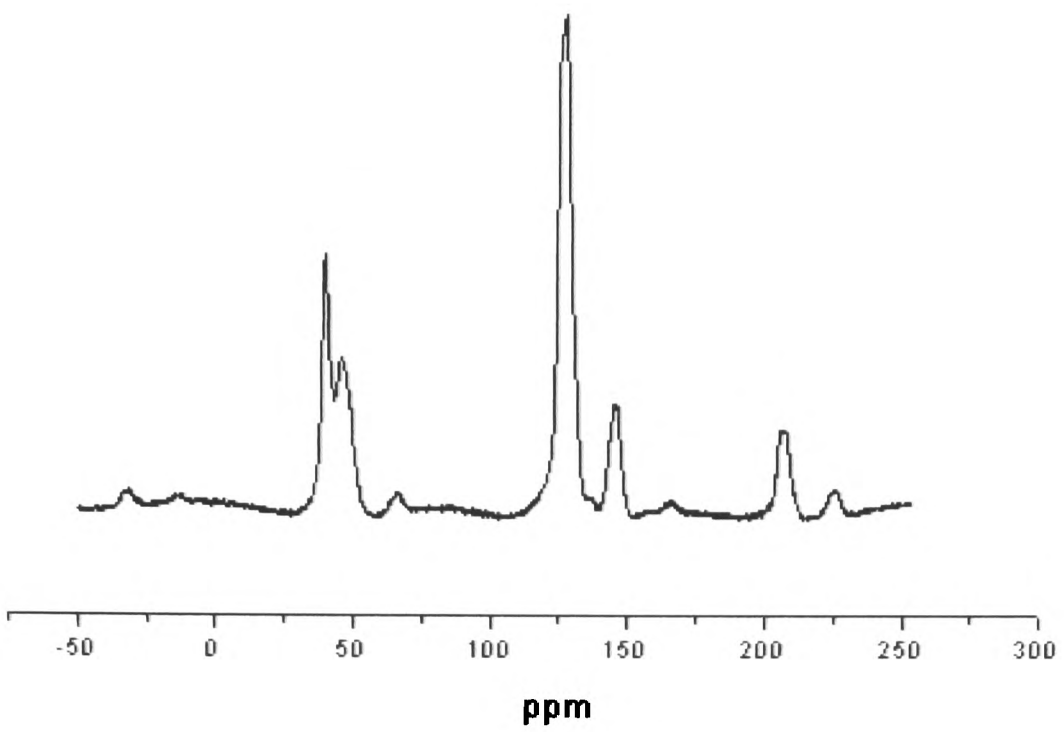

Figure 3.10.3: solid-state ^{13}C analysis of the 10% composition latex.

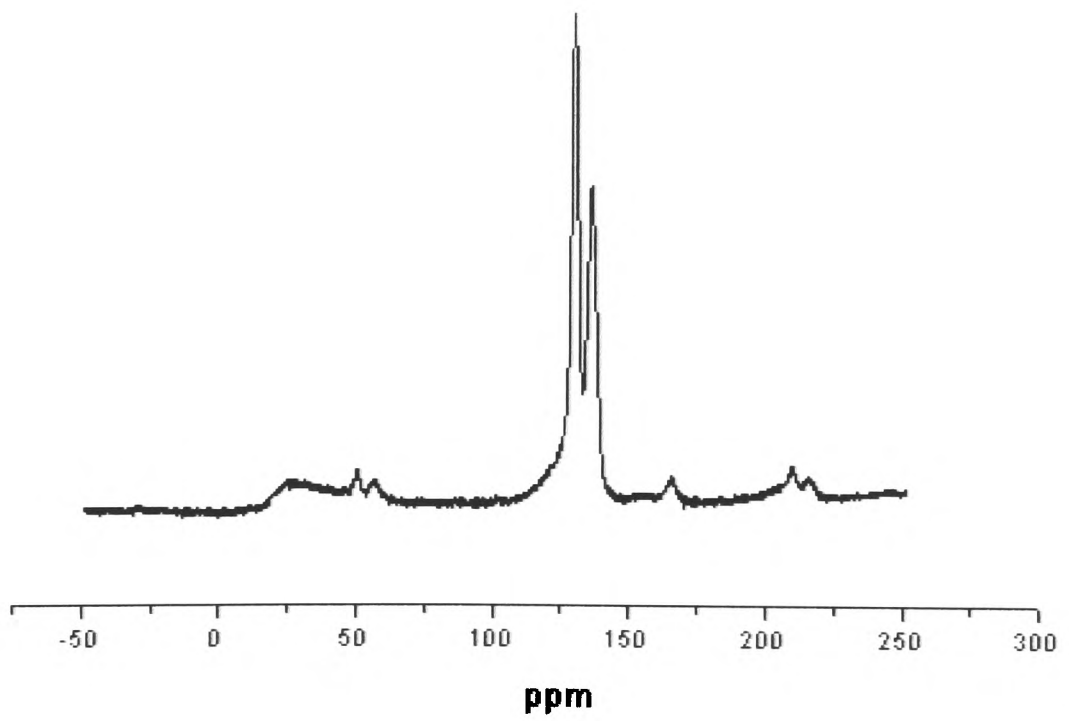

Figure 3.10.4: solid-state ^{13}C analysis of the 90% composition latex.

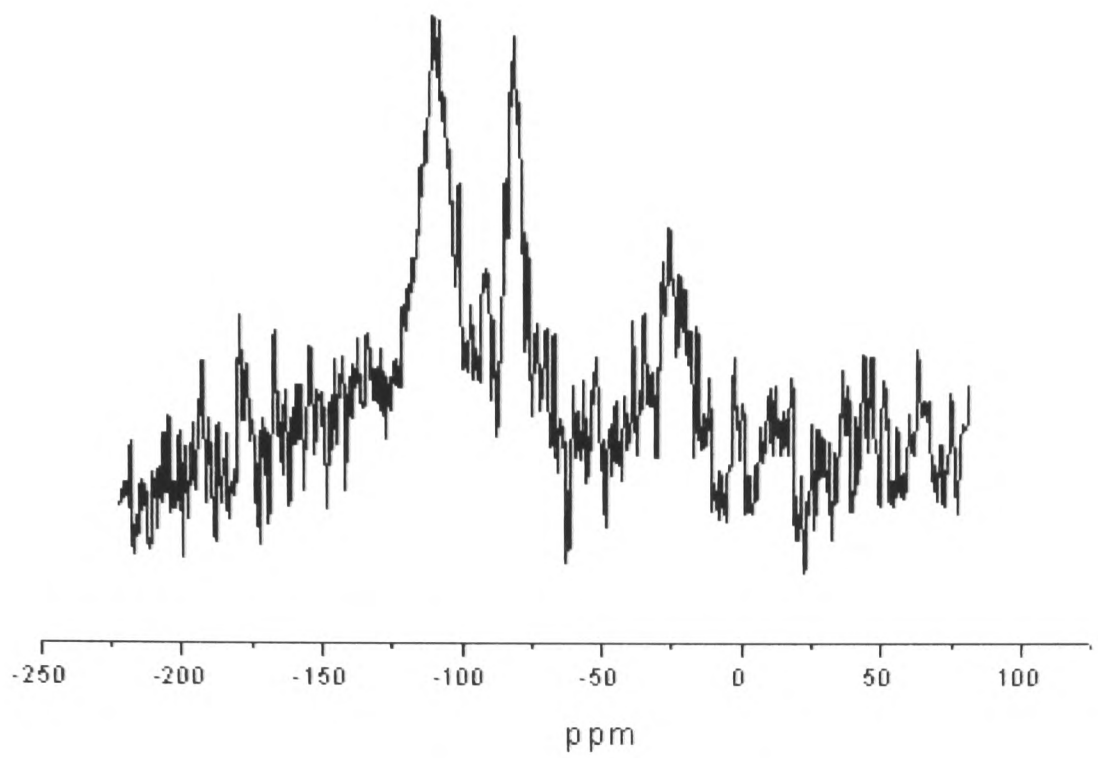

Figure 3.10.5: solid-state ^{29}Si analysis of the 10% composition latex.

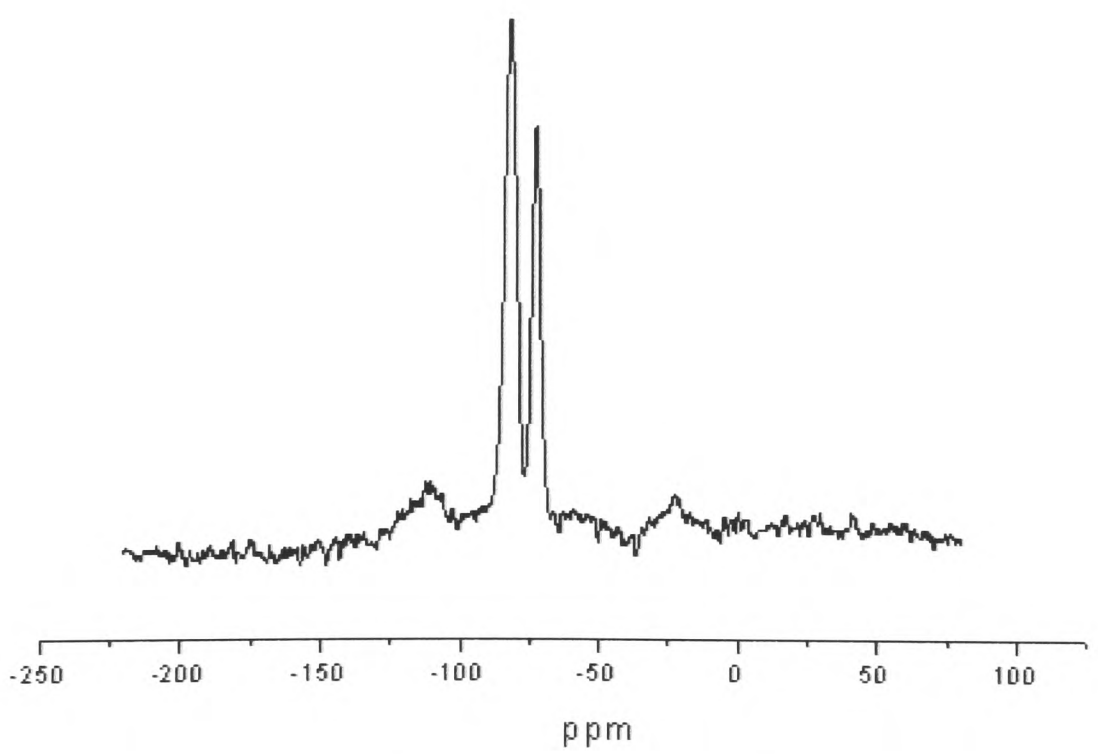

Figure 3.10.6: solid-state ^{29}Si analysis of the 90% composition latex.

3.10.4 LIGHT SCATTERING ANALYSIS

Light scattering techniques are used to the study of polymers because of the large size of such molecules. The hydrodynamic particle size (nm) and zeta potential of the vinyltrimethoxysilane: styrene latex particles were measured. **Table 3.10.3** summarizes these results.

Table 3.10.3: Light scattering results of the vinyl containing latexes

% composition	Zeta Potential (mV)	Particle Size (nm)
0 (no vinyltrimethoxysilane)	-38.7±0.4	673.5±8.0
10	-34.4±0.3	316.7±0.8
20	-33.1±0.3	274.4±0.8
30	-26.6±0.3	208.2±2.6
40	-30.4±0.1	996.2±4.7
50	-33.9±0.2	258.3±2.2
60	-28.7±0.5	188.4±1.1
70	-31.7±0.4	201.5±0.9
80	-27.0±0.5	274.8±3.3
90	-26.5±1.0	255.7±2.0

These values are shown graphically below, at **Figure 3.10.7** representing the % composition of the latexes versus the zeta potential measurements and **Figure 3.10.8** showing the % composition of the latexes versus the particle size measurements. There is no apparent increase or decrease on the zeta potential values or the size particles of the latexes. More or less the values are the same, suggesting that the addition of vinyltrimethoxysilane in the styrene latex has not affected its size. A simple explanation is that during the reaction the styrene surrounds the silicate polymer and any extra addition of the vinyltrimethoxysilane does not react with the stryrene to increase the particle size of the latex. However, the 40% composition latex appears to be anomalous probably due to a error in the zetalizer, which show to aggregate during the analysis.

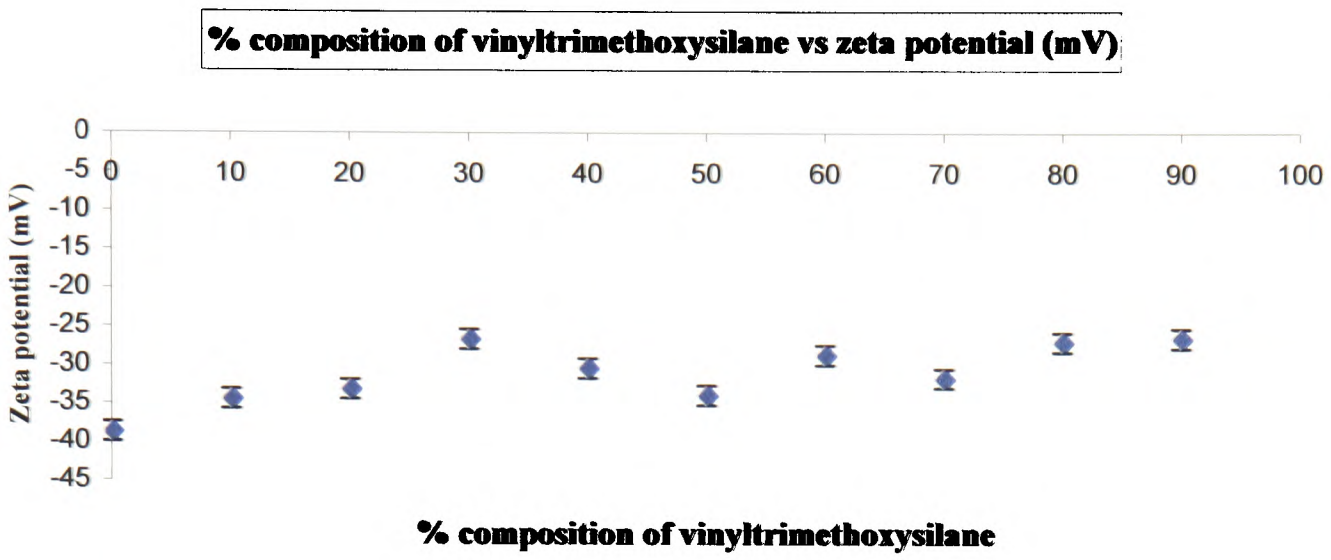

Figure 3.10.7: Graph of % composition of vinyltrimethoxysilane versus zeta potential (mV)

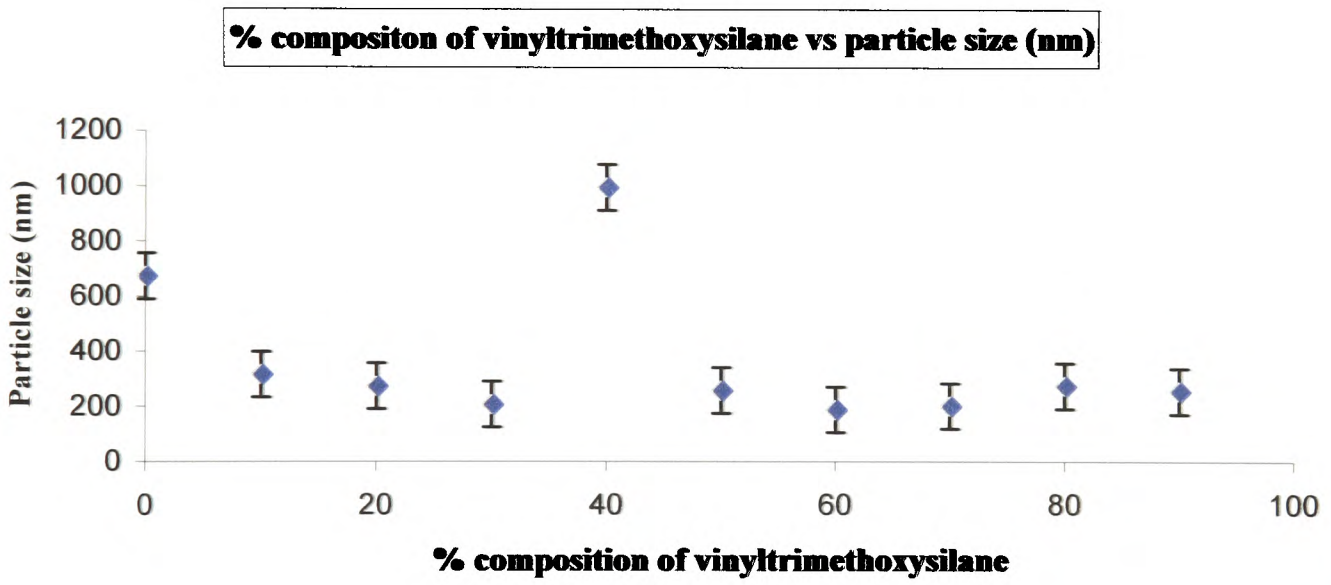

Figure 3.10.8: Graph of % composition of vinyltrimethoxysilane versus particle size (nm)

3.10.5 SCANNING ELECTRON MICROSCOPY (SEM) ANALYSIS

Scanning Electron Microscopy (SEM) is a very effective technique for the study of polymer morphology. The table below **(Table 3.10.4)** summarizes the particle sizes found from the SEM analysis.

Table 3.10.4: Particle size measurements from the SEM analysis

% composition	Particle size measurement taken from SEM (nm)
10	250
20	40-180
30	260 and some 160
40	60-200
50	80-200
60	odd shapes 60-200
70	100-160
80	70-100
90	4 μm-20 nm

Below is a diagram of the comparison between the particle size results taken from the light scattering analysis and the results from the SEM measurements.

It can be seen that there is no apparent difference between the two measurements.

Figure 3.10.9 and **Figure 3.10.10** gives the SEM micrographs of the 20% composition vinyl-containing latexes and the 60% composition.

Comparison of the particle size measurements using light scattering and particle sizes using SEM measurements.

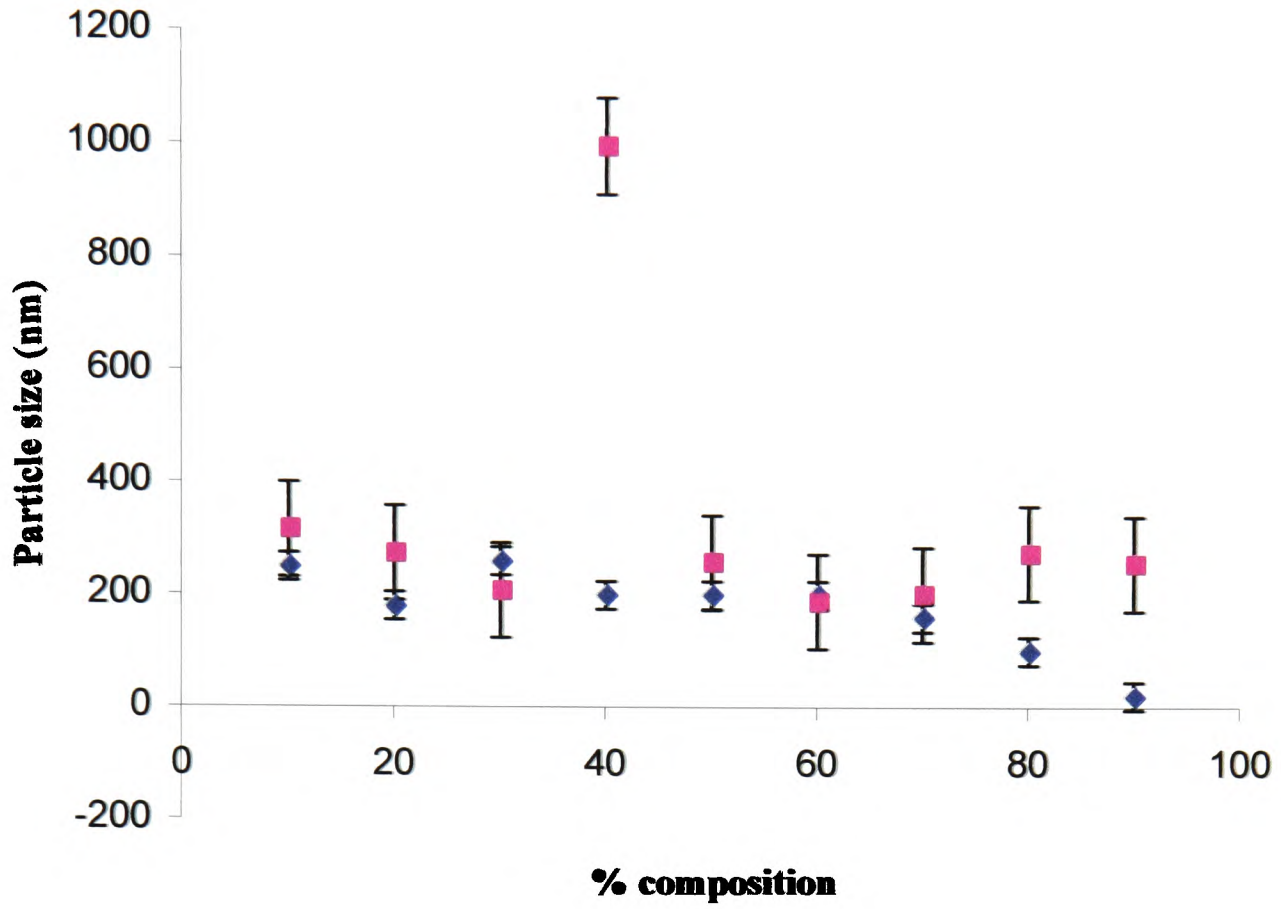

The results have indicated that the most favourable structure of the latex can be **[3]**. Unfortunately not all the results from the analysis performed were suggesting that e.g. the CHN analysis was suggesting that the structural presentation of the latex could be **[2]**. Feher had actually suggested that this type of structure is more possible to appear comparing to the other two.

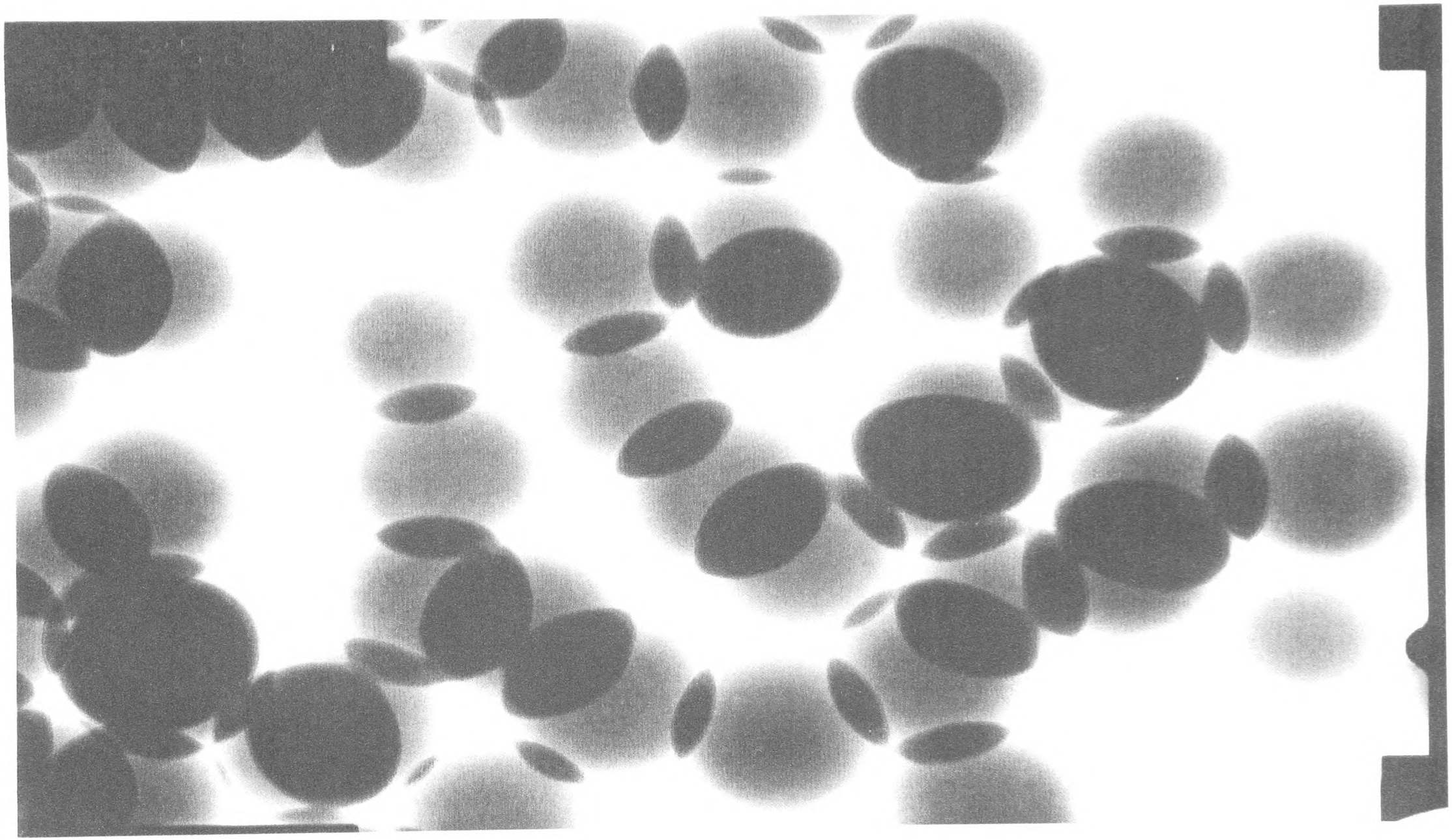

Figure 3.10.9: SEM micrograph of 20% composition latex.

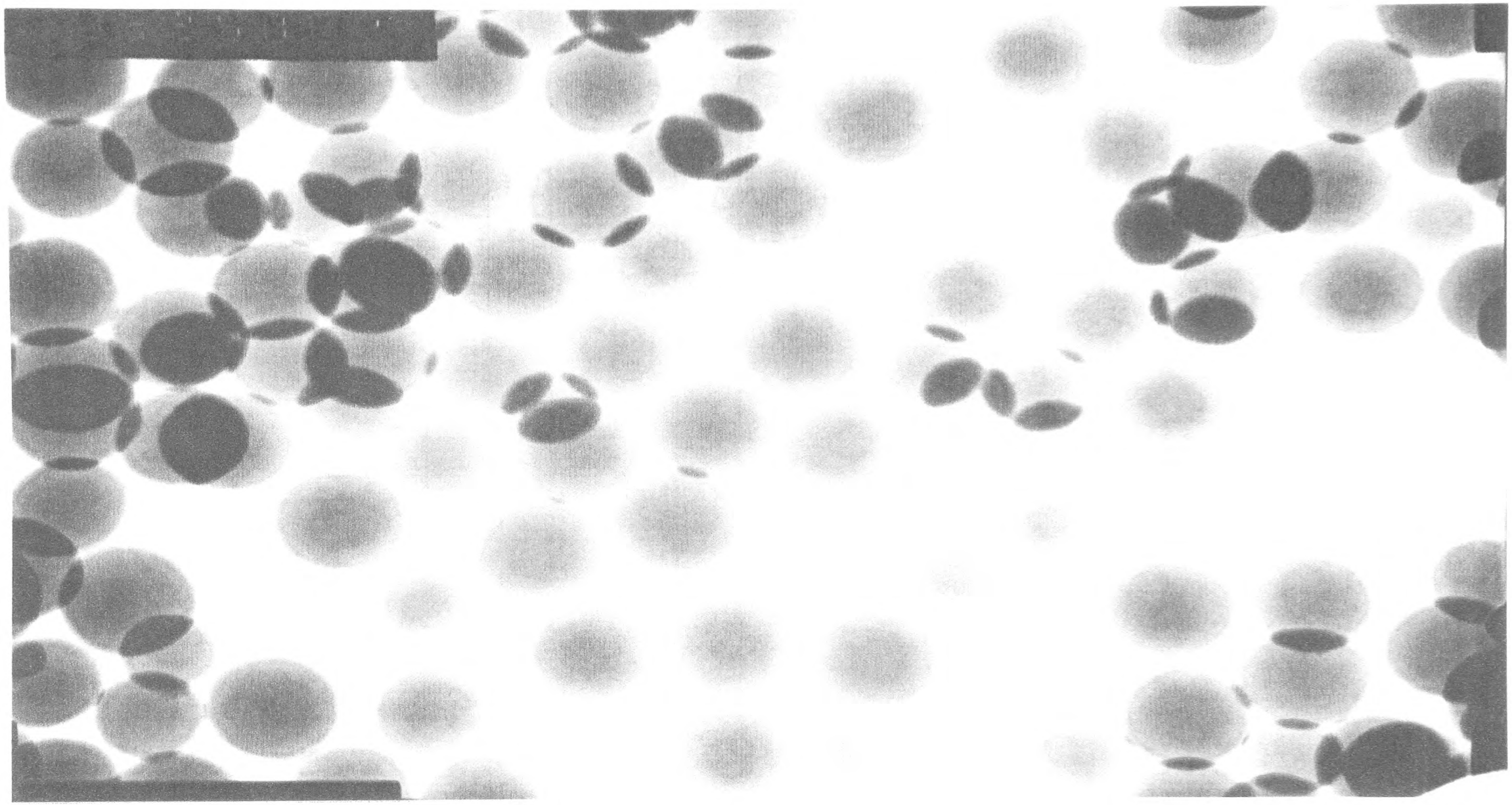

Figure 3.10.10: SEM micrograph of 80% composition latex.

3.11 ANALYSIS OF ORGANICALLY MODIFIED SILICATES

Mesostructured silica was prepared under acid conditions with tetraethoxysilane (TEOS) as the silica precursor and cetyltrimethylammonium bromide (CTAB) as the structure directing agent. A synthesis mixture of composition 2.2TEOS:1.lCTAB:75HCI:1000H_2O gave a well ordered material with a range of different structures [146]. Vinyltrimethoxysilane was added at different values to give organically modified silicas.

Table 3.11.1 summarizes the experiments performed with the relevant amounts used.

Table 3.11.1: TEOS:Vinyltrimethoxysilane:CTAB:HCI:H_2O ratios used for this experiment.

Mole ratio TEOS:Vinyltrimethoxysilane:CTAB:HCl:H_20	**Sample**
2.2: 0.0: 1.1: 75: 1000	EK69
2.2: 0.09: 1.1: 75: 1000	EK78
2.2: 0.16: 1.1: 75: 1000	EK79
2.0: 0.25: 1.1: 75: 1000	EK80
2.0: 0.09: 1.1: 75: 1000	EK81
2.0: 0.09: 1.1: 45: 1000	EK82
2.1: 0.32: 1.2: 75: 1000	EK83
2.0: 0.29: 1.1: 45: 1000	EK84
2.0: 0.31: 1.2: 66: 1000	EK84

Before any treatment, infrared analysis all the samples was performed and comparing the spectrum of EK69 with the rest of the spectra we were hoping to see some distinguishing peaks as a result of vinyltrimethoxysilane. Unfortunately, there were no noticeable differences involving the product containing no vinyltrimethoxysilane and the rest prepared with different ratios of vinyltrimethoxysilane. This was not unexpected because of the low levels of incorporation of vinyltrimethoxysilane into the silica. The C-H vibrations at 3000cm^{-1} are due to the presence of the CTAB in the pore of the silica. For example, **Figure 3.11.1** and **Figure 3.11.2** are the infrared spectrum of EK69 and EK82 respectively.

X-ray analysis was also performed on the un-treated samples and the results showed that all samples were amorphous.

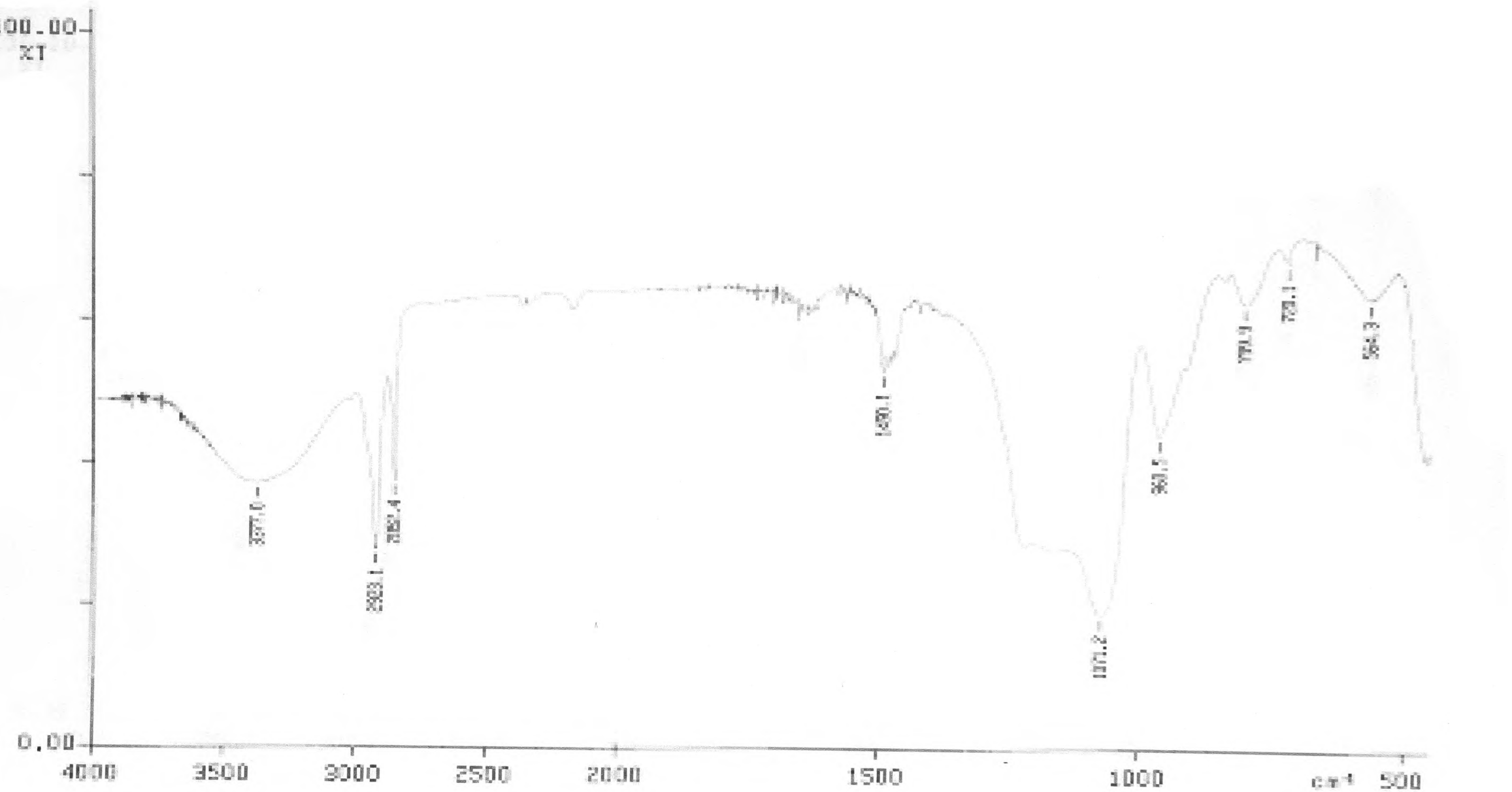

Figure 3.11.1: Infrared spectrum of EK69.

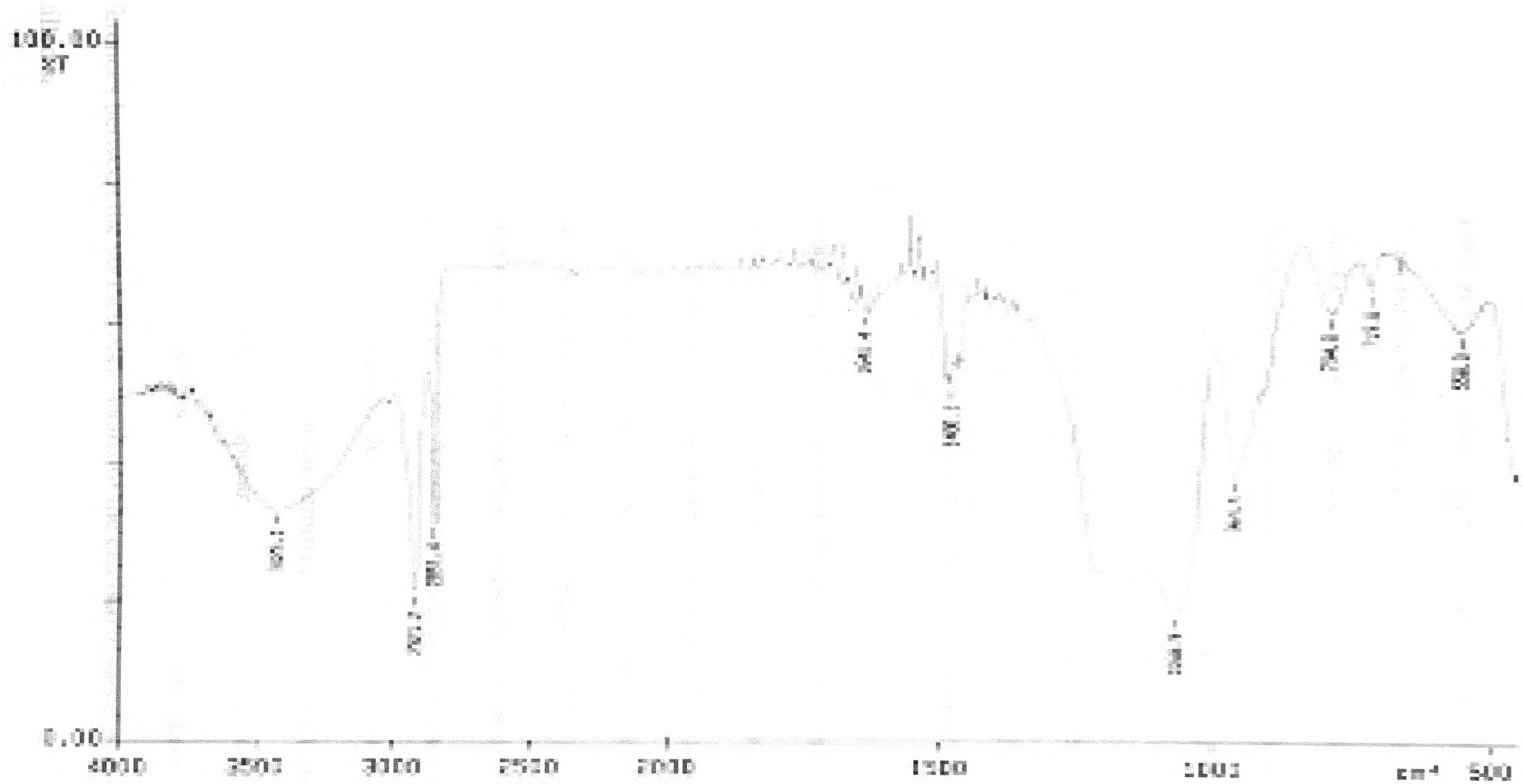

Figure 3.11.2: Infrared spectrum of EK82.

All the compounds were calcined in a tube furnace, under flowing nitrogen. Samples were heated from 1°C min^{-1} to 540°C maintaining that flowing nitrogen for 6 hours. The calcination at that high temperature should burn off all of the organic groups that probably surround the silica structure as well as the CTAB in the pores, giving a clearer image of the structure of the silica. The same compositions were treated by azeotropic distillation using toluene to remove the water from the pores such a way that the pore structure was maintained. CTAB should also have been removed at this point.

To see the differences between the samples treated under those two different methods, a 5-point surface area analysis was performed for all the compounds to obtain the surface area of the products. **Table 3.11.2** lists the results from the surface area analysis.

We can see the big surface area values of the samples after calcination, going up to 1600sq m/g. This value is very large surface compared to values obtained previously. These appear to be no correlation between the starting composition and the surface area. It should be noted however that it is likely that rates of stirring or other external factors may contribute to the products characteristics. Comparing the surface areas of the calcined samples and samples taken after azeotropic distillation there is a big difference on the pore size. Azeotropic distillation is used to remove any water from the samples without actually destroying the structure of the compound. The calcinations process is more used for the removal of the organics and any excess water. But after calcination the particles appear to be smaller which means the samples would have higher surface area. **Figure 3.11.3** is a graph showing the big differences between the surface area results of the calcinated samples and azeotropic distilled samples.

Table 3.11.2: Surface area results of the organically modified silicas treated under two different ways

Name of product	Surface area (sq m/g) after calcinations of the samples	Surface area (sq m/g) after azeotropic distillation
EK69	916.2	304.8
EK78	1356.8	518.5
EK79	1221.3	345.9
EK80	1291.1	477.8
EK81	1608.5	377.6
EK82	1601.7	43.4
EK83	1215.3	429.8
EK84	1486.9	512.0
EK85	1349.0	233.7

The results from the 5-point surface area analysis show that the calcined samples gave much higher surface area results comparing to the ones from the azeotropic distillation. That is to be expected since the breakage of the particles into smaller units gives a much higher surface area on the compound. **Figure 3.11.3** actually shows the big drop on the surface area results between the two compounds.

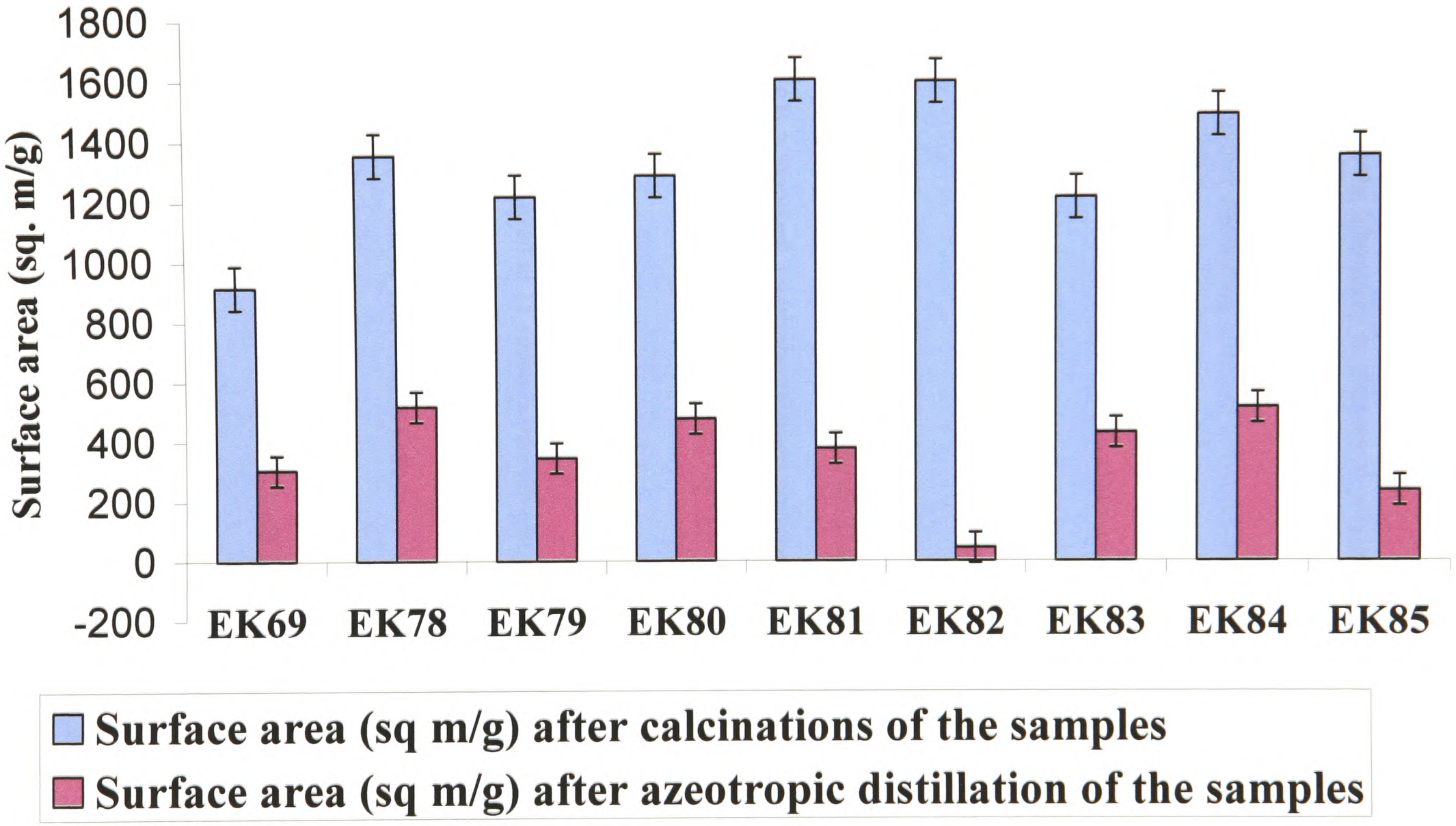

Figure 3.11.3 Surface area differences between the two different treated samples.

3.12 FIRE TESTS ON ORGANICALLY MODIFIED SILICATES

Seven samples were prepared and burned using cone calorimeter. Two of them were prepared in the laboratory as plaques of poly(methyl) methacrylate (PMMA) suitable for cone calorimetric experiments (Standard 1 and 2) and the rest were the PMMA copolymer containing different polymers that were purified by two different methods, one after calcinations and the other one after treating it under Dean and Stark extraction. The names of the samples that were given from me for reasons of simplicity are:

No. 1D = Standard 1 with the azeotropic distillation treated polymer-EK81

No. 1B = Standard 1 with the calcined polymer-EK81

No. 2D = Standard 2 with the azeotropic distillation treated polymer-EK82

No. 2AB = Standard 2 with the calcined polymer (Run A)-EK82

No. 2BB = Standard 2 with the calcined polymer (Run B)-EK82

For the Standard 1 sample, clear in colour, there was some white smoke before ignition, which occurred at 15 seconds into the test. After ignition the sample burnt to give black smoke and a strong yellow flame. There was a little intumescence of about 10mm. The sample then continued to burn until flaming out at 525 seconds and then smouldered until the test was stopped after a further 2 minutes. There was no residue.

For the Standard 2 sample, clear in colour, there was some white smoke before ignition, which occurred at 12 seconds into the test. After ignition the sample burnt to give black smoke and a strong yellow flame. There was a little intumescence of about

l0mm. The sample then continued to burn until flaming out at 498 seconds and then smouldered until the test was stopped after a further 2 minutes. There was no residue.

For the No. 1D sample, clear in colour, there was some white smoke before ignition, which occurred at 13 seconds into the test. After ignition the sample burnt to give black smoke and a strong yellow flame. There was no intumescence. The sample then continued to bum until flaming out at 809 seconds and then smouldered until the test was stopped after a further 2 minutes. The residue consisted of a thin layer of light grey char.

For the No.1B sample, clear in colour, there was some white smoke before ignition, which occurred at 8 seconds into the test. After ignition the sample burnt to give black smoke and a strong yellow flame. There was no intumescence. The sample then continued to burn until flaming out at 883 seconds and then smouldered until the test was stopped after a further 2 minutes. The residue consisted of a thin layer of light grey char.

For the No.2D sample, clear in colour, there was some white smoke before ignition, which occurred at 11 seconds into the test. After ignition the sample burnt to give black smoke and a strong yellow flame. There was no intumescence. The sample then continued to burn until flaming out at 925 seconds and then smouldered until the test was stopped after a further 2 minutes. The residue consisted of a thin layer of light grey char.

For the No.2AB sample, clear in colour, there was some white smoke before ignition, which occurred at 6 seconds into the test. After ignition the sample burnt to give black smoke and a strong yellow flame. There were no intumescences. The

sample then continued to bum until flaming out at 309 seconds and then smouldered until the test was stopped after a further 2 minutes. The residue consisted of a thin layer of light grey char.

For the No.2BB sample, clear in colour, there was some white smoke before ignition, which occurred at 6 seconds into the test. After ignition the sample burnt to give black smoke and a strong yellow flame. There were no intumescences. The sample then continued to burn until flaming out at 246 seconds and then smouldered until the test was stopped after a further 2 minutes. The residue consisted of a thin layer of light grey char.

The **Table 3.12.1** shows the cone calorimeter test results at heat release of 50 kWm^{-2}.

Fire Performance Index (FPI) relates to the time available for escape in a real fire. This parameter is defined as:

$$\text{FPI (in } m^2 \text{ s } kW^{-1}) = \frac{\text{ignition time}}{\text{peak rate of heat release}}$$

High values of FPI indicate less fire hazard. Obviously, the FPI values of these samples are extremely low, meaning there are great fire risks.

Table 3.12.1: Cone calorimeter test results at Heat Flux of 50 kWm^{-2}.

	Standard 1	Standard 2	No. 1D	No.1B	No. 2D	No.2AB	No. 2BB
Time Of Ignition (sec)	15.00	12.00	13.00	8.00	11.00	6.00	6.00
Peak Rate Of Heat Release (kWm^{-2})	886.73	690.41	714.24	749.74	718.01	630.61	641.50
Total Heat Release (MJm^{-2})	240.40	173.51	375.64	407.34	416.09	102.08	83.43
Fire Performance Index ($mskW^{-1}$)	0.02	0.02	0.02	0.01	0.02	0.01	0.01
Smoke Parameter ($MWkg^{-1}$)	132.13	95.17	105.98	117.75	105.00	85.16	89.75
Average from ignition to 3 minutes							
Rate Of Heat Release (kWm^{-2})	516.10	538.60	352.10	426.30	457.30	500.80	443.80
Effective Heat Combustion ($MJKg^{-1}$)	22.30	22.40	21.40	22.60	22.20	23.00	22.40
Specific Extinction Area (m^2Kg^{-1})	126.10	116.30	135.20	134.60	124.90	122.70	136.60
CO ($kg.kg^{-1}$)	0.01	0.01	0.01	0.01	0.01	0.01	0.01
CO_2 ($kg.kg^{-1}$)	1.64	1.72	1.63	1.65	1.65	1.76	1.80
Average for complete run							
Rate Of Heat Release (kWm^{-2})	471.56	356.76	472.42	464.95	454.70	336.49	347.16
Effective Heat Of Combustion ($MJkg^{-1}$)	23.52	23.37	22.37	23.29	22.73	23.24	22.54
Specific Extinction Areas (m^2kg^{-1})	149.01	137.84	148.38	157.05	146.24	135.05	139.91
CO ($kg.kg^{-1}$)	0.01	0.01	0.01	0.01	0.01	0.01	0.01
CO_2 ($kg.kg^{-1}$)	1.92	1.91	1.85	1.86	1.87	1.88	1.85

Looking at the average rate of heat release of complete run we can see that all seven samples are fully developed fire models **(Table 3.12.2).**

Table 3.12.2: Range of fire intensities

Heat Flux (kWm^{-2})	**Effect**
10-20	Poor repeatability; too close to minimum heat flux for pilot ignition.
25	Initial fire growth model. Good discrimination between non-FR materials. Recommended level for carpets and domestic upholstery
35	Developing fire model. General good repeatability. Recommended level for upholstery used in public and high risk areas.
50	Developed fire model. Good repeatability for FR materials.
75-100	Fully developed fire model; often encountered in very severe fires (e.g. aircraft fires). Little discrimination between many organic materials.

The results were disappointing for the fire tests of the organically modified silicates used as fire retardants. **Figure 3.12.1** and **Figure 3.12.2** shows the heat release of the Standard one and No. 2D. All seven samples cone calorimeter single run data can be seen in the Appendix.

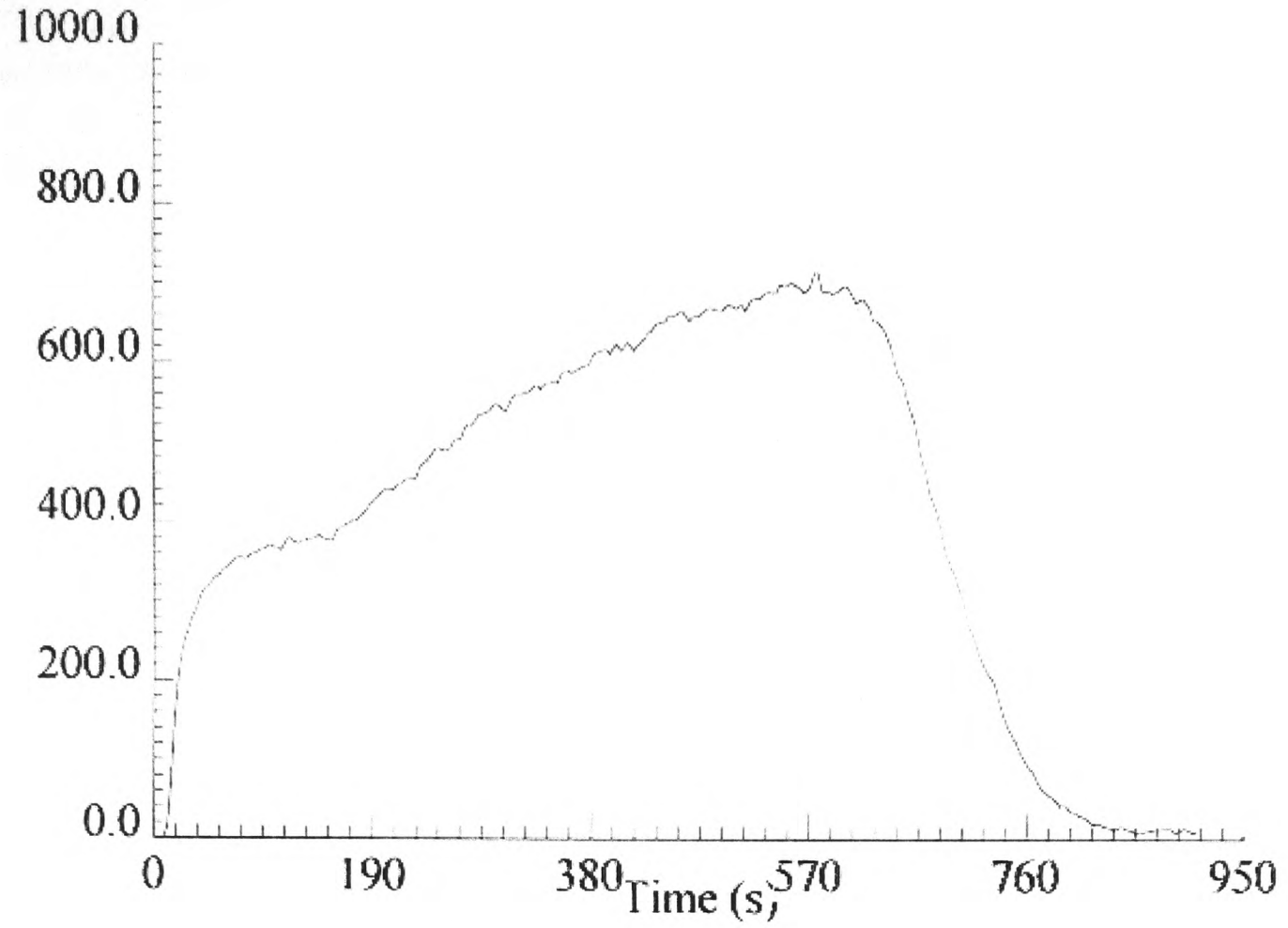

Figure 3.12.1: Heat release (kW/m^2) curve for Standard 1.

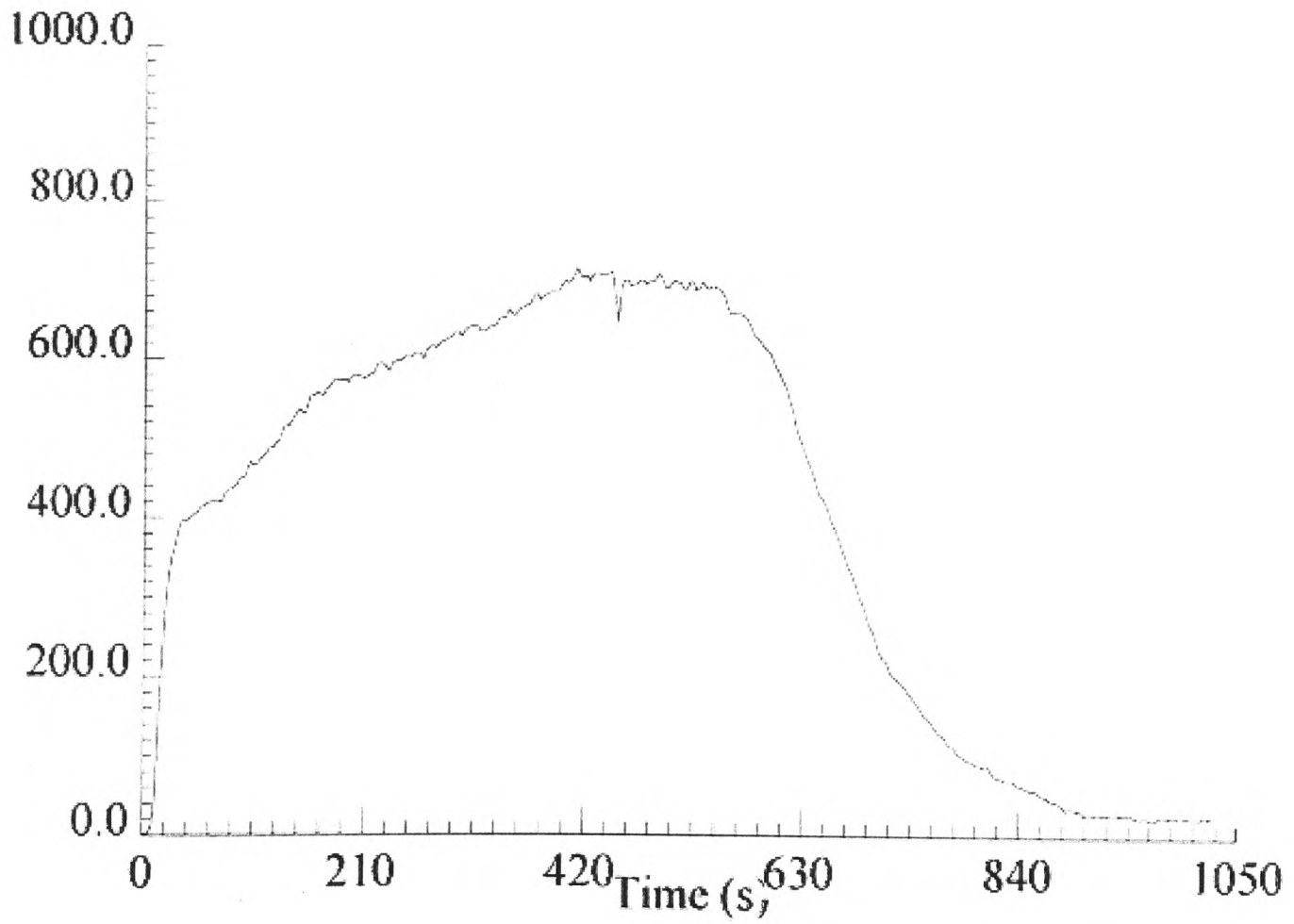

Figure 3.12.2: Heat release (kW/m^2) curve for No. 2D.

CHAPTER 4: - CONCLUSIONS

The main aim of this work was to synthesise and characterise a range of inorganic/organic hybrid polymers containing pendant vinyl groups and to study their uses in a range of applications, such as fire retandancy.

Organically modified silicas, containing pendant vinyl groups, have been successfully prepared and characterization by nitrogen adsorption and infrared and NMR spectroscopy. Surface areas of around $400m^2g^{-1}$ were obtained but the values depended on the amount of organic-containing silicon species added to the reaction mixture although no clear trend was apparent. Extremely large surface area silicas were obtained when these materials were calcined. Unfortunately neither the organically modified silica nor the silica itself enhanced the thermal stability of poly(methylmethacrylate).

A series of silica-containing co-polymer latexes were prepared and characterised. The samples had very narrow size distributions but there was no trend between zeta potential and composition, suggesting that the silica could form a core around which the styrene polymerised.

Some novel, new vinyl-containing compounds were prepared but although a range of analytical techniques were used for their study, their structures could not be confirmed.

4.1 SUGGESTIONS FOR FURTHER WORK

A major area which warrants further investigation is the application of silicas as fire retardants since it has been shown previously that in some circumstances silica has fire retardant properties. In this work no such properties were found but it should be noted that because of time constraining only two compositions were investigated., one containing vinyl groups and one where the organic groups have been calcined off. A more systematic study of organically-modified silicas in fire applications is needed. The effect of additive distribution in PMMA plaques and the consequent effect on heat release rates needs further investigation. This could be achieved by the manufacture of a template with adjustable groove regions **(Figure 4.1.1)**. The additive would be pushed under pressure to introduce it as a sheet.

Alternatively, a more homogeneous distribution of the additive could be achieved by micronising it before it is incorporated into the polymer.

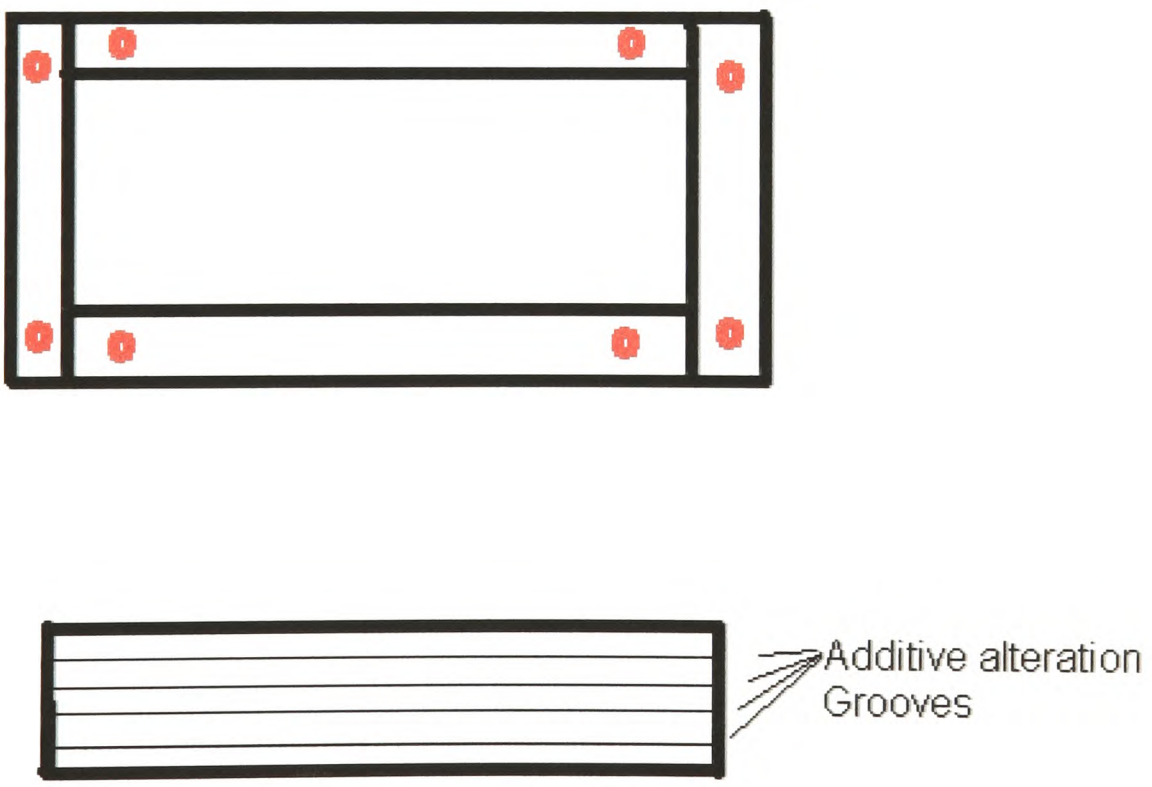

Figure 4.1.1: Template with adjustable additive groove.

A more detailed work could be done for the preparation of organically modified silicates. Different mole rations of TEOS:Vinyltrimethoxysilane:CTAB:HCl:H_2O could result to the synthesis of materials with different particle shape and size.

Further work also needs to be carried out in order to completely characterise materials obtained in this work.

CHAPTER 5: - REFERENCES

1. Ahmad H., Benee L. S., Snowden M. J., Thomas M. J. K., Vidgeon E. A., **2001,** *Colloids And Surfaces-A*, 186: 221-228

2. Chowdhry B. Z., Snowden M. J., Benee L. S., **2002**, *Langmuir*, 18: 6025-6030

3. Loy D. A., Shea K. J., **1995,** *Chem. Rev.*, 95, 1431-1442.

4. Noll W., *Chemistry and Technology of Silicone*, Academic Press, New York, **1968**

5. Brinker C. J., Scherer G. W., *The Physics And Chemistry Of Sol-Gel Processing*, Academic Press, San Diego, **1990**

6. Brook M. A., *Silicon In Organic, Organometallic And Polymer Chemistry*, John Wiley & Sons, Canada, **2000**

7. Schmidt H., Scholze H., Kaiser A., **1984**, *J. Non-Cryst Solids*, 63: 1-11

8. Mann S., Ozin G. A., **1996,** *Nature*, 382: 313-319

9. Mann S., **1995**, *J. Mater. Chem.*, 5: 935-946

10. Ou D. L., Seddon A. B., **1997**, *J. Non-Cryst Solids*, 210: 187-186

11. Ou D. L., Seddon A. B., **1997**, *J. Sol-Gel Sci. Technol.*, 8: 139-145

12. Schmidt H., **1985**, *J. Non-Cryst. Solids*, 100: 51-64

13. www.isc.fraunhofer.de

14. http://optoweb.fis.uniroma2.it/opto/index.html

15. Pierre A. C., *Introduction to Sol Gel Processing*, Kluwer Academic, Boston, **1998**

16. Collinson M. M., *Mikrochim. Acta*, **1998**, 129: 149-165

17. Vorotilov K. A., Vasiljen V. A., Sobolevsky M. V., Afanasyeve N. I., **1996**, *Thin Solids Films*, 288: 57-63

18. Hook R. J., **1996,** *J. Non-Cryst. Solids*, 195: 1-15

19. Bommel M. J., Bernards T. N. M, Boonstra A. H., **1991,** *J. Non-Cryst. Solids,* 128: 231-246

20. Collinson M. M., **2002**, *Trends Anal. Chem.*, 21: 30-38

21. www.sigma-aldrich.com

22. Feher F. J., *Chem. Comm.*, **1997**, 13: 1185-1186

23. Sellinger A, Laine R. M., **1996**, *Macromolecules*, 29; 2327-2330

24. Sellinger A., **1996**, *J. of Mater. Chem.*, 8: 1592-1995

25. Lichtenhan J. D., **1995**, *Comments Inorg. Chem.*, 17: 115-121

26. Tsuchida A., **1997,** *Macromolecules*, 30: 2818-2824

27. Feher F. J., Newman D. A., Walzer J., **1989**, *J. of Am. Soc.*, 111: 1741-1748

28. Haddad T. S., Lichtenhan J. D., **1996,** *Macromolecules,* 29: 7302-7304

29. Feher F. J., Newman D., **1990**, *J. of Am. Chem. Soc.*, 112: 1931-1936

30. Feher F. J., **1991**, *Organometallics*, 10: 2526-2528

31. Feher F. J., **1995**, *Organometallics*, 14: 2009-2017

32. Burns G. T., **1992**, *Chem. Mater.*, 4: 1313-1323

33. White D. A., **1987**, *Adv. Ceramic Mater.*, 2: 45-46

34. White D. A., **1987**, *Adv. Ceramic Mater.*, 2: 53-55

35. Kamiya K., **1986**, *J. Non-Cryst. Solids*, 83: 208-222

36. Laine R. M., *Ultrastructure Processing Of Advanced Ceramics*, Wiley, New York, **1988**

37. Feher F. J., **1992**, *J. of Am. Chem. Soc.*, 114: 9686-9688

38. Feher F. J., Weller, K. J., **1990**, *Organometallics*, 9: 2638-2640

39. Mantz R. A., **1996**, *Chem. Mater.*, 8: 1250-1255

40. Lee S., Makan S., Banaszak Holl M. M., McFeely F. R., **1994**, *J. of Am. Chem. Soc.*, 116: 11819-11826

41. Asua J. M., *Polymeric dispersions: principles and applications,* Kluwer Academic, Dordrecht, Boston, **1997**

42. Daniels E. S., Sudol E. D., El-Aasser M. S., *Polymer Latexes: Preparation, Characterisation and Applications*, ACS Symposium Series 492, American Chemical Society, Washington, DC, **1992**

43. Piirma I., *Emulsion Polymerisation,* Academic Press, New York, **1982**

44. Lovell P. A., El-Aasser M. S., *Emulsion polymerisation and emulsion polymers,* Wiley, Chichester, **1997**

45. Kim J., Ko J., Park J., Jun J., Chang I., Suh K., **2002**, *J. Appl. Polym. Sci.*, 85: 328-332

46. Snowden M. J., Chowdhry B. Z., **1995**, *Chemistry In Britain*, 943-945

47. Kurihara S., Minagoshi A., Nomaka T., **1996**, *J. Appl. Polym. Sci.*, 62: 153-159

48. http://www.chemfinder.com, *Chemical Structures*

49. Shaw D. J., *Introduction To Colloid And Surface Chemistry*, 3rd Edition, Butterworth, Oxford, Boston, **1992**

50. Solomons T. W. G., *Organic Chemistry*, John Wiley 7 Sons, 6th Edition, New York, **1996**

51. Brydson J. A., *Plastics Materials*, Butterworth-Heinemann, 5th Edition, Oxford, **1999**

52. Lyons J. W., *The Chemistry And Use Of Fire Retardants*, John Wiley & Sons, New York, **1970**

53. Aseeva M., Zaikov G., *Combustion Of Polymer Materials*, Carl Hanser Verlag, Munich, Vienna, New York, **1985**

54. http://www.sriconsulting.com

55. Ayen R. J., Iacobucci P. A., **1988**, *Rev. Chem. Eng.*, 5: 157-198

56. Gesser H. D., Goswami P. C., **1989**, *Chem. Rev.*, 89: 765-788

57. Pajock G. M., **1991**, *Appl. Catal.*, 72: 217-266

58. Fricke J., Emmerling A., **1992**, *Struct. Bond.*, 77: 37-87

59. Schneider M., Baiker A., **1995**, *Cat. Rev. - Sci. Eng.*, 37: 515-556

60. Hüsing N., Schubert U, **1998**, *Angewandte Chemie*, 110: 22-47; *Angewandte Chemie International Edition in English*, **1998**, 37: 22-45

61. Rolison D. R., Dunn B., **2001**, *J. Mater. Chem.*, 11: 963-980

62. Kresge C. T., Leonowicz M. E., Roth W. J., Vartuli J. C., Beck J. S., **1992**, *Nature*, 359: 710-712

63. Sanchez C., Ribot F., *New J. Chem.*, **1994**, 18: 1007–1047

64. Corriu R. J. P., Leclercq D., *Angew. Chem. Int. Ed.*, **1996,** 35: 1420–1436

65. Schubert U., Husing N., Lorenz A., **1995,** *Chem. Mater.*, 7: 2010–2027

66. Brinker J., Scherer G., *Sol-Gel Science: The Physics and Chemistry of Sol-Gel Processing*, Academic Press, New York, **1990**

67. Brinker C. J., **1988**, *J. Non-Cryst. Solids*, 100: 31–50

68. Schubert U., Hüsing N., Lorenz A., **1995**, *Chem. Mater.*, 7: 2010-2027

69. Raman N. K., Anderson M. T., Brinker C. J., **1996,** *Chem. Mater.*, 8: 1682-1701

70. Wen J., Wilkes G. L., **1996**, *Chem. Mater.*, 8: 1667-1681

71. Interrante L. V., Hampden-Smith M. J., *Chemistry of Advanced Materials, An Overview*, Wiley-VCH, New York, **1998**

72. Bescher E., Mackenzie J. D., *Hybrid Organic-Inorganic Sensors, Materials Sciences and Engineering*, Chap. 6, pages 145-154, **1998**

73. Collinson M. M., **1998**, *Mikrochim. Acta*, 129: 149–165

74. Collinson M. M., **2002,** *Trends in Analytical Chemistry,* 21: 30–38

75. Burkett S. L., Sims S. D., Mann S., **1996,** *Chem. Comm.*, 11: 1367-1368

76. Macquarrie D. J., **1996,** *Chem. Comm.*, 16: 1961-1962

77. Maschmeyer T., **1998,** *Curr. Opin. Solid State Mater. Sci.*, 3: 71-78

78. Stein A., Melde B. J., Schroden R. C., **2000,** *Adv. Mater.*, 12: 1403

79. Lindlar B., Lüchinger M., Röthlisberger A., Haouas M., Pirngruber G., Kogelbauer A., Prins R, **2002,** *J. Mater. Chem.*, 12: 528-533

80. Stein A., Melde B. J., Schroden R. C., **2000,** *Adv. Mater.*, 12: 1403

81. Morey M. S., Davidson A., Stucky G. D., **1998,** *J. Porous Mater.,* 5: 195-204

82. Alfredsson V., Anderson M. W., **1996,** *Chem. Mater.*, 8: 1141-1146

83. Clark J. H., Macquarrie D. J., **1998,** *Chem. Comm.*, 1367

84. Corma A., Garcia H., Navarro M. T., Palomares E. J., Rey F., **2000,** *Chem. Mater.*, 12: 3068-3072

85. Evans J., Zaki A. B., El-Sheikh M. Y., El-Safty S. A., **2000,** *J. Phys. Chem. - B*, 104: 10271-10281

86. Jaenicke S., Chuah G. K., Lin X. H., Hu X. C., **2000,** *Microporous Mesoporous Mater.*, 35-36: 143-153

87. Sorokin A. B., Tuel A., **2000,** *Catal. Today*, 57: 45-59

88. Yamamoto K., Tatsumi T., **2000,** *Chem. Lett.*, 6: 624-625

89. Ryoo R., Ko C. H., Kruk M., Antochshuk V., Jaroniec M. J., **2000,** *J. Phys. Chem. – B*, 104: 11465-11471

90. Jaenicke S., Chuah G. K., Lin X. H., Hu X. C., **2000,** *Microporous Mesoporous Mater.*, 35-36: 143-153

91. Choudary B. M., Lakshmi M. K., Sreekanth P., Bandopadhyay T., Figuera F., Tuel A., **1999,** *J. Mol. Catal. A: Chem.*, 142: 361-365

92. Cauvel A., Renard G., Brunel D., **1997**, *J. Org. Chem.*, 62: 749-751

93. Xuanhao L., Chuah G. K., Jaenicke S., **1999**, *J. Mol. Catal. A: Chem.*, 150: 287-294

94. Bossaert W. D., De Vos D. E., Van Rhijn W. M., Bullen J., Grobet P. J., Jacobs P. A., **1999**, *J. Catal.*, 182: 156-164

95. Wen J., Wilkes G. L., **1996**, *Chem. Mater.*, 8: 1667-1681

96. Edler K. J., Roser S. J., **2001**, *Int. Rev. Phys. Chem.*, 20: 387-466

97. Moller K., Bein T., **1998**, *Chem. Mater.*, 10: 2950-2963

98. Corma A., **1997**, *Chem. Rev.*, 97: 2373-2419

99. Lim M. H., Blanford C. F., Stein A., **1997**, *J. Am. Chem. Soc.*, 119: 4090-4091

100. Lim M. H., Stein A., **1999**, *Chem. Mater.*, 11: 3285-3295

101. Lin H. P., Yang L. Y., Mou C. Y., Liu S. B., Lee H. K., **2000**, *New J. Chem.*, 24: 253-255

102. Brown J., Richer R., Mercier L., **2000**, *Microporous Mesoporous Mater.*, 37: 41-48

103. Adachi M., Harada T., Harada M., **1999**, *Langmuir*, 15: 7097-7100

104. Feng X., Fryxell G. E., Wang L. Q., Kim A. Y., Liu J., Kemmer K. M., **1997**, *Science*, 276: 923-926

105. Liu A. M., Hidajat K., Kawi S., Zhao D. Y., **2000**, *Chem. Comm.*, 13: 1145-1146

106. Hall S. R., Fowler C. E., Lebeau B., Mann S., **1999**, *Chem. Comm.*, 19: 201-202

107. Diaz I., Marquez-Alvarez C., Mohino F., Perez-Pariente J., Sastre E. J., **2000**, *J. Catal.*, 193: 283-294

108. Margolese D., Melero J. A., Christiansen S. C., Chmelka B. F., Stucky G. D., **2000**, *Chem. Mater.*, 12: 2448-2459

109. Anwander R., Nagr I., Widenmeyer M., Engelhardt G., Groeger O., Palm C., Röser T., **2000**, *J. Phys. Chem. – B*, 104: 3532-3544

110. Anwander R., Palm C., Stelzer J., Groeger O., Engelhardt G., **1998**, *Stud. Surf. Sci. Catal.*, 117: 135

111. Baltes M., **1999**, *Langmuir*,15: 5841-5845

112. Ryoo R., Ko C. H., Kruk M., Antochshuk V., Jaroniec M., **2000**, *J. Phys. Chem.- B,* 104: 11465-11471

113. Kimura T., Saeki S., Sugahara Y., Kuroda K., **1999**, *Langmuir*, 15: 2794-2798

114. Lin H. P., Yang L. Y., Mou C. Y., Liu S. B., Lee H. K., **2000**, *New J. Chem.*, 24: 253-255

115. Antochshuk V., Jaroniec M., **2000**, *Chem. Mater.*, 12: 2496-2501

116. Jaroniec M., Sayari, A, *Nanoporous Materials III (Studies in Surface Science and Catalysis)*, Elsevier, Amsterdam, Boston, **2002**

117. Antochshuk V., Jaroniec M., **1999**, *Chem. Comm.*, 23: 2373-2374

118. Jaroniec C. P., Kruk M., Jaroniec M., Sayari A., **1998**, *J. Phys. Chem. – B*, 102: 5503-5510

119. Anwander R., Roesky R., **1997**, *J. Chem. Soc., Dalton Trans.*, 2: 137-138

120. Richer R., Mercier L., **1998**, *Chem. Comm.*, 16: 1775-1777

121. Joo J., Hyeon T., Hyeon-Lee J., **2000**, *Chem. Comm.*, 16: 1487-1488

122. Bhaumik A., Tatsumi T, **2000**, *J. Catal.*, 189: 31-39

123. Margolese D., Melero J. A., Christiansen S. C., Chmelka B. F., Stucky G. D., **2000**, *Chem. Mater.*, 12: 2448-2459

124. Brown J., Mercier L., Pinnavaia T, **1999**, *J. Chem. Comm.*, 1: 69-70

125. Bhaumik A., Tatsumi T., **2000**, *Catal. Lett.*, 66: 181-184

126. Anwander R., Nagl I., Widenmeyer M., Engelhardt G., Groeger O., Palm C., Röser T., **2000**, *J. Phys. Chem. – B*, 104: 3532-3544

127. Wood D. L., Rabinovich E. M., **1989**, *J. Non-Cryst. Solids*, 107: 199-211

128. Niznanski D, Rehspringer J. L., **1995**, *J. Non-Cryst. Solids*, 180: 191-196

129. Schraml-Marth M., Walther K. L., Wokaun A., Handy B. E., Baiker A., **1992**, *J. Non-Cryst. Solids*, 143: 92-100

130. Wen J., Wikes G. L., **1996**, *Chem. Mater.*, 8: 1667-1681

131. Sanchez C., Ribot F., **1994**, *New J. Chem.*, 18: 1007-1047

132. Corriu R. J. P., Leclercq D., *Angew. Chem. Int. Ed.*, **1996,** 35: 1420–1436

133. Schubert U., Husing N, Lorenz A. **1995**, *Chem. Mater.*, 7: 2010-2027

134. Walcarius A., Lüthi N., Blin J.-L., Su B.-L., Lamberts L., **1999**, *Electrochim. Acta*, 44: 4601

135. Lim M. H., Blanford C. F., Stein A., **1998**, *Chem. Mater.*, 10: 467-470

136. Mercier L., Pinavaia T. J., **1999**, *Adv. Mater.*, 9: 500

137. Brown J., Mercier L., Pinnavaia T. J., **1999**, *Chem. Comm.*, 1: 69-70

138. Zhao X. S., Lu G. Q., **1998**, *J. Phys. Chem. – B*, 102: 1556-1561

139. Lim M. H., Stein A., **1999**, *Chem. Mater.*, 11, 3285-3295

140. Melde B. J., Holland H. T., Blanford C. F., Stein A., **1999**, *Chem. Mater.*, 11: 3302-3308

141. Macquarrie D. J., **1999**, *Green Chemistry*, 1: 195-198

142. Perrin D. D., Armarego W. L. F., Perrin D. R., *Purification of laboratory chemicals*, 2nd edition, Permagon Press, Oxford, New York, **1982**

143. Chan H. B. S., Budd, P. M., Naylor, T., **2000**, *J. Mater. Chem.*, 11: 951-957

APPENDIX

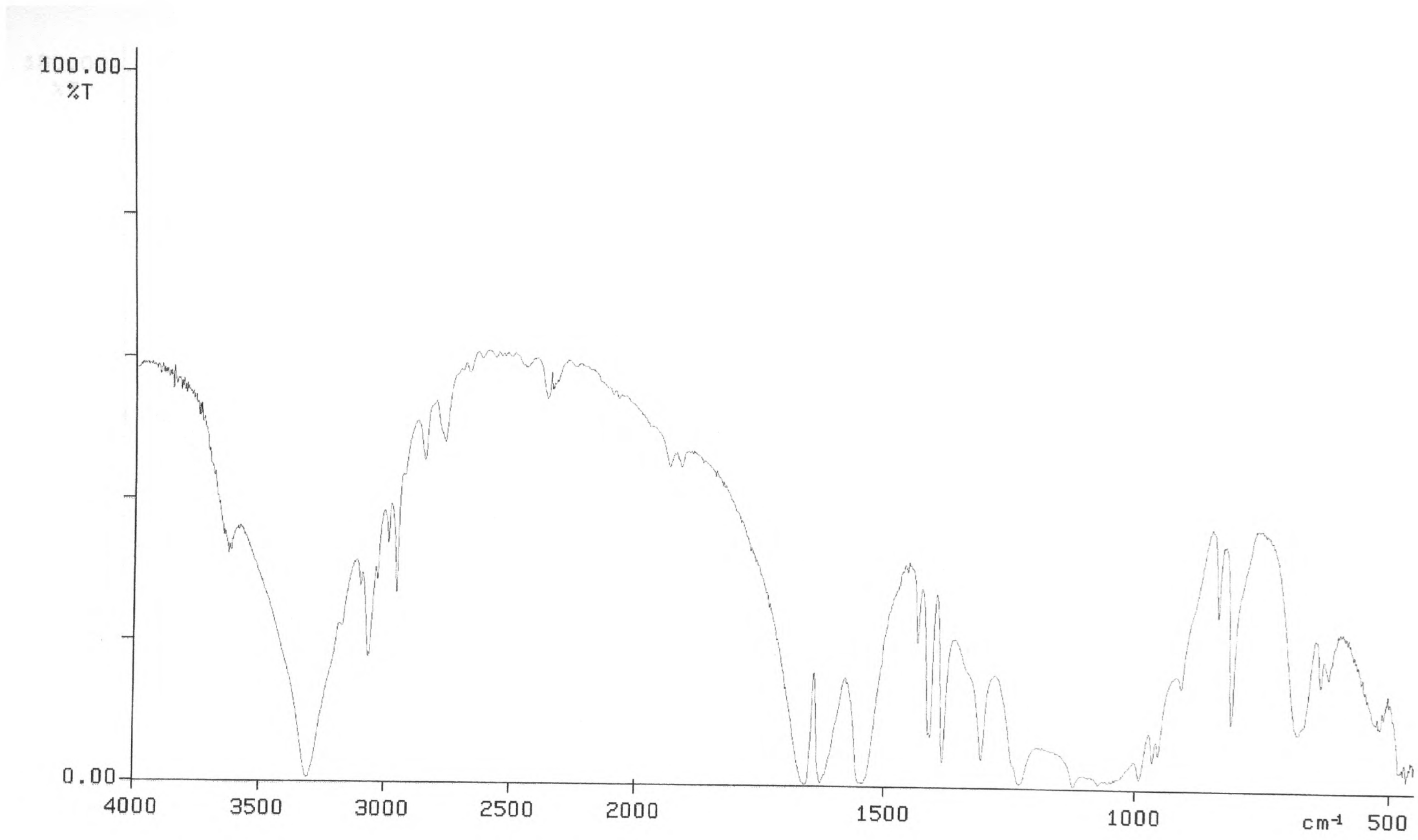

Infrared spectrum of K10 with NIPAM (2:1.5)

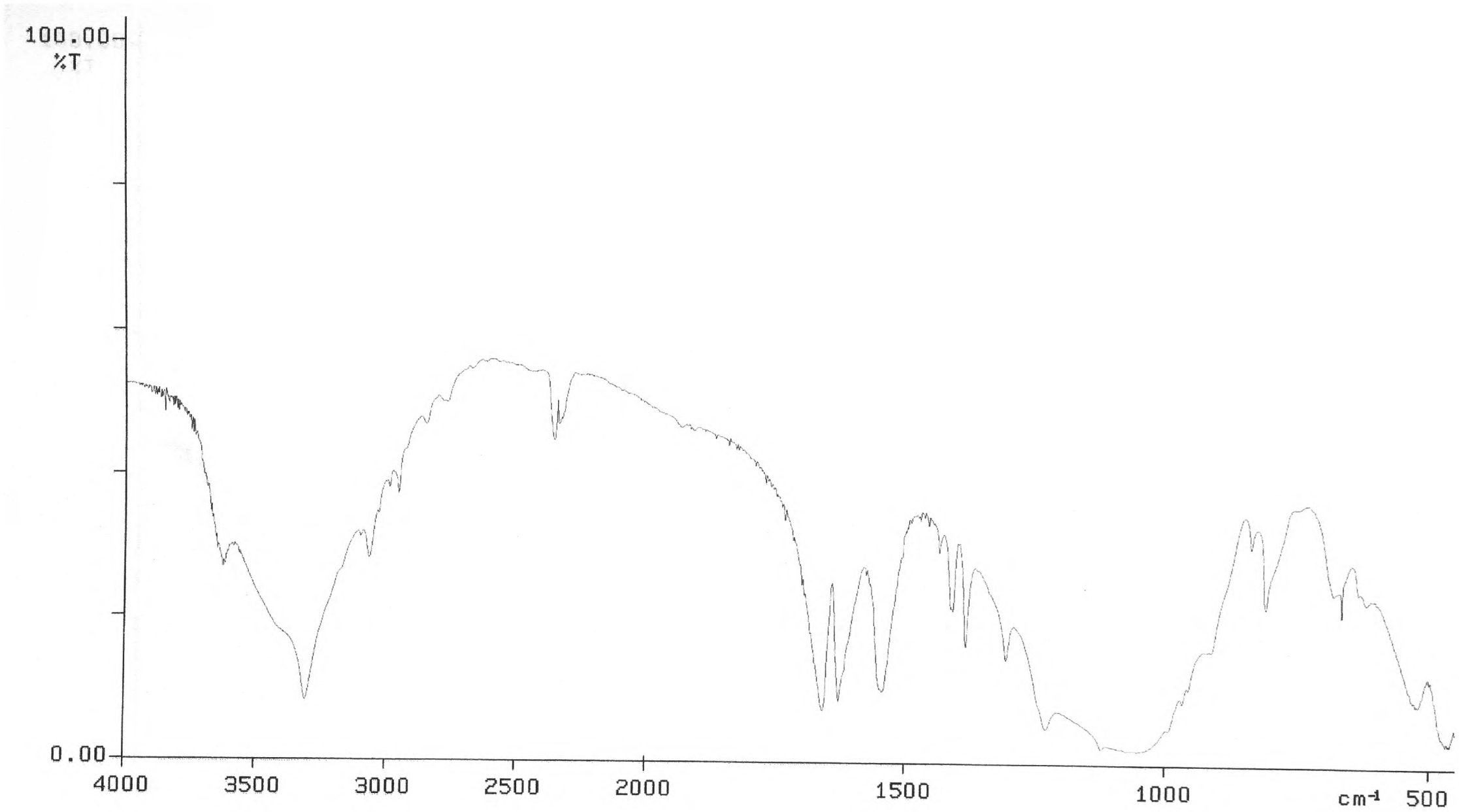

Infrared spectrum of K10 with NIPAM (2:1)

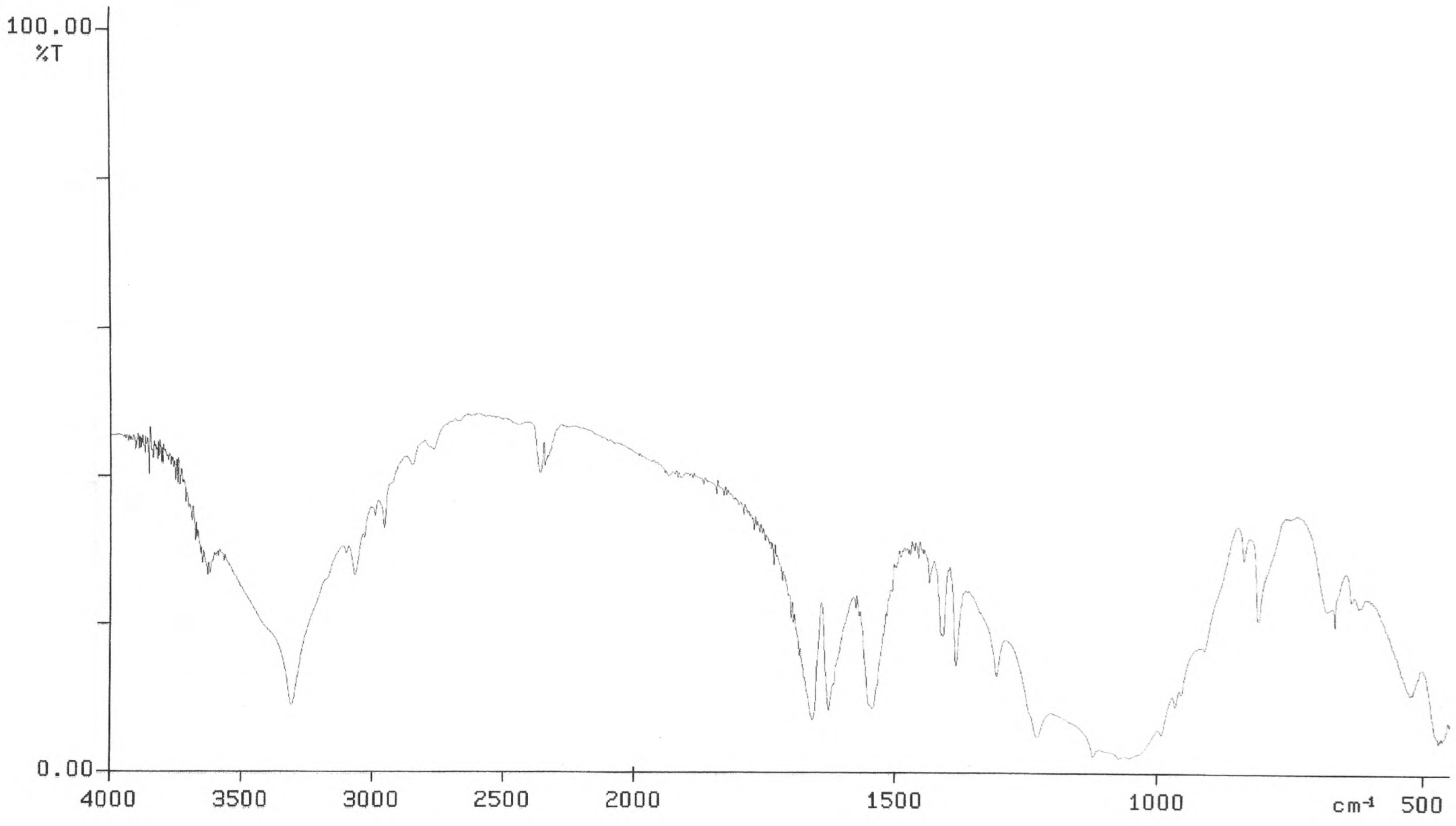

Infrared spectrum of K10 with NIPAM (2:0.5)

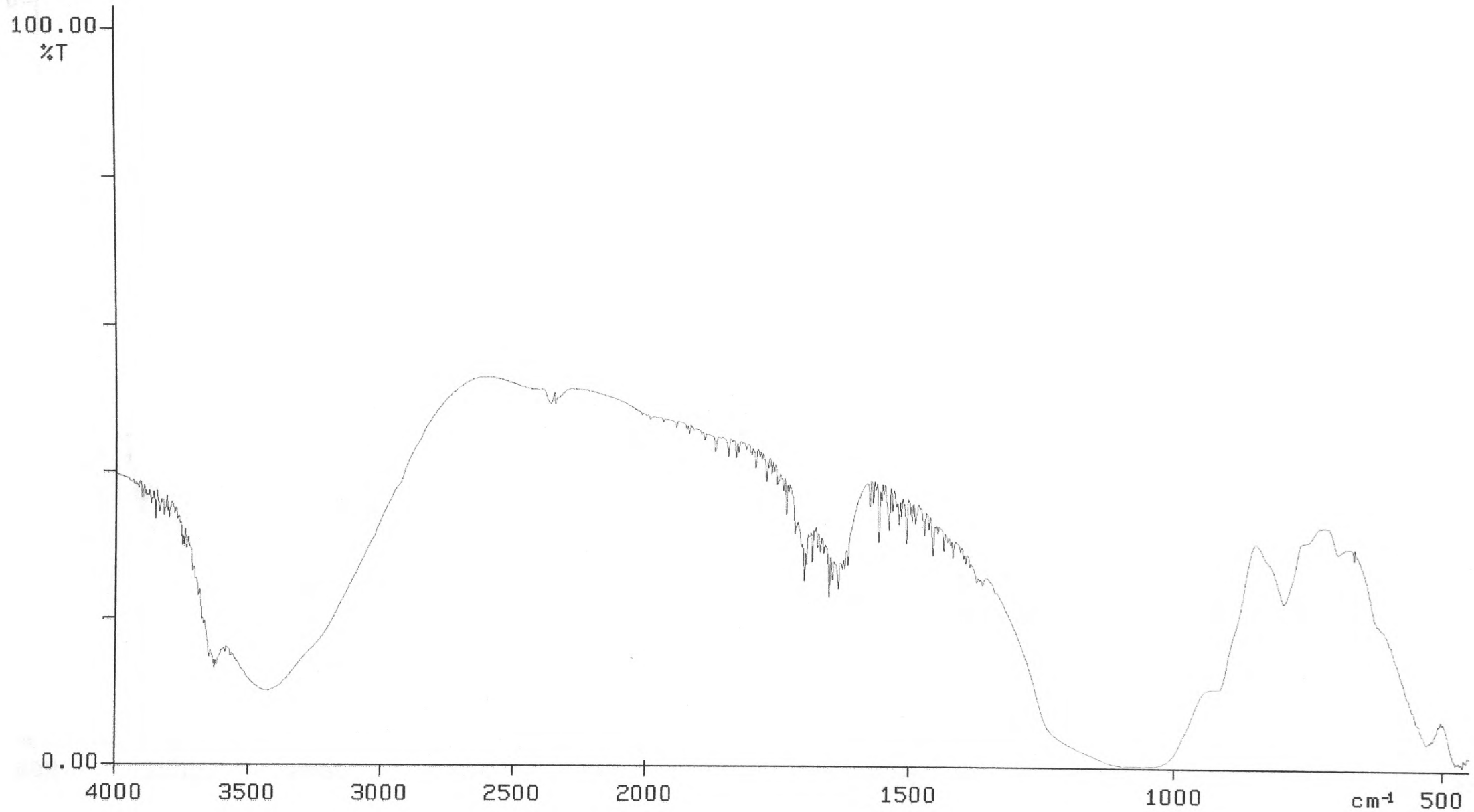

Infrared spectrum of K10 with styrene (2:1.5)

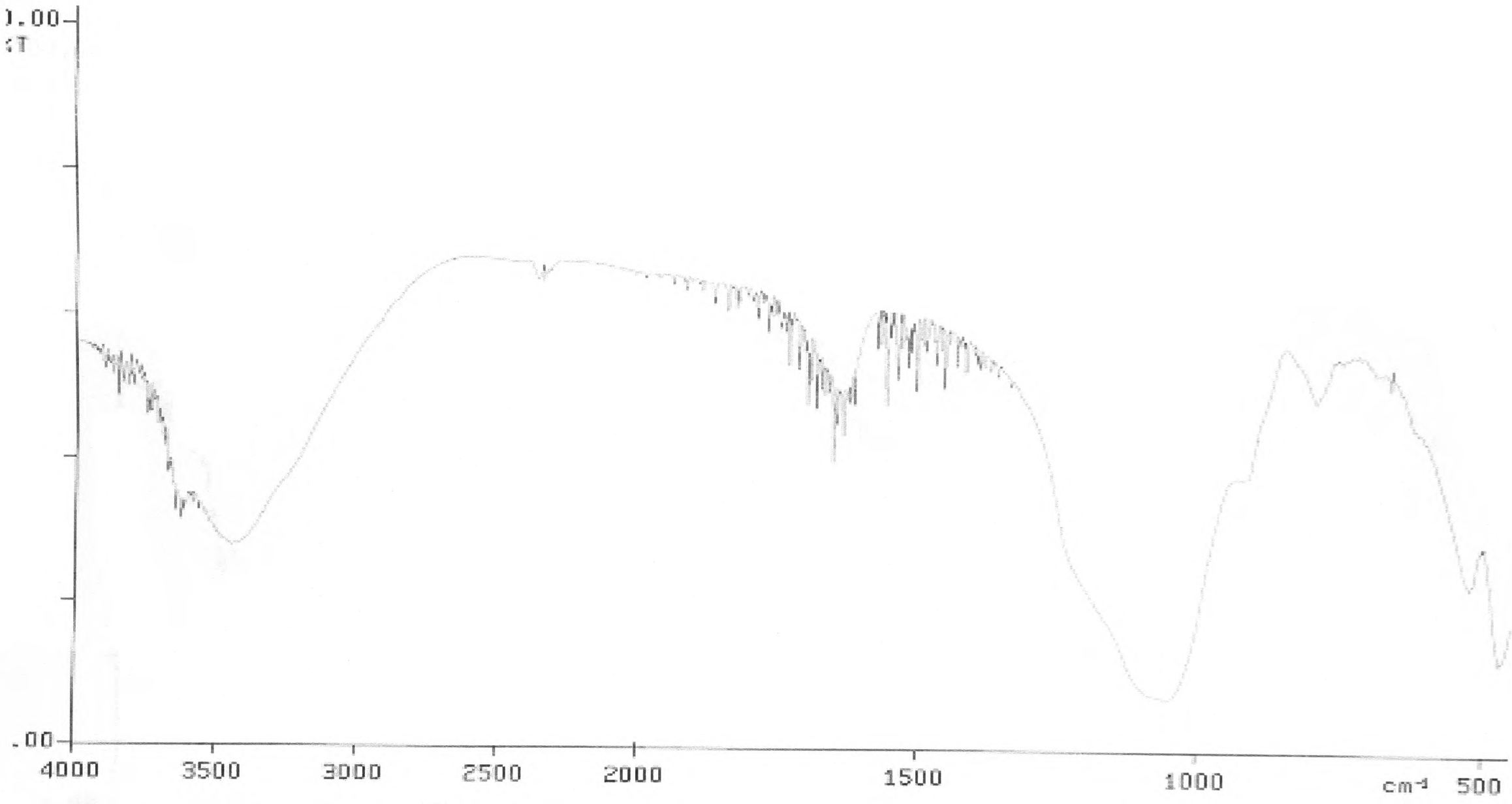

Infrared spectrum of K10 with styrene (2:1)

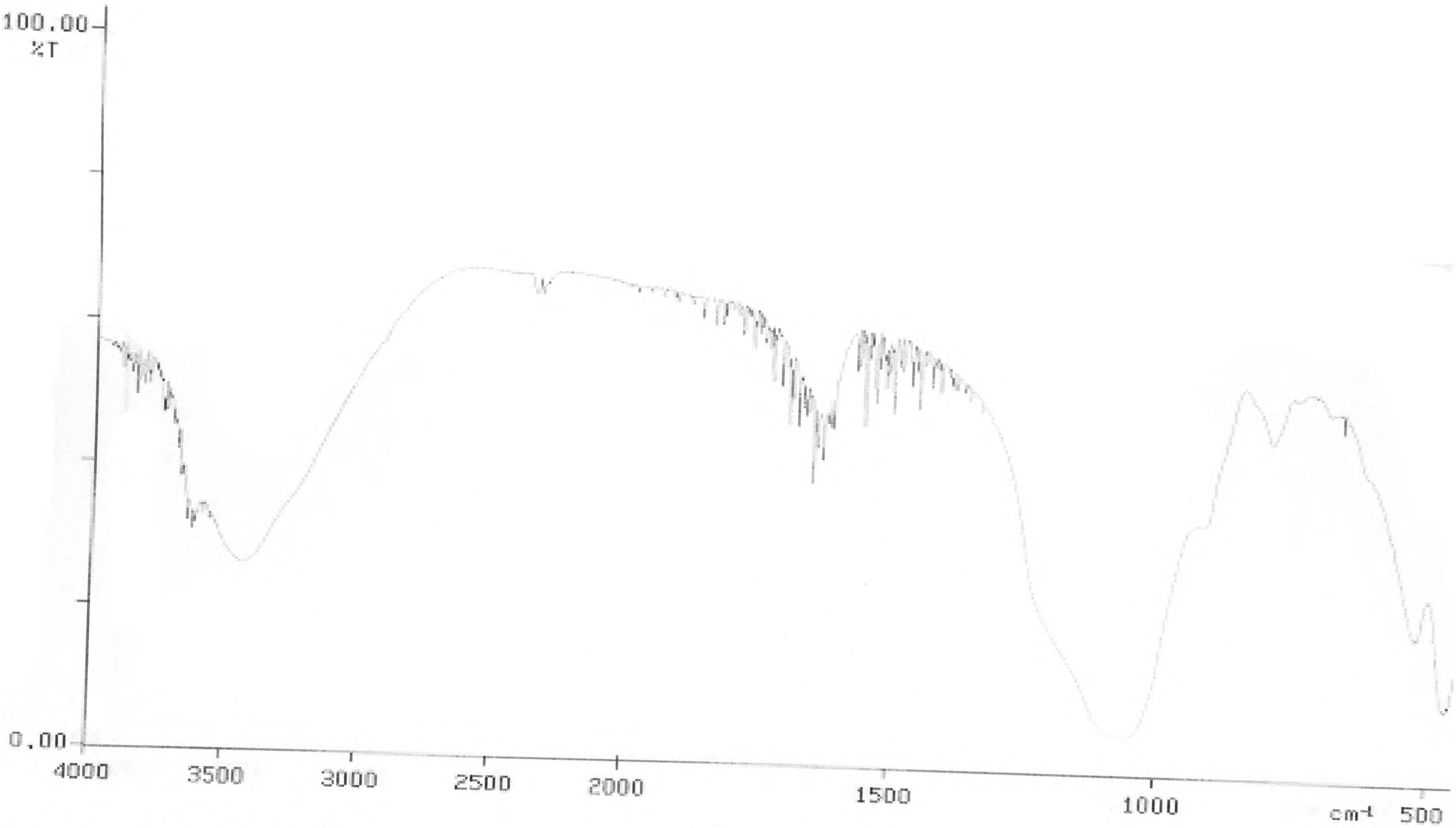

Infrared spectrum of K10 with styrene (2:0.5)

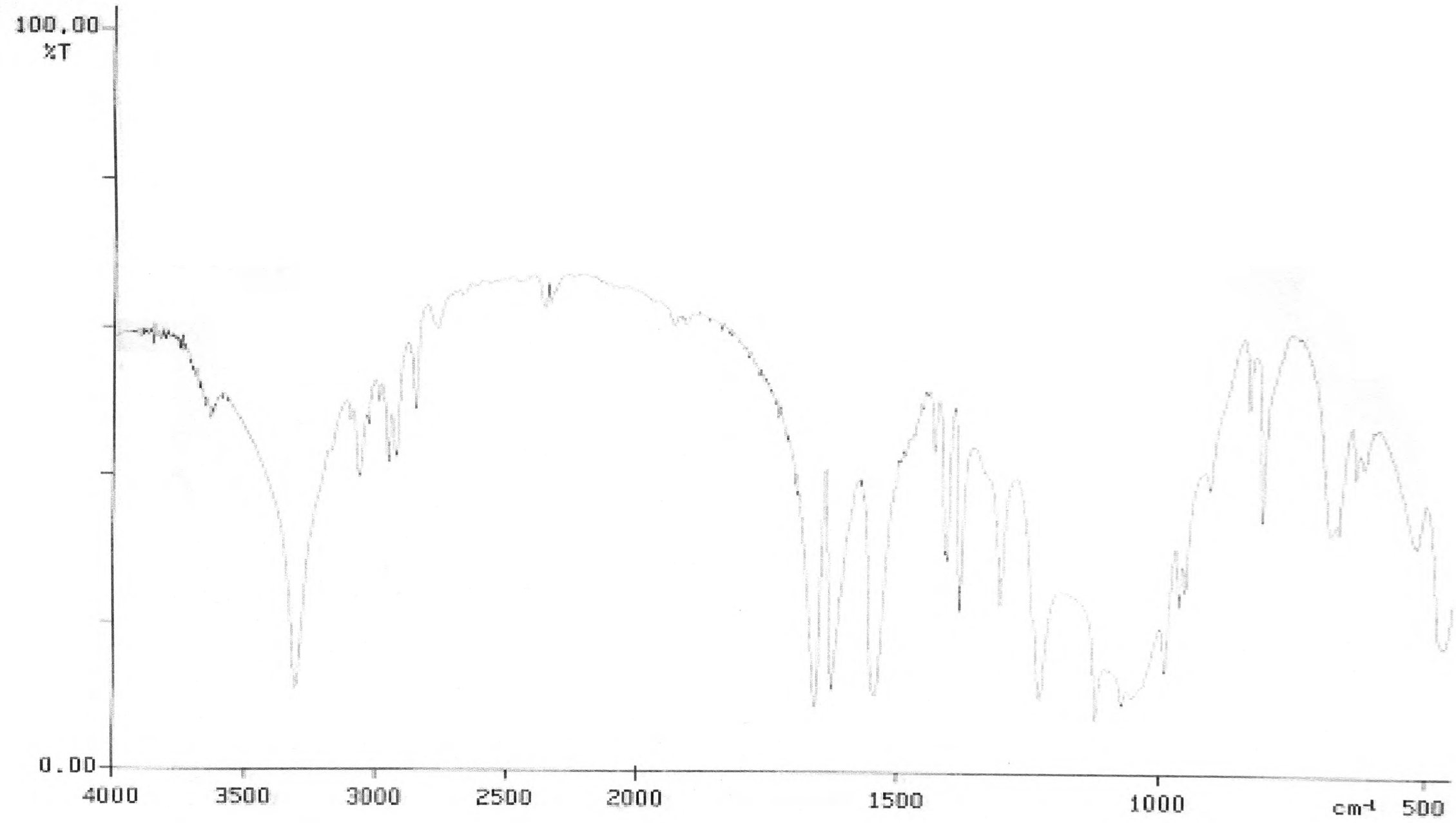

Infrared spectrum of organophilic K10 with NIPAM (2:1.5)

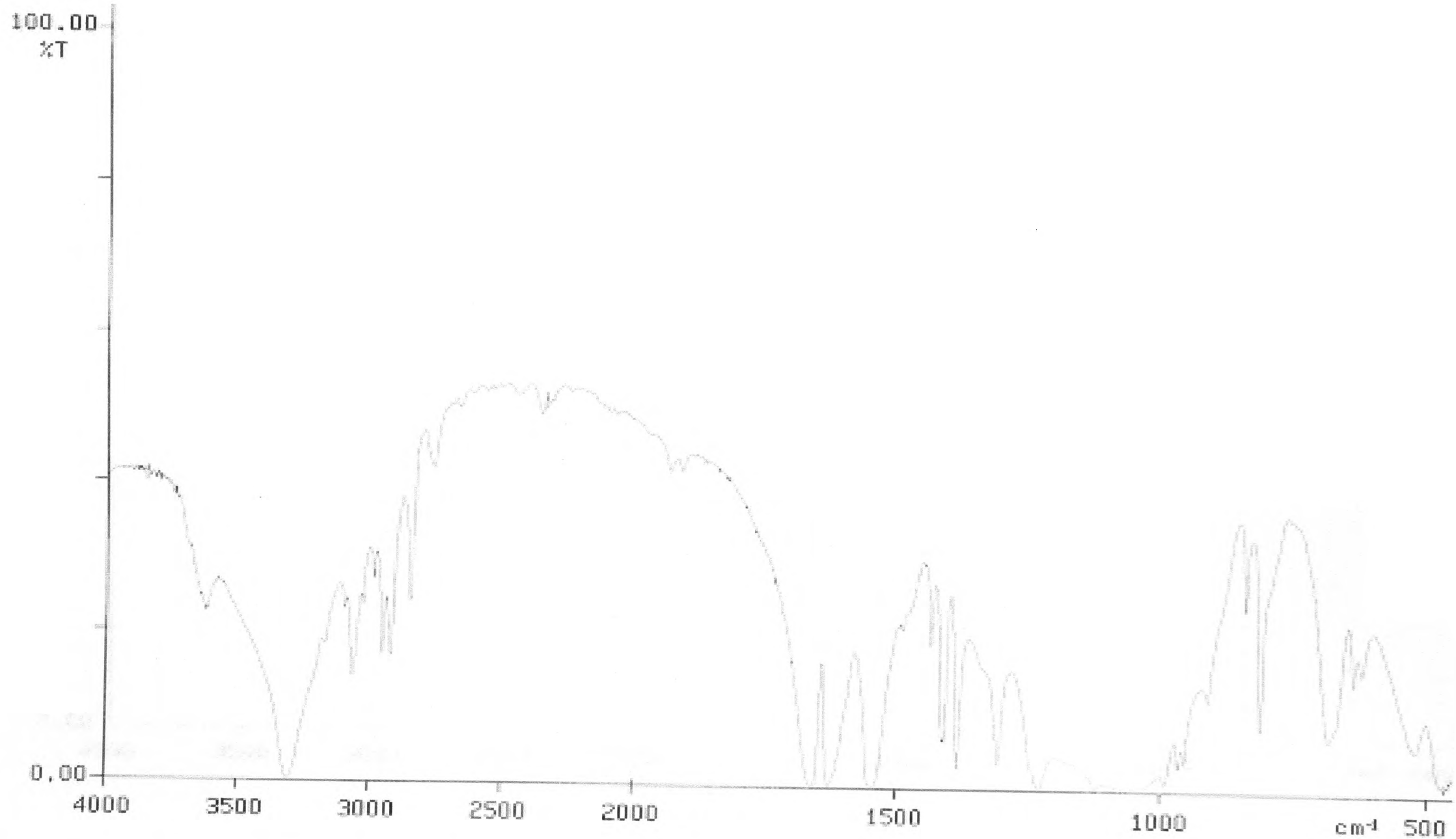

Infrared spectrum of organophilic K10 with NIPAM (2:1)

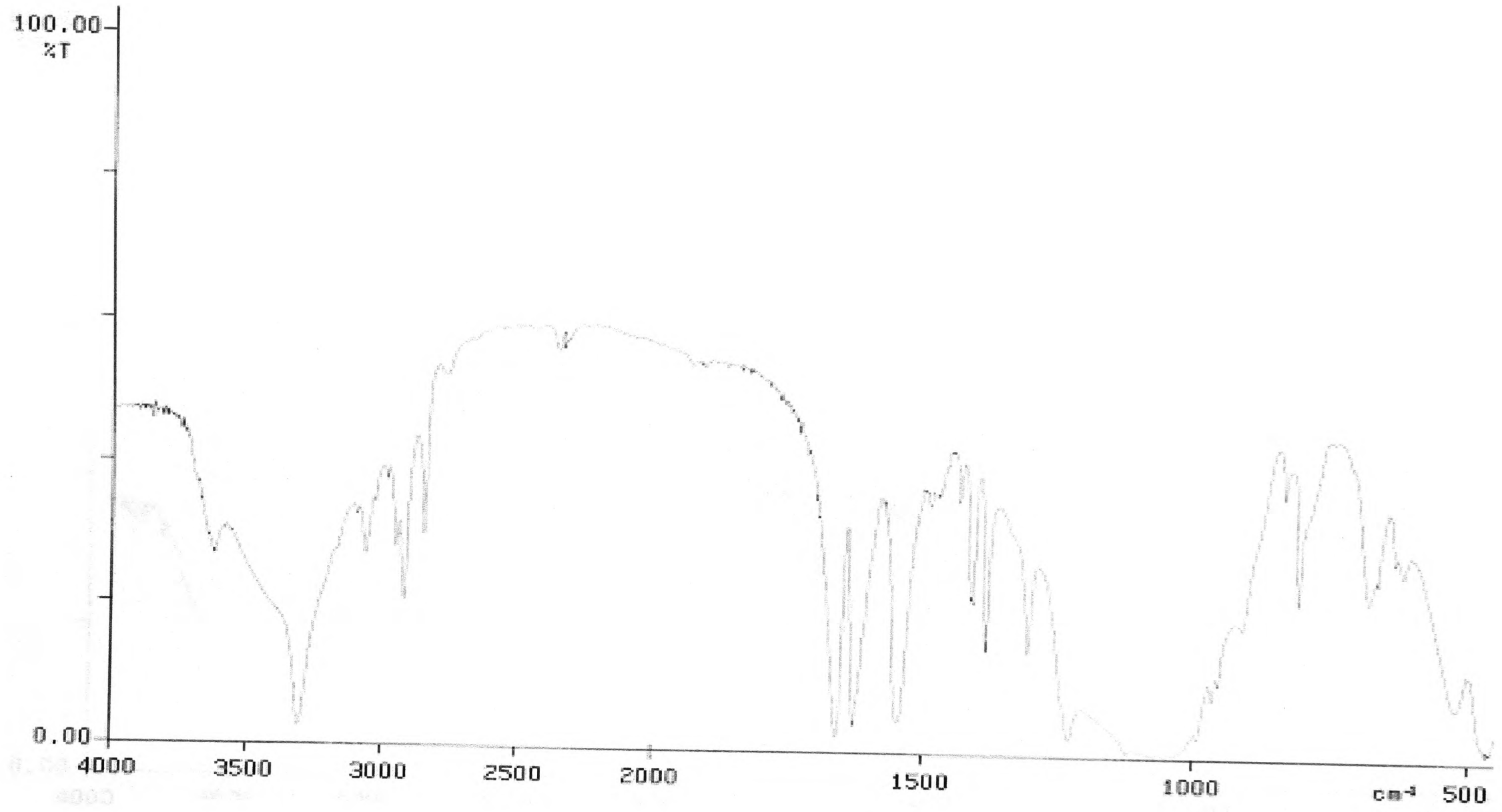

Infrared spectrum of organophilic K10 with NIPAM (2:0.5)

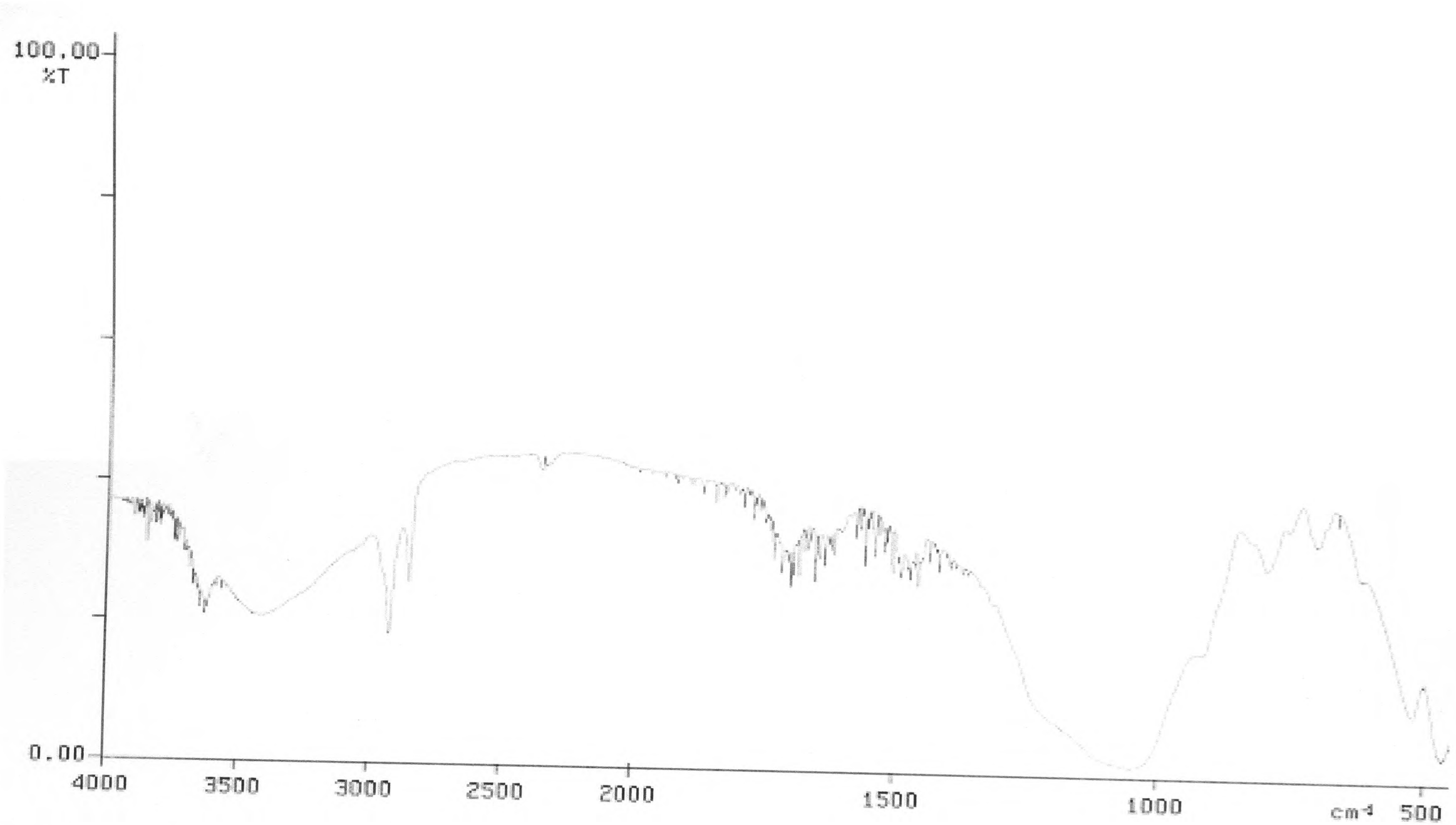

Infrared spectrum of organophilic K10 with styrene (2:1.5)

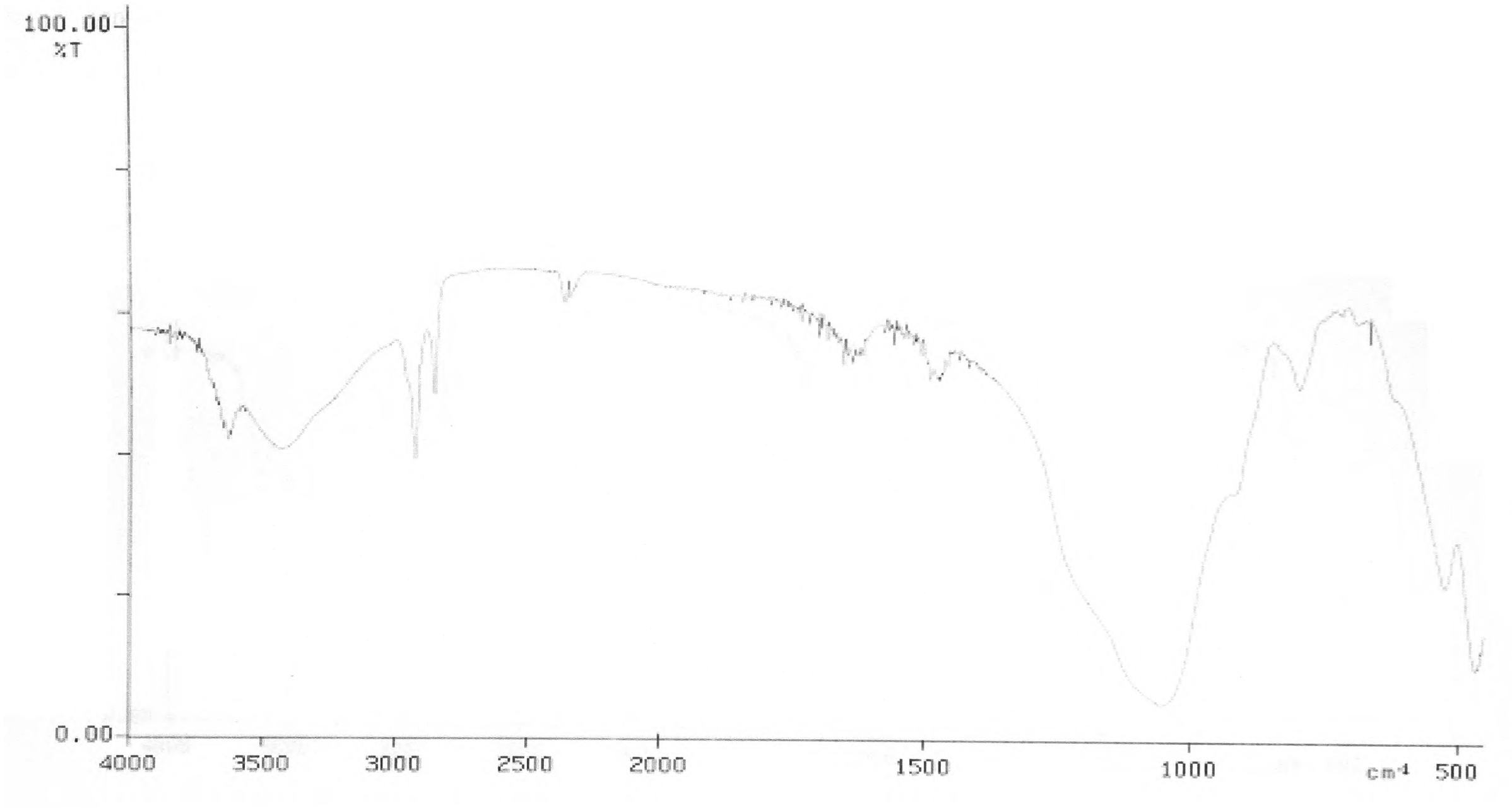

Infrared spectrum of organophilic K10 with styrene (2:1)

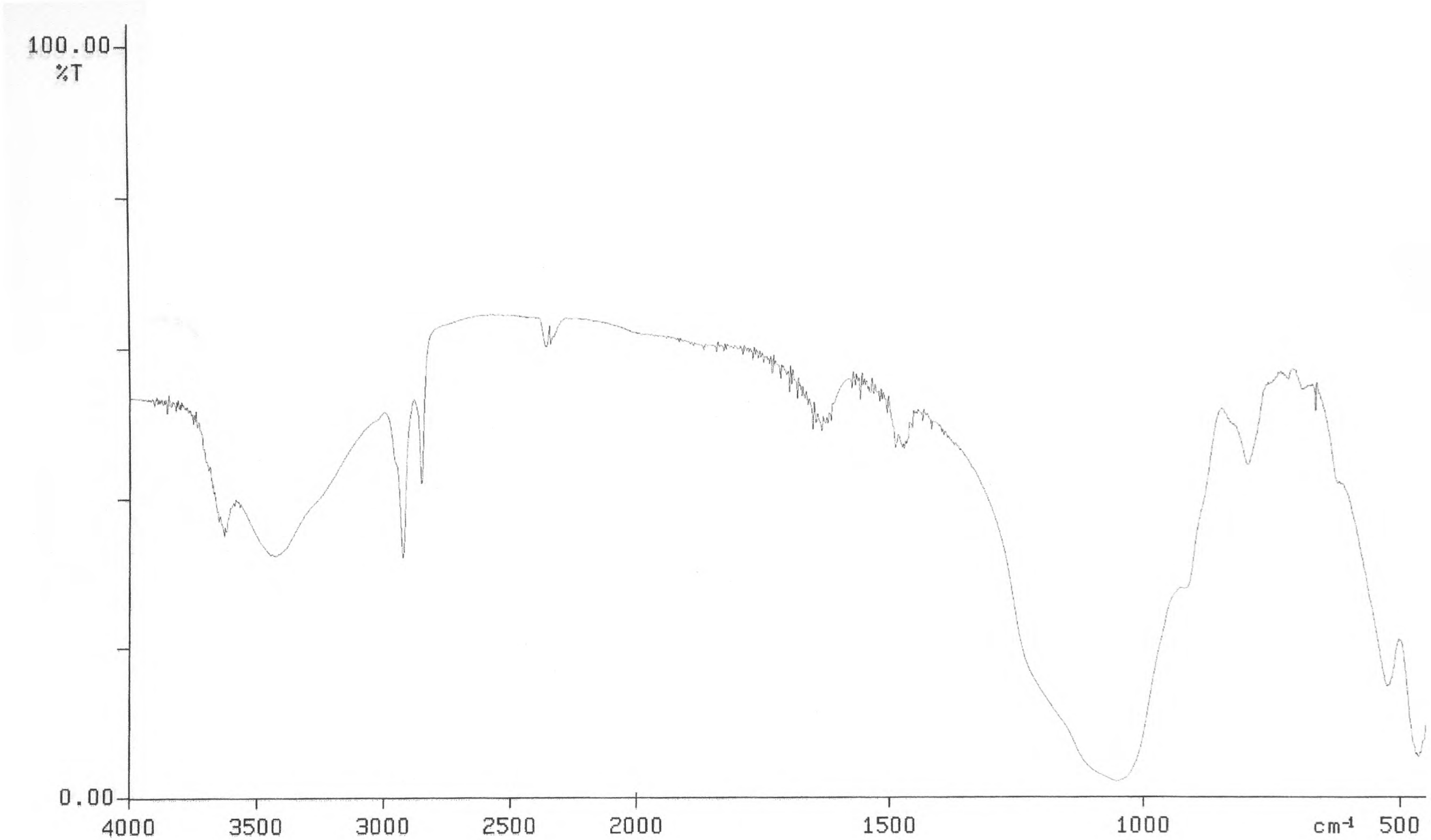

Infrared spectrum of organophilic K10 with styrene (2:0.5)

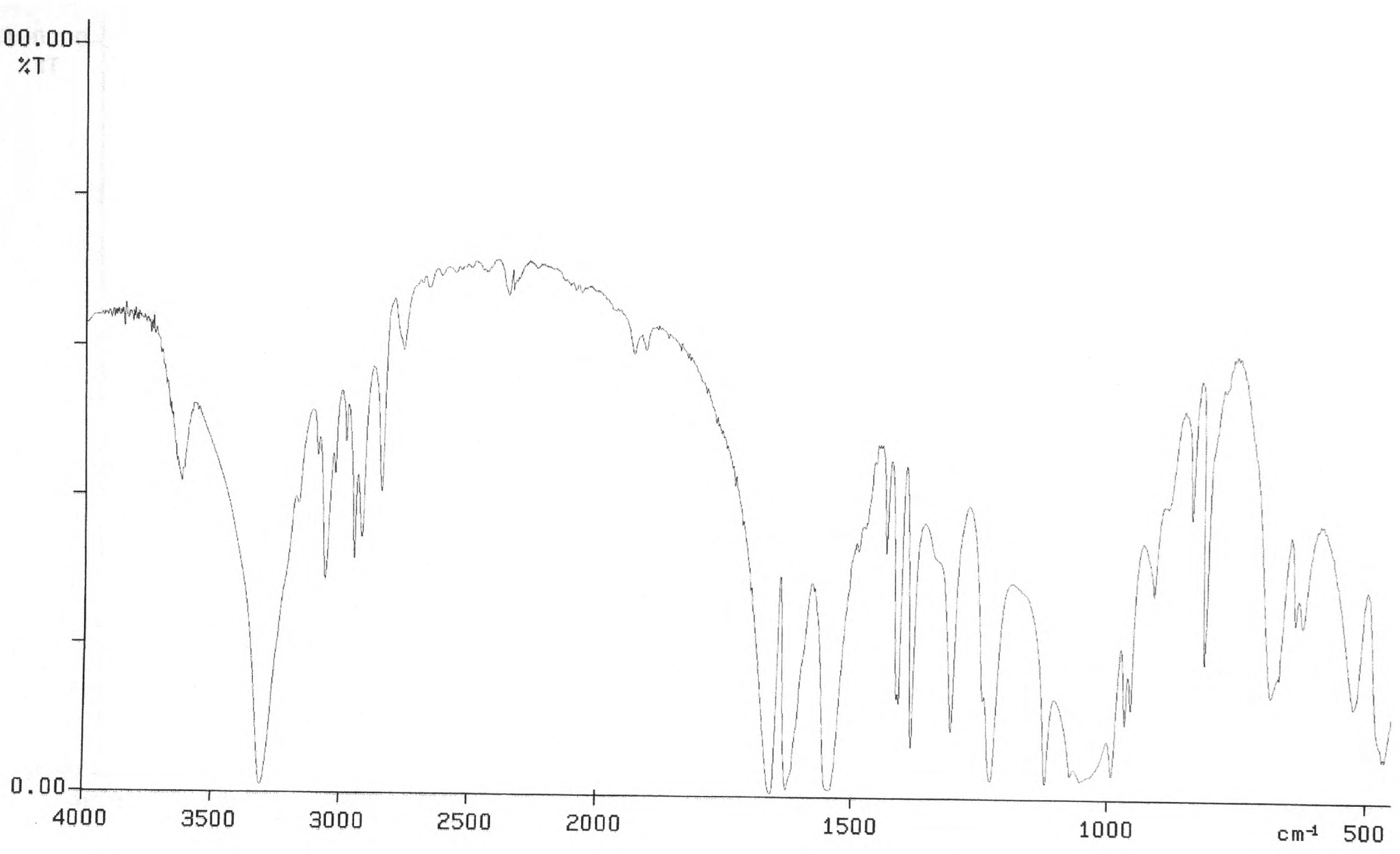

Infrared spectrum of organophilic bentonite with NIPAM (2:1.5)

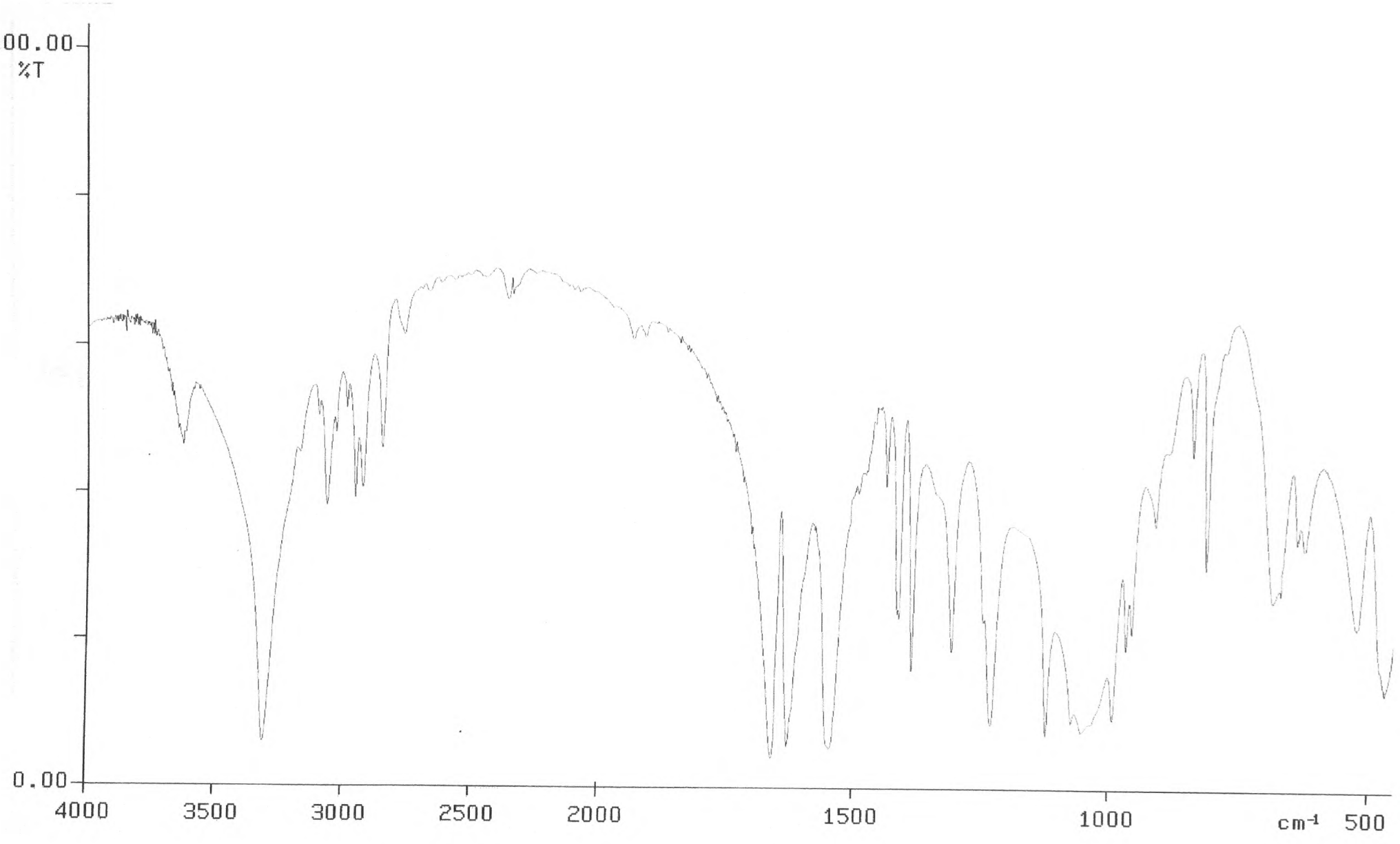

Infrared spectrum of organophilic bentonite with NIPAM (2:1)

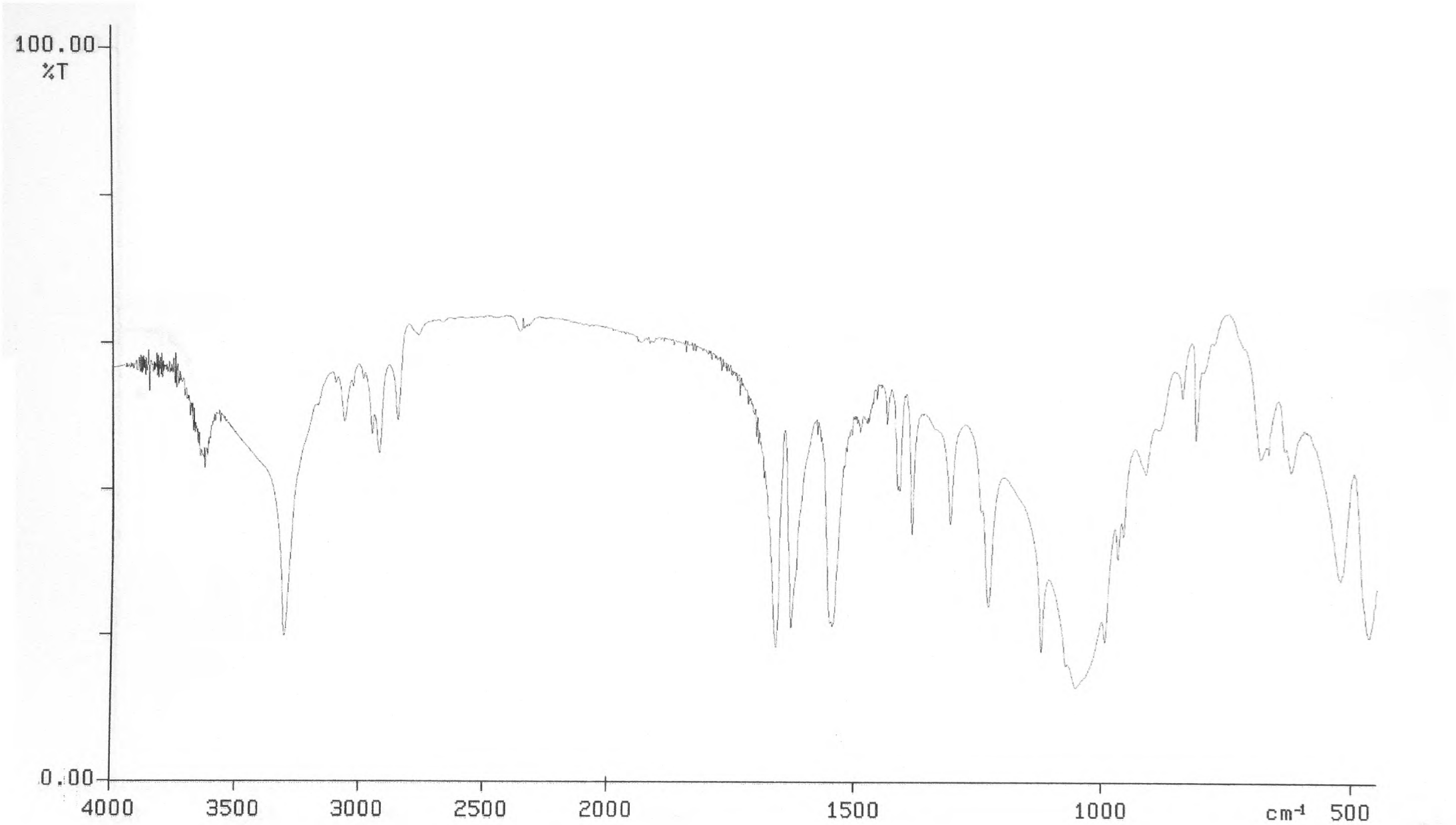

Infrared spectrum of organophilic bentonite with NIPAM (2:0.5)

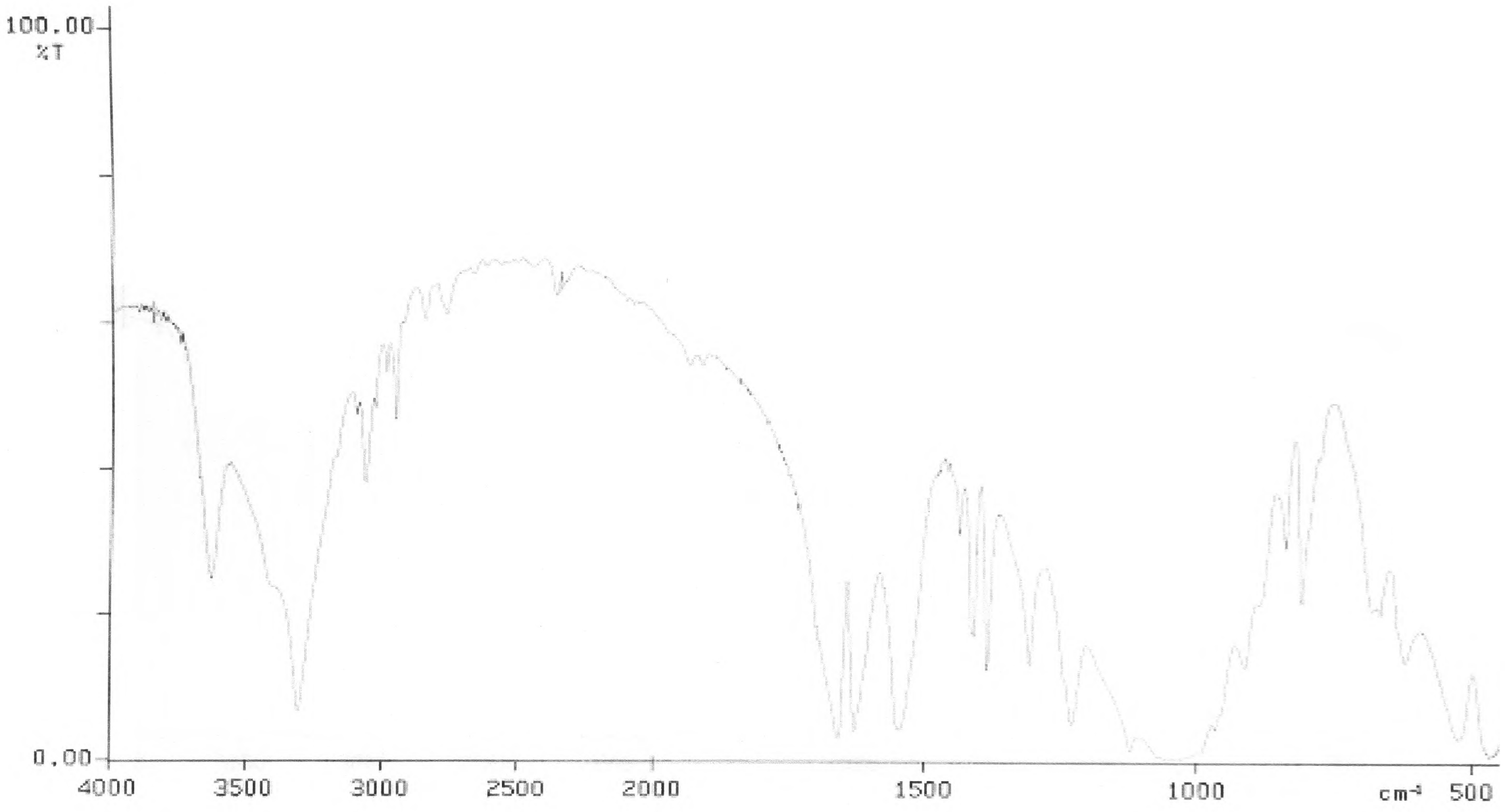

Infrared spectrum of bentonite with NIPAM (2:1.5)

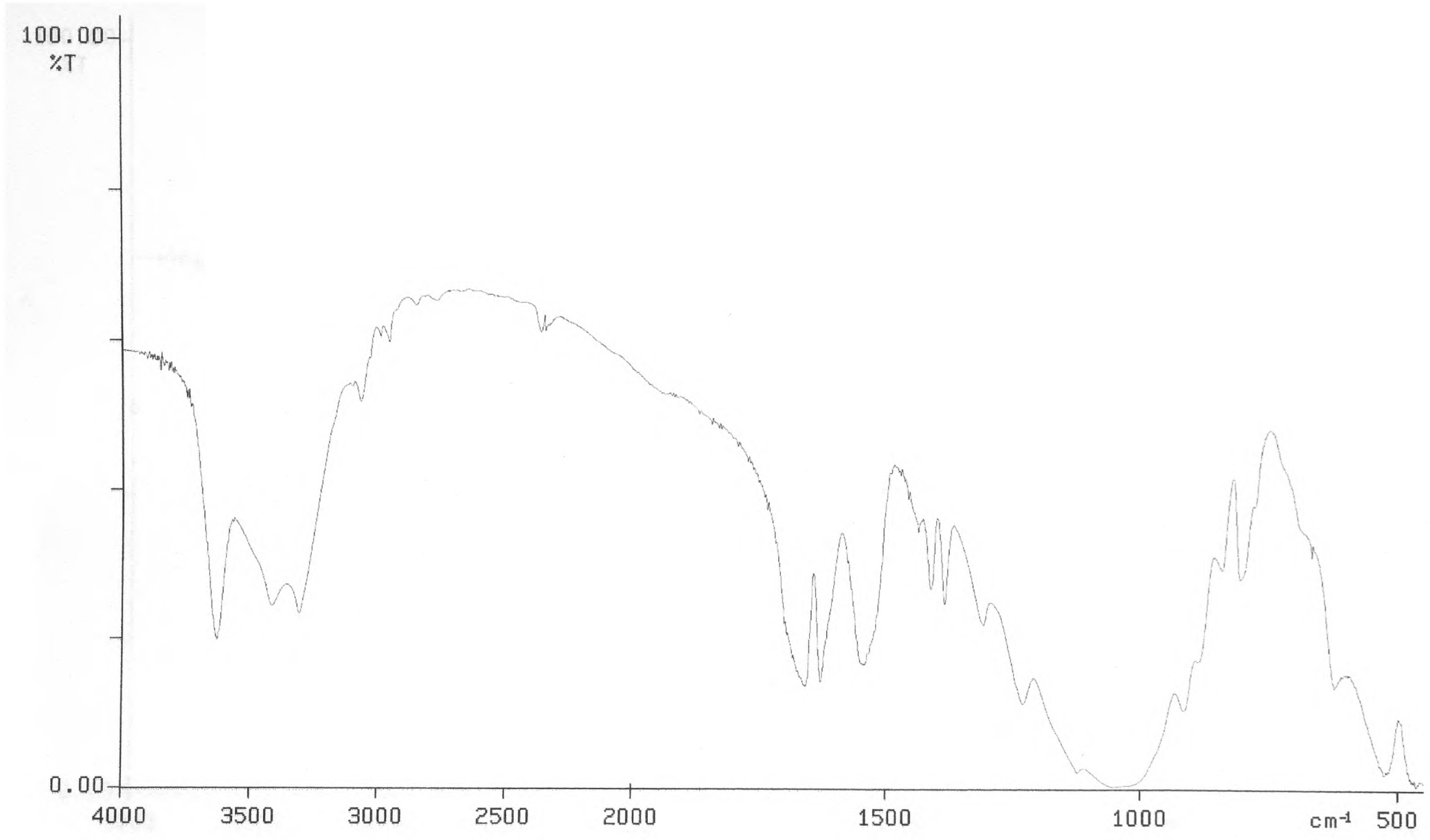

Infrared spectrum of bentonite with NIPAM (2:1)

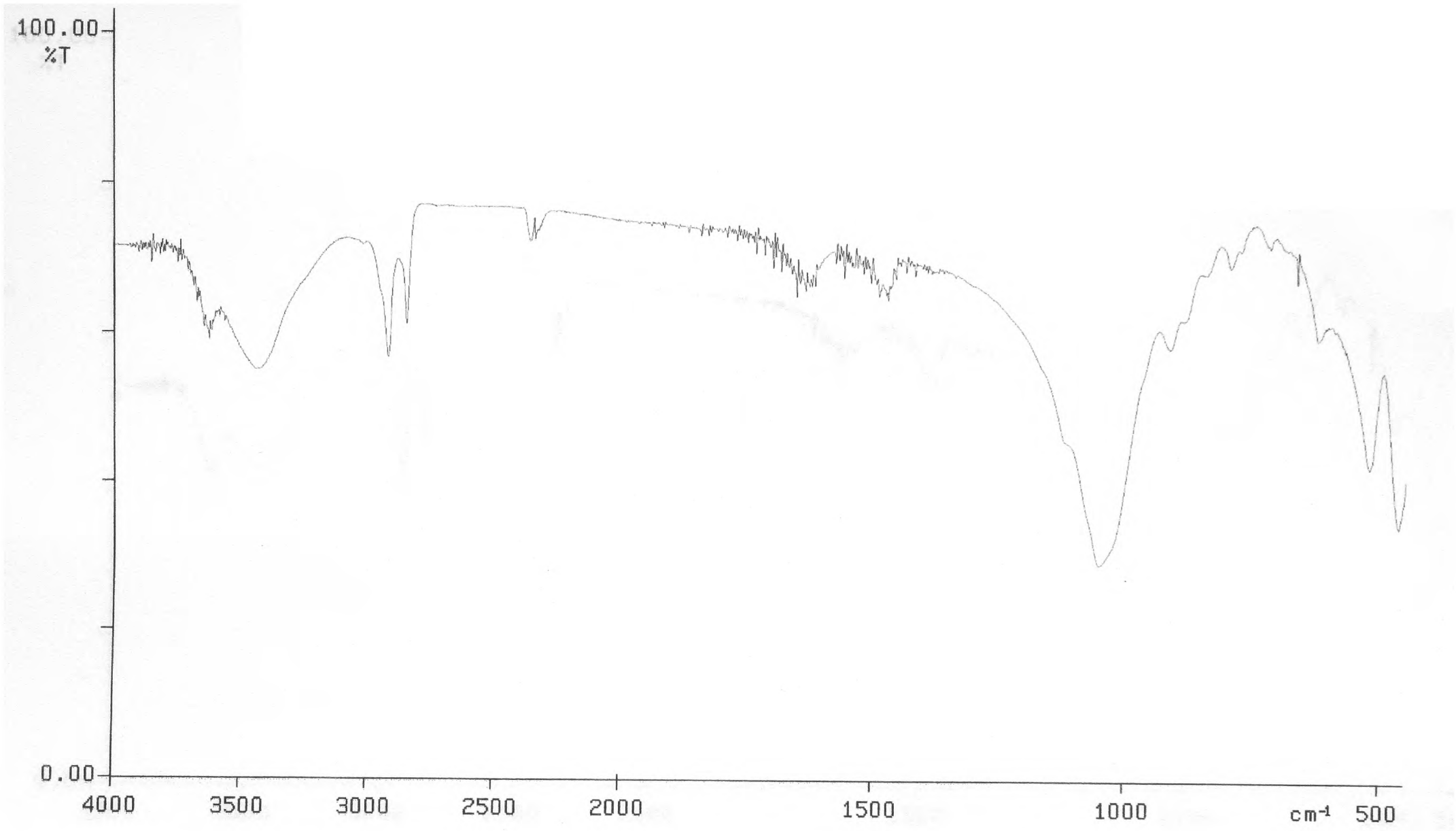

Infrared spectrum of bentonite with NIPAM (2:0.5)

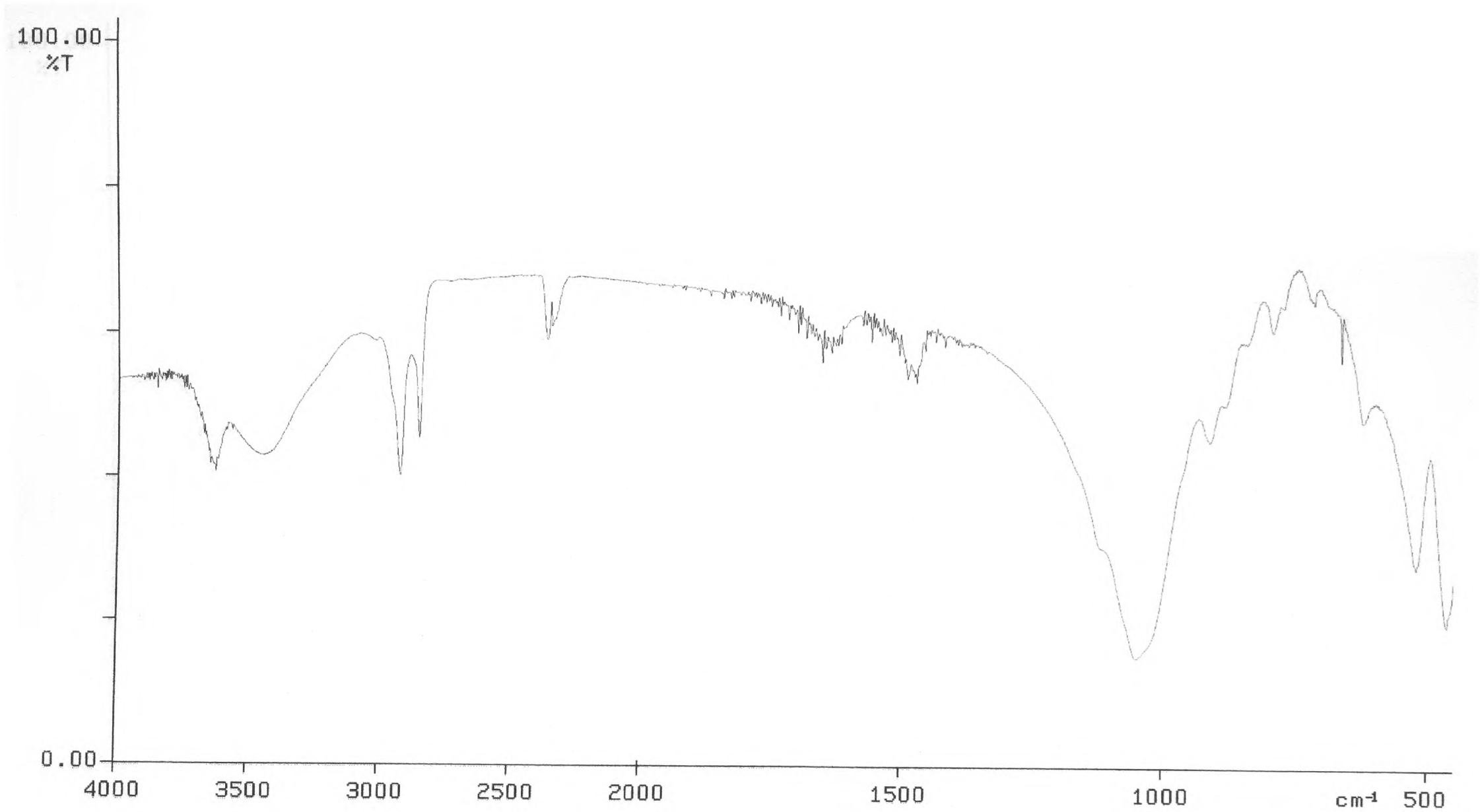

Infrared spectrum of organophilic bentonite with styrene (2:1.5)

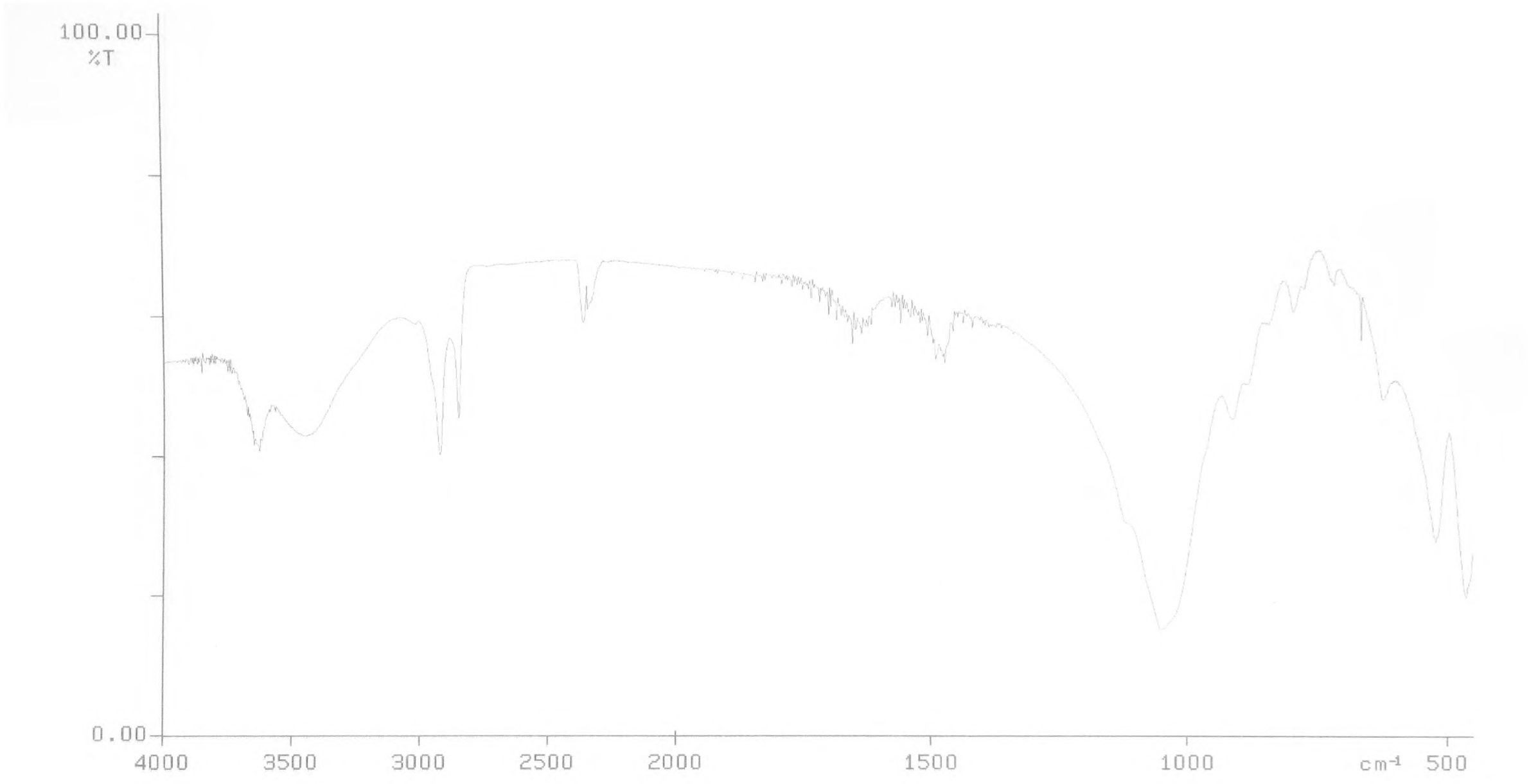

Infrared spectrum of organophilic bentonite with styrene (2:1)

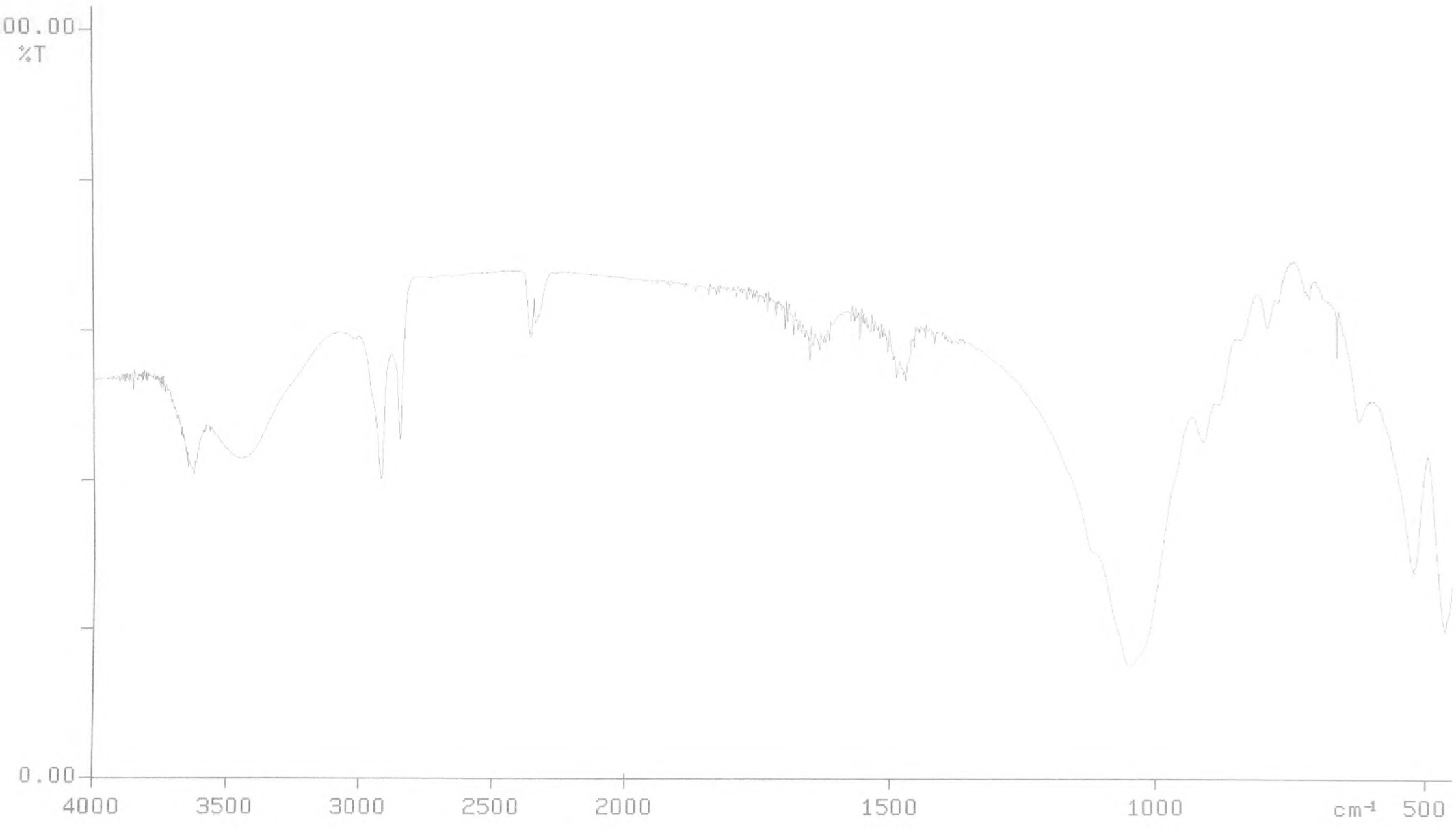

Infrared spectrum of organophilic bentonite with styrene (2:1)

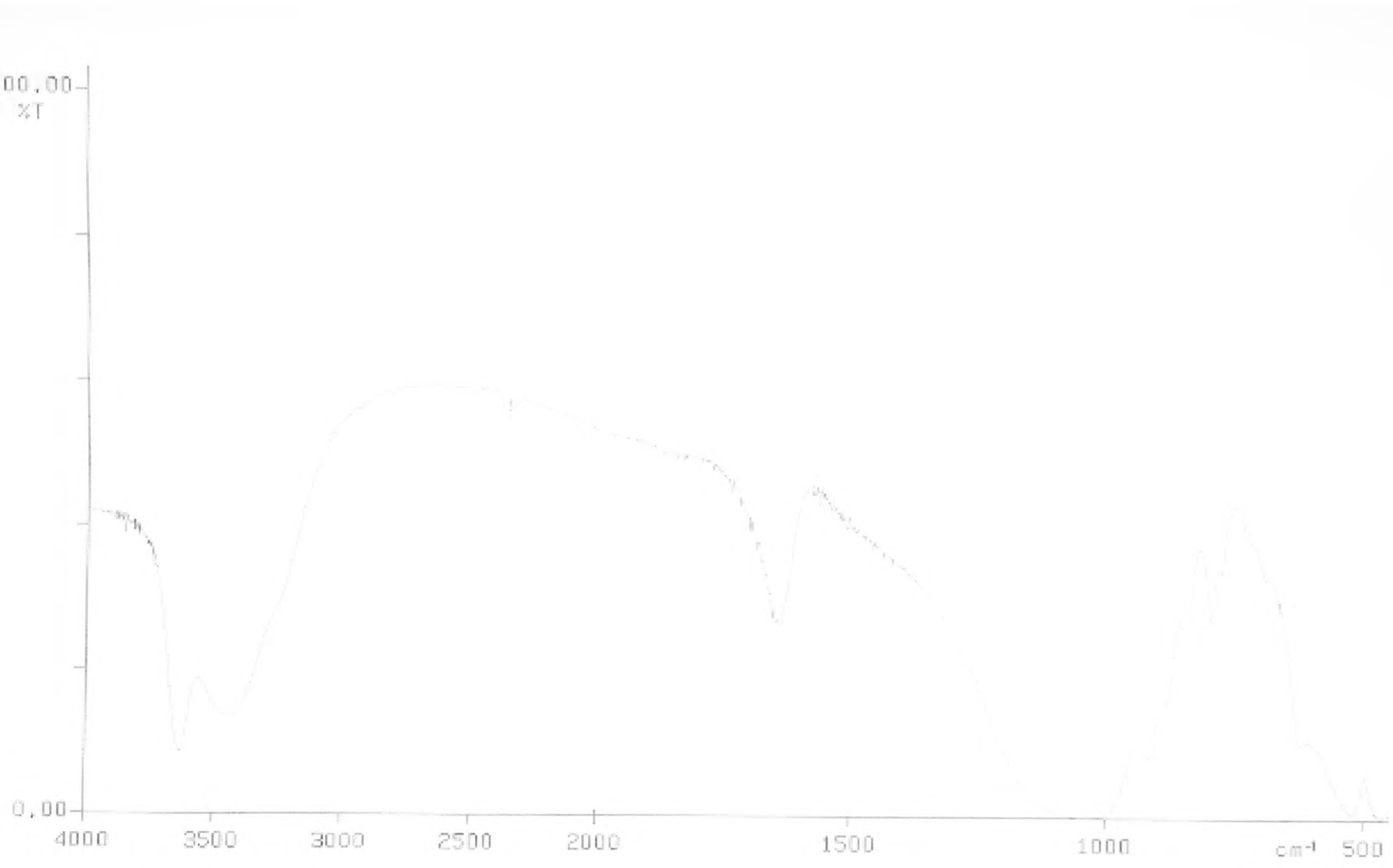

Infrared spectrum of organophilic bentonite with styrene (2:0.5)

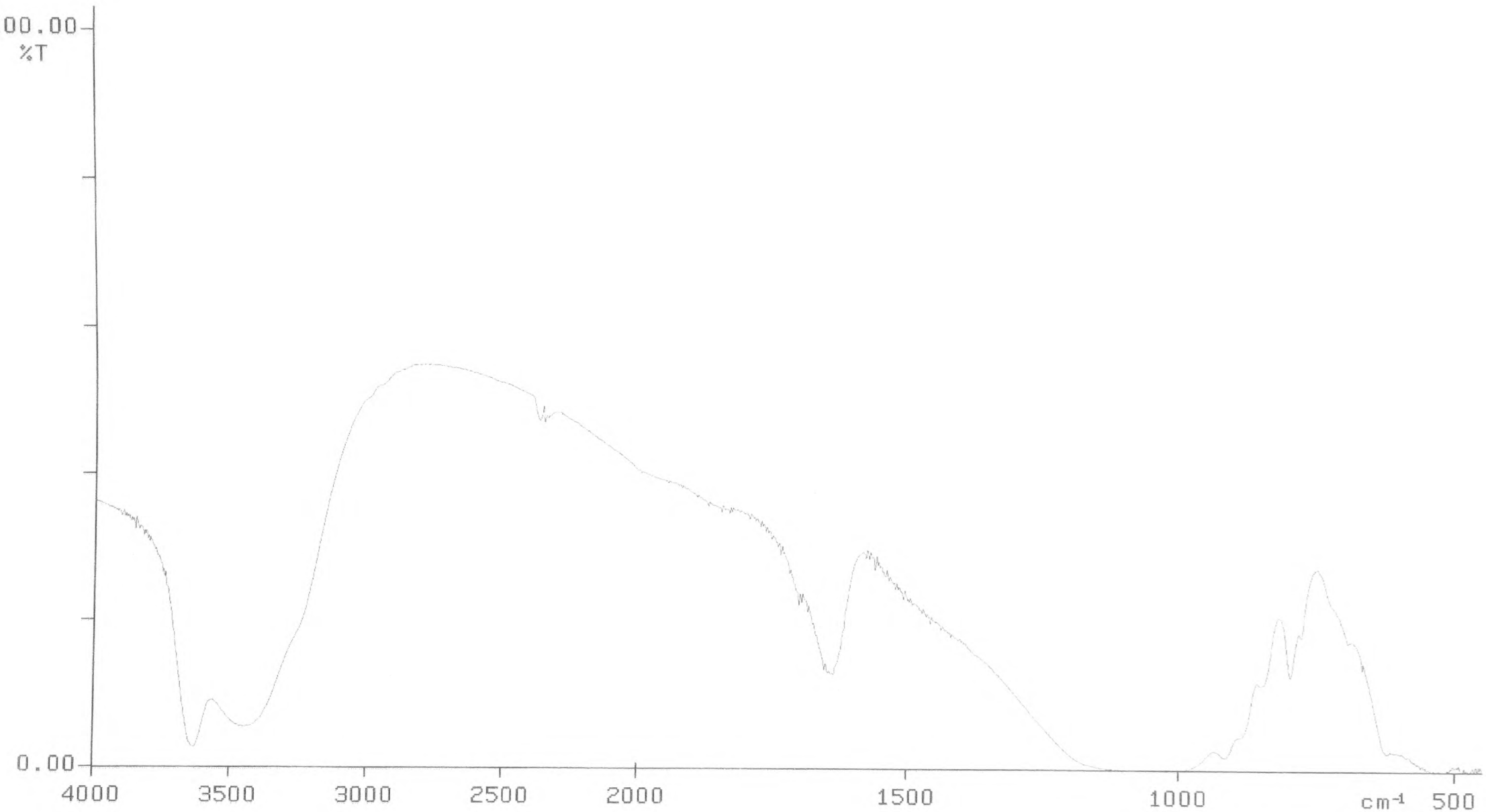

Infrared spectrum of bentonite with styrene (2:1.5)

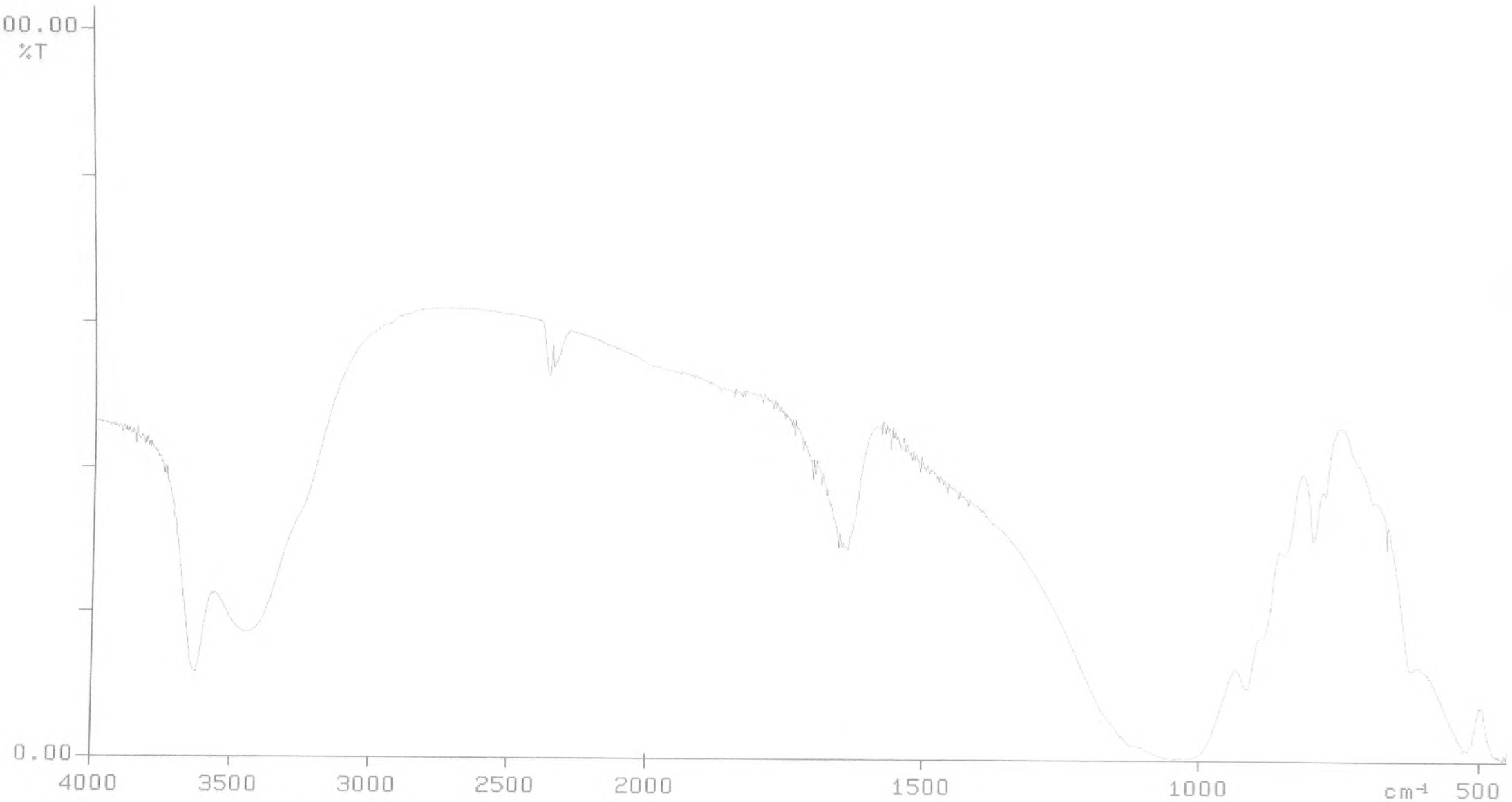

Infrared spectrum of organophilic bentonite with styrene (2:1)

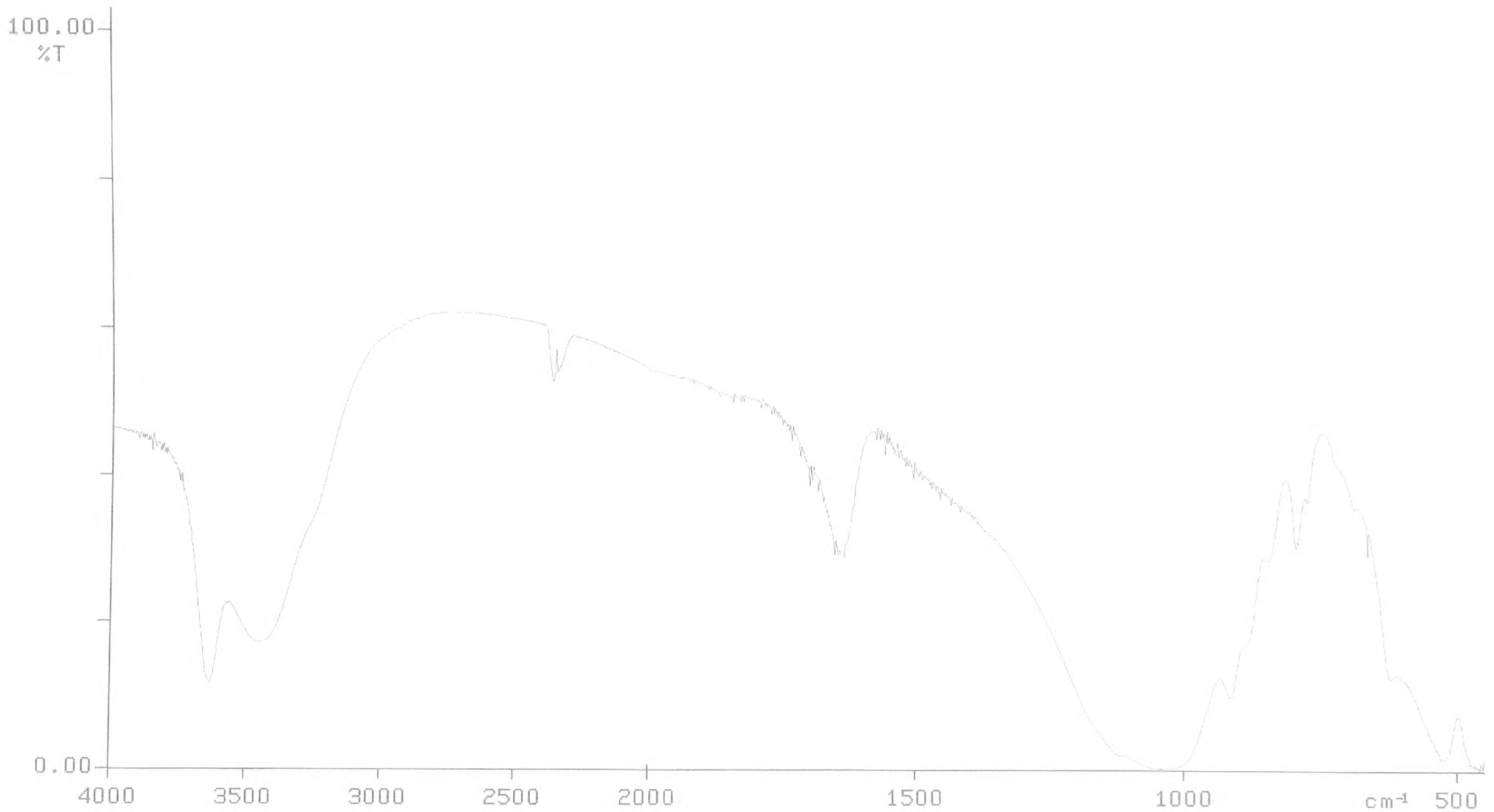

Infrared spectrum of organophilic bentonite with styrene (2:0.5)

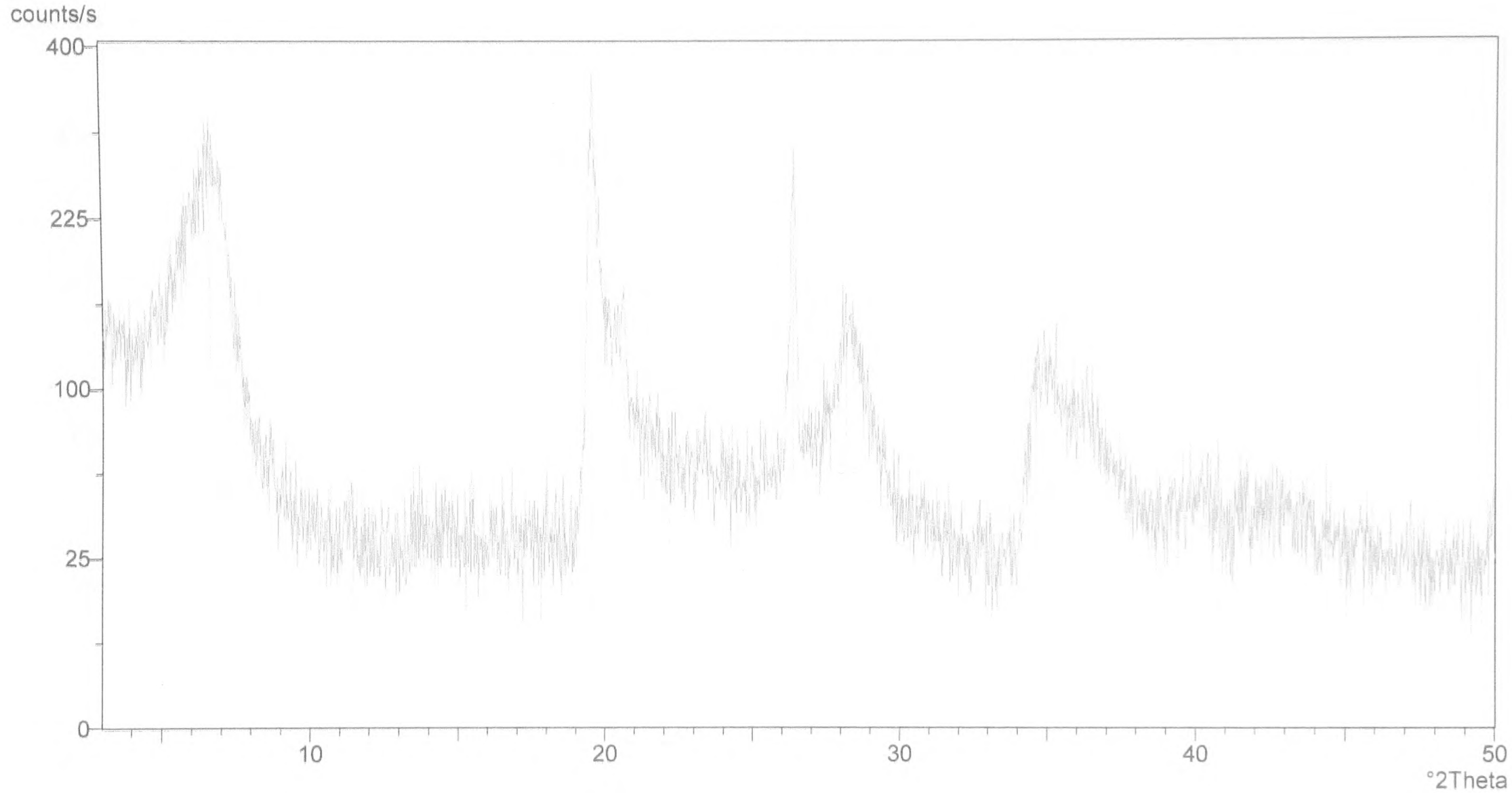

X-ray diffraction pattern of organophilic K10 with NIPAM (2:1.5)

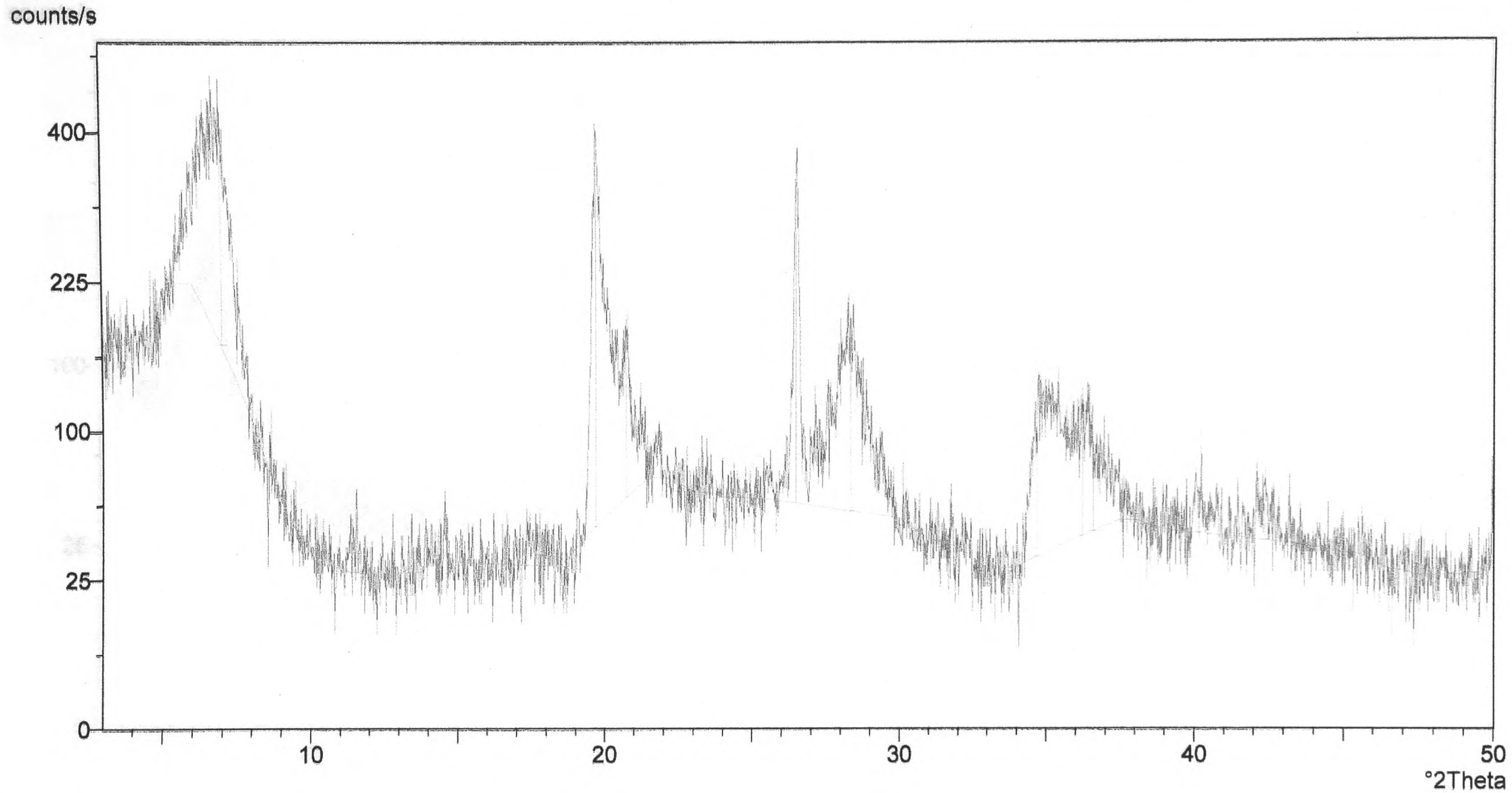

X-ray diffraction pattern of organophilic K10 with NIPAM (2:1)

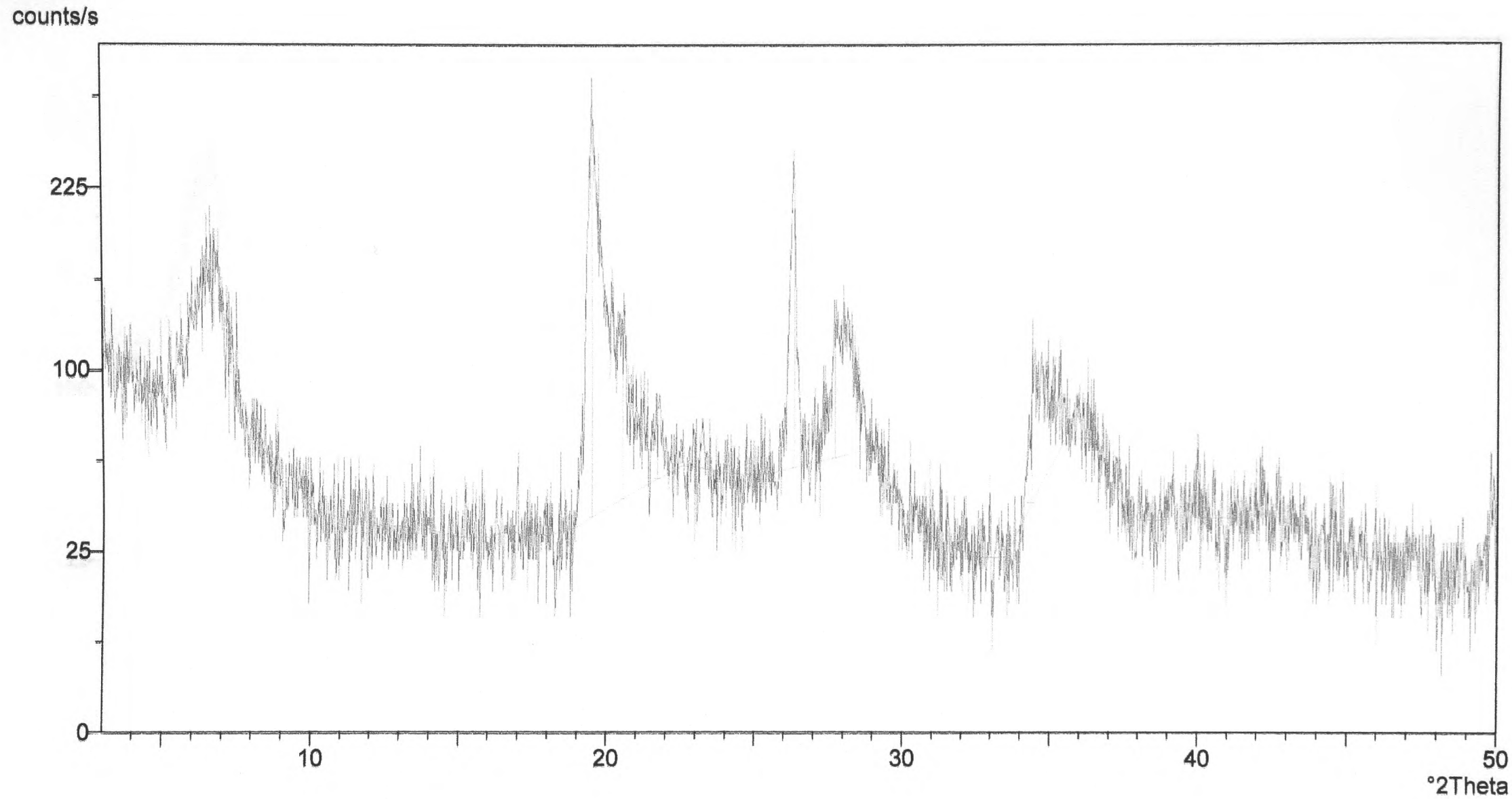

X-ray diffraction pattern of organophilic K10 with NIPAM (2:0.5)

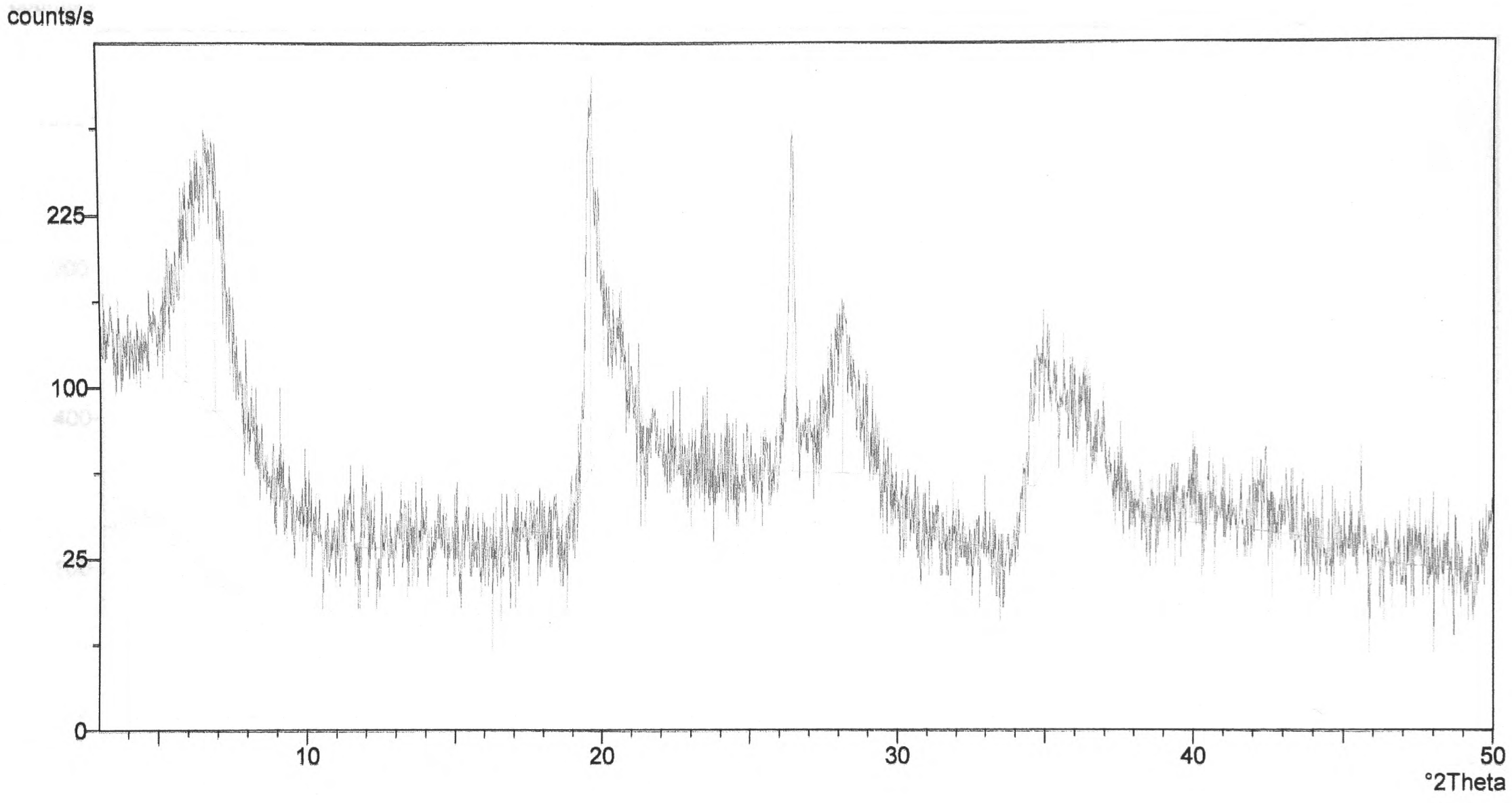

X-ray diffraction pattern of K10 with NIPAM (2:1.5)

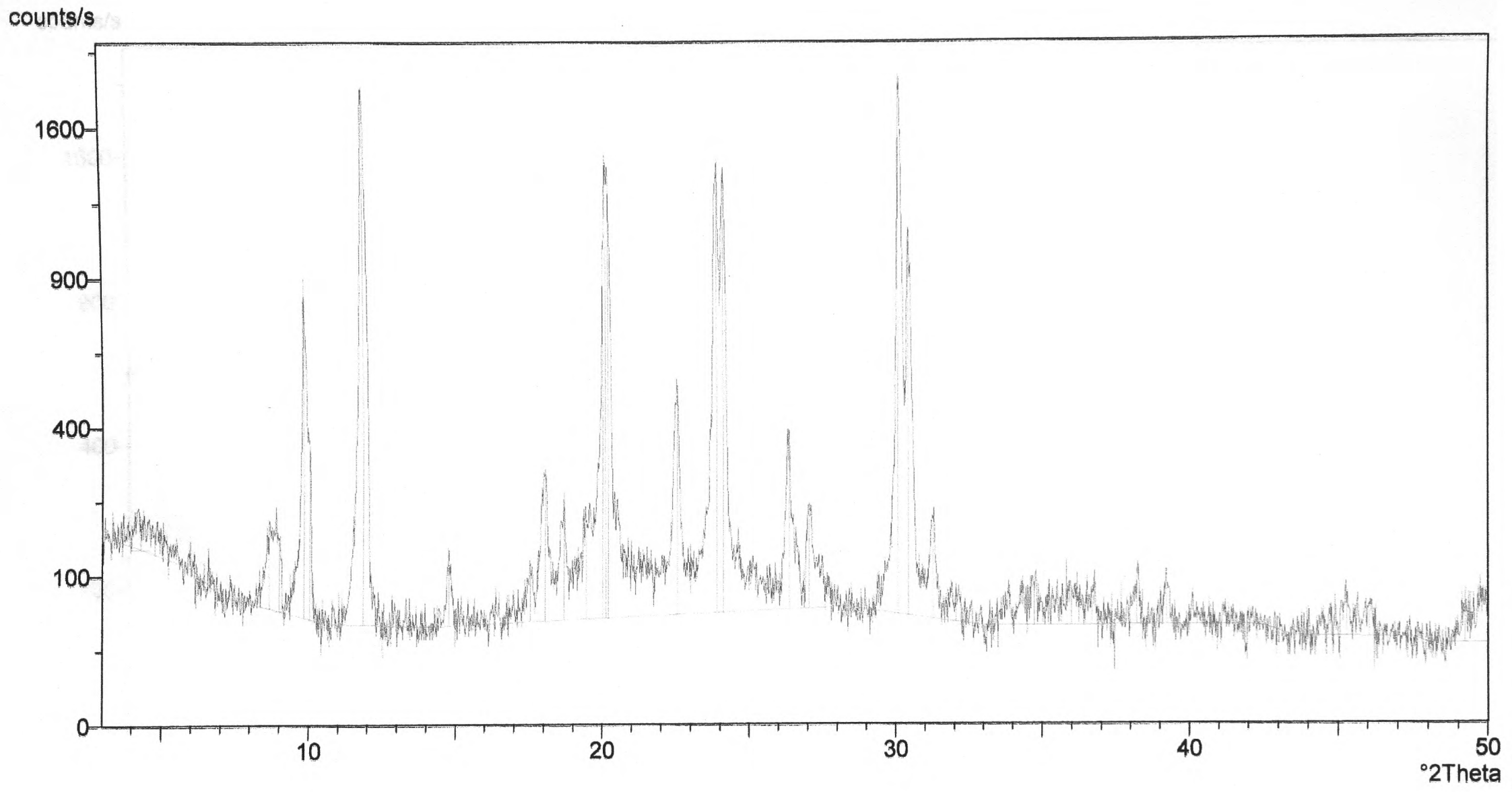

X-ray diffraction pattern of K10 with NIPAM (2:1)

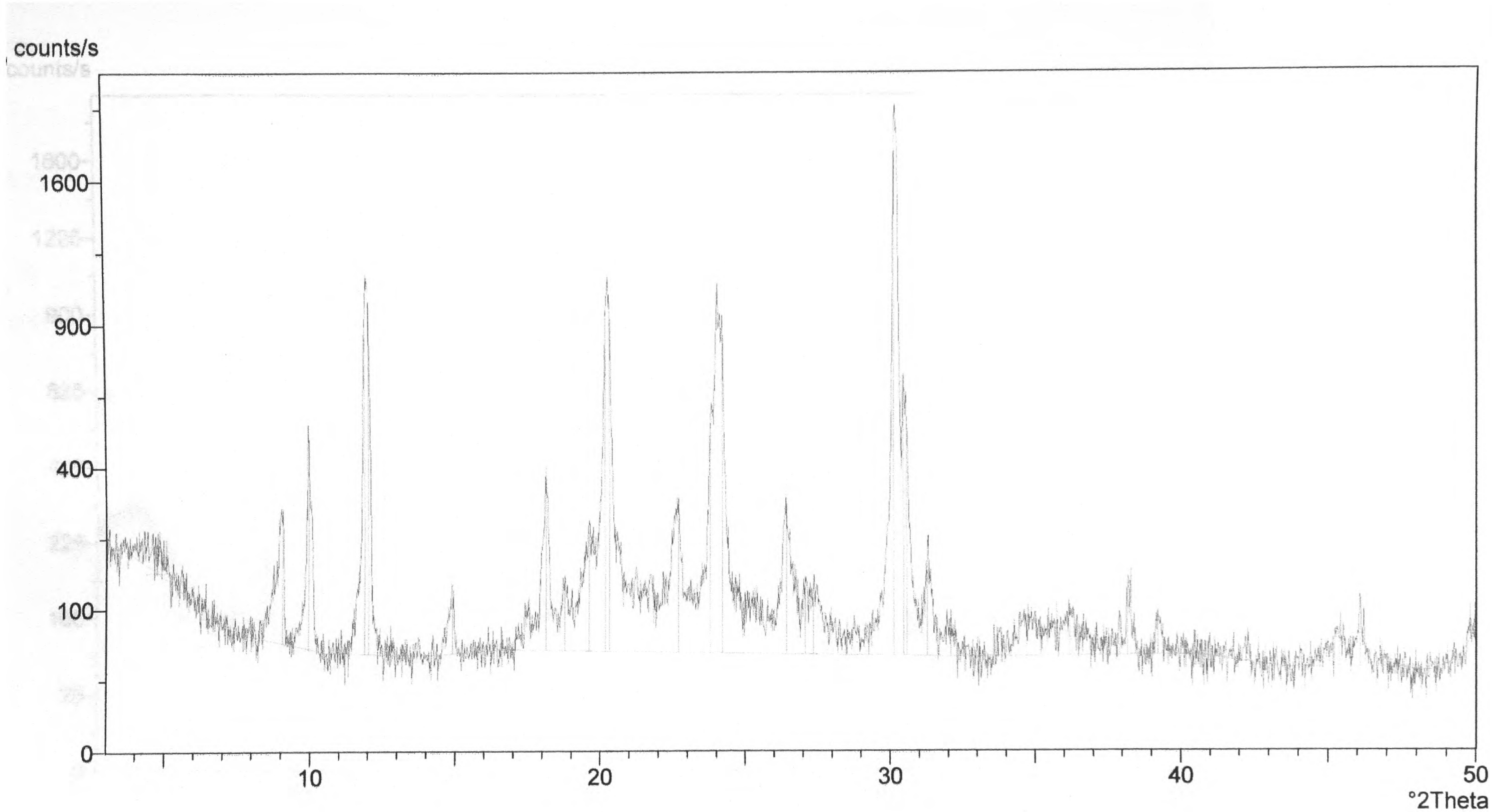

X-ray diffraction pattern of K10 with NIPAM (2:0.5)

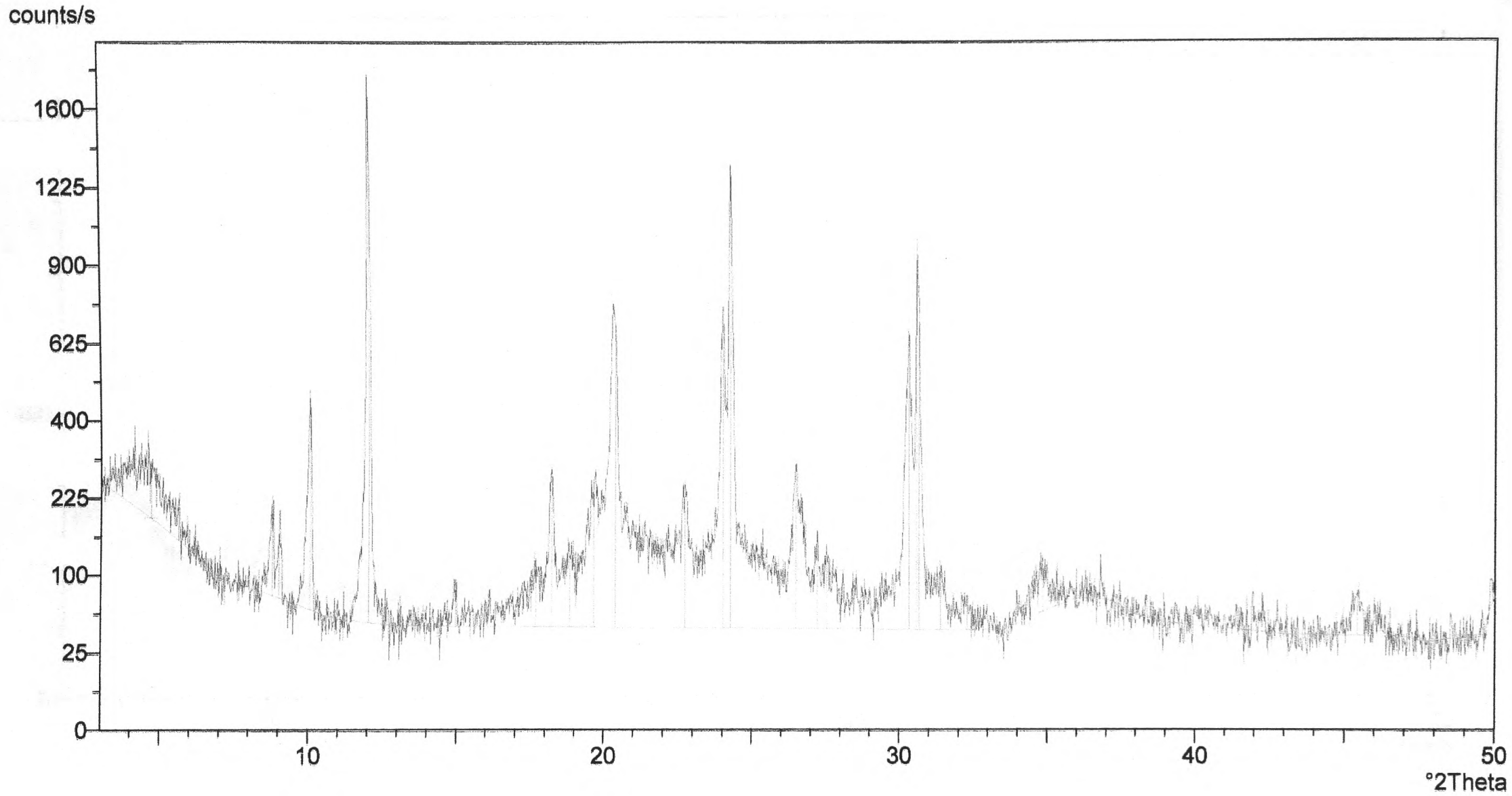

X-ray diffraction pattern of organophilic K10 with styrene (2:2)

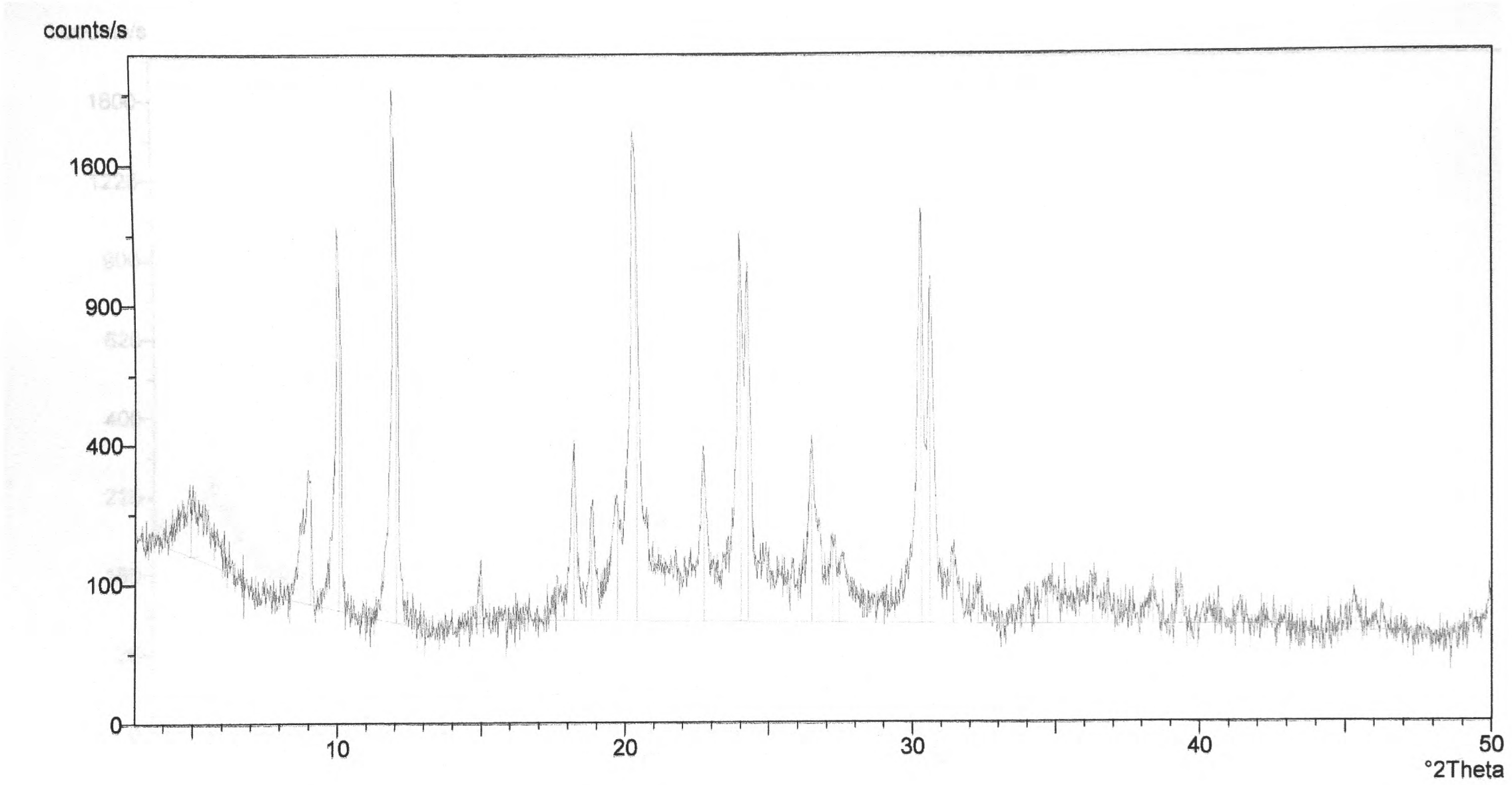

X-ray diffraction pattern of organophilic K10 with styrene (2:1.5)

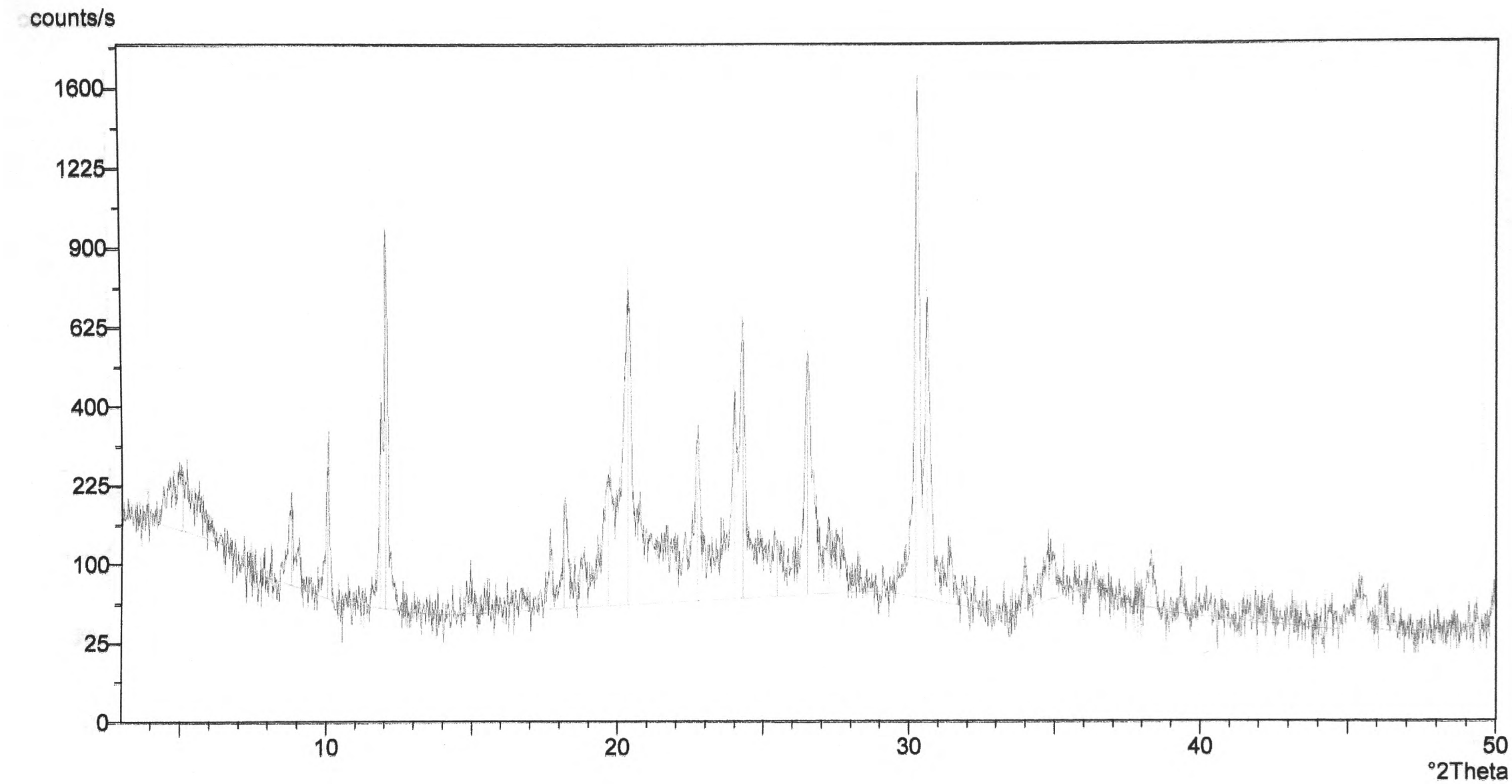

X-ray diffraction pattern of organophilic K10 with styrene (2:1)

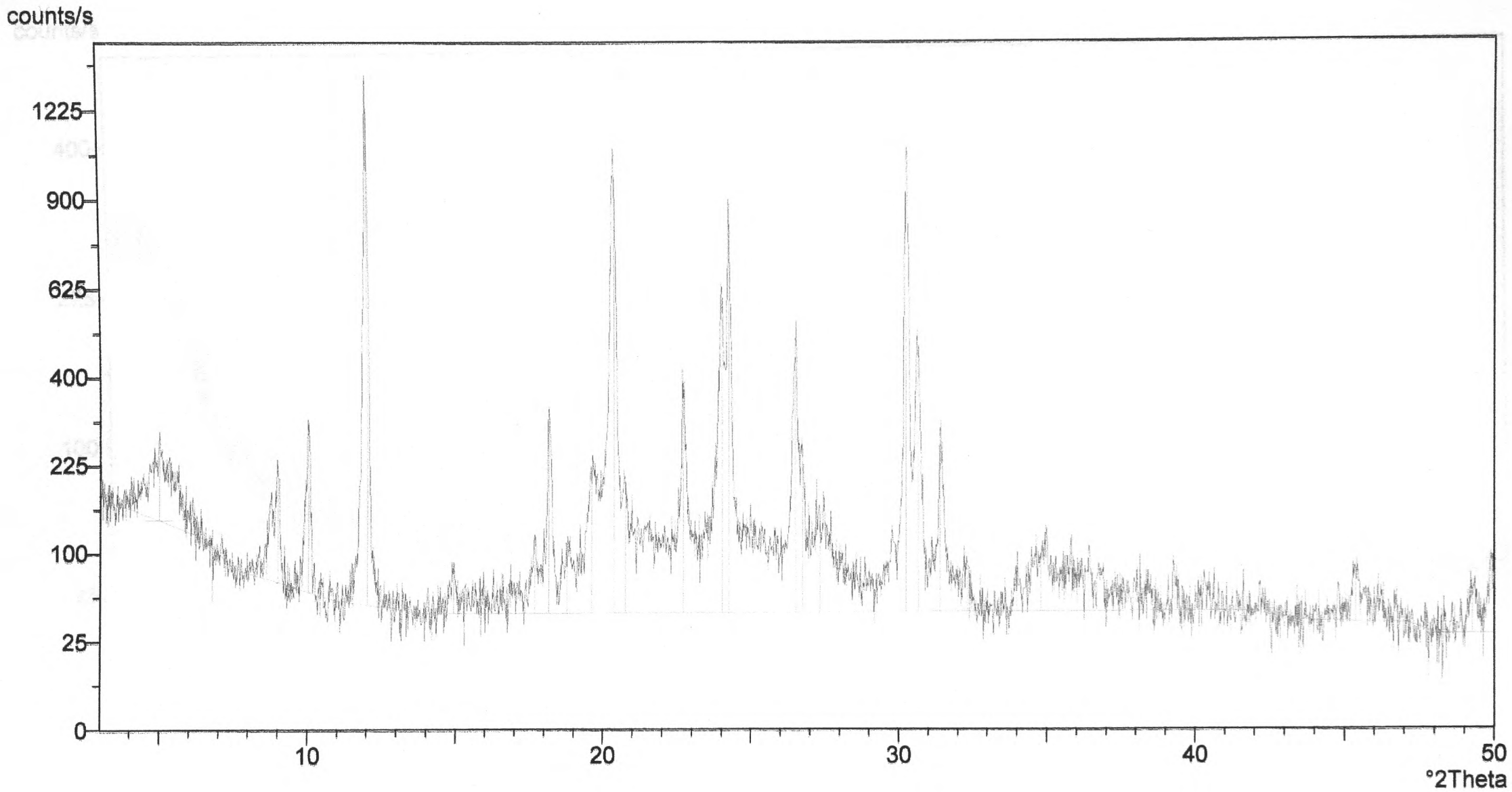

X-ray diffraction pattern of organophilic K10 with styrene (2:0.5)

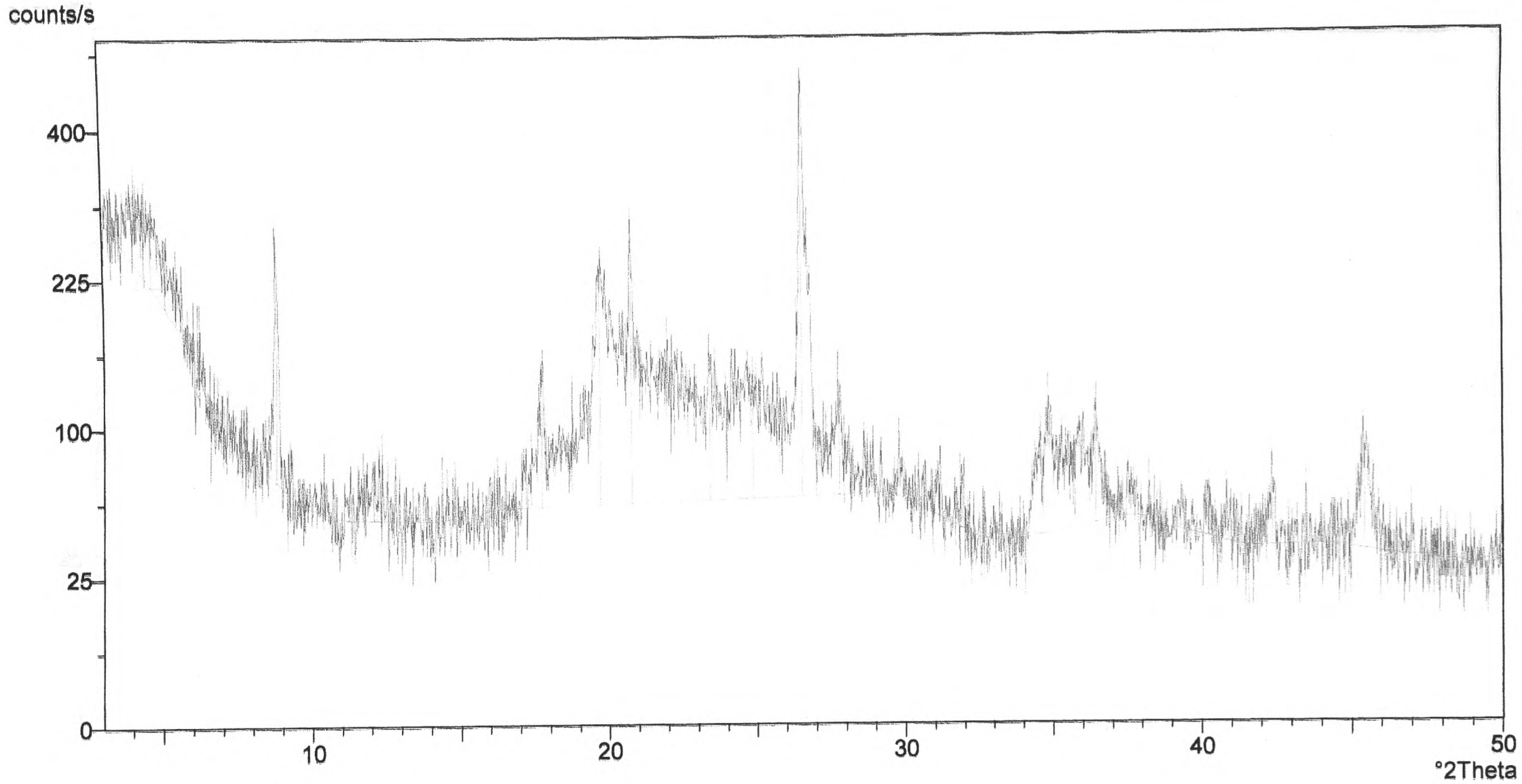

X-ray diffraction pattern of K10 with styrene (2:2)

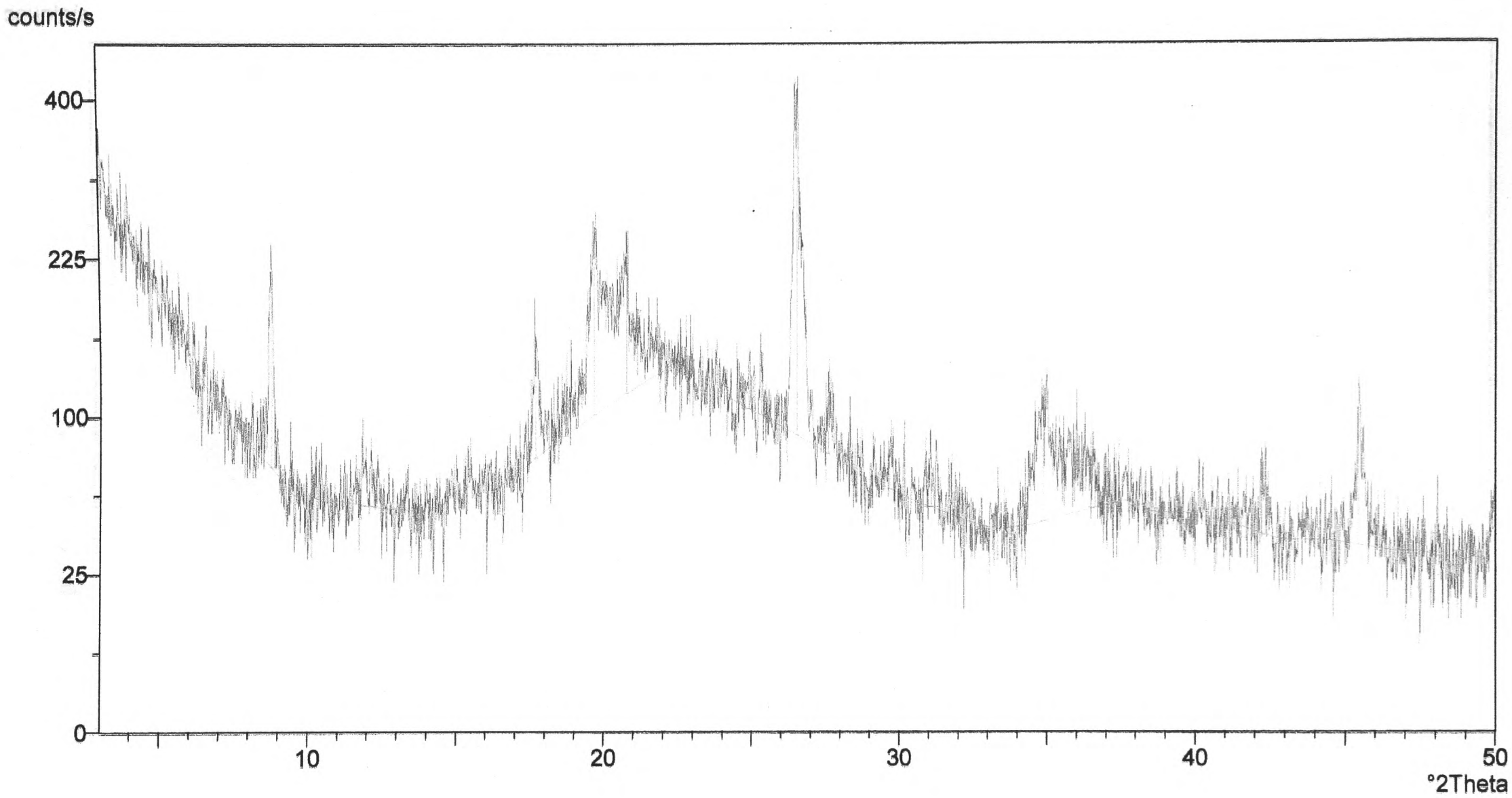

X-ray diffraction pattern of K10 with styrene (2:1.5)

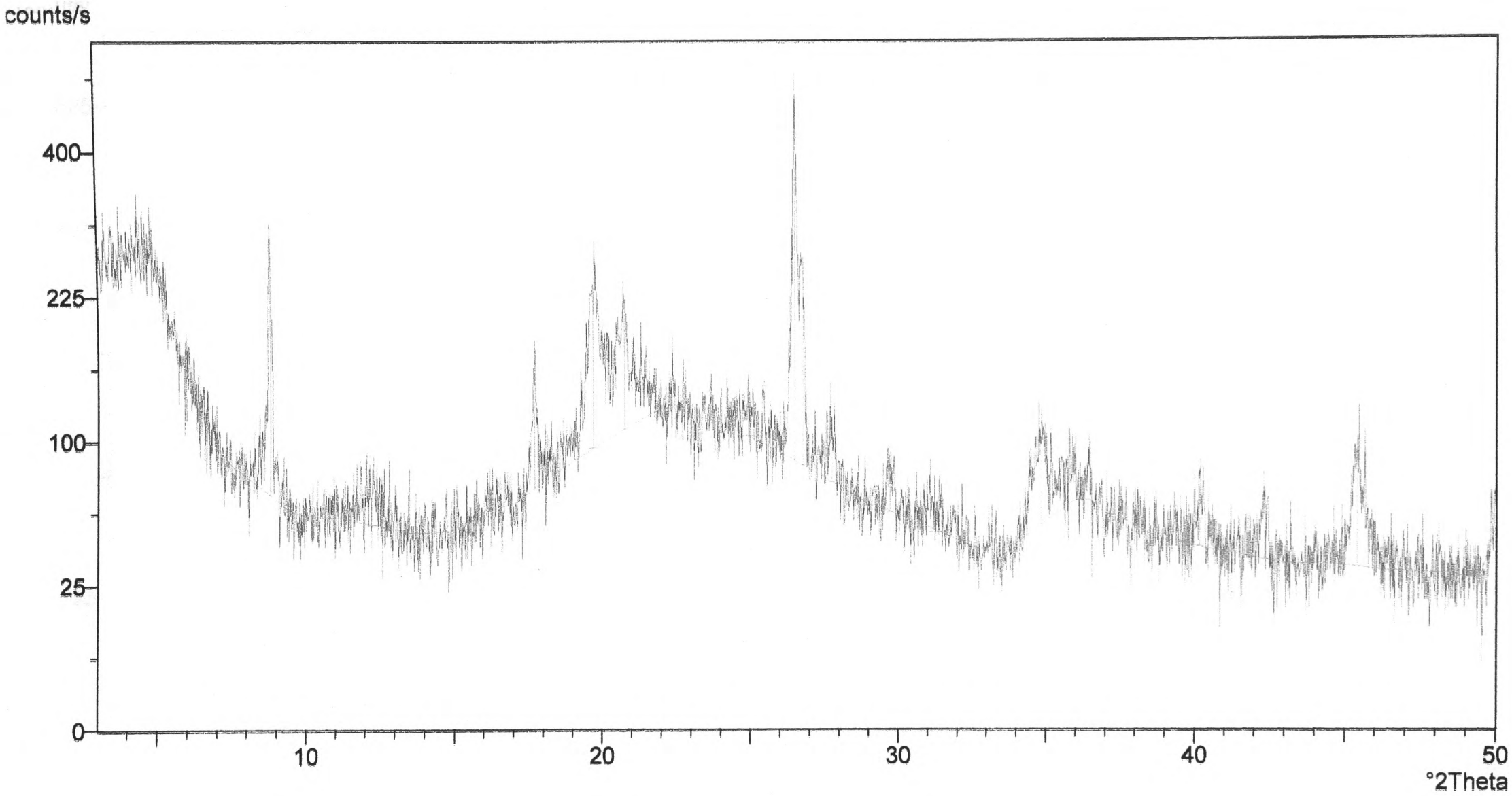

X-ray diffraction pattern of K10 with styrene (2:1)

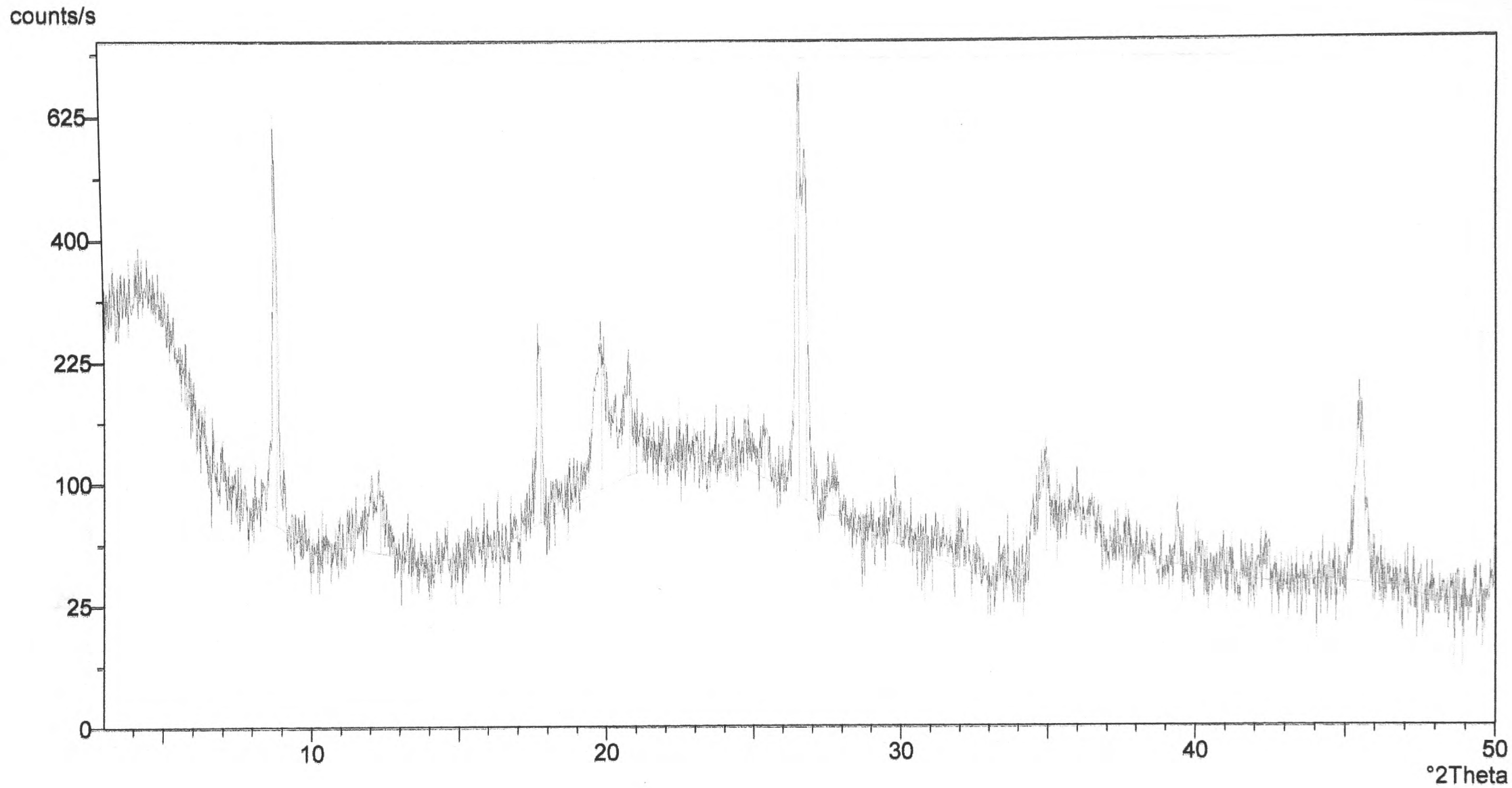

X-ray diffraction pattern of K10 with styrene (2:0.5)

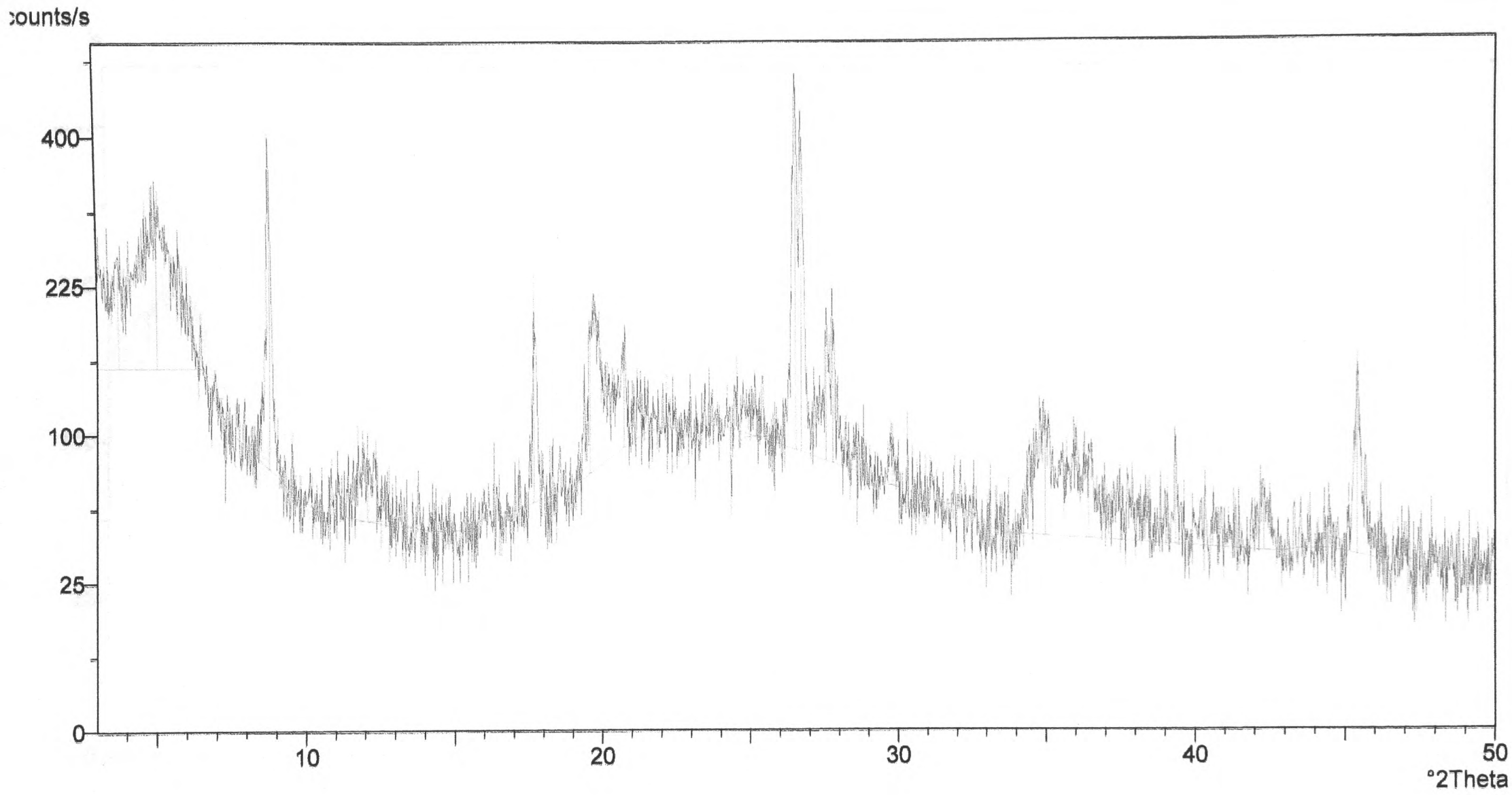

X-ray diffraction pattern of organophilic bentonite with NIPAM (2:2)

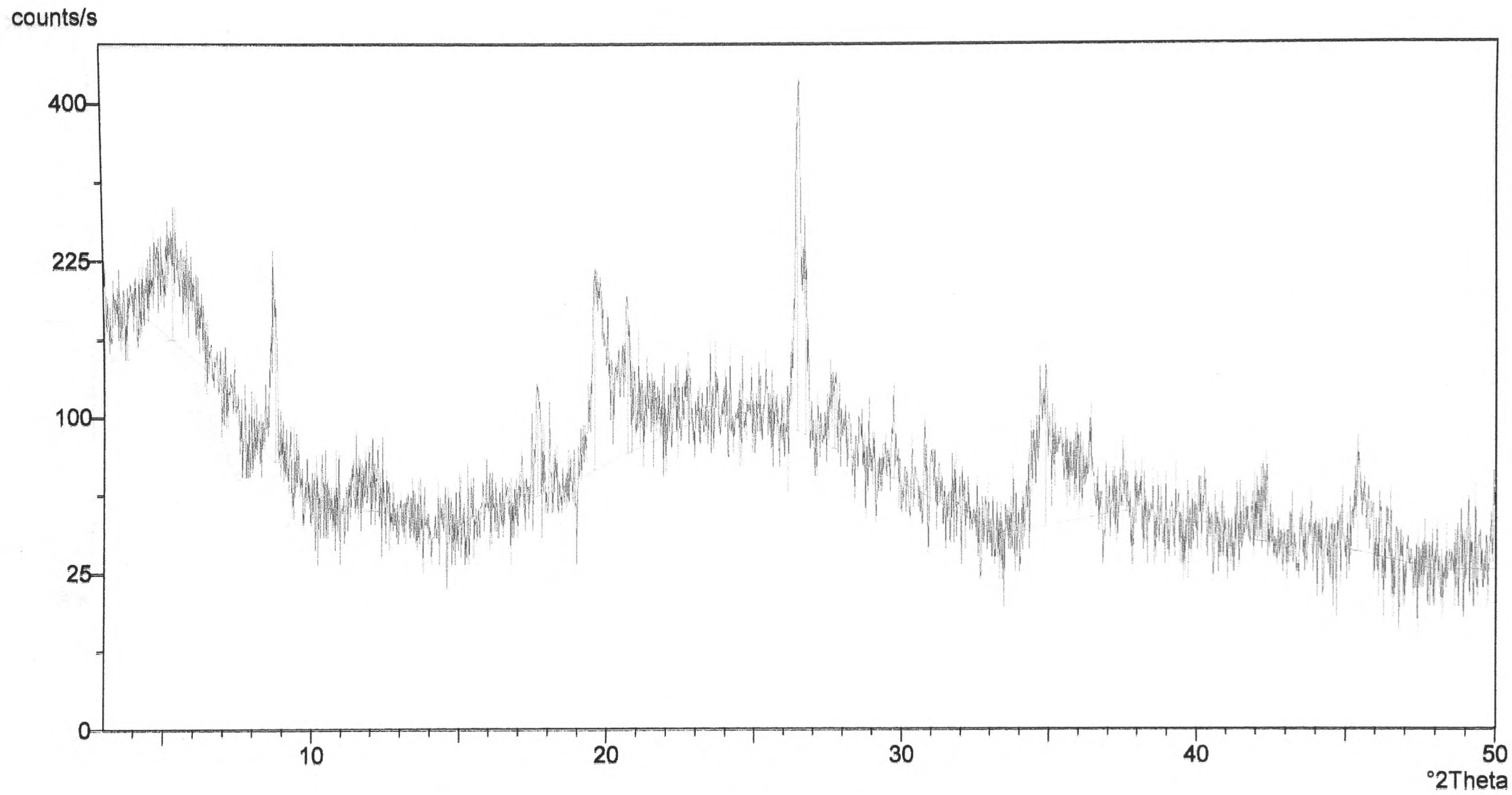

X-ray diffraction pattern of organophilic bentonite with NIPAM (2:1.5)

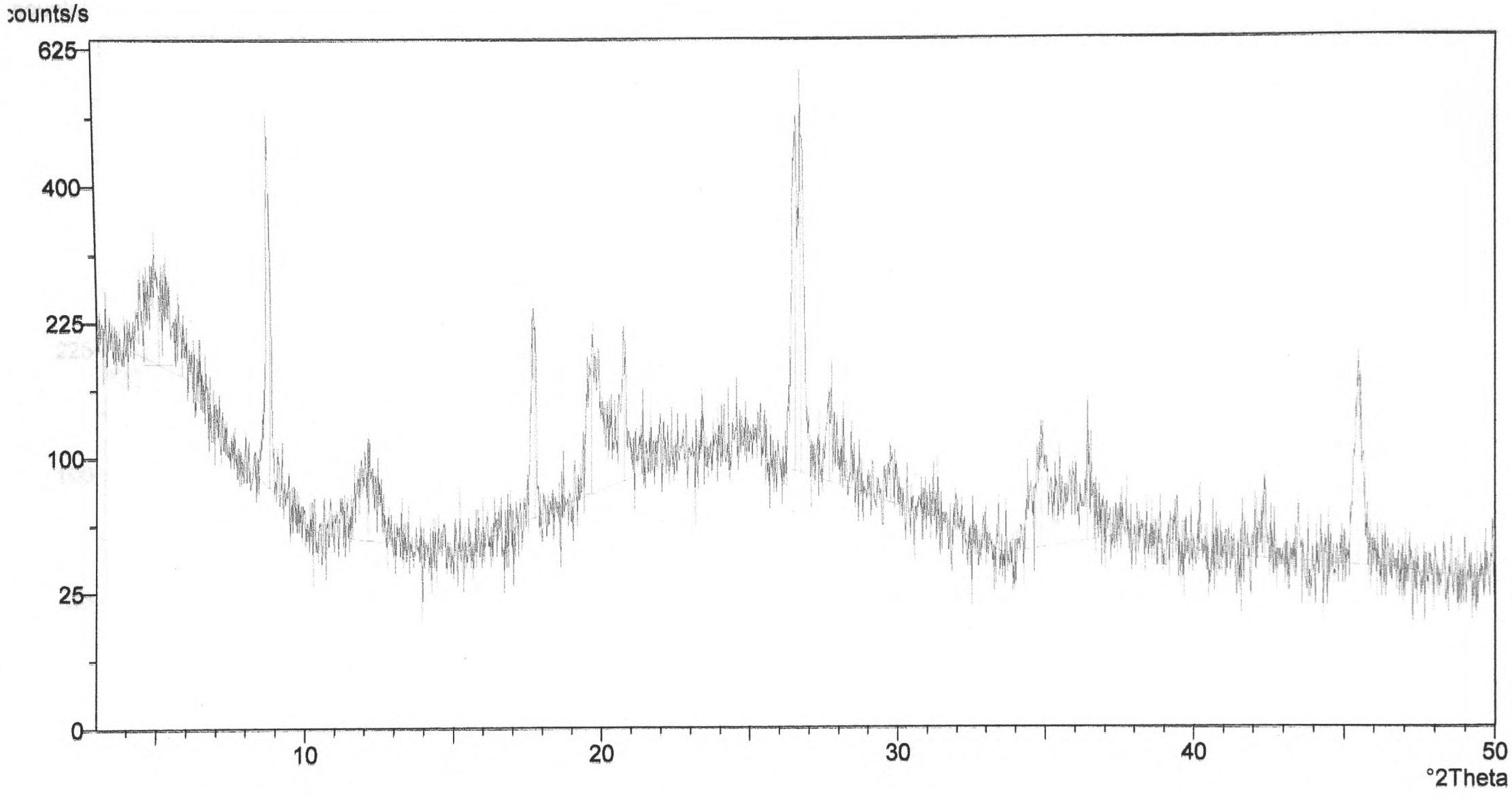

X-ray diffraction pattern of organophilic bentonite with NIPAM (2:1)

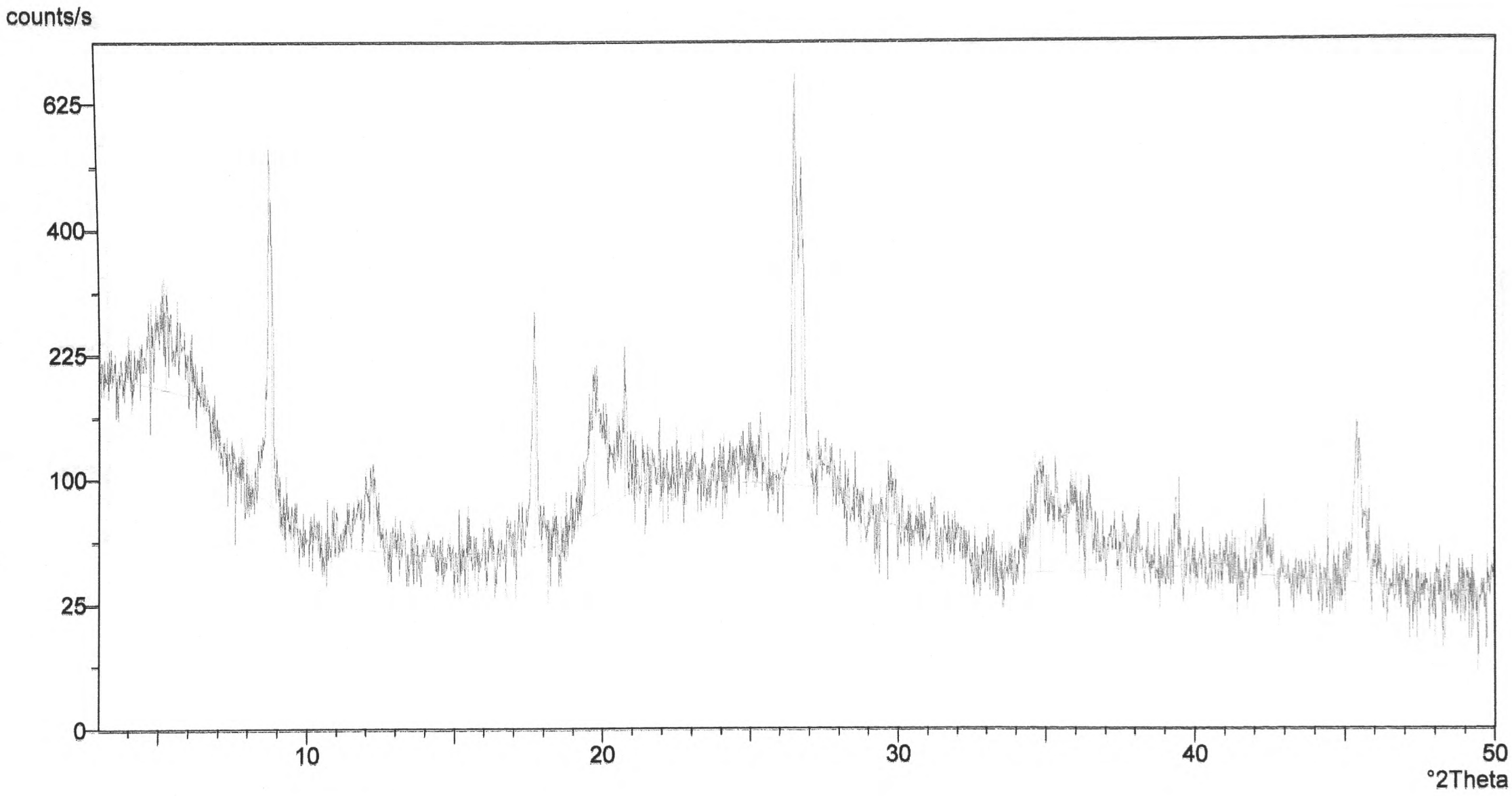

X-ray diffraction pattern of organophilic bentonite with NIPAM (2:0.5)

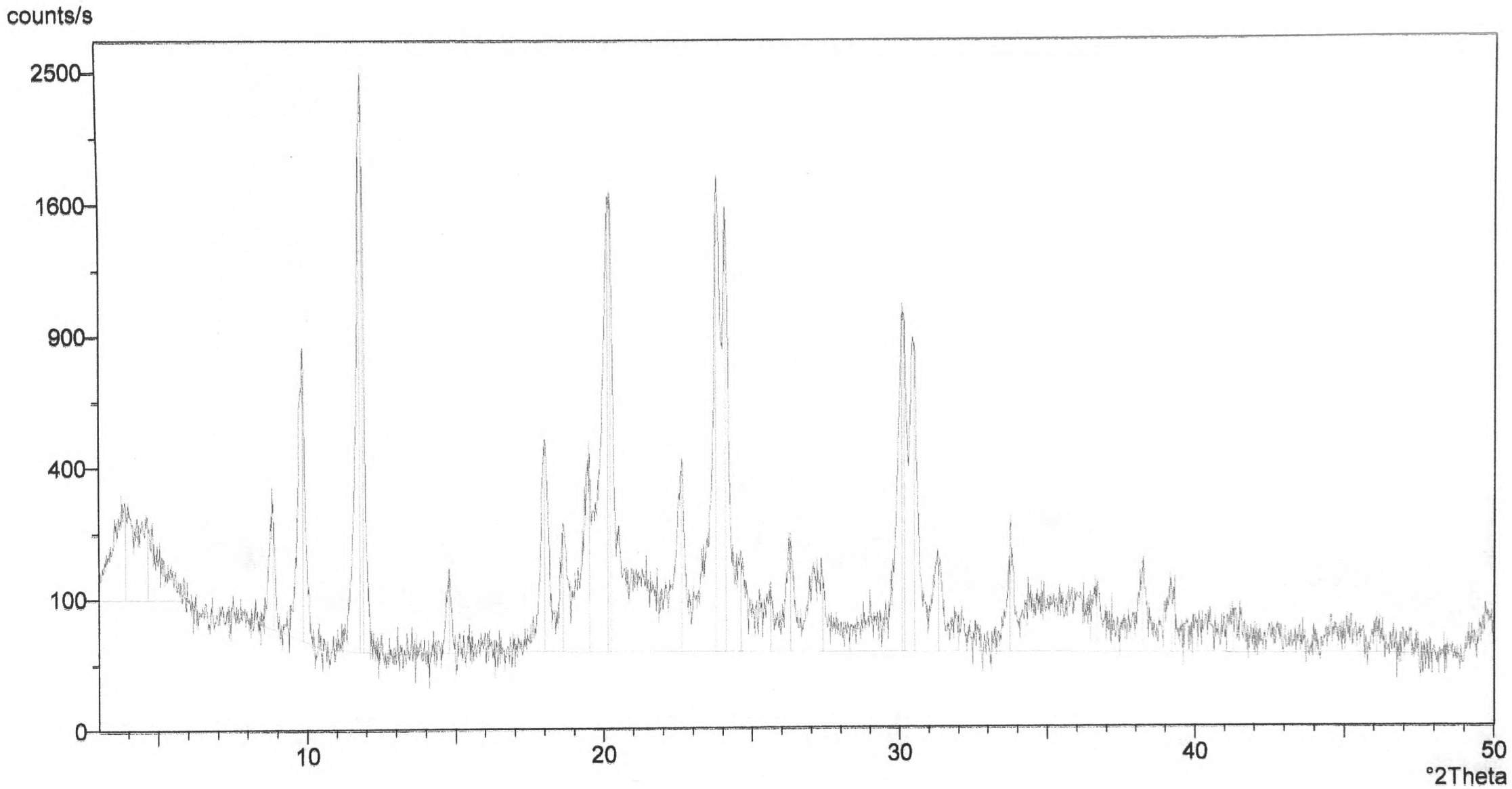

X-ray diffraction pattern of bentonite with NIPAM (2:2)

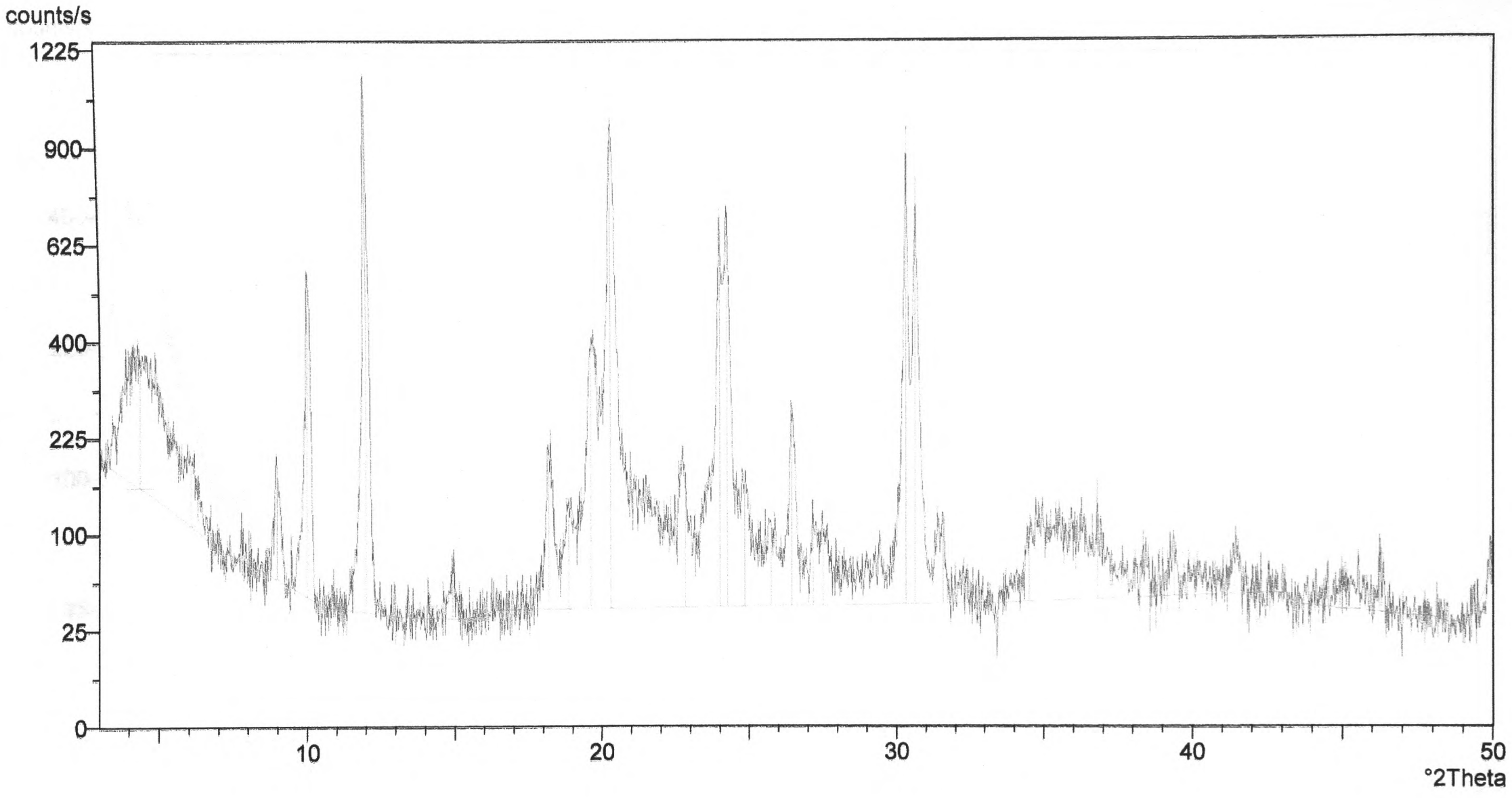

X-ray diffraction pattern of bentonite with NIPAM (2:1.5)

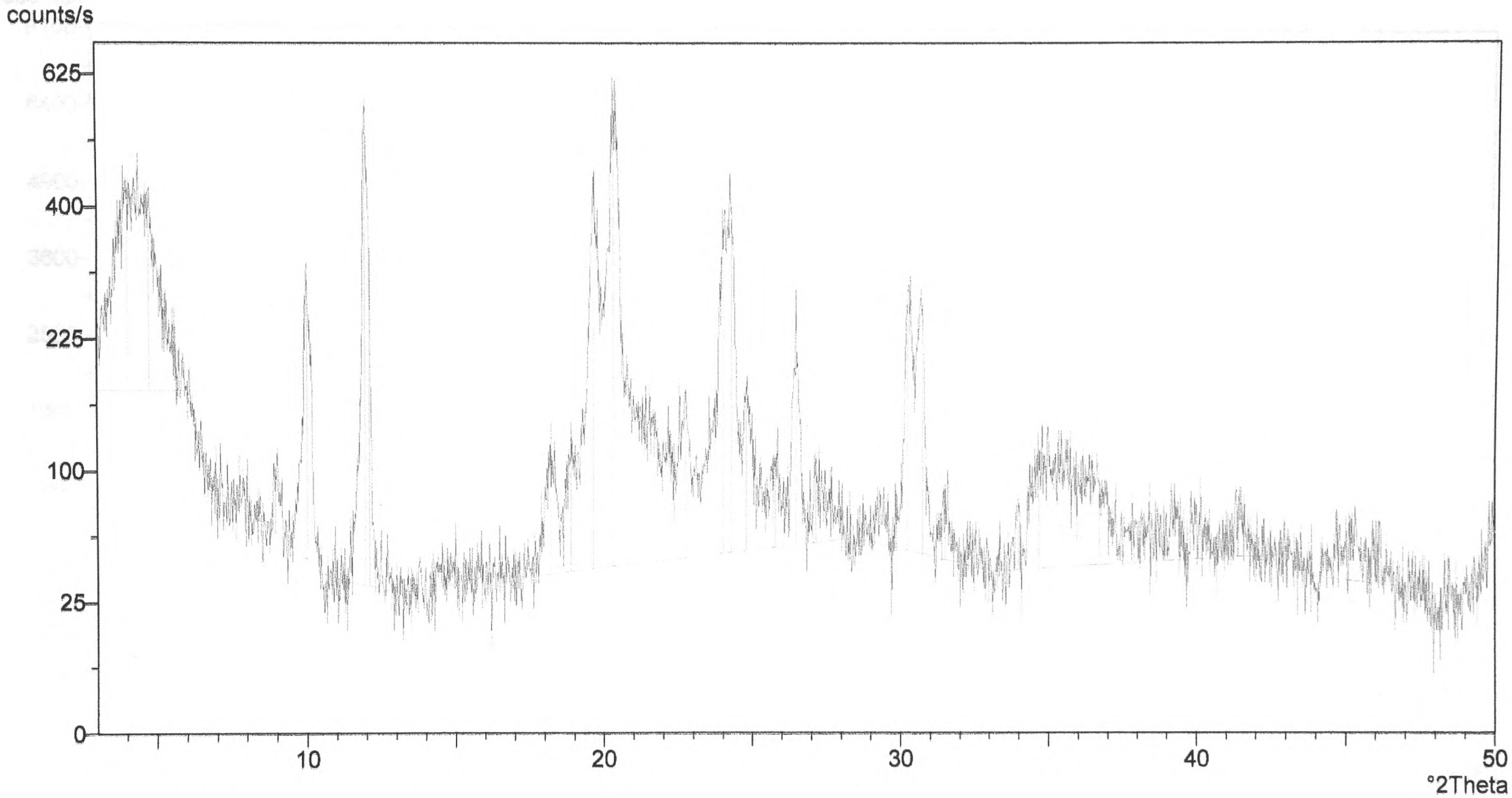

X-ray diffraction pattern of bentonite with NIPAM (2:1)

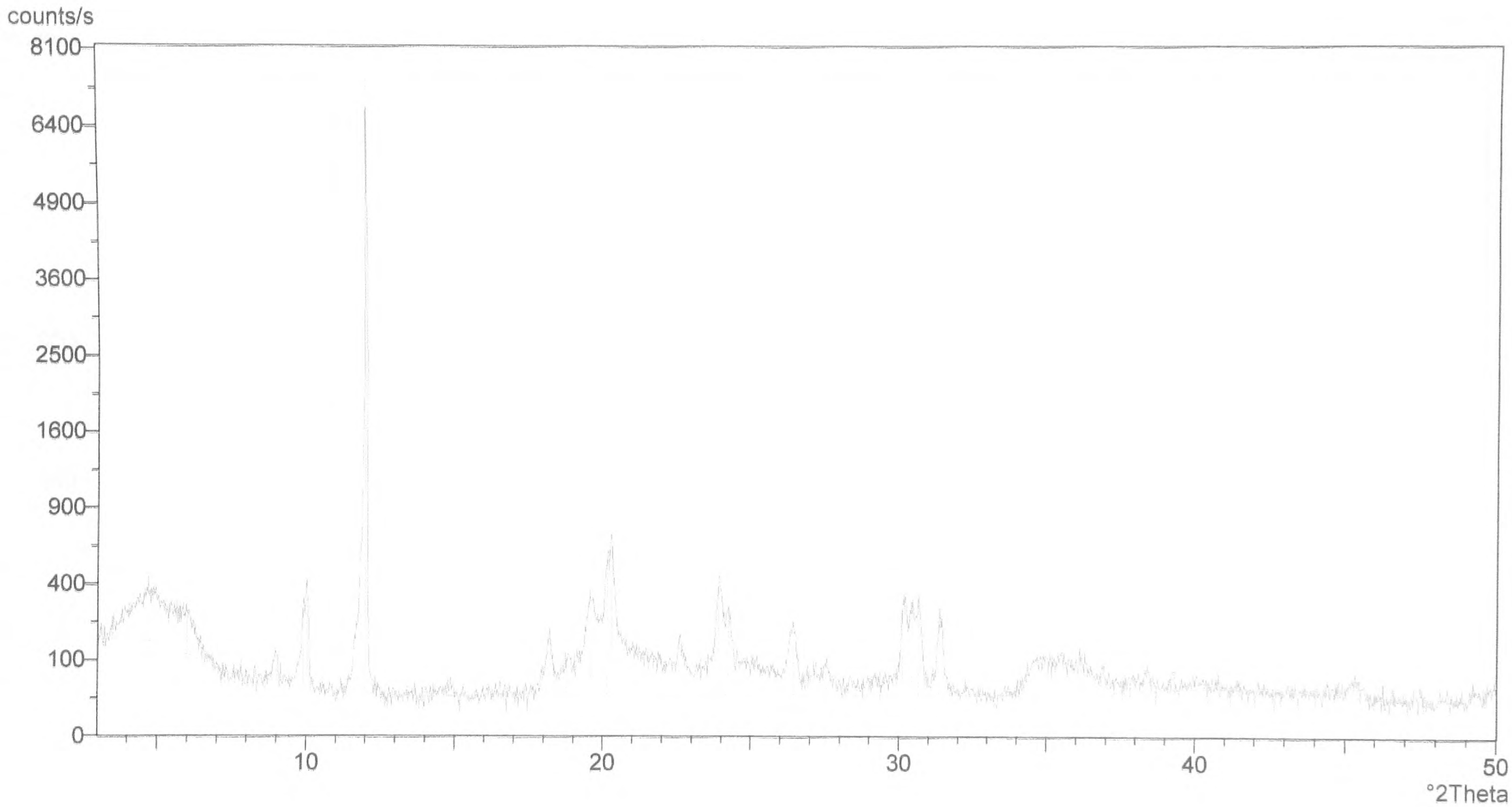

X-ray diffraction pattern of bentonite with NIPAM (2:0.5)

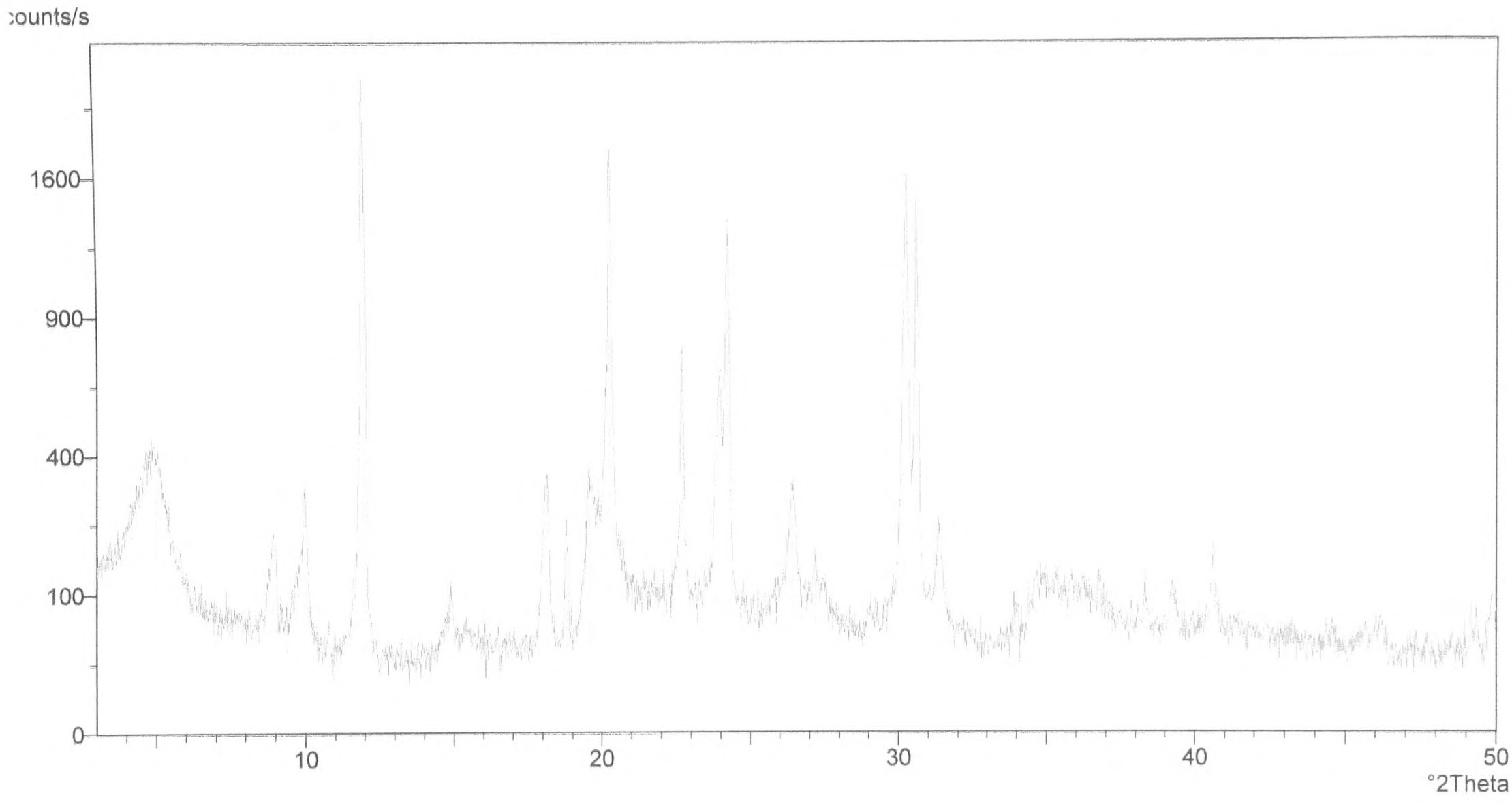

X-ray diffraction pattern of organophilic bentonite with styrene (2:2)

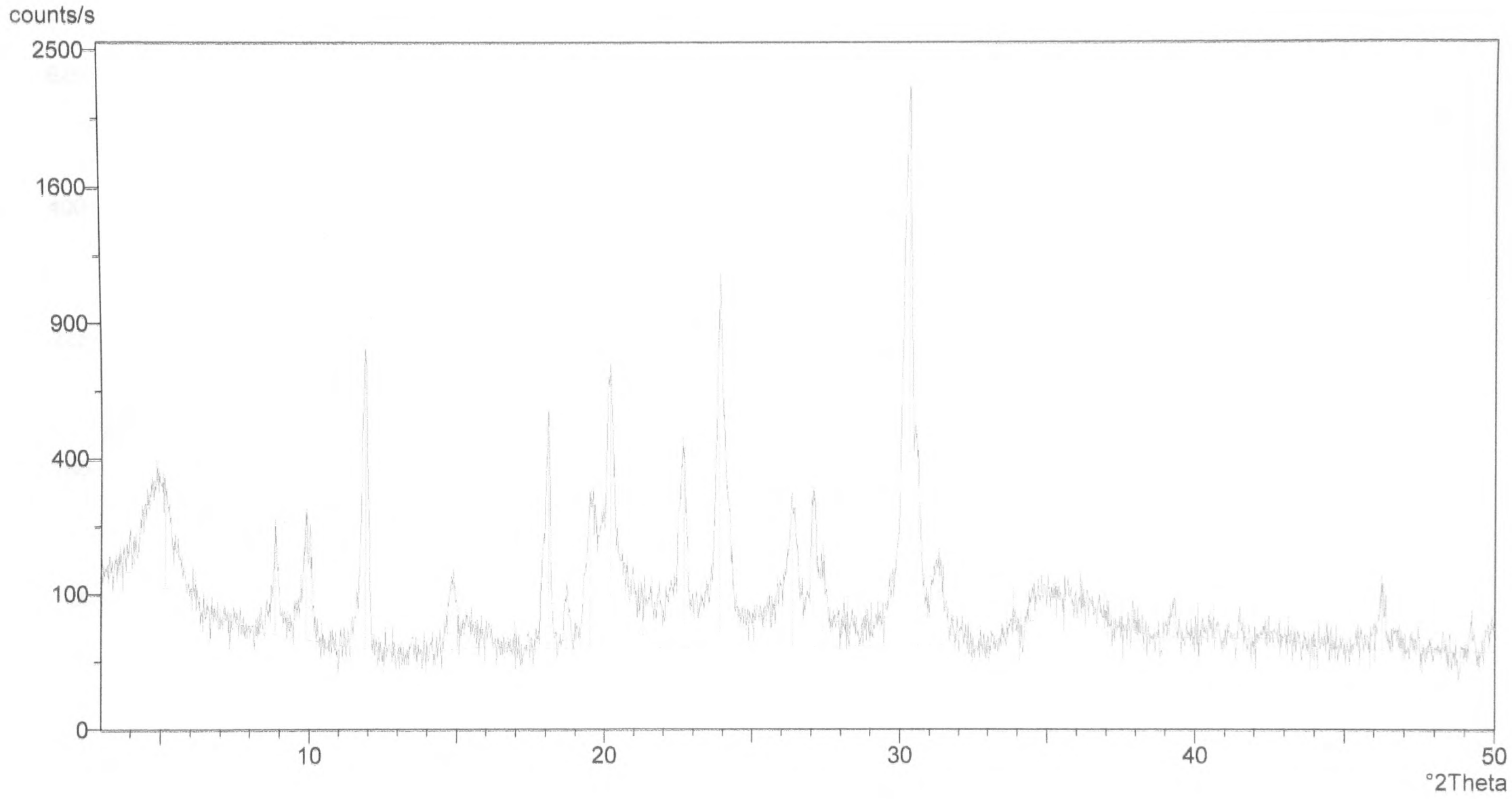

X-ray diffraction pattern of organophilic bentonite with styrene (2:1.5)

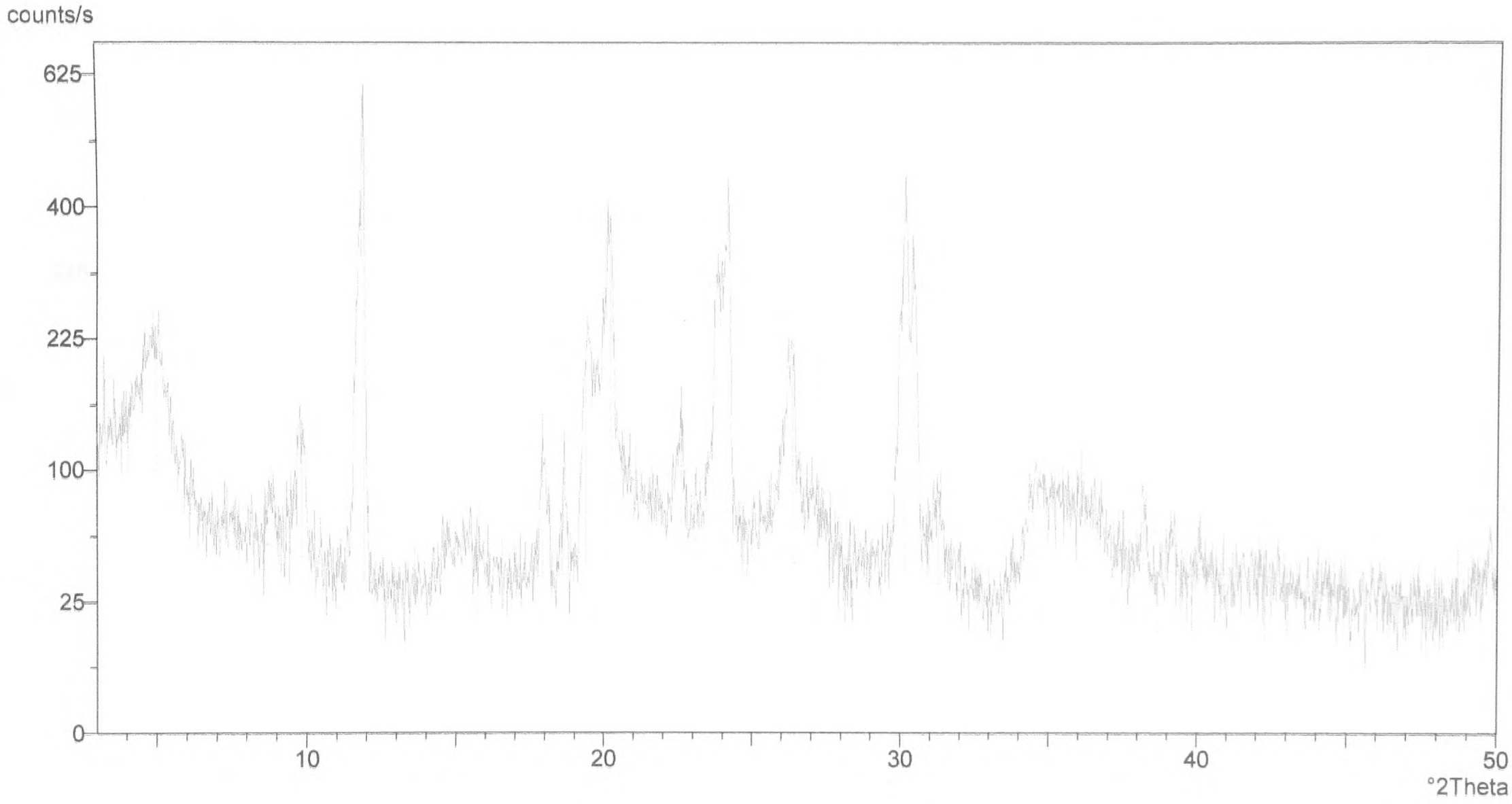

X-ray diffraction pattern of organophilic bentonite with styrene (2:1)

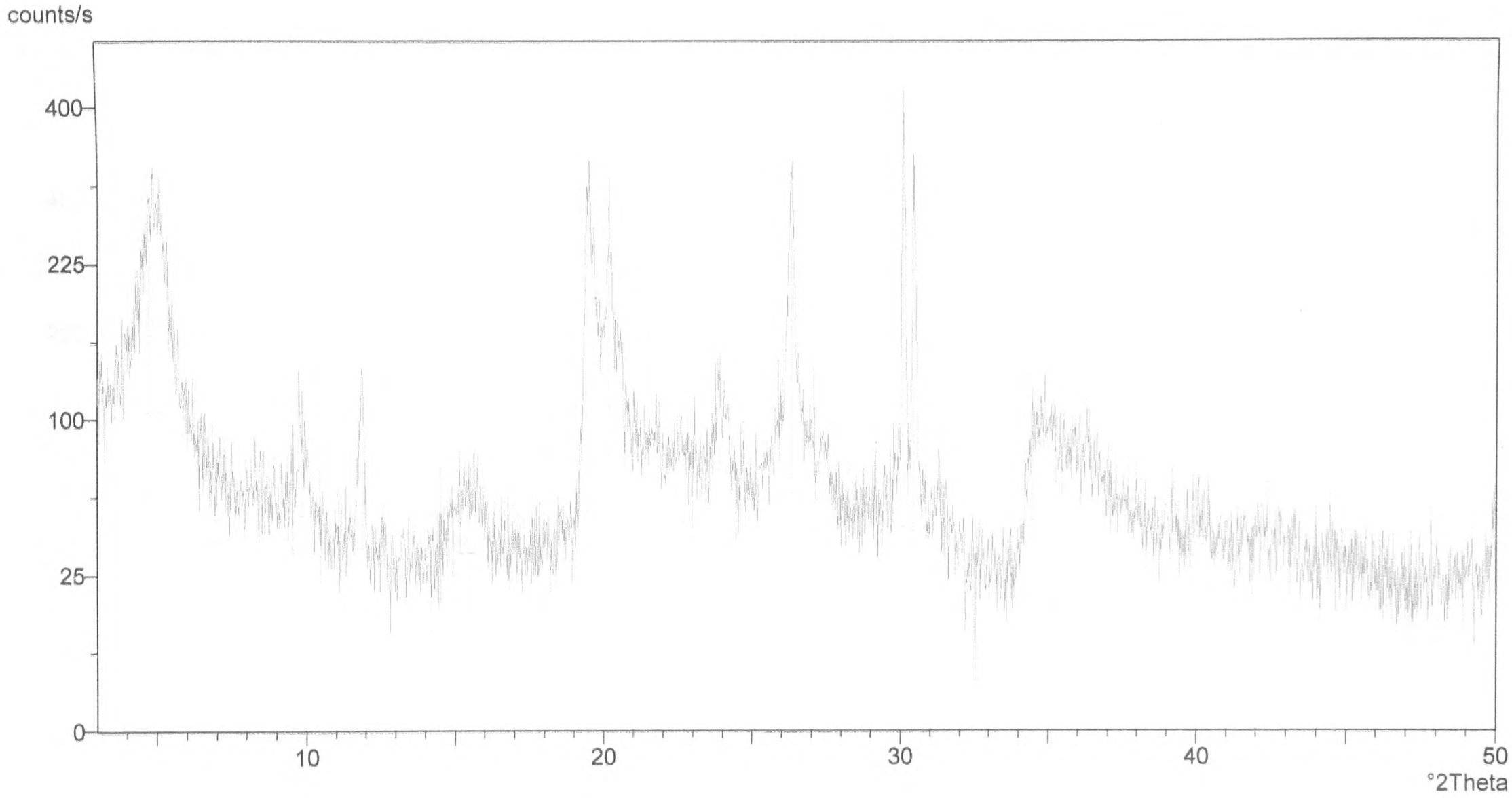

X-ray diffraction pattern of organophilic bentonite with styrene (2:0.5)

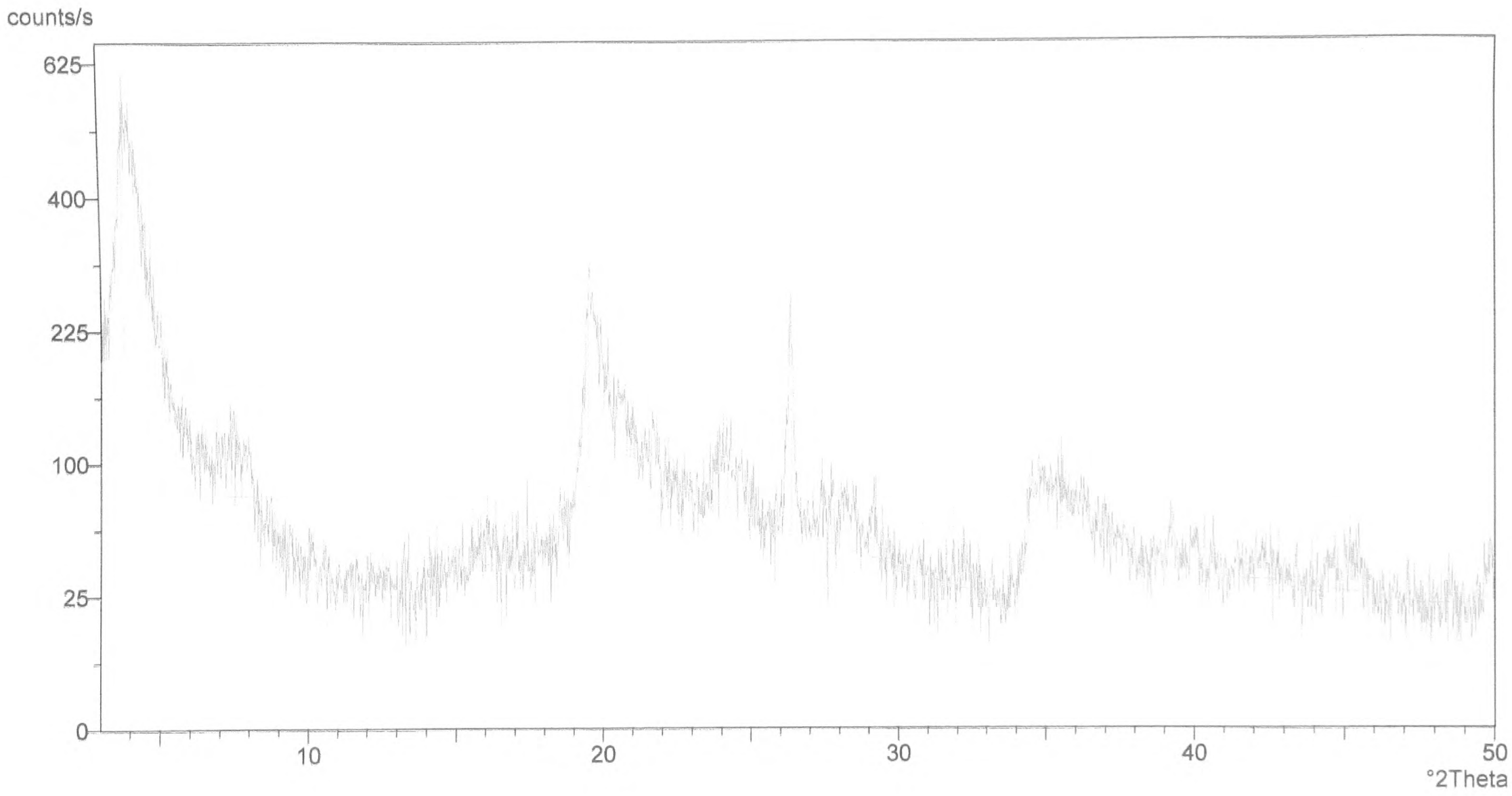

X-ray diffraction pattern of bentonite with styrene (2:2)

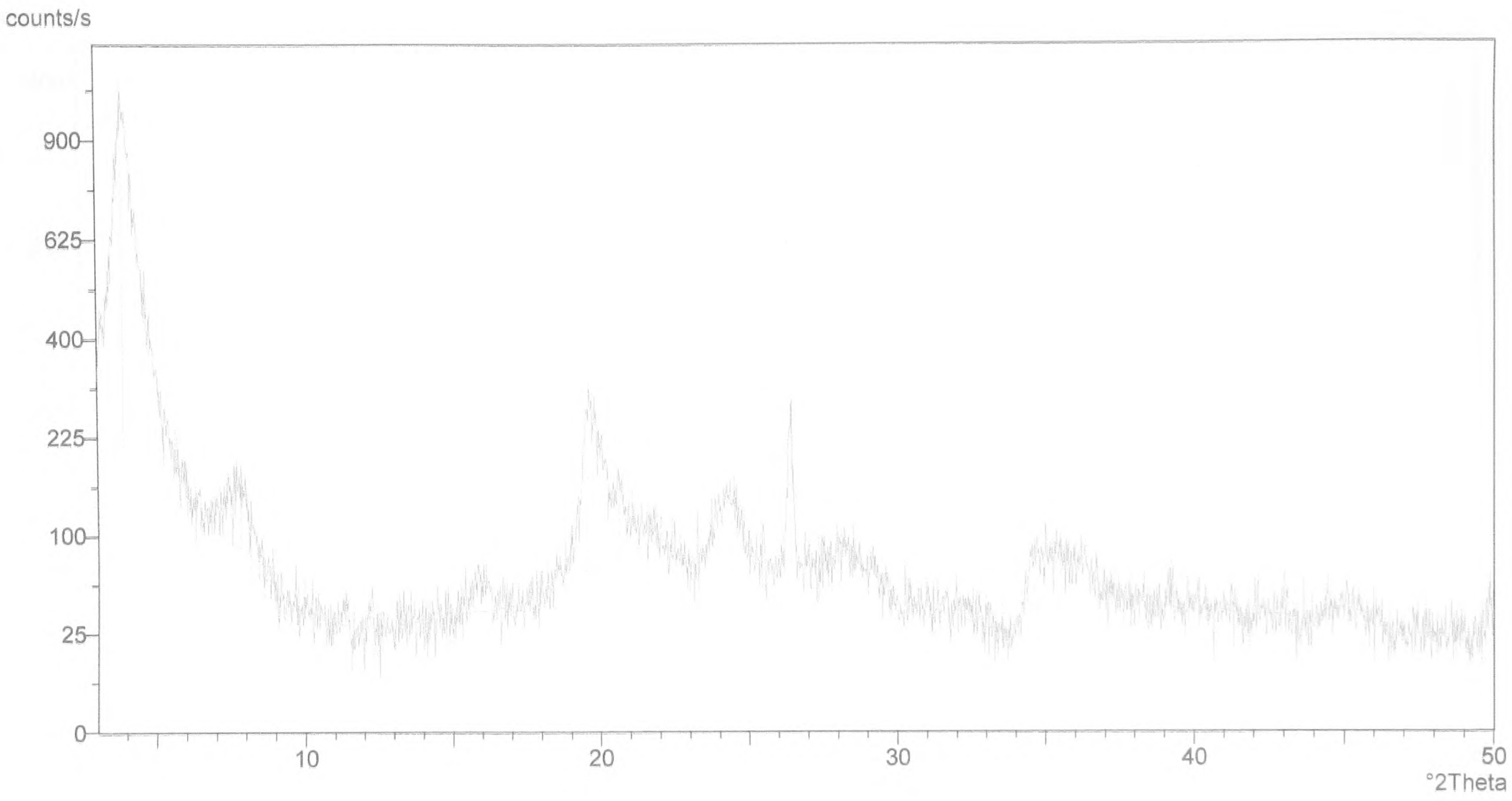

X-ray diffraction pattern of bentonite with styrene (2:1.5)

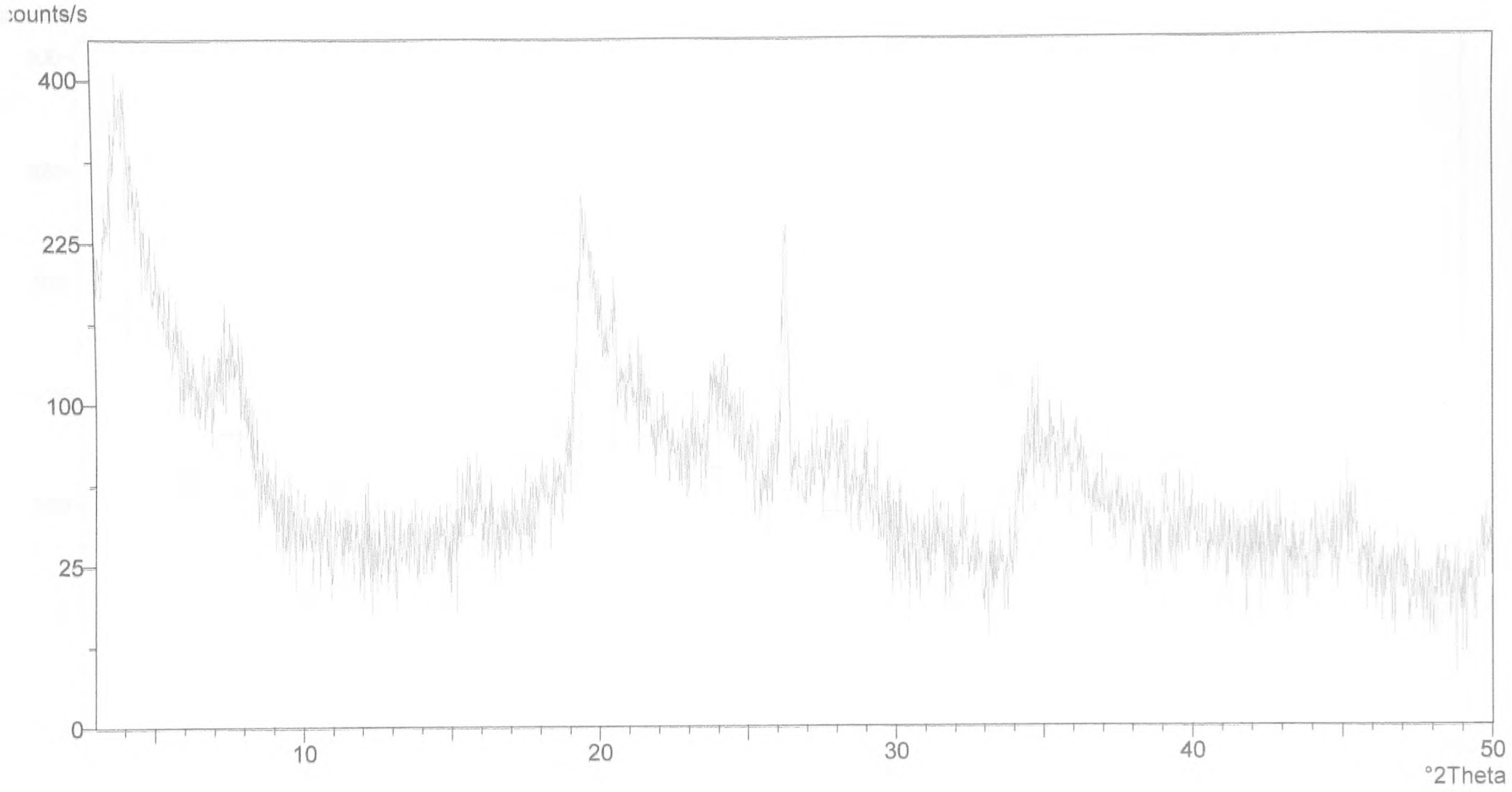

X-ray diffraction pattern of bentonite with styrene (2:1)

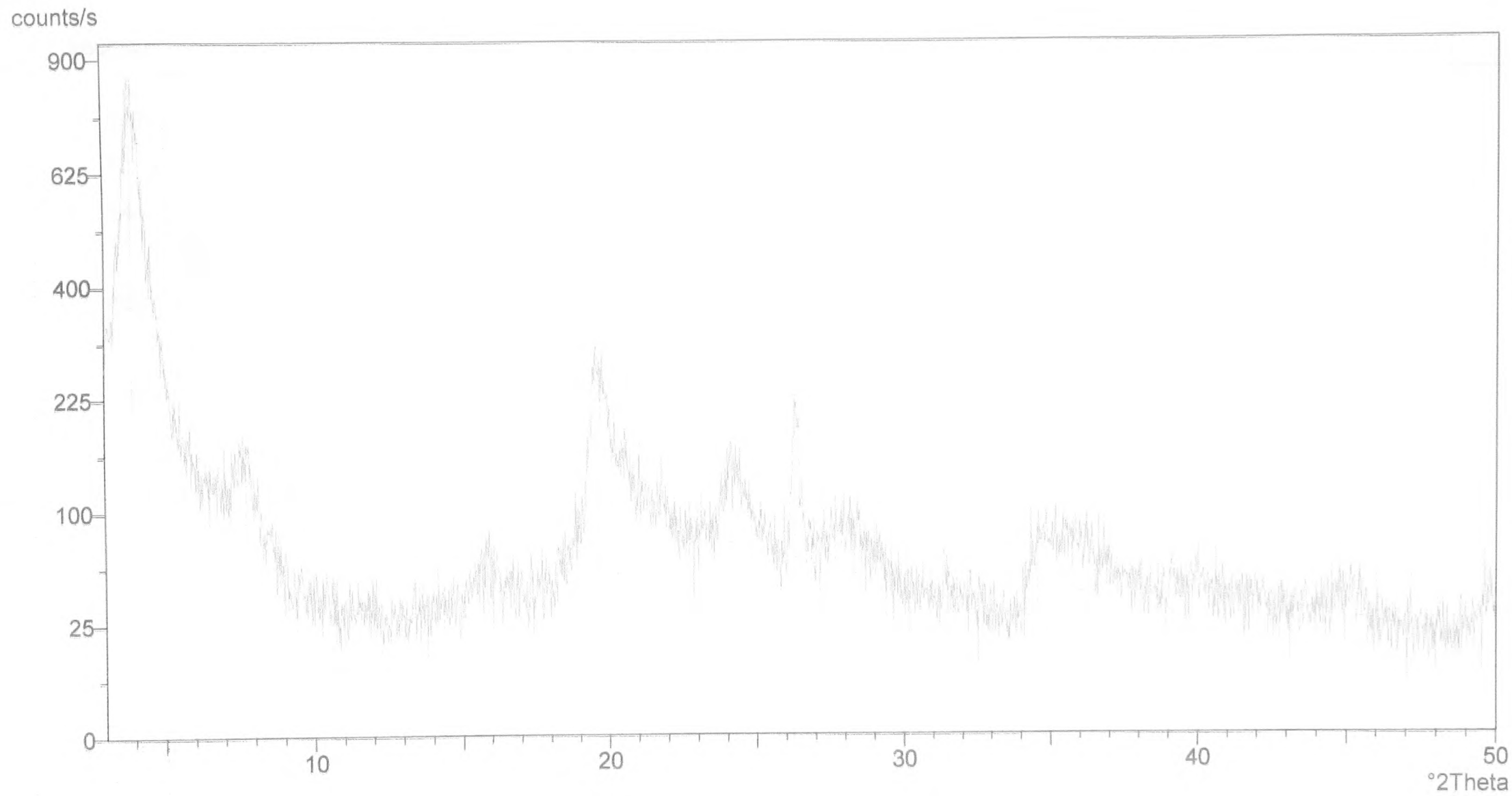

X-ray diffraction pattern of bentonite with styrene (2:0.5)

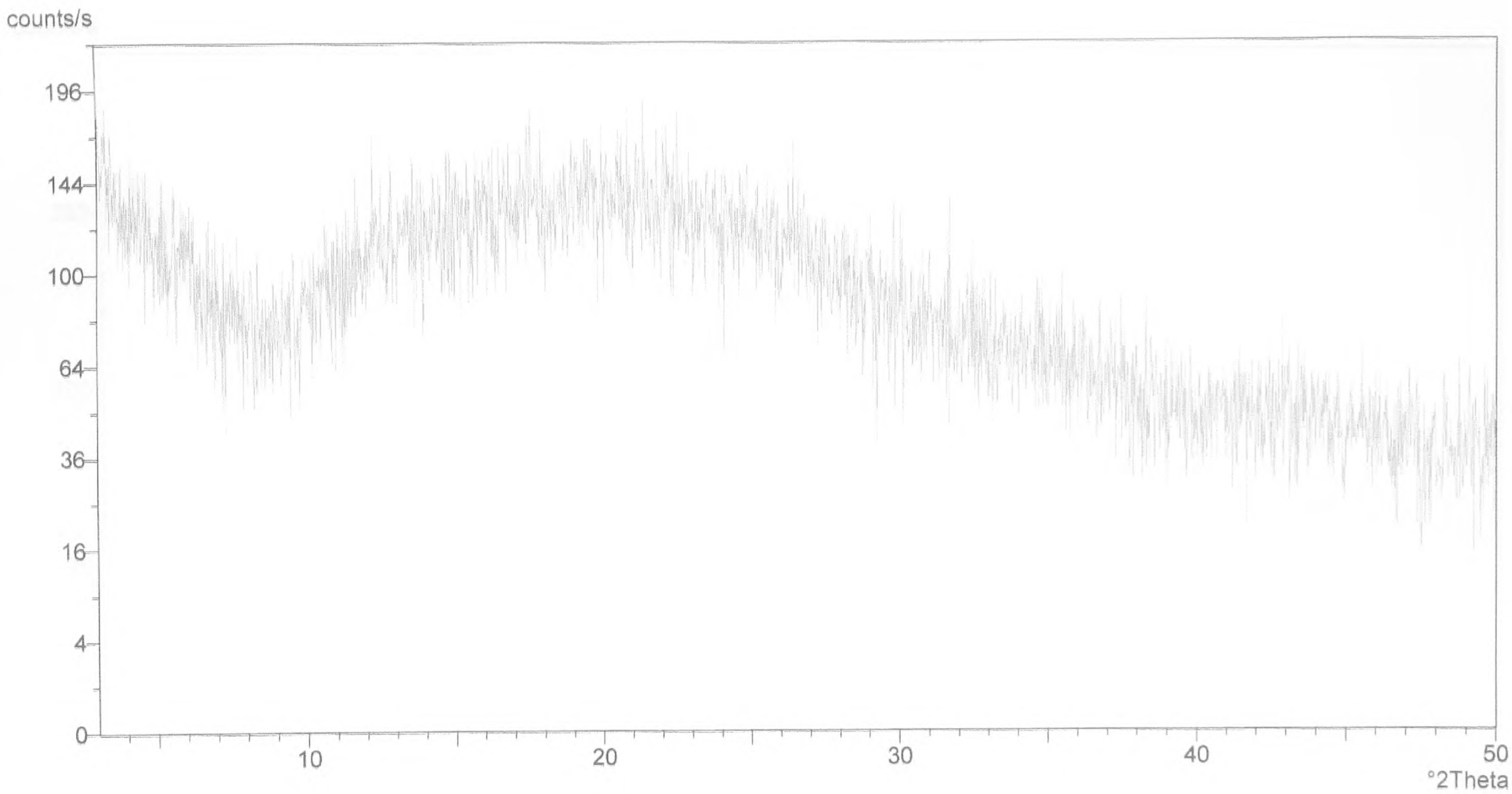

X-ray diffraction pattern of bentonite-C_{16}-NIPAM (6 hours)

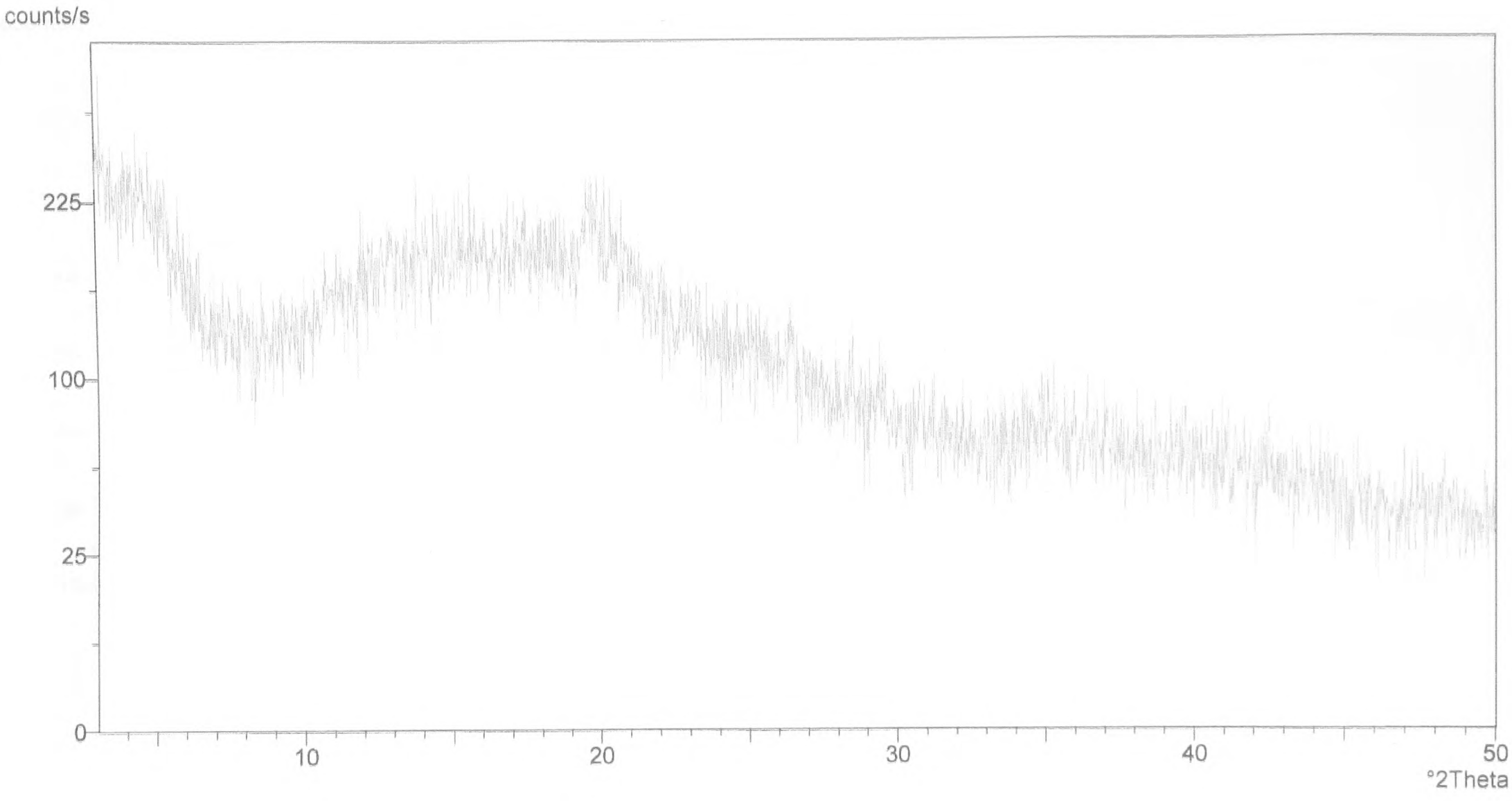

X-ray diffraction pattern of bentonite-C_{16}-NIPAM (4 hours)

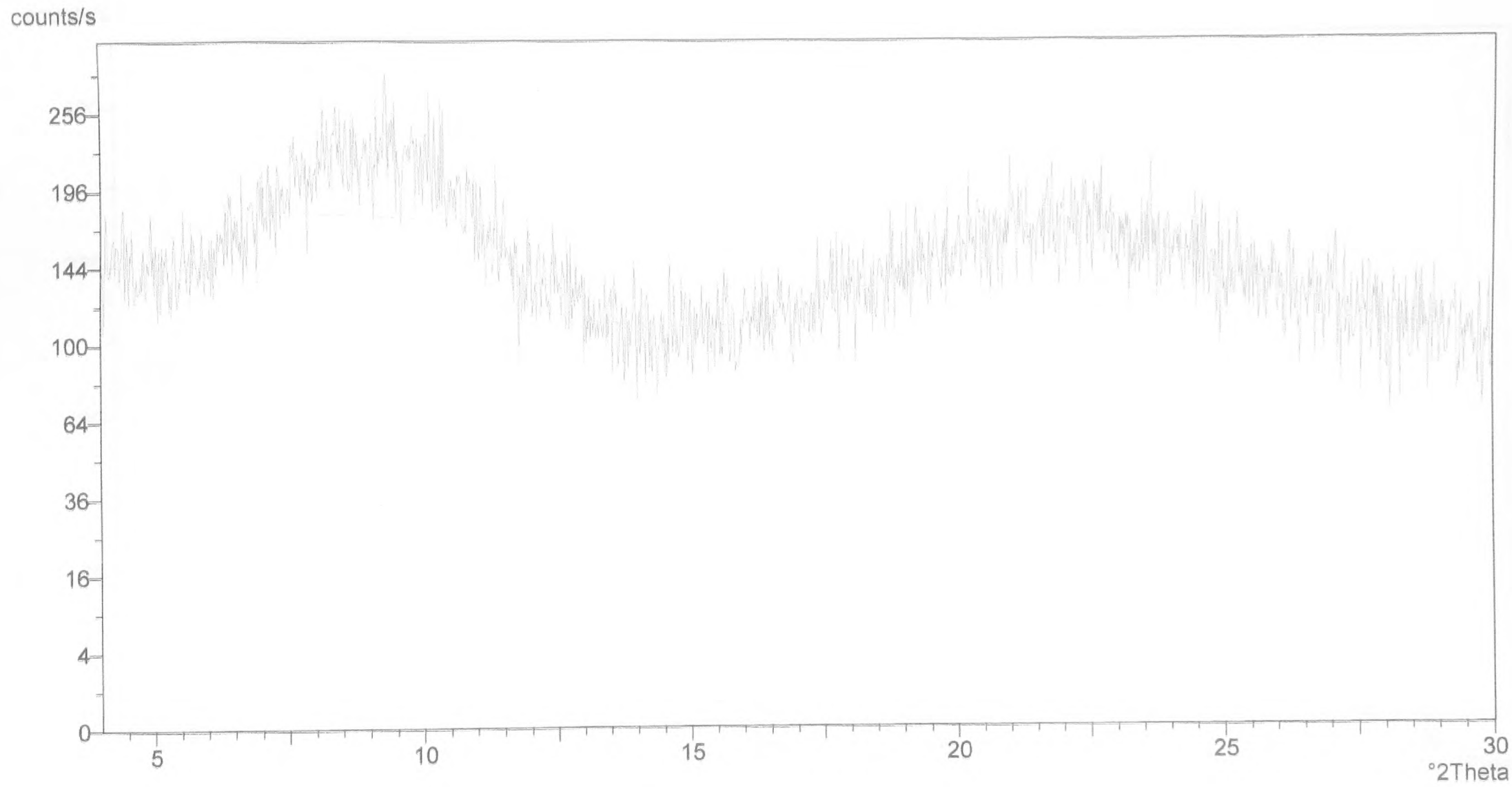

X-ray diffraction pattern of the vinyltrichlorosilane polymer

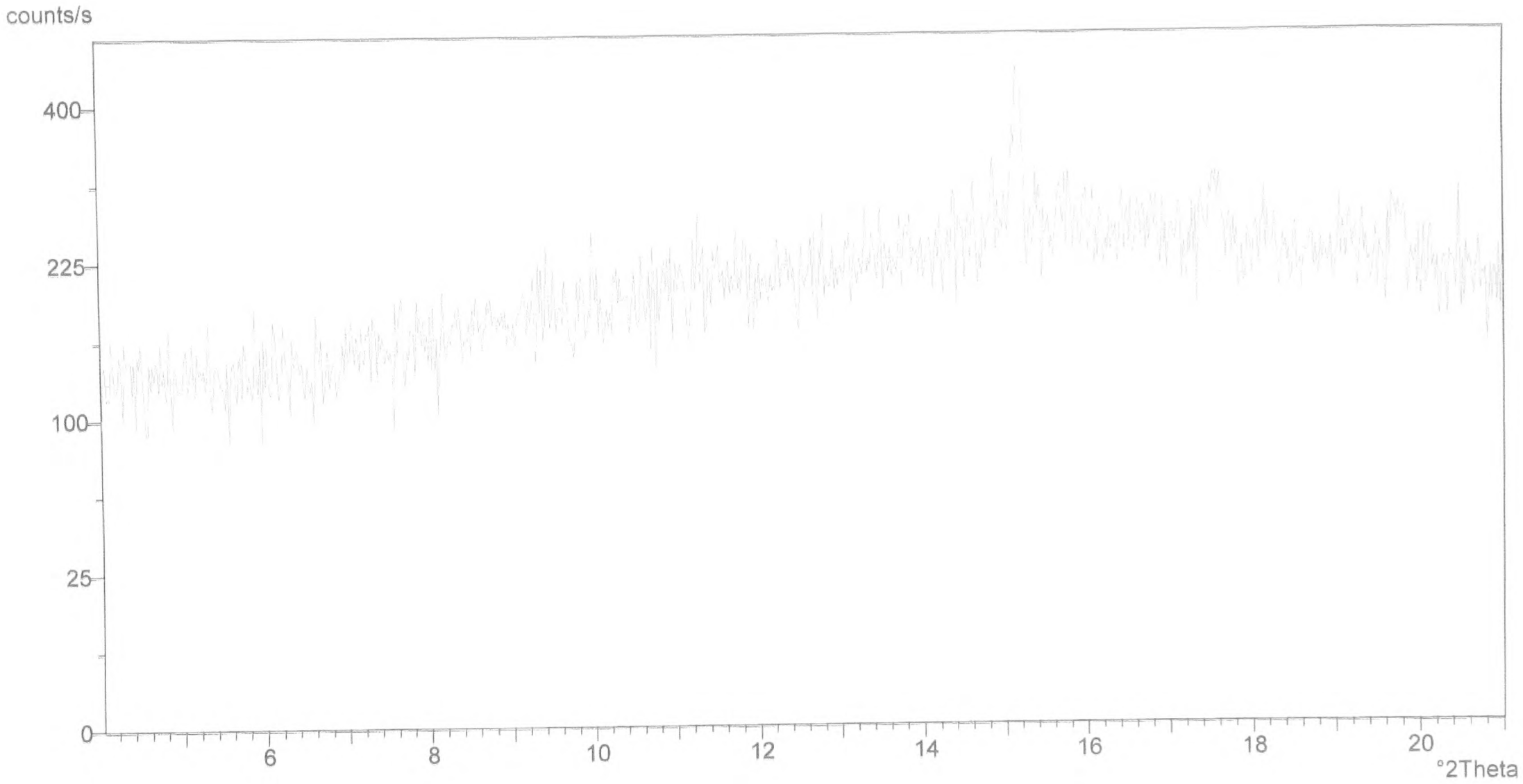

X-ray diffraction pattern of the vinyltrimethoxysilane polymer

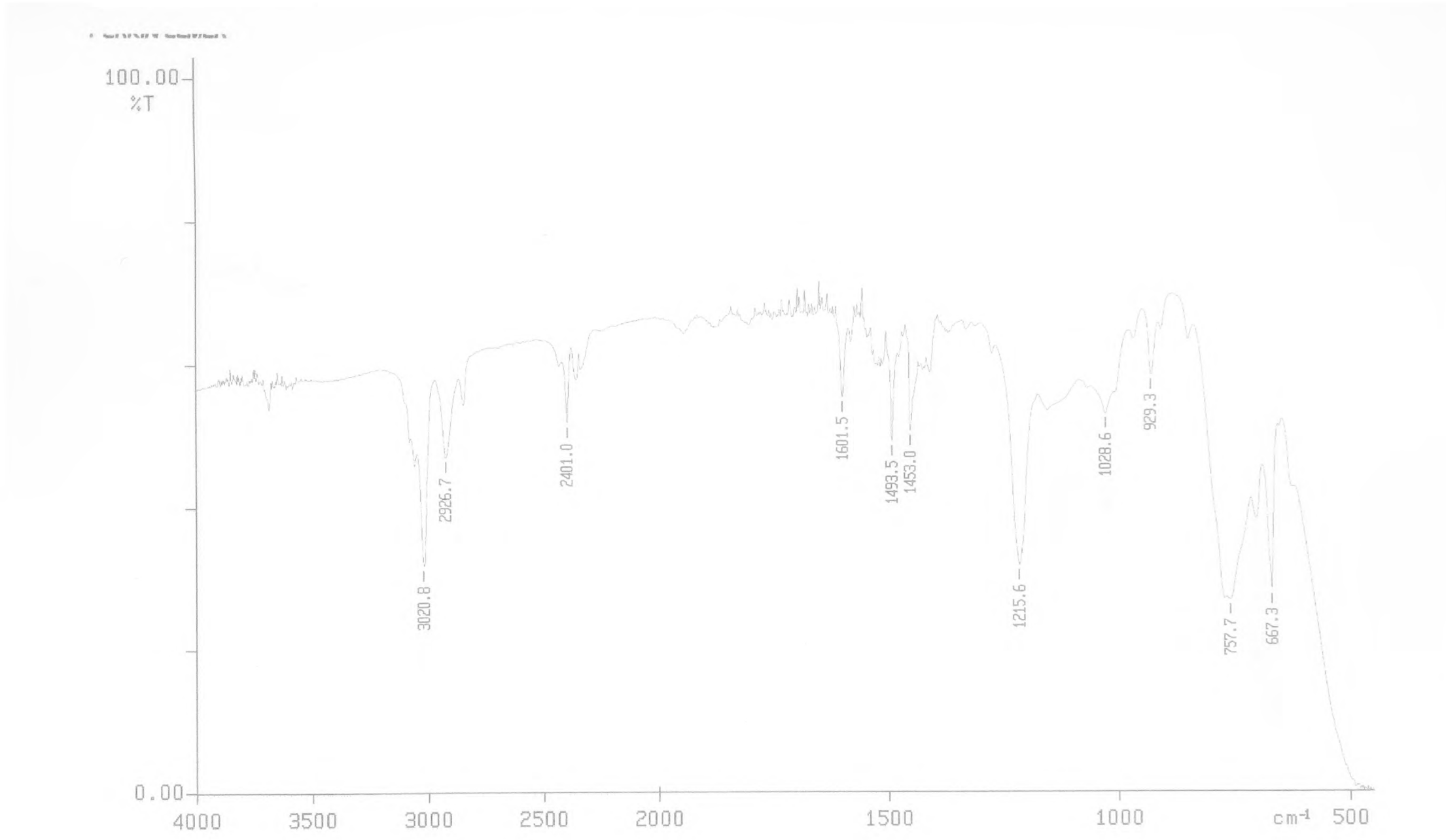

Infrared spectrum of the 20% composition of the vinyl-containing latex

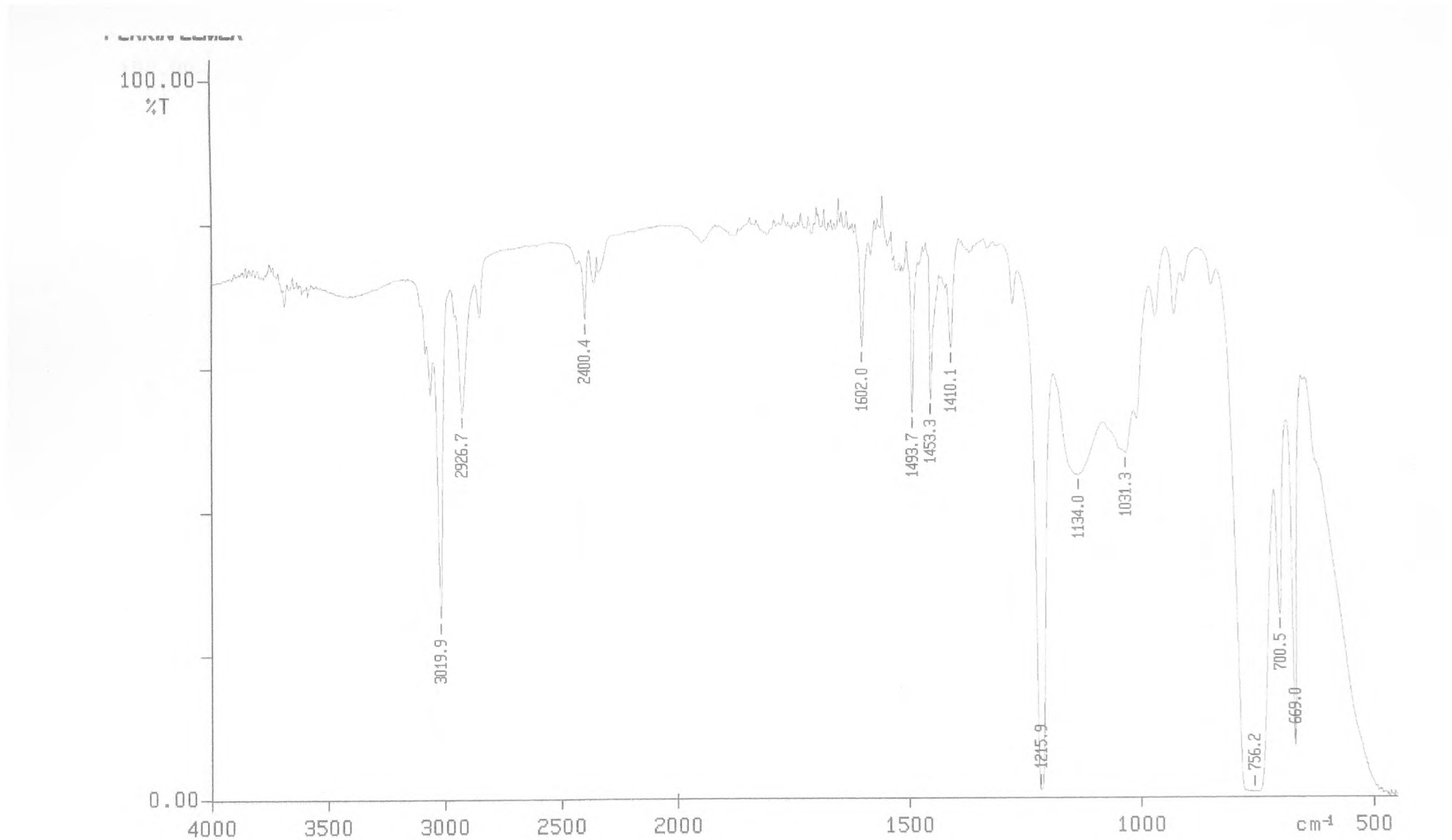

Infrared spectrum of the 30% composition of the vinyl-containing latex

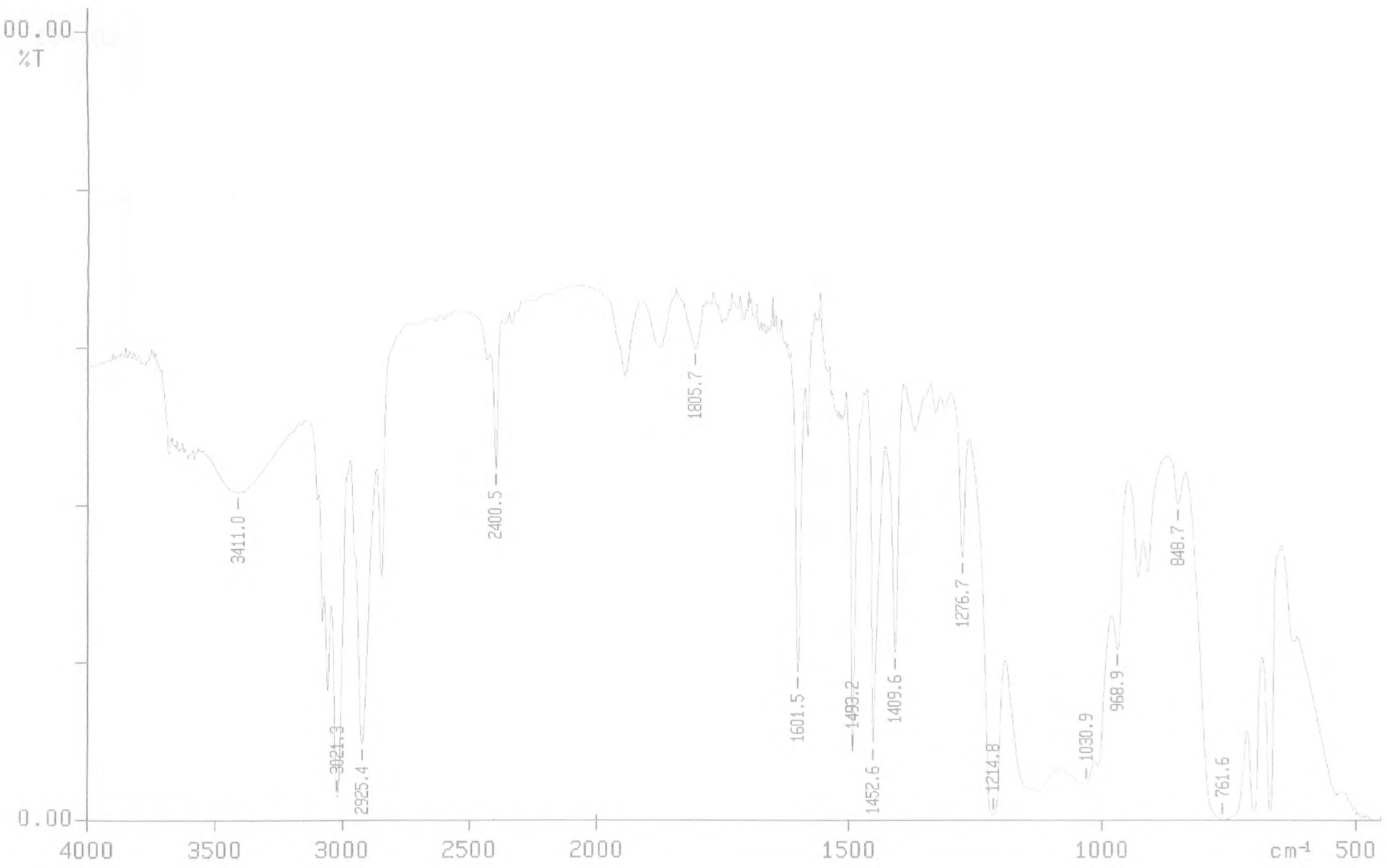

Infrared spectrum of the 40% composition of the vinyl-containing latex

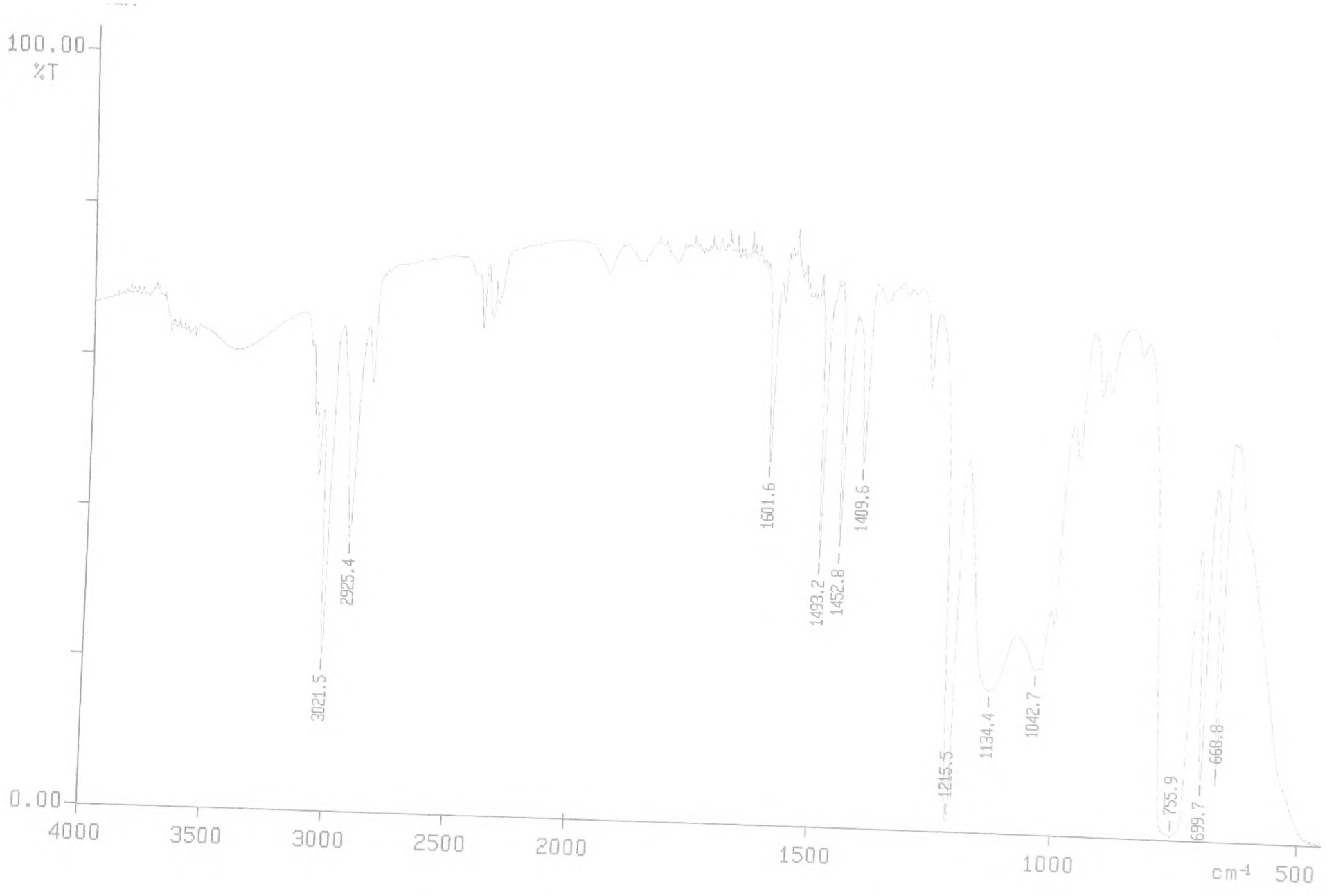

Infrared spectrum of the 50% composition of the vinyl-containing latex

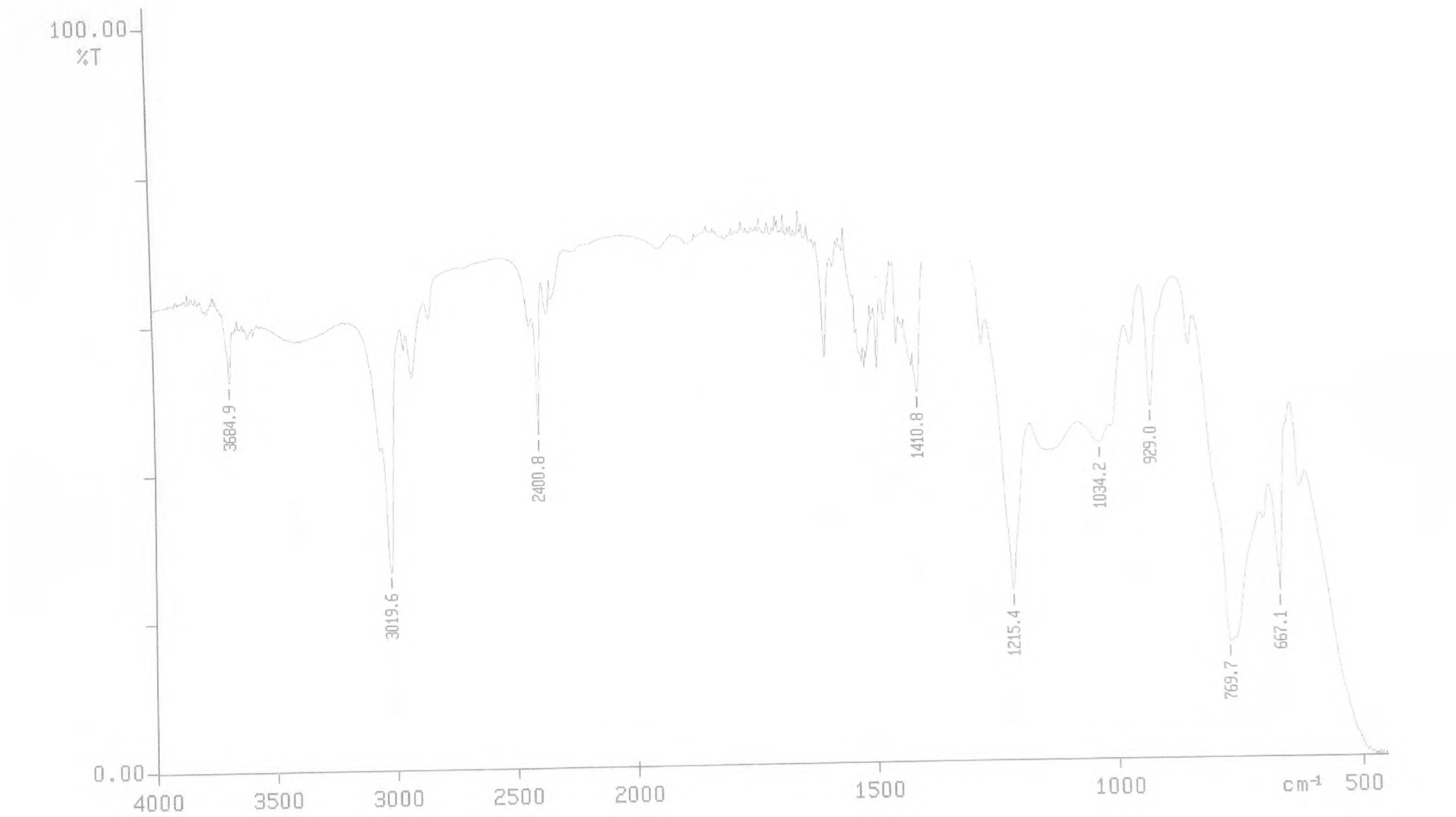

Infrared spectrum of the 60% composition of the vinyl-containing latex

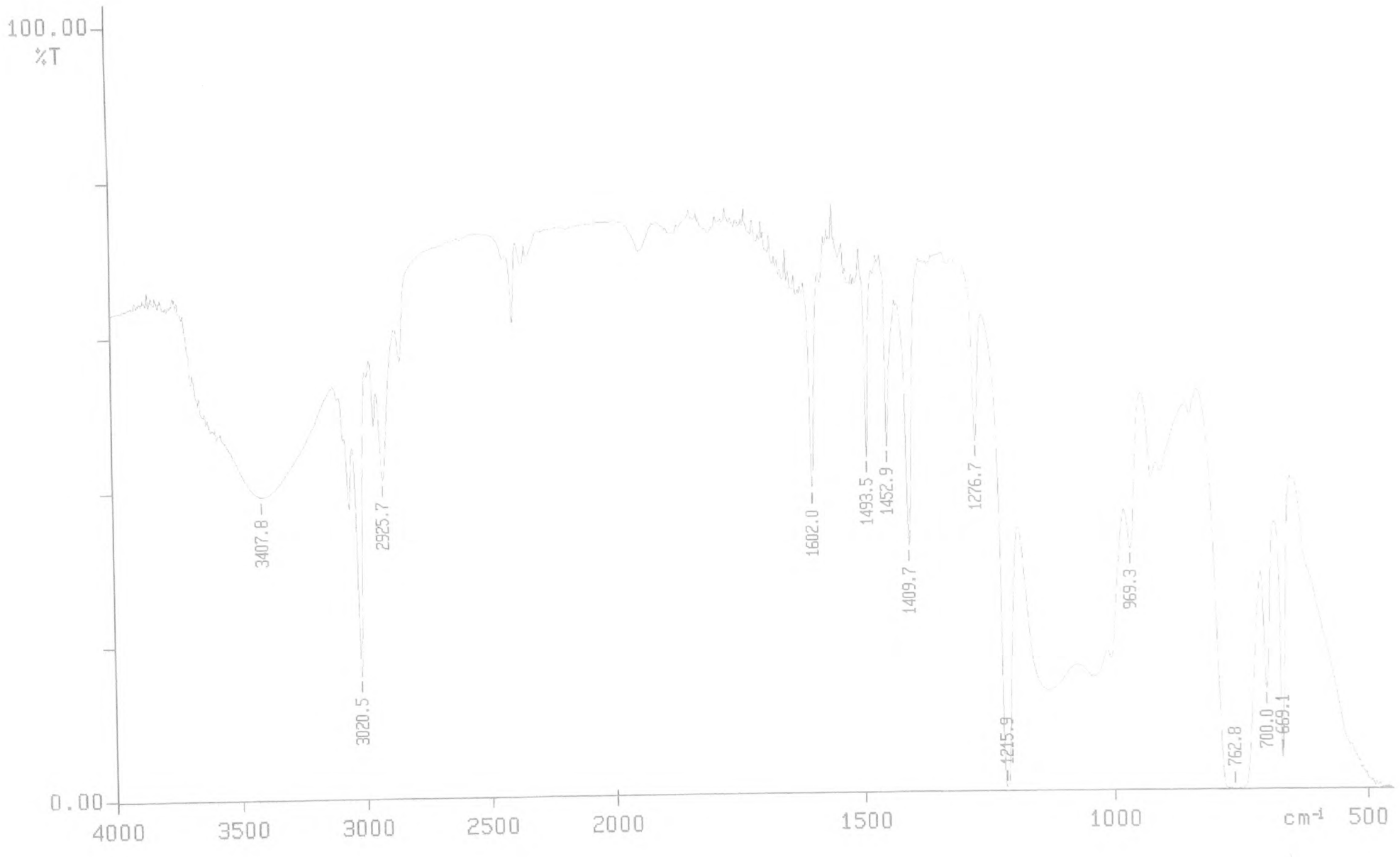

Infrared spectrum of the 70% composition of the vinyl-containing latex

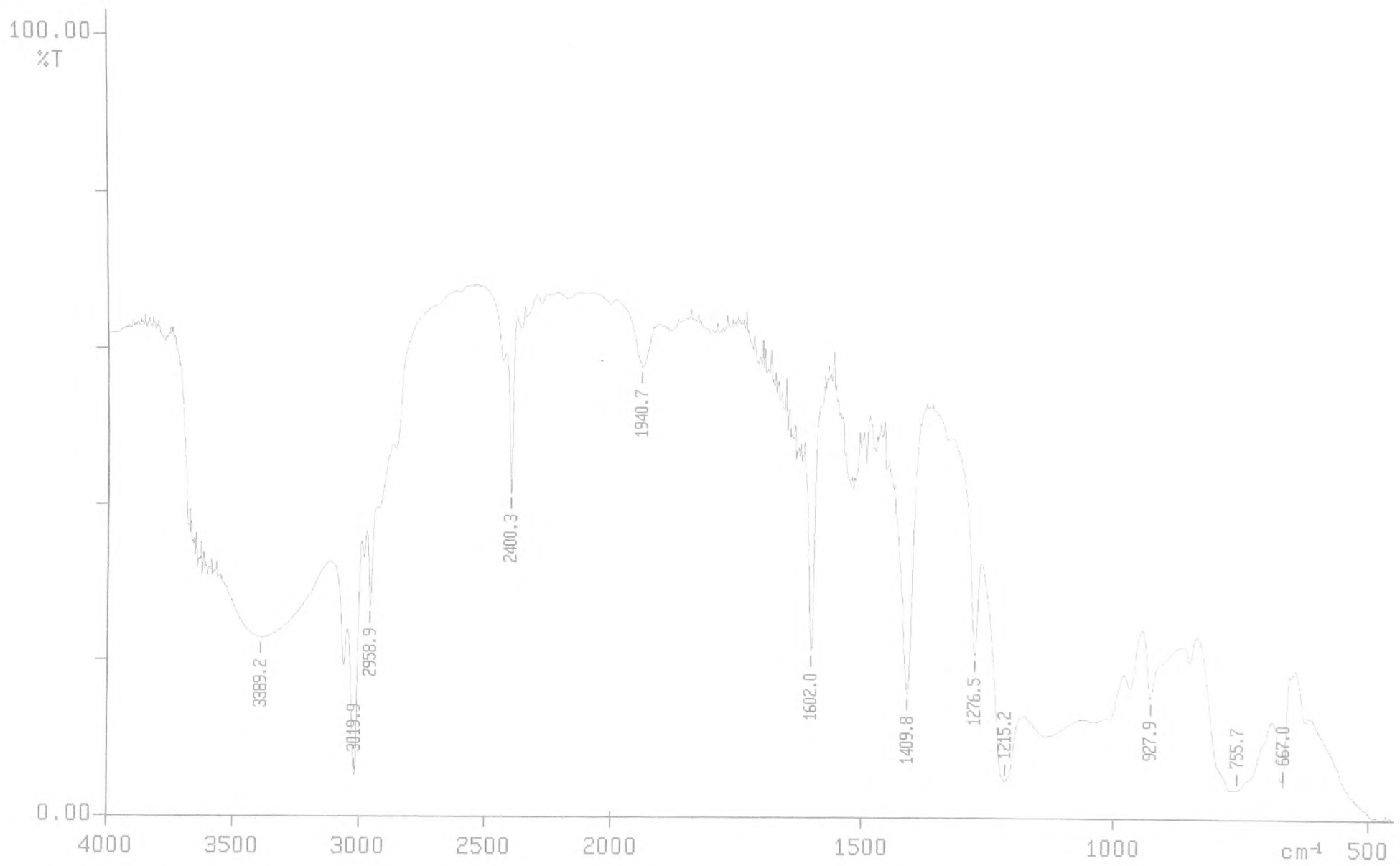

Infrared spectrum of the 90% composition of the vinyl-containing latex

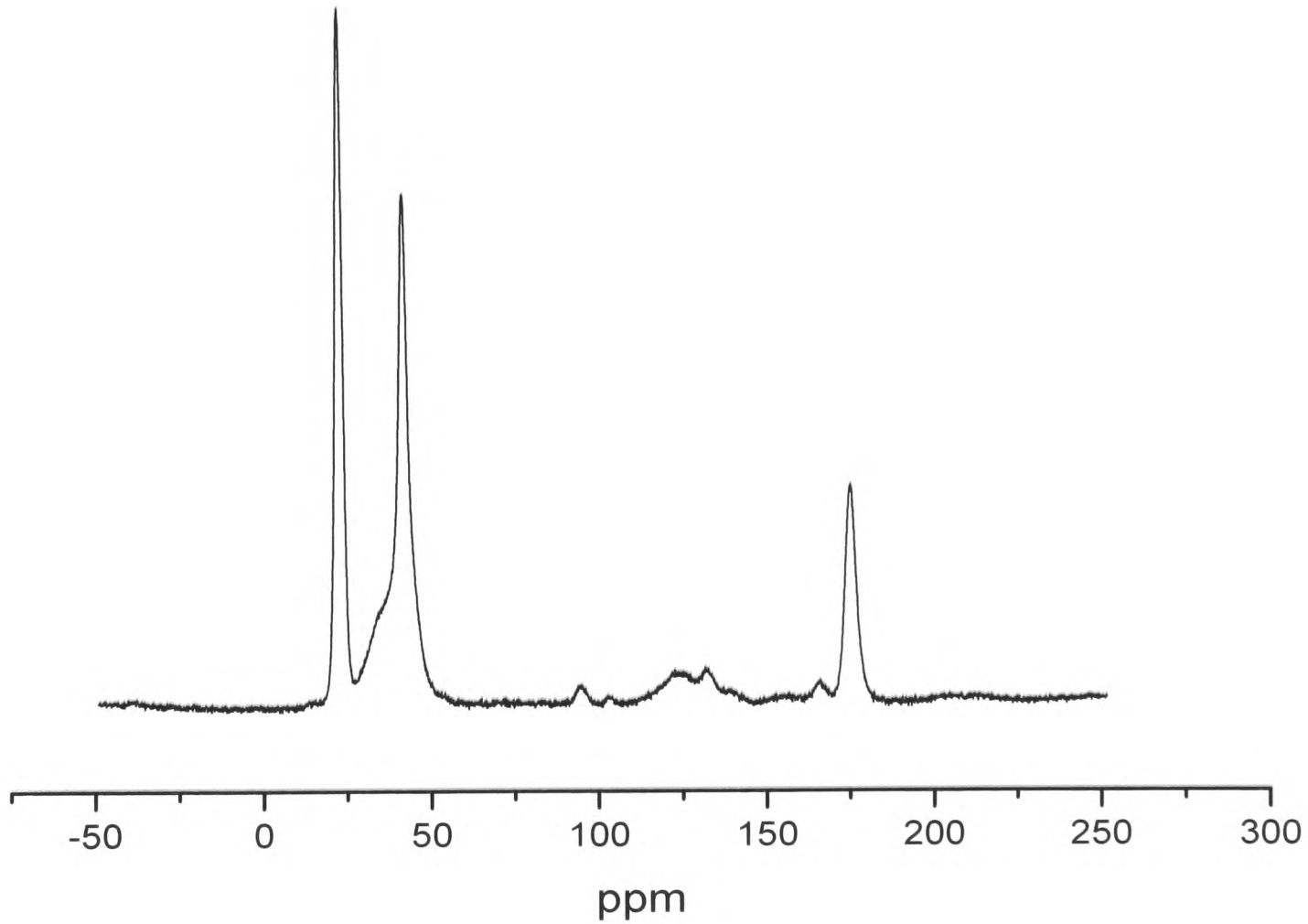

Solid state ^{13}C NMR analysis of 0% composition latex

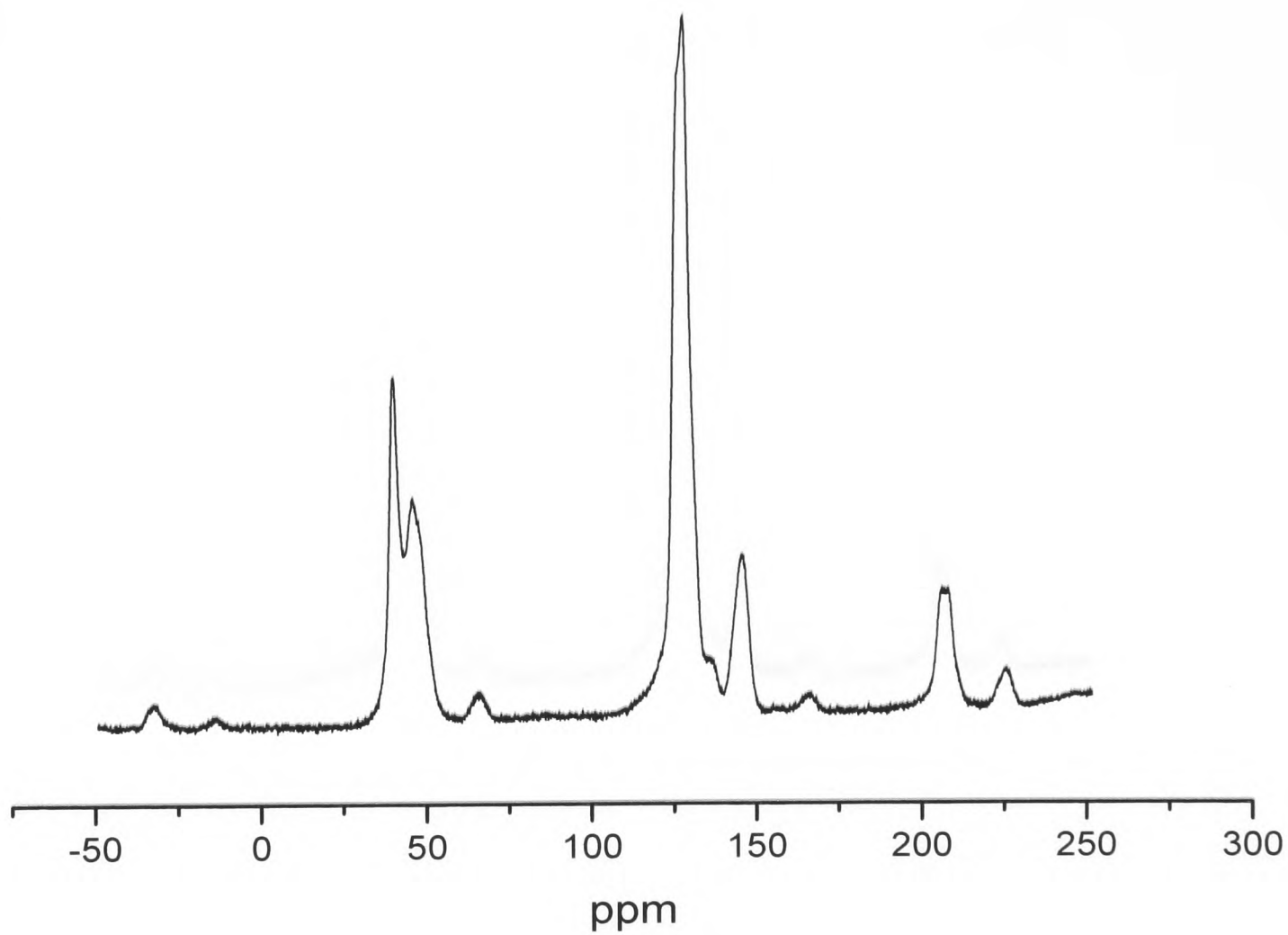

Solid state ^{13}C NMR analysis of 20% composition latex

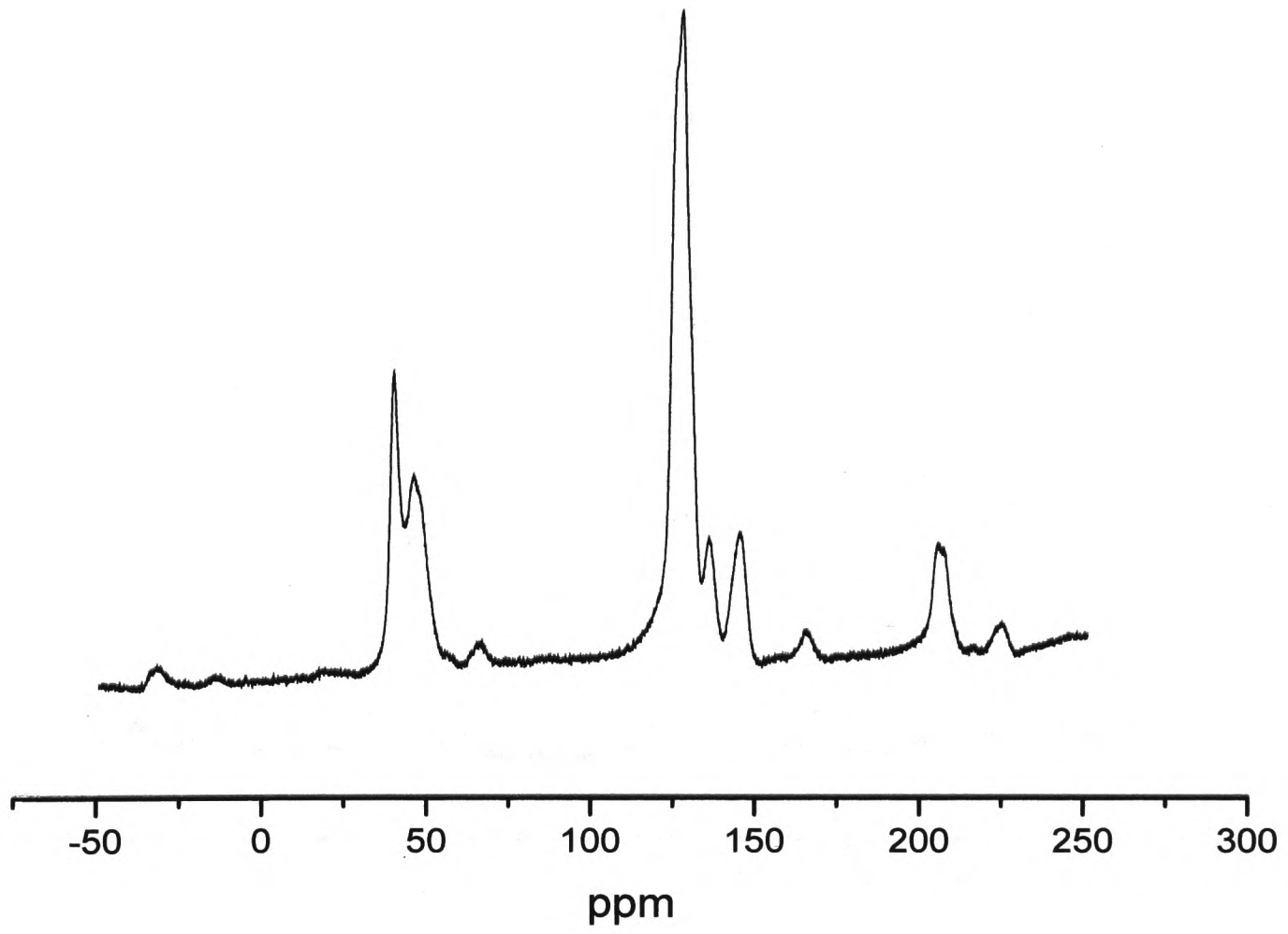

Solid state ^{13}C NMR analysis of 30% composition latex

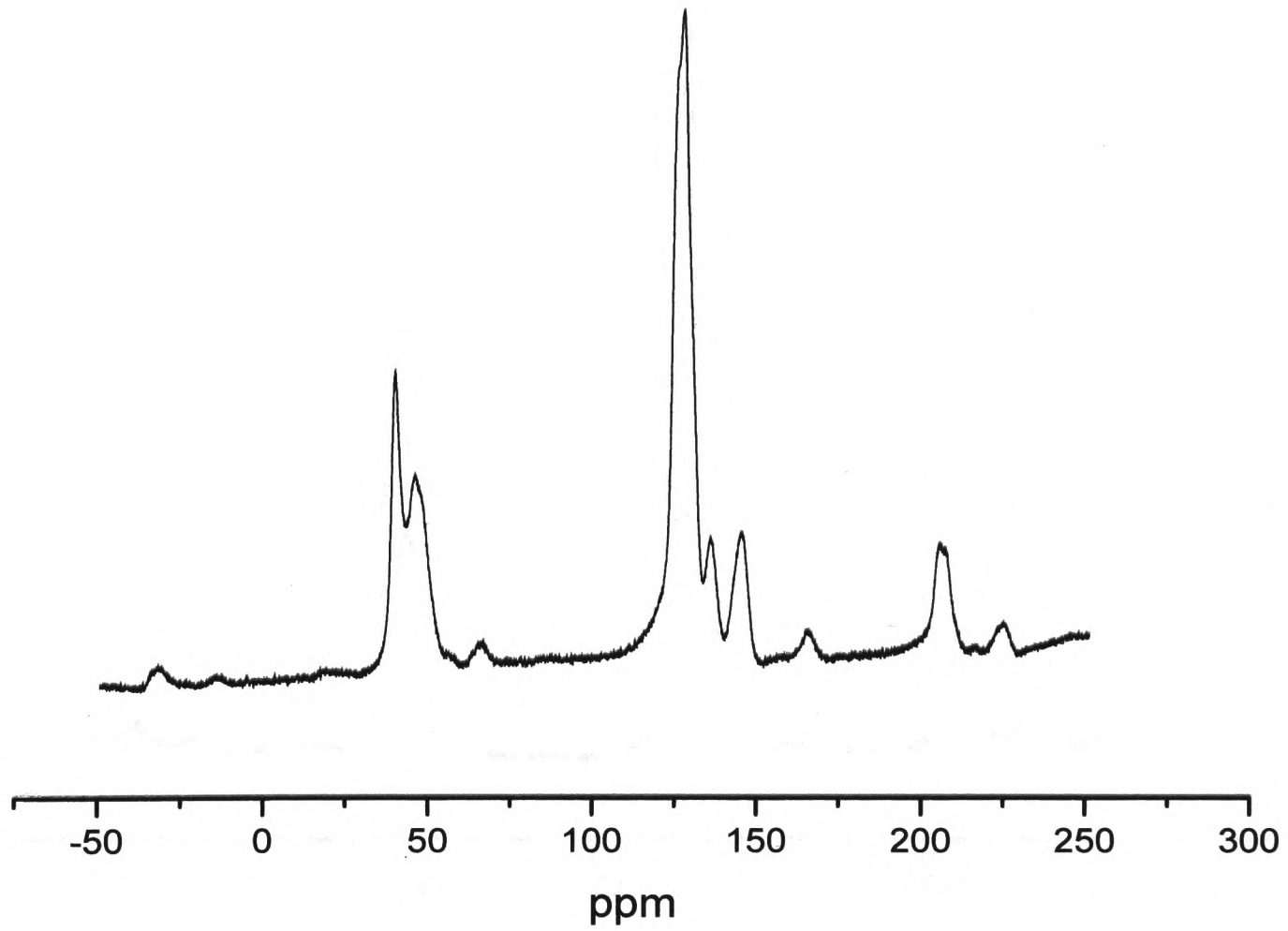

Solid state ^{13}C NMR analysis of 40% composition latex

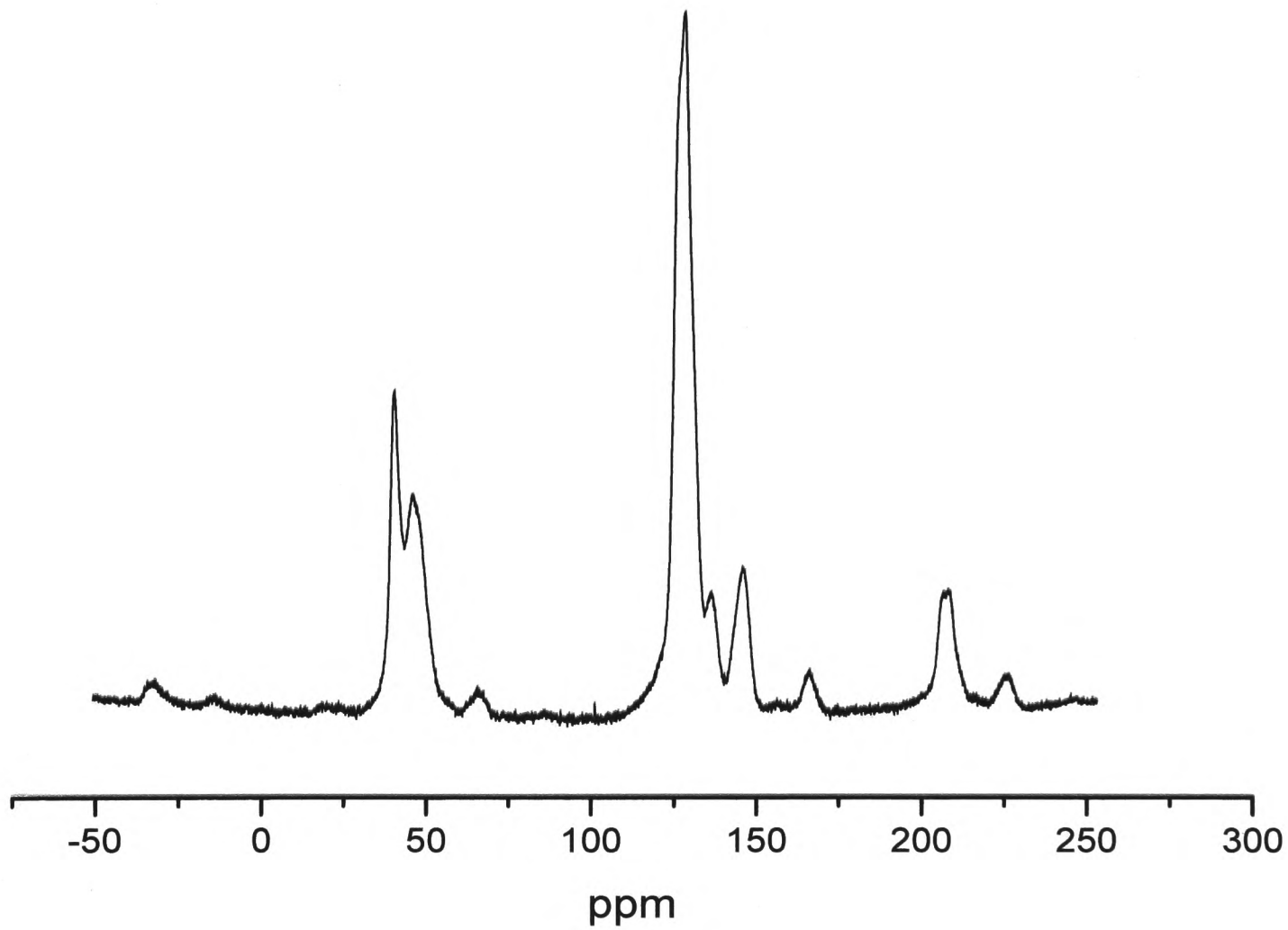

Solid state ^{13}C NMR analysis of 50% composition latex

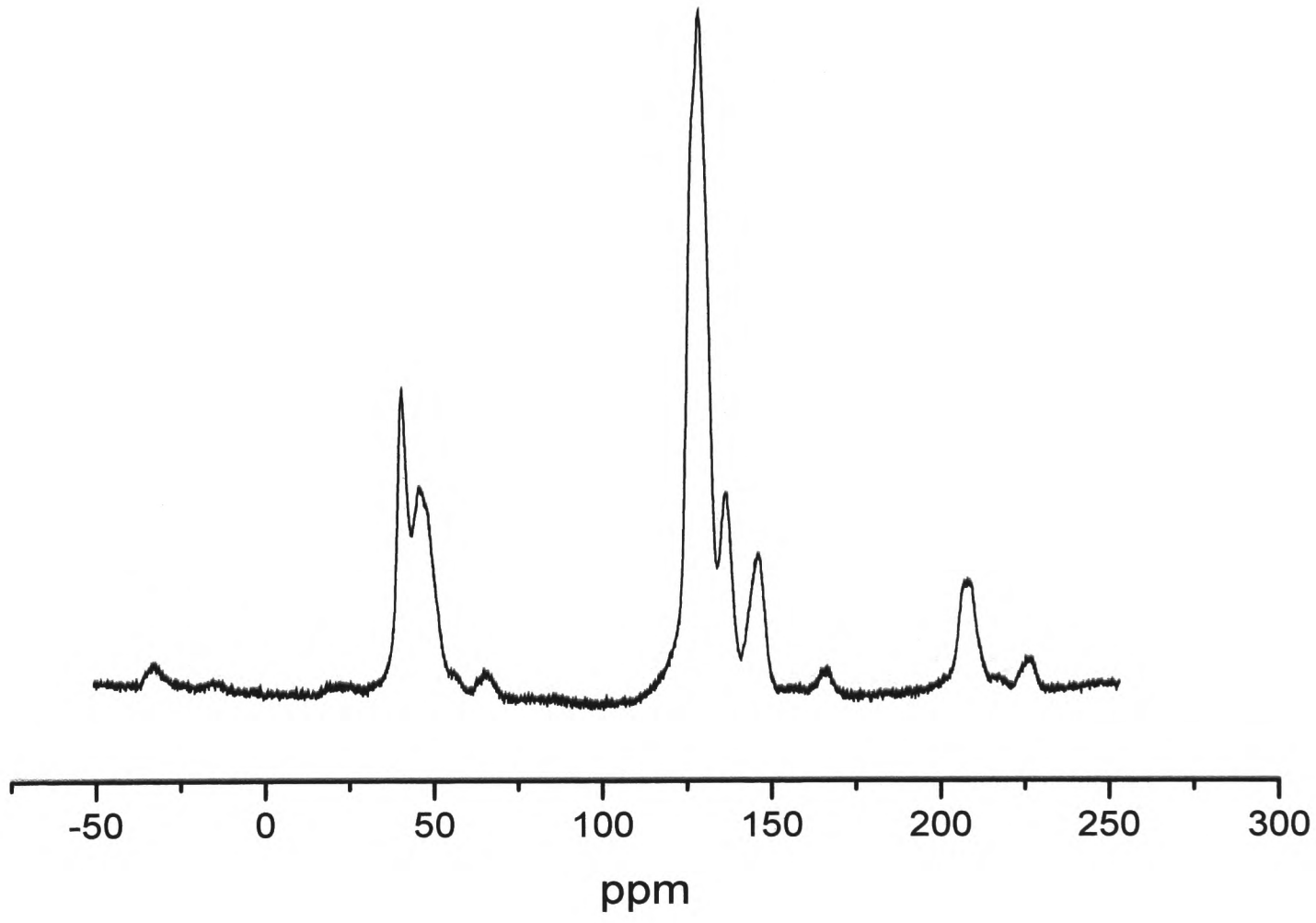

Solid state ^{13}C NMR analysis of 60% composition latex

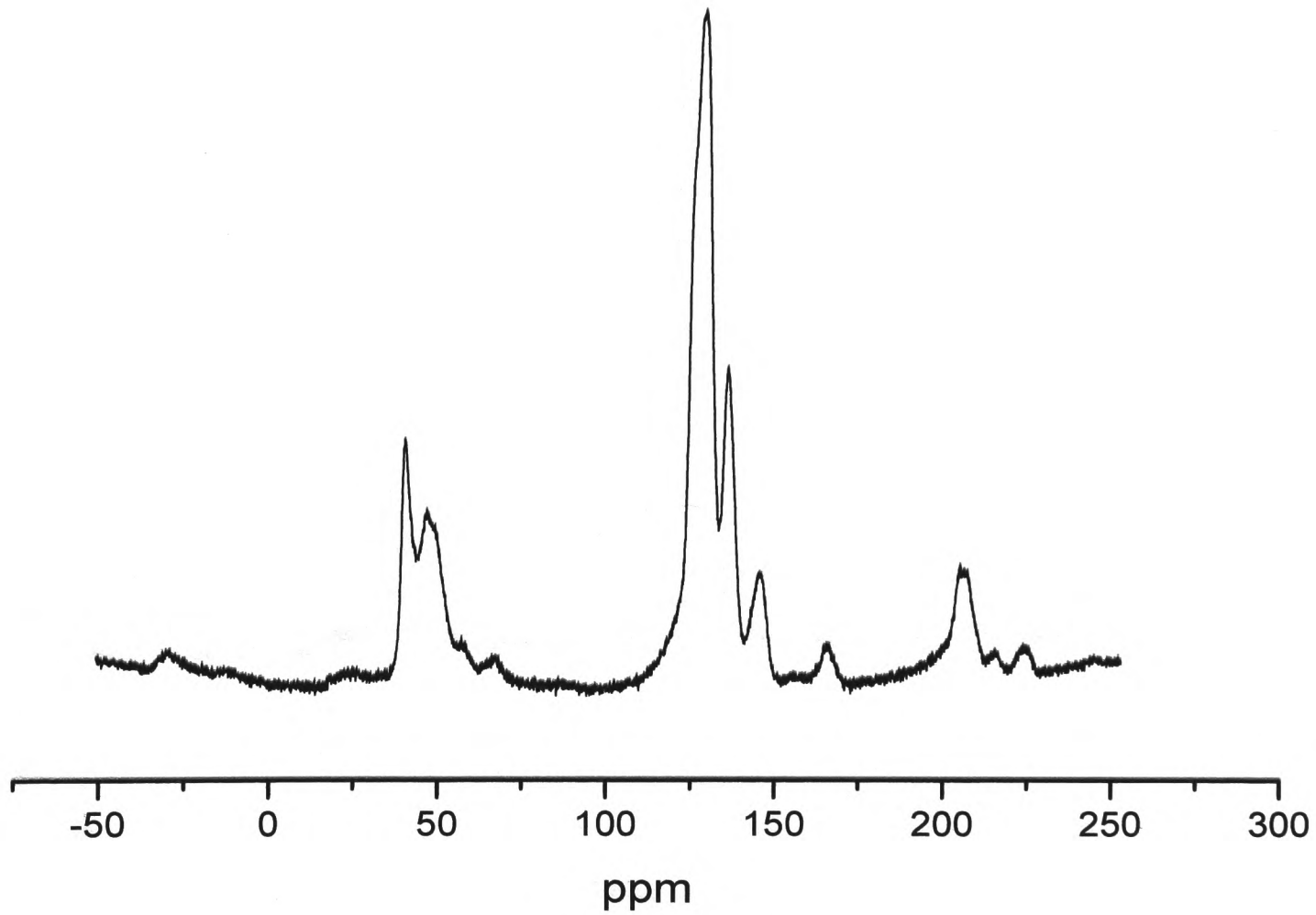

Solid state ^{13}C NMR analysis of 70% composition latex

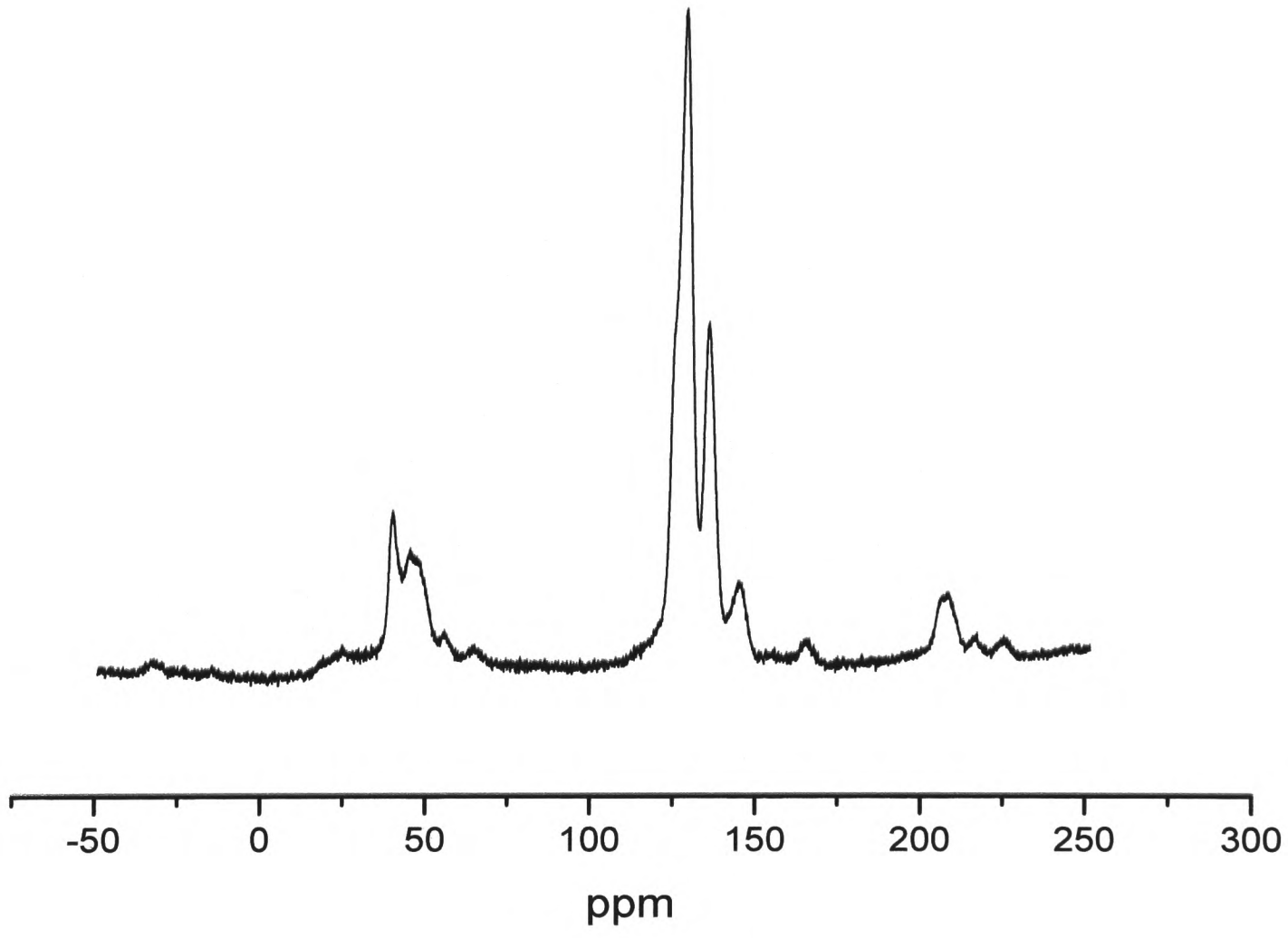

Solid state ^{13}C NMR analysis of 80% composition latex

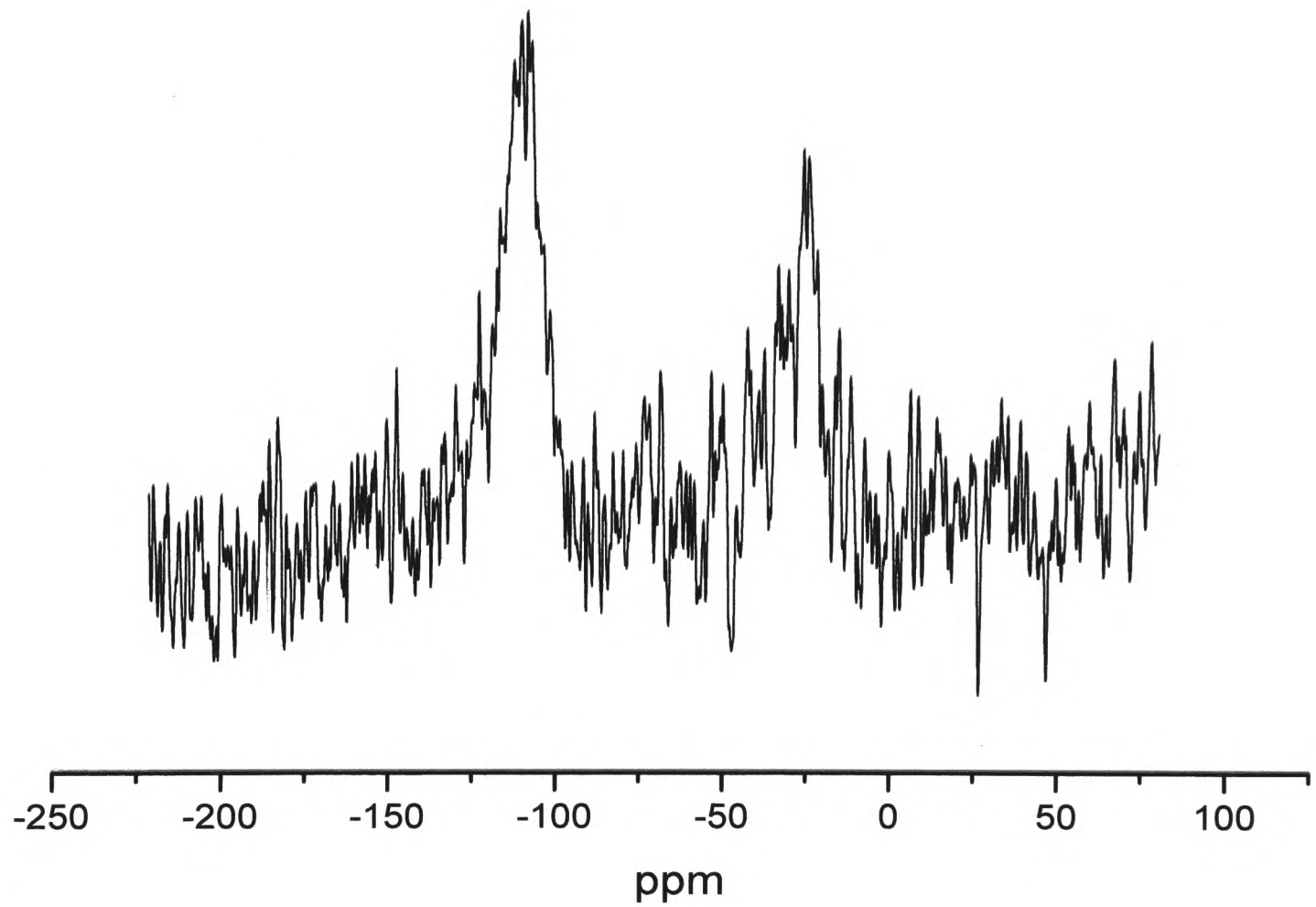

Solid state ^{29}Si NMR analysis of 0% composition latex

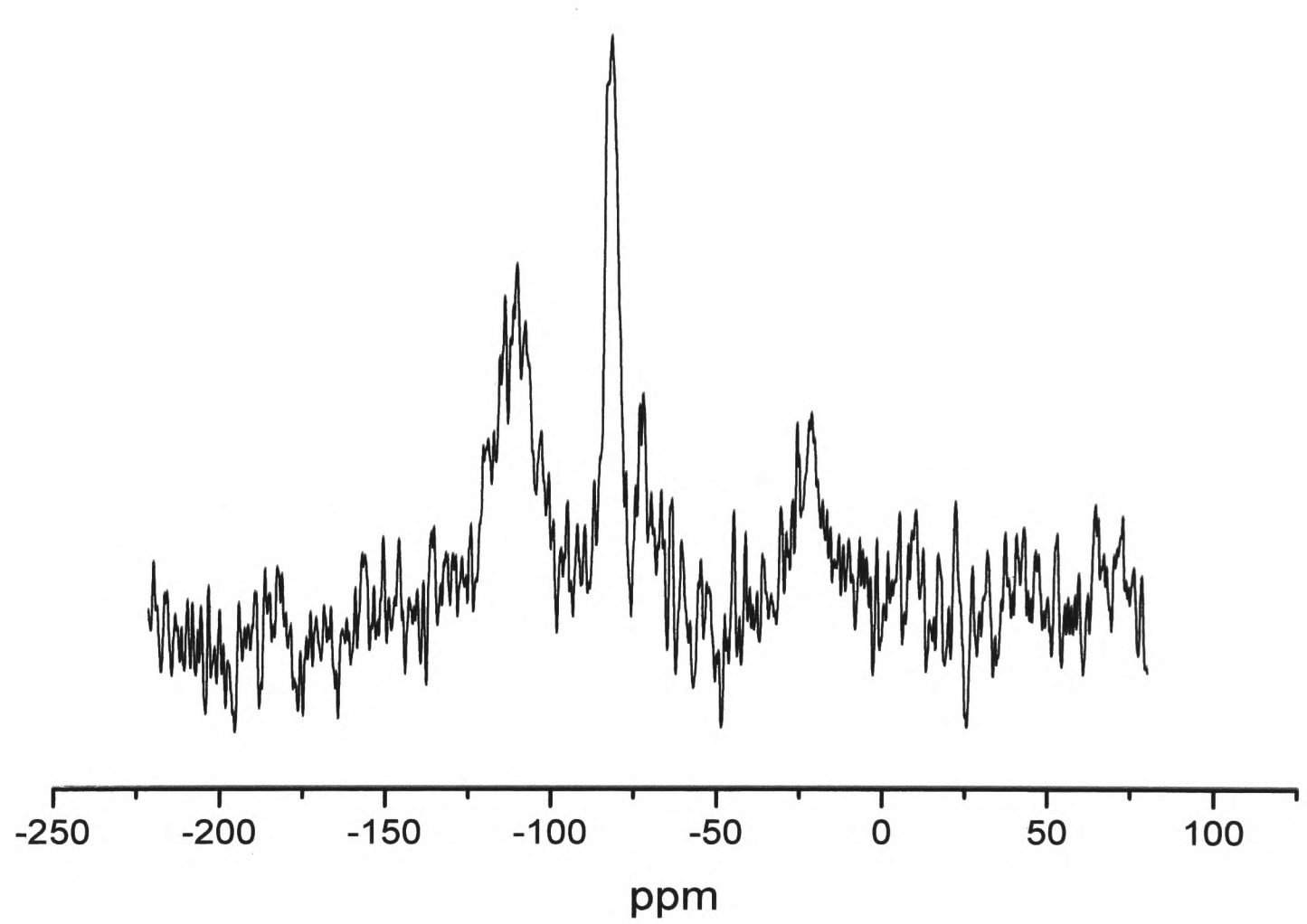

Solid state ^{29}Si NMR analysis of 20% composition latex

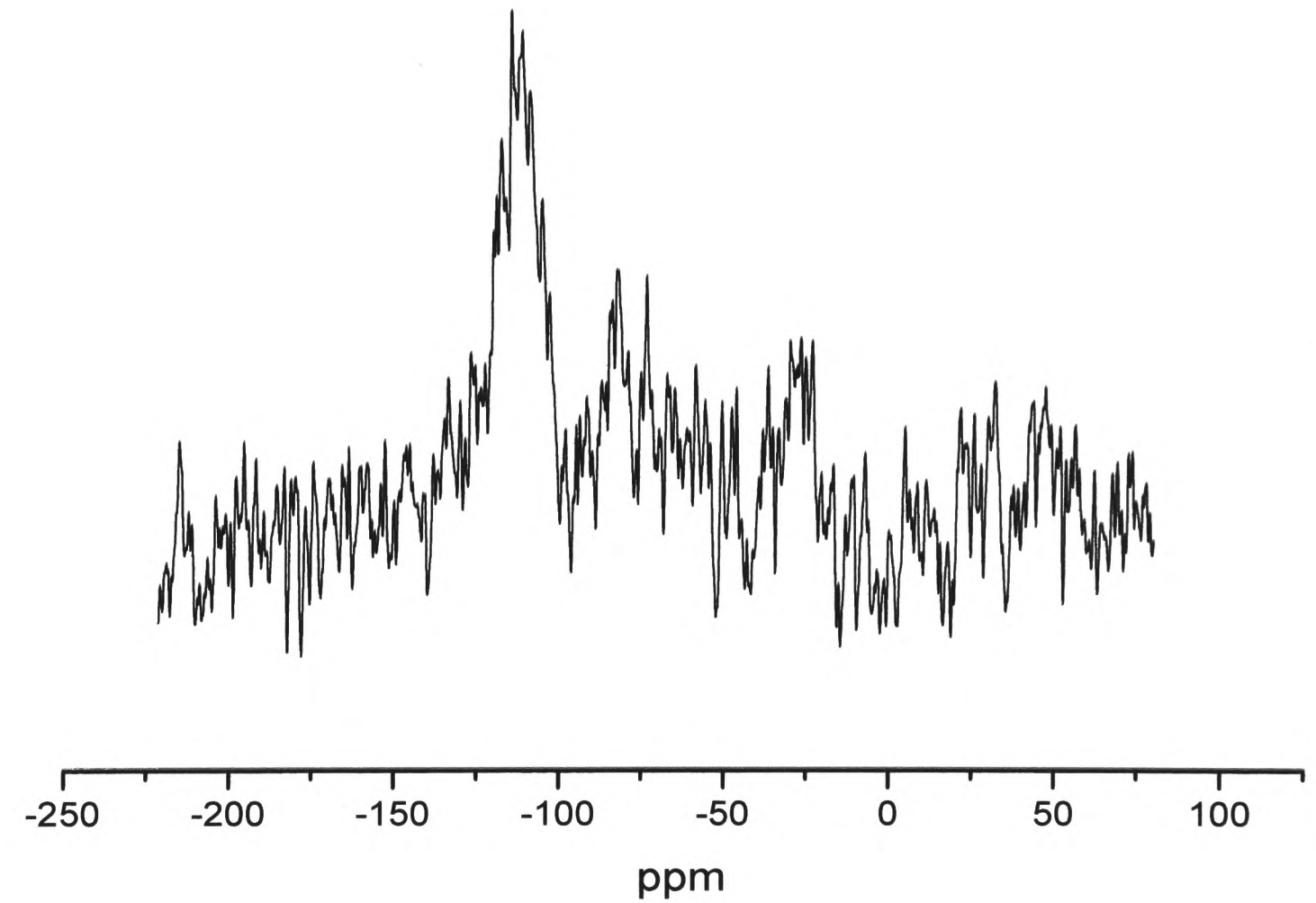

Solid state ^{29}Si NMR analysis of 30% composition latex

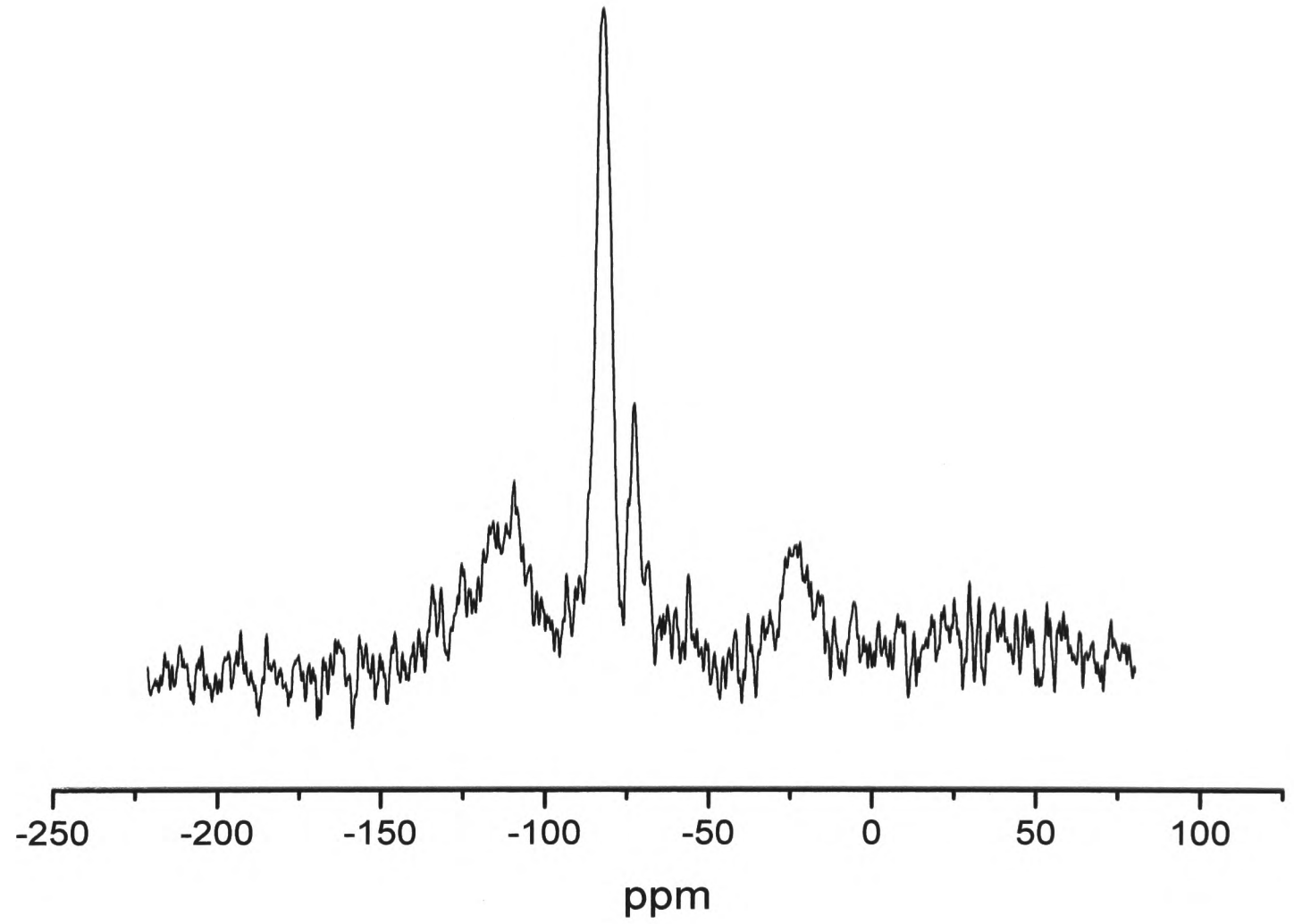

Solid state ^{29}Si NMR analysis of 40% composition latex

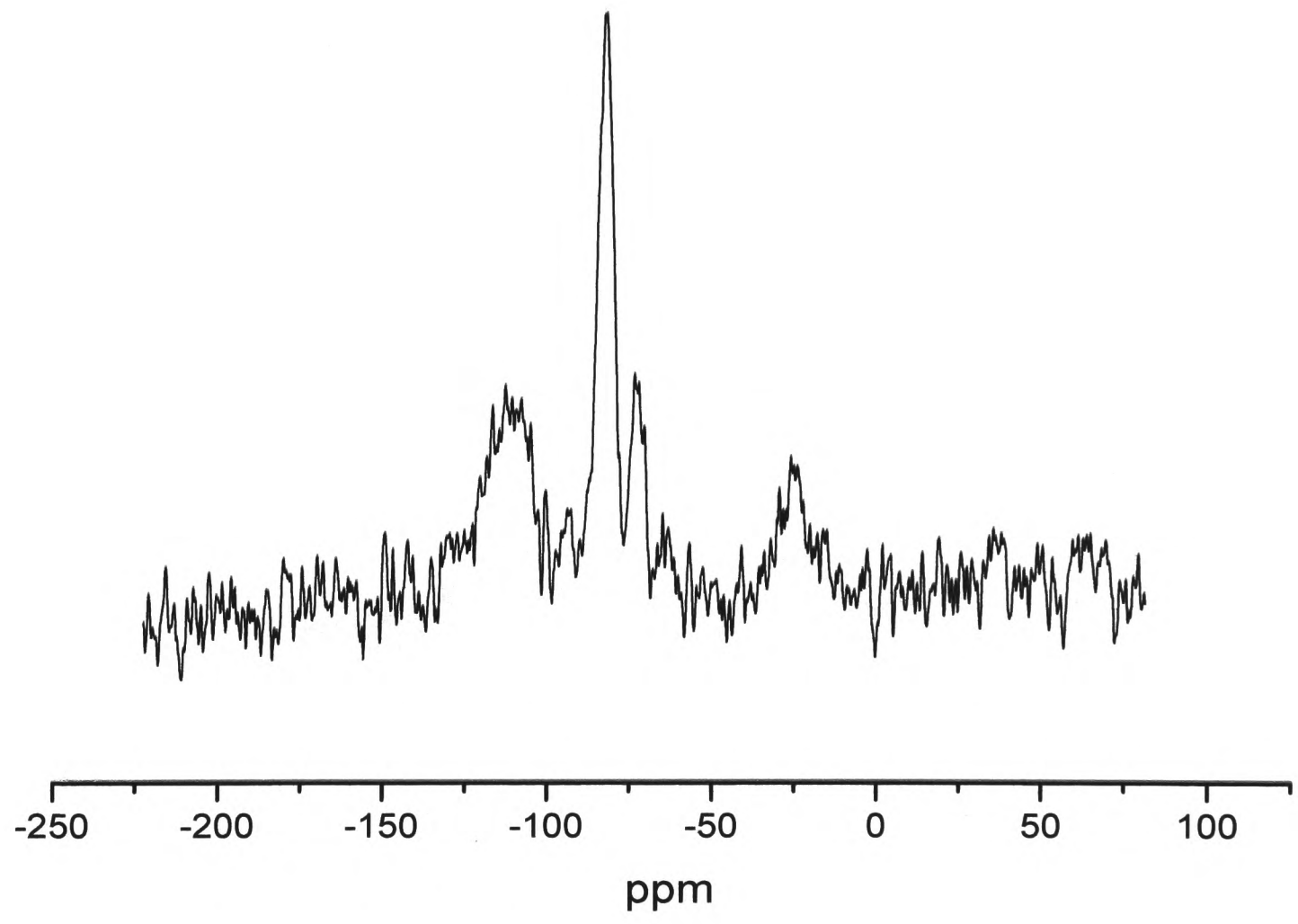

Solid state ^{29}Si NMR analysis of 50% composition latex

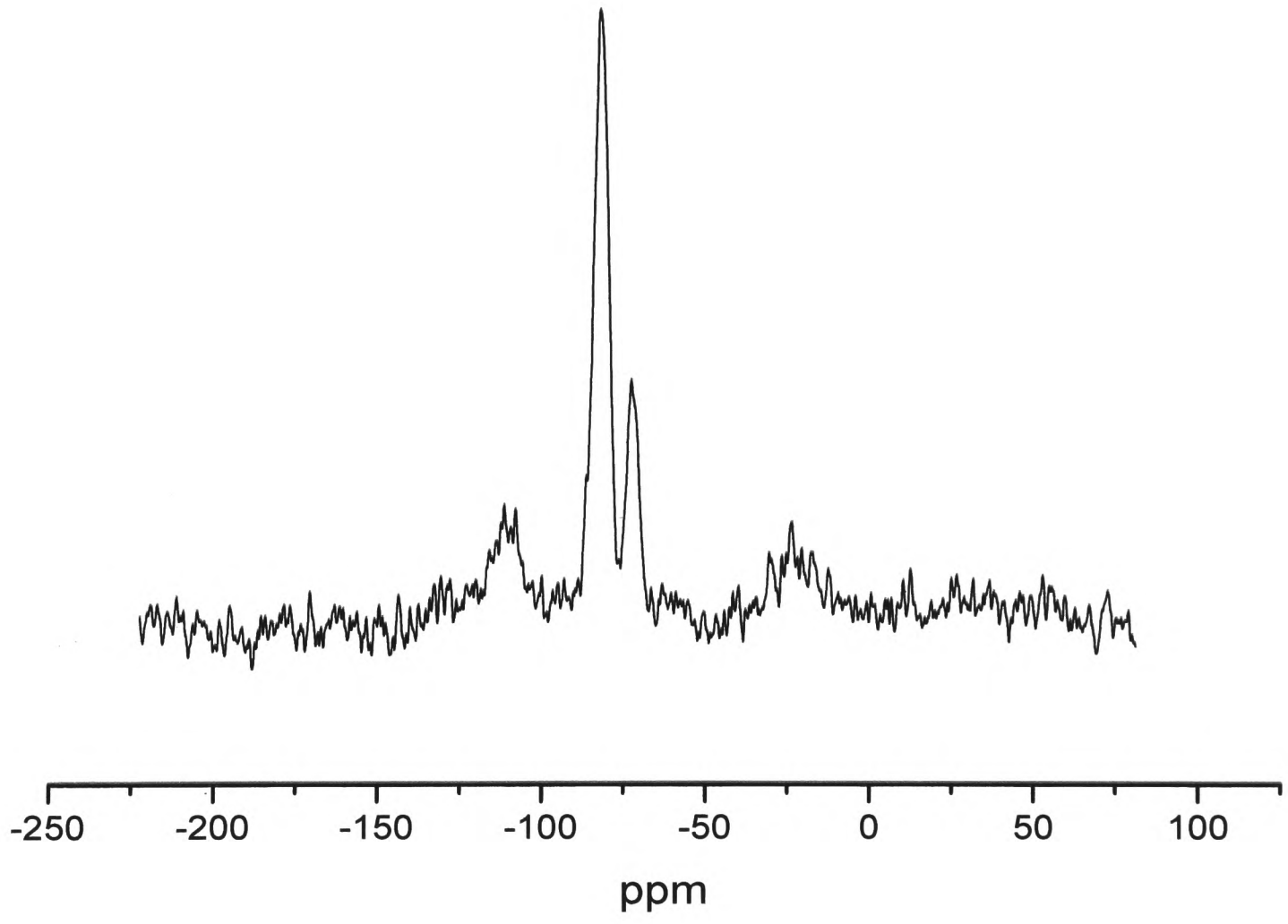

Solid state ^{29}Si NMR analysis of 60% composition latex

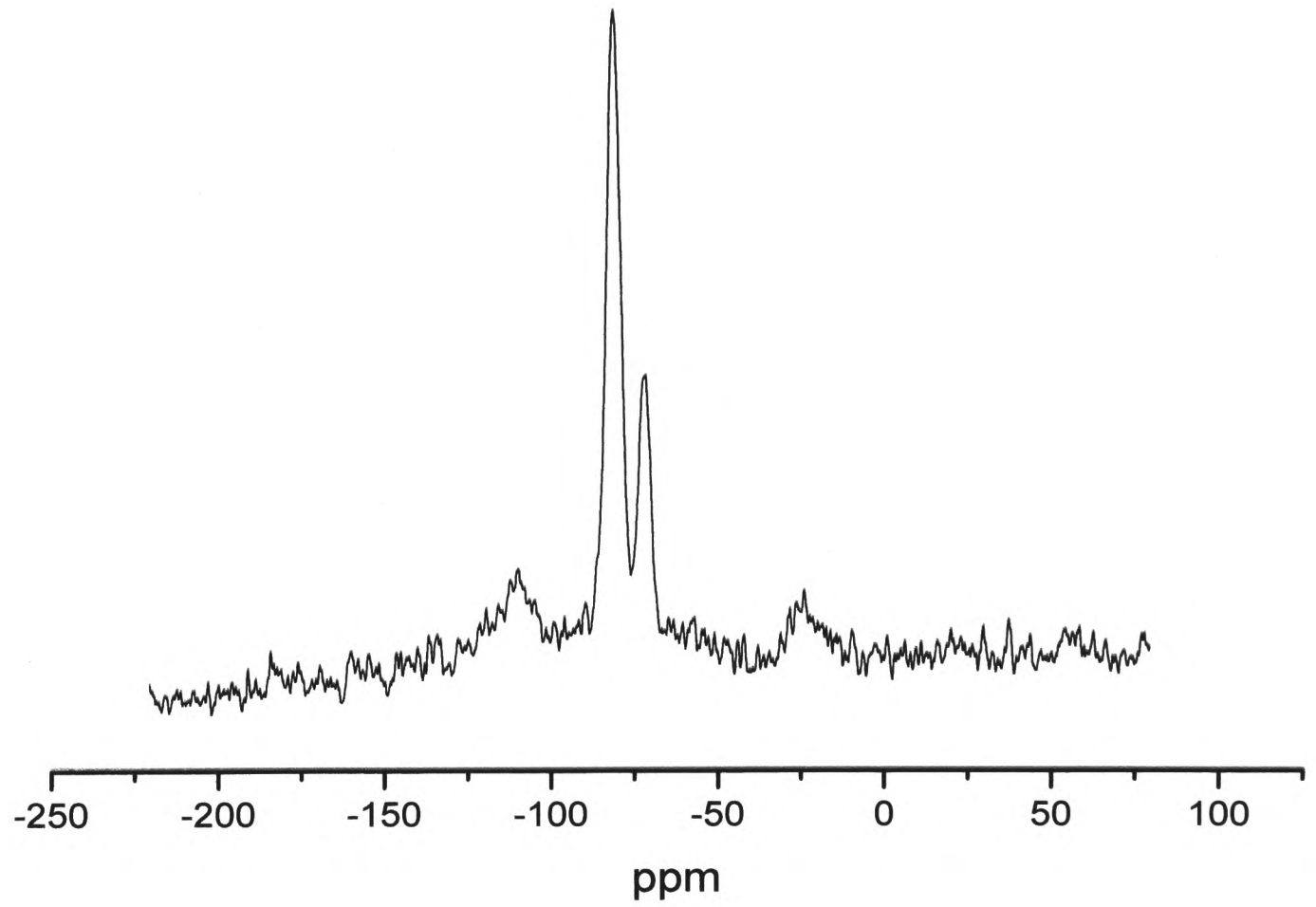

Solid state ^{29}Si NMR analysis of 70% composition latex

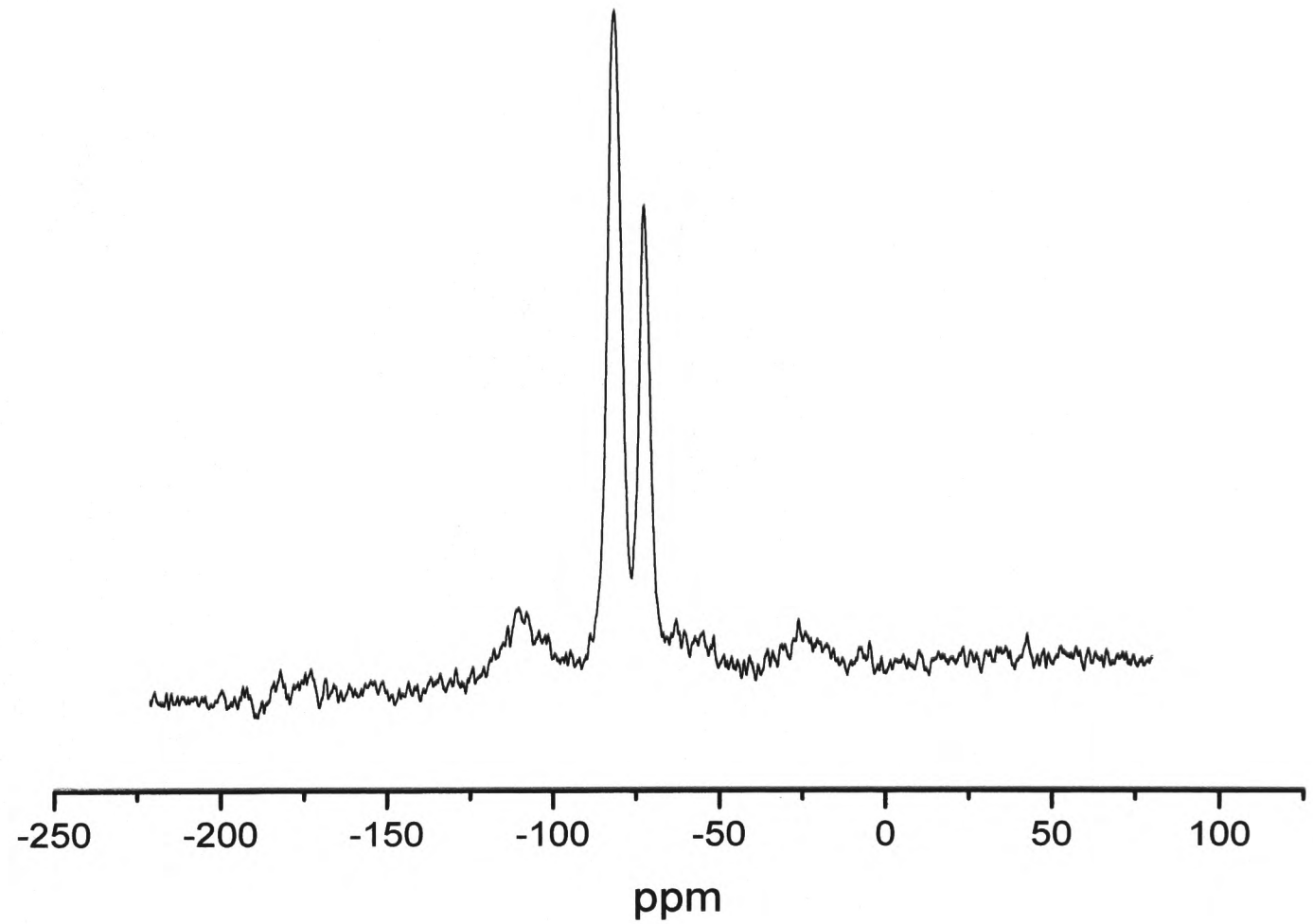

Solid state ^{29}Si NMR analysis of 80% composition latex

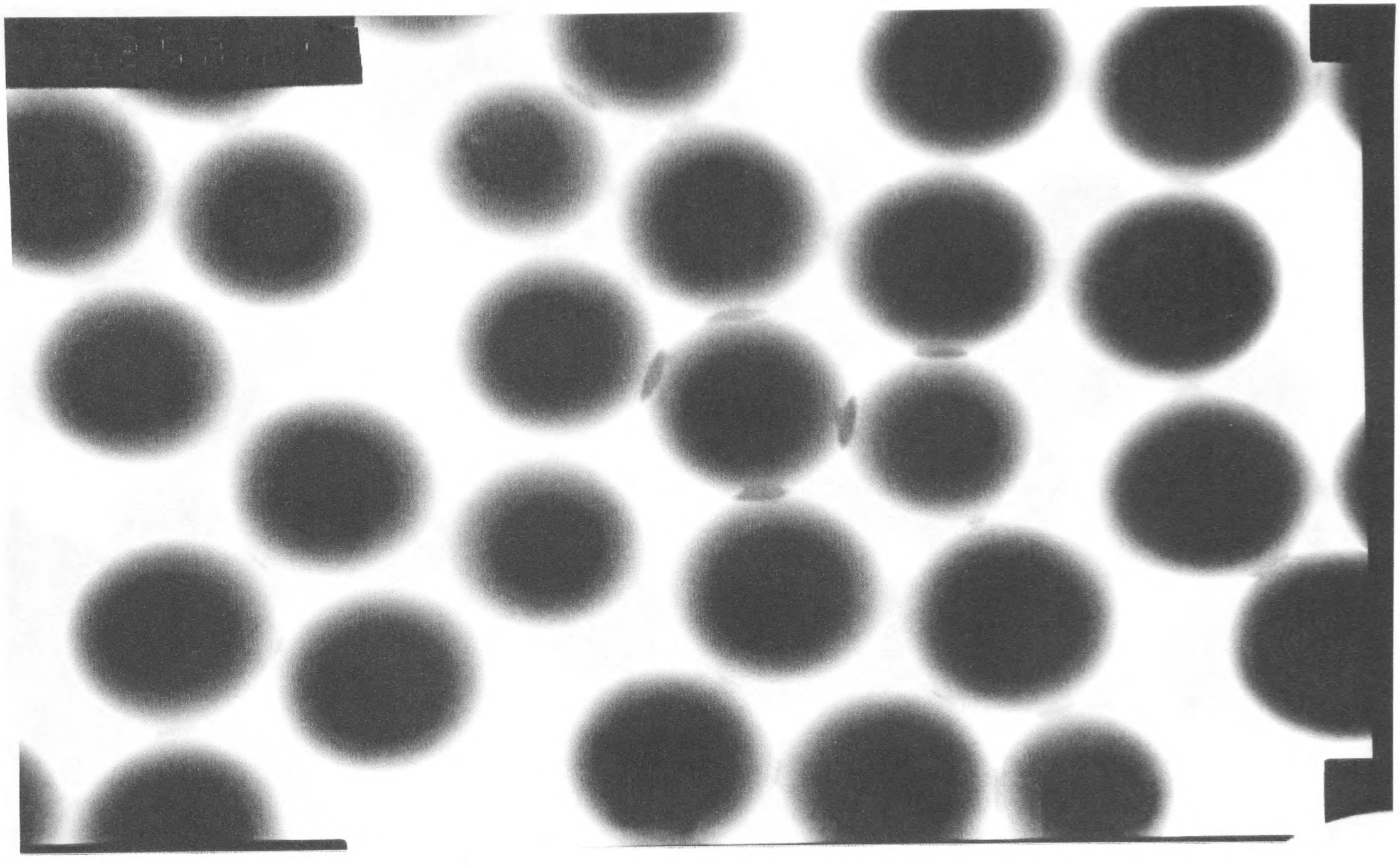

SEM micrograph of 10% composition

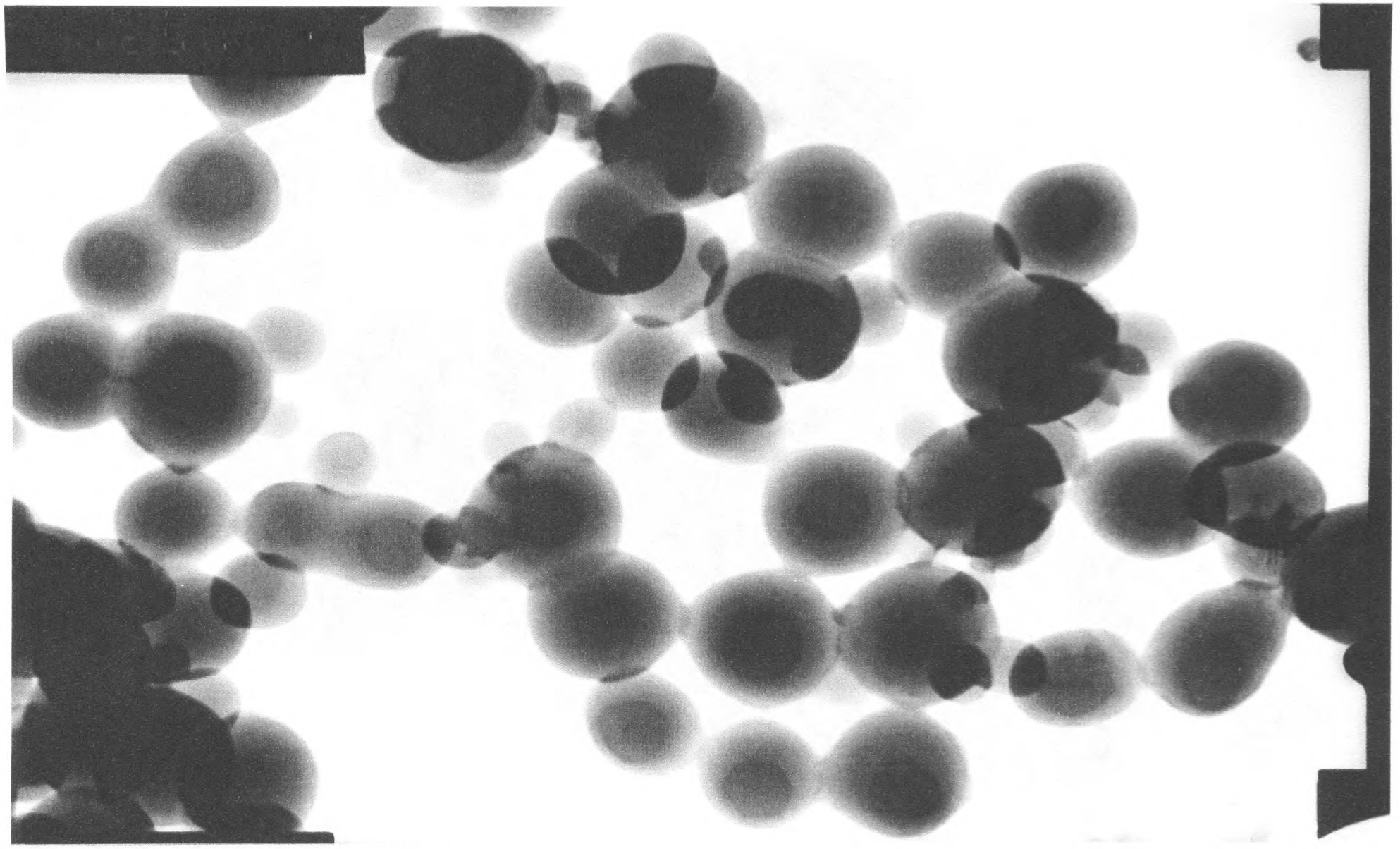

SEM micrograph of 30% composition

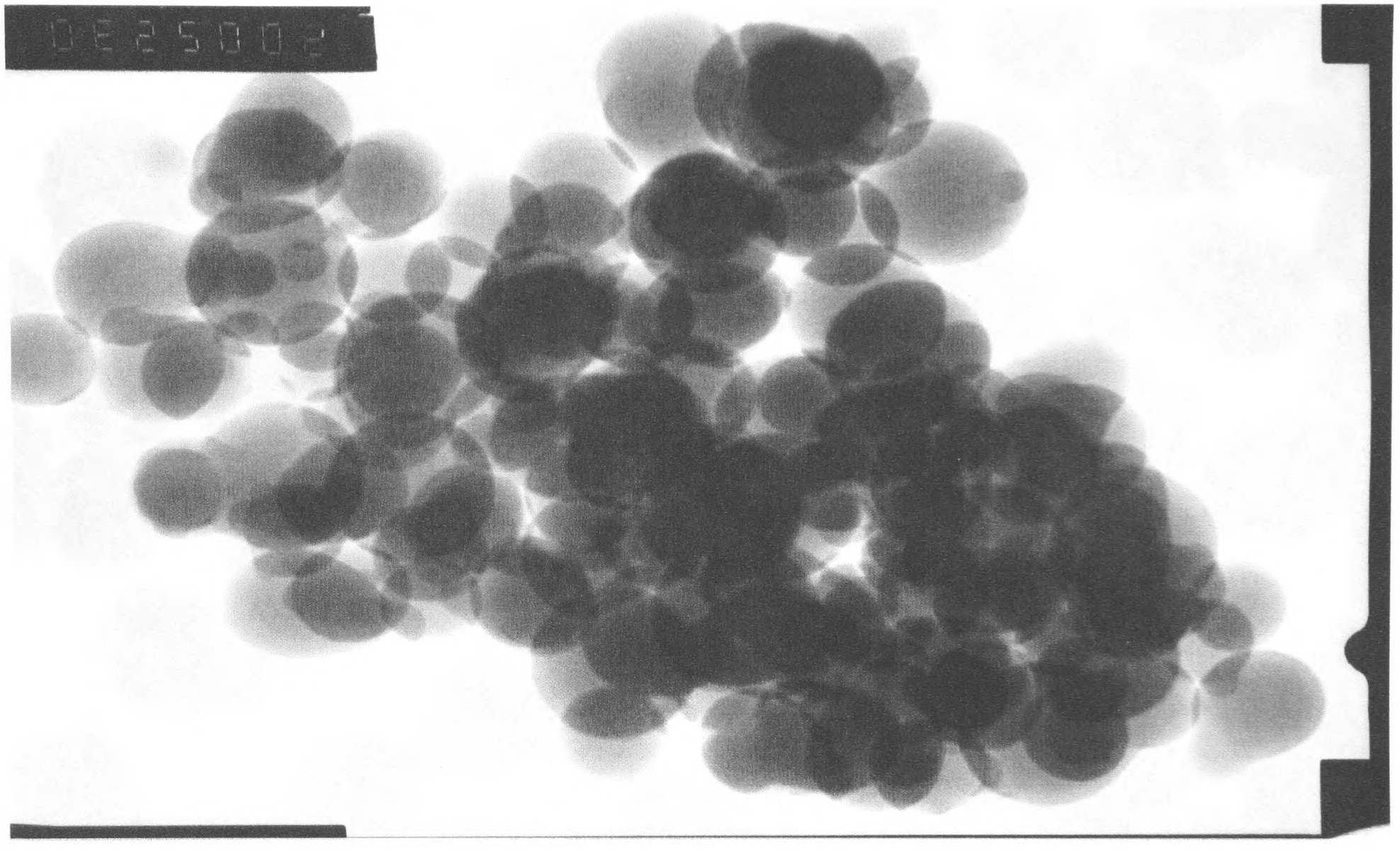

SEM micrograph of 40% composition

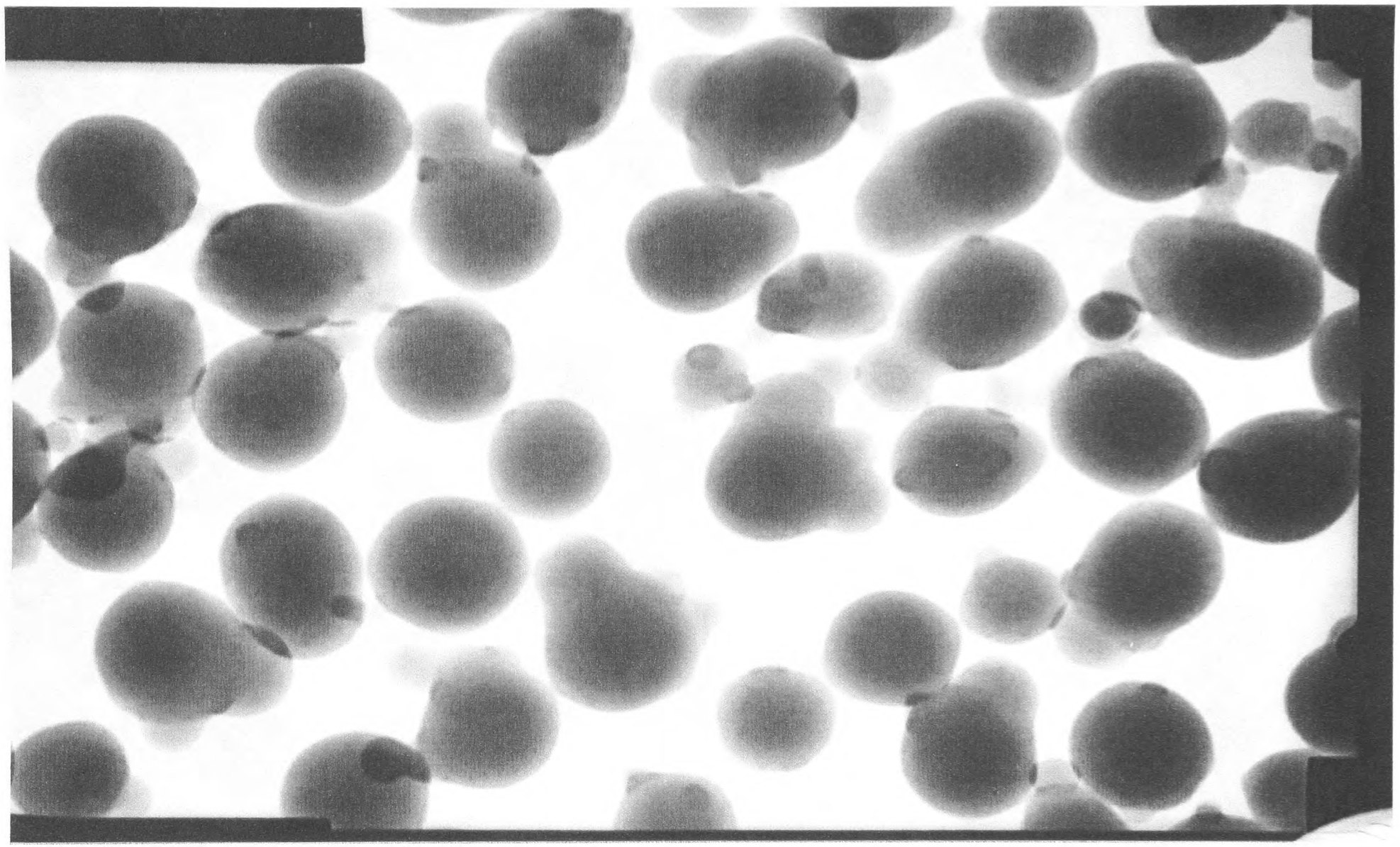

SEM micrograph of 50% composition

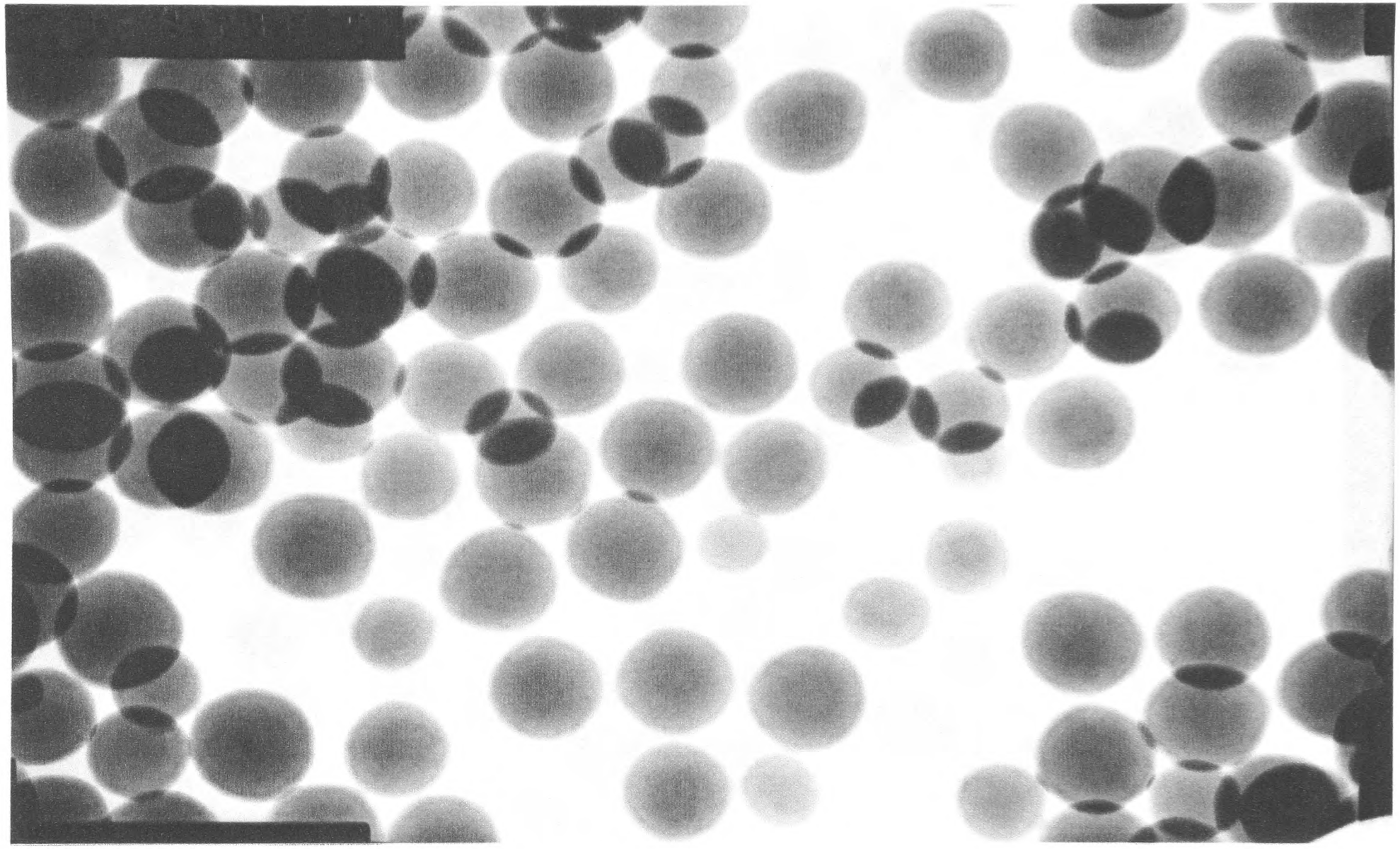

SEM micrograph of 60% composition

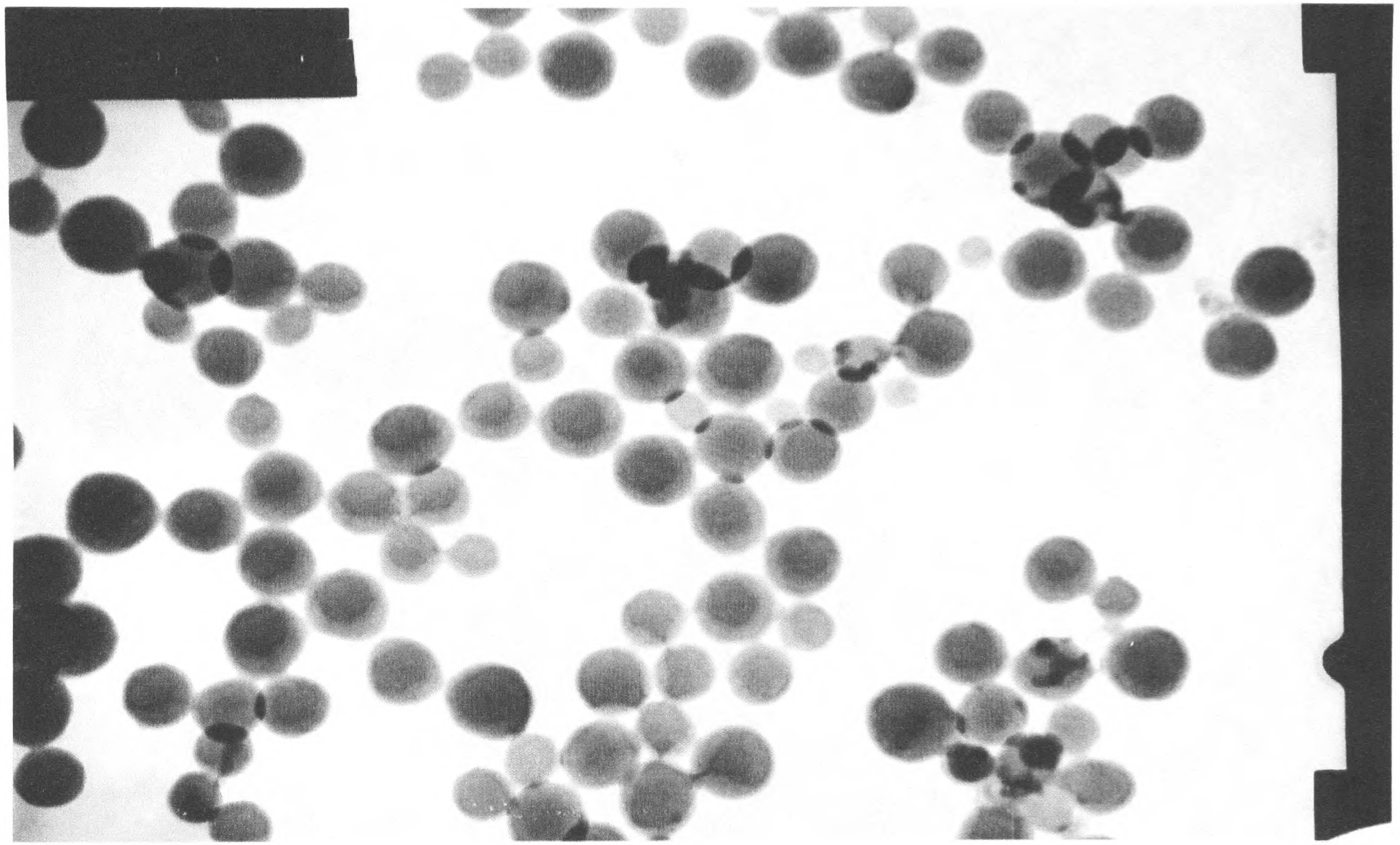

SEM micrograph of 70% composition

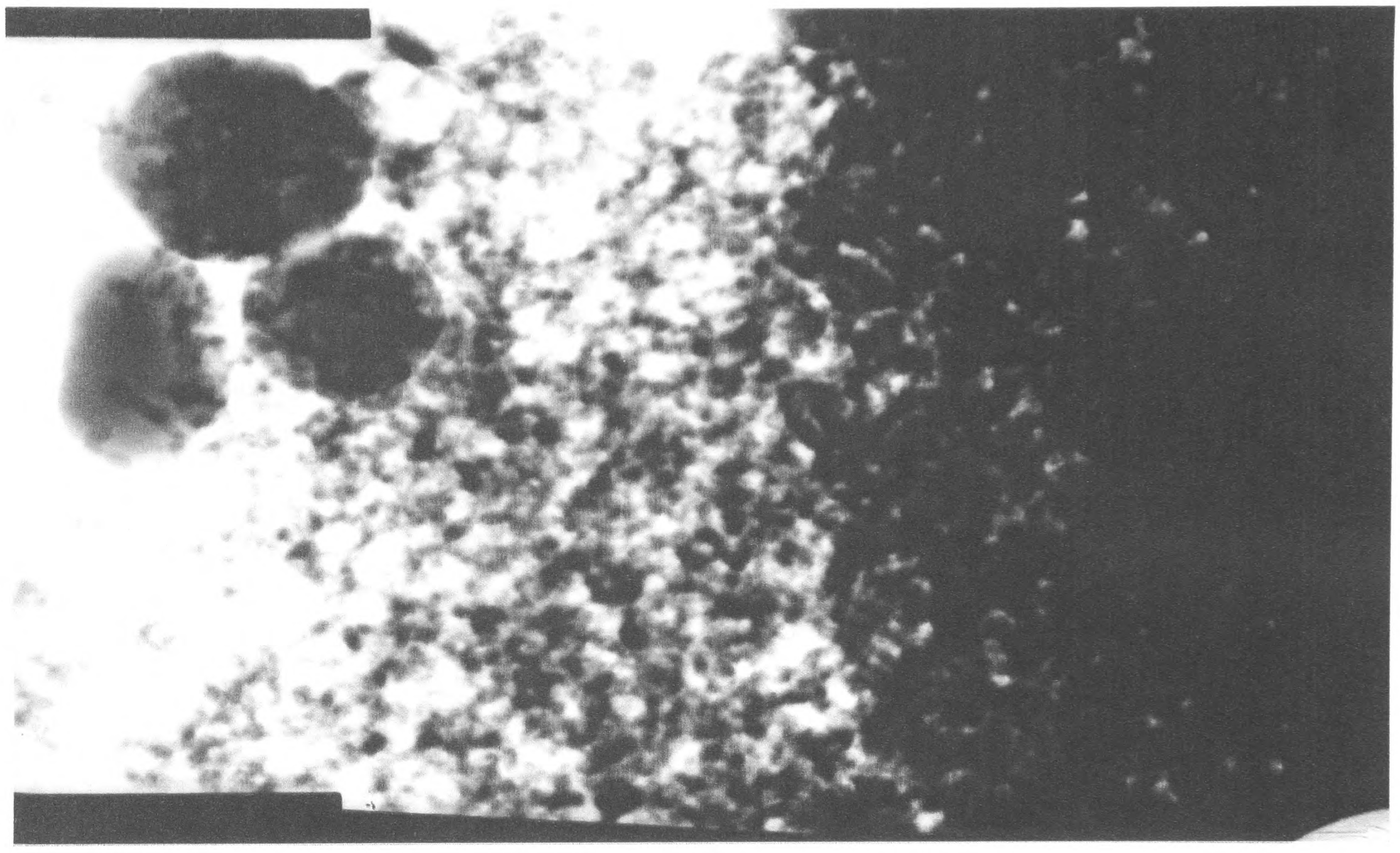

SEM micrograph of 90% composition

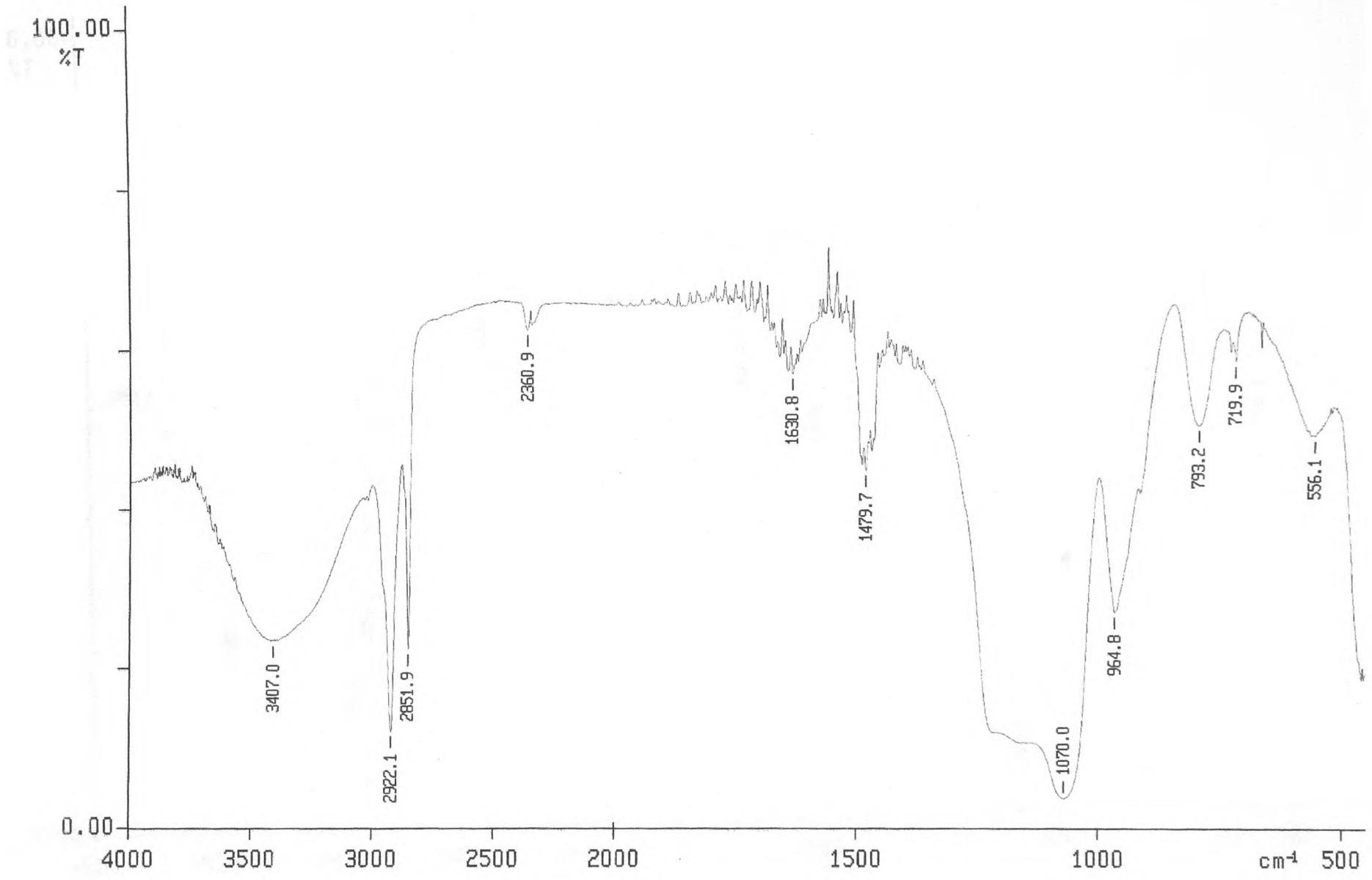

Infrared spectrum of EK78

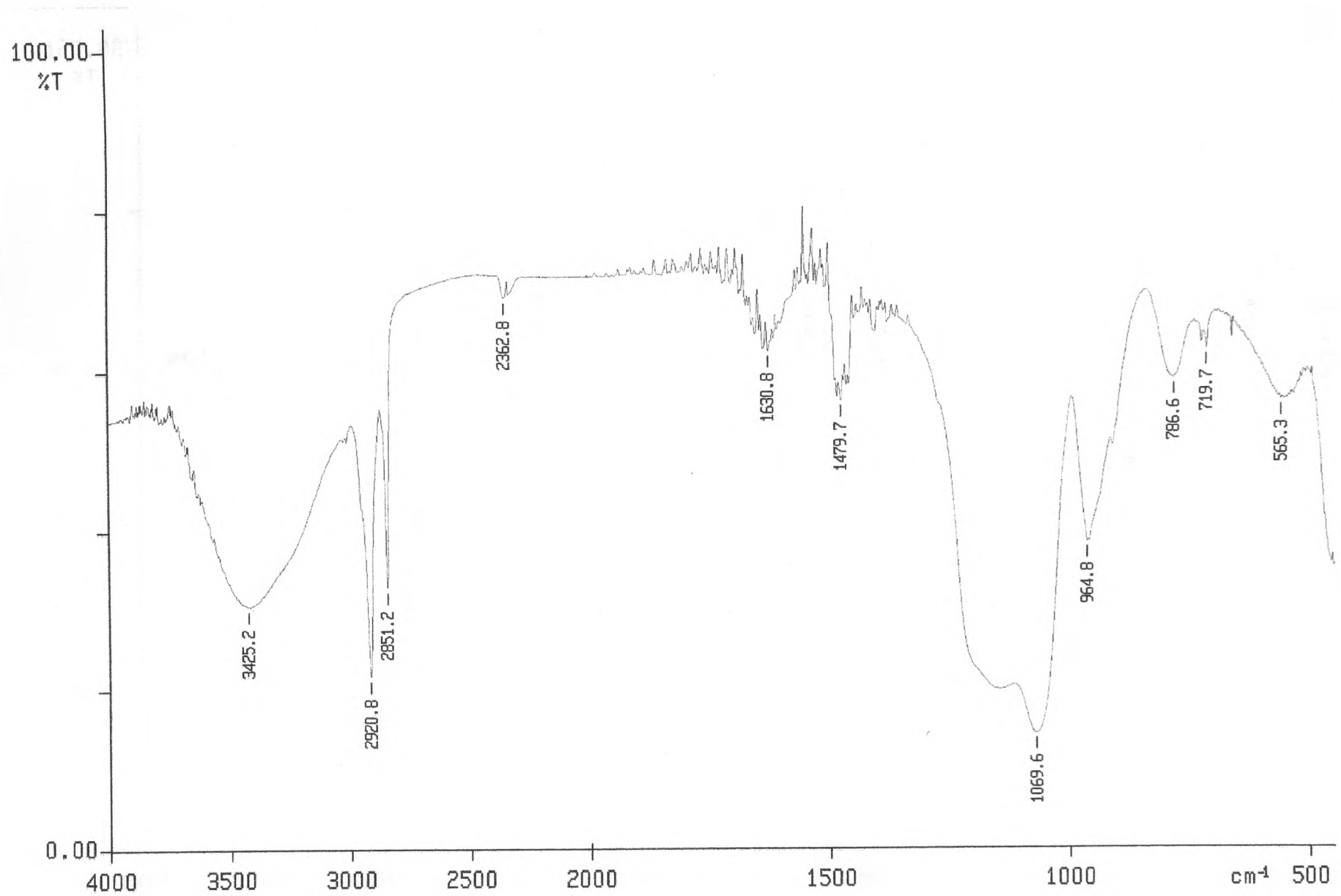

Infrared spectrum of EK79

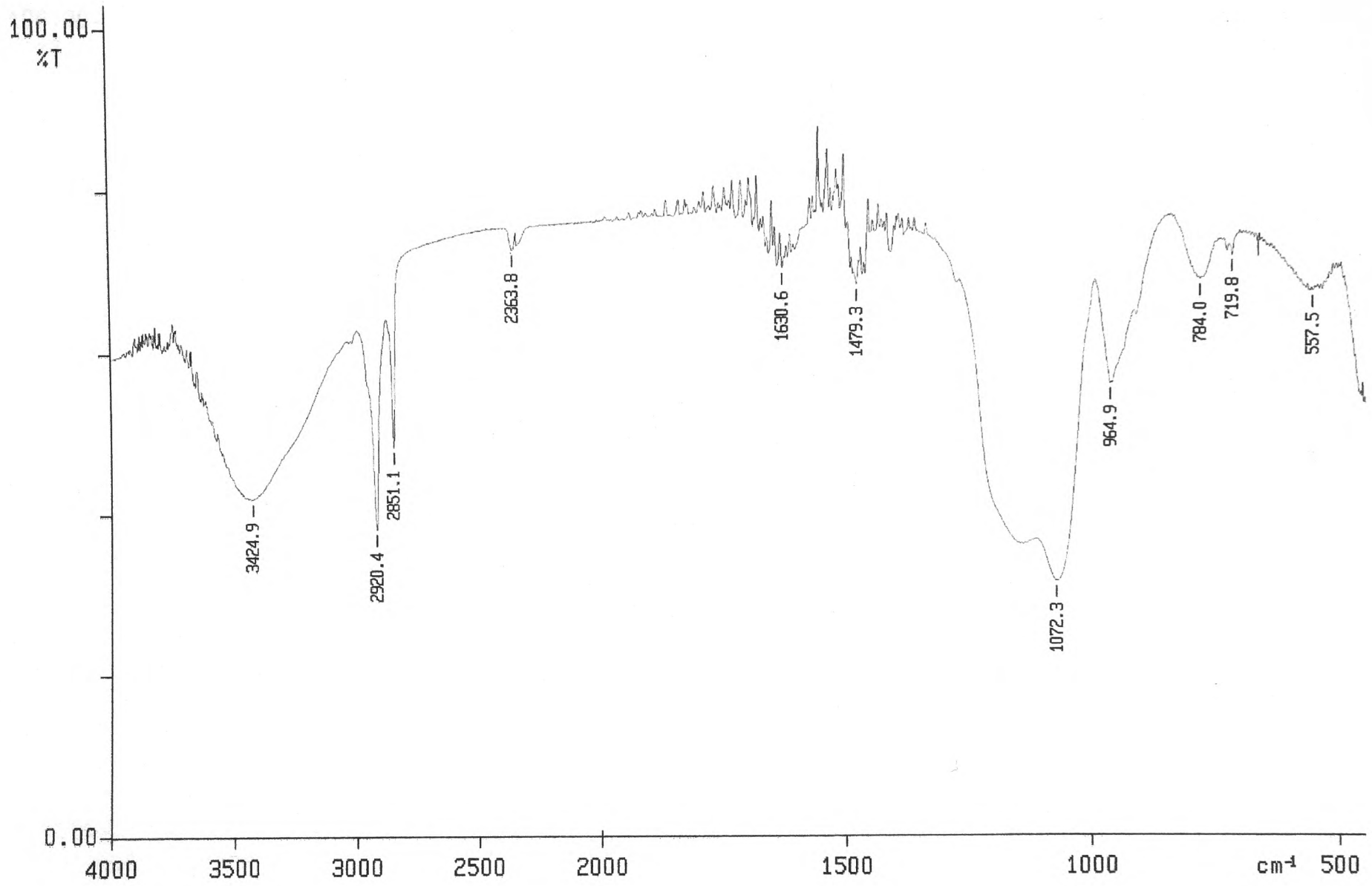

Infrared spectrum of EK80

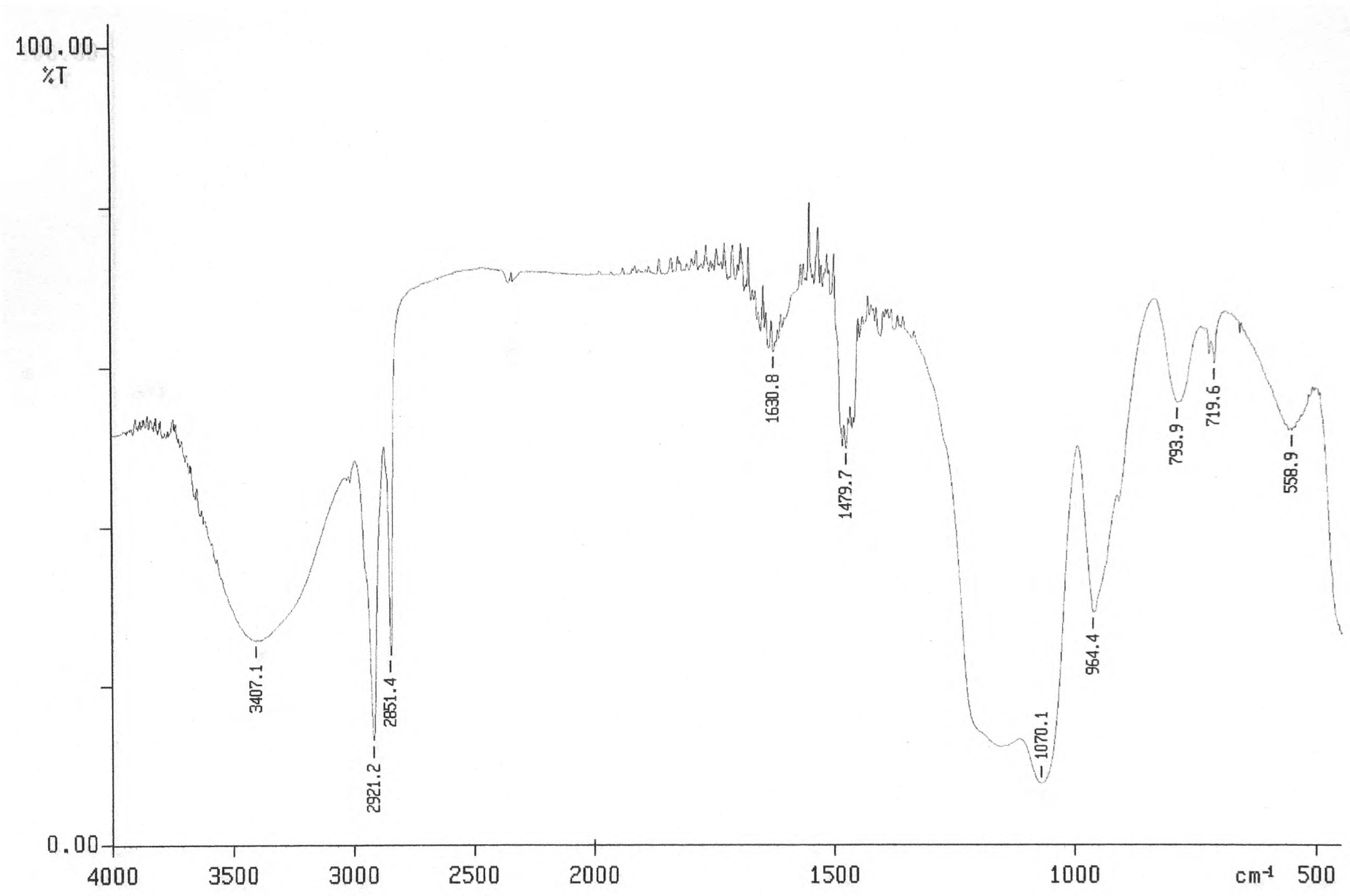

Infrared spectrum of EK81

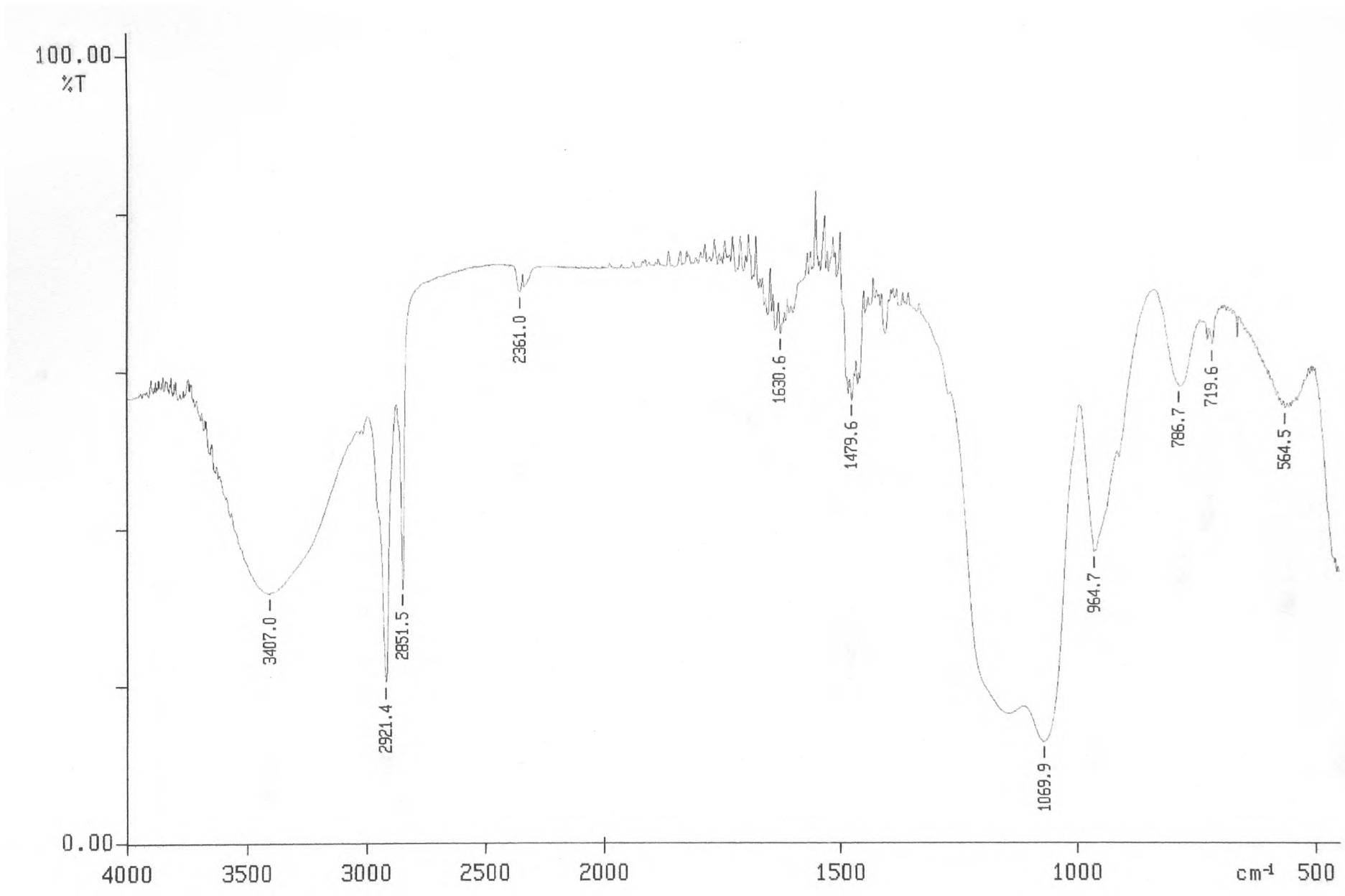

Infrared spectrum of EK83

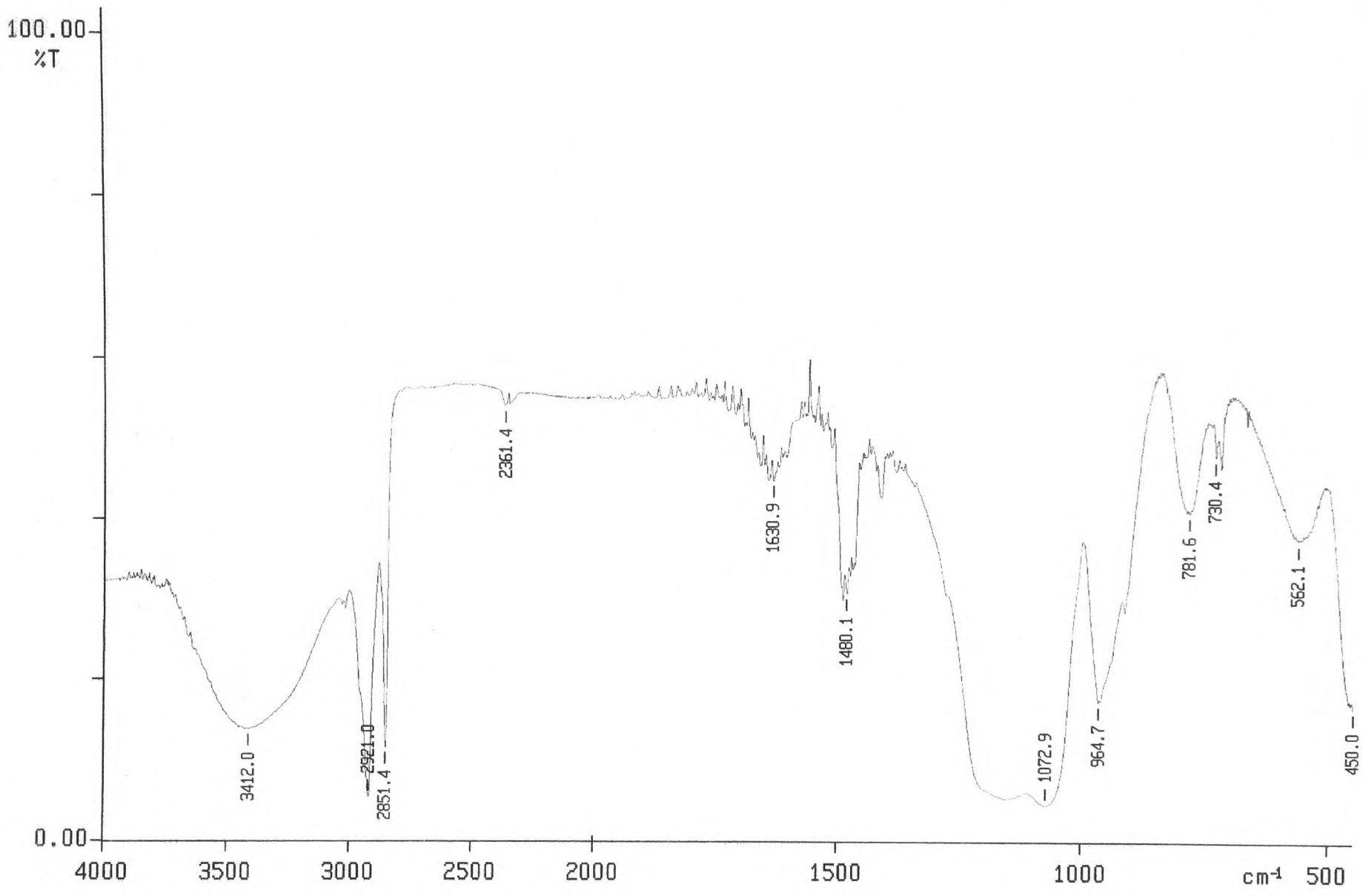

Infrared spectrum of EK84

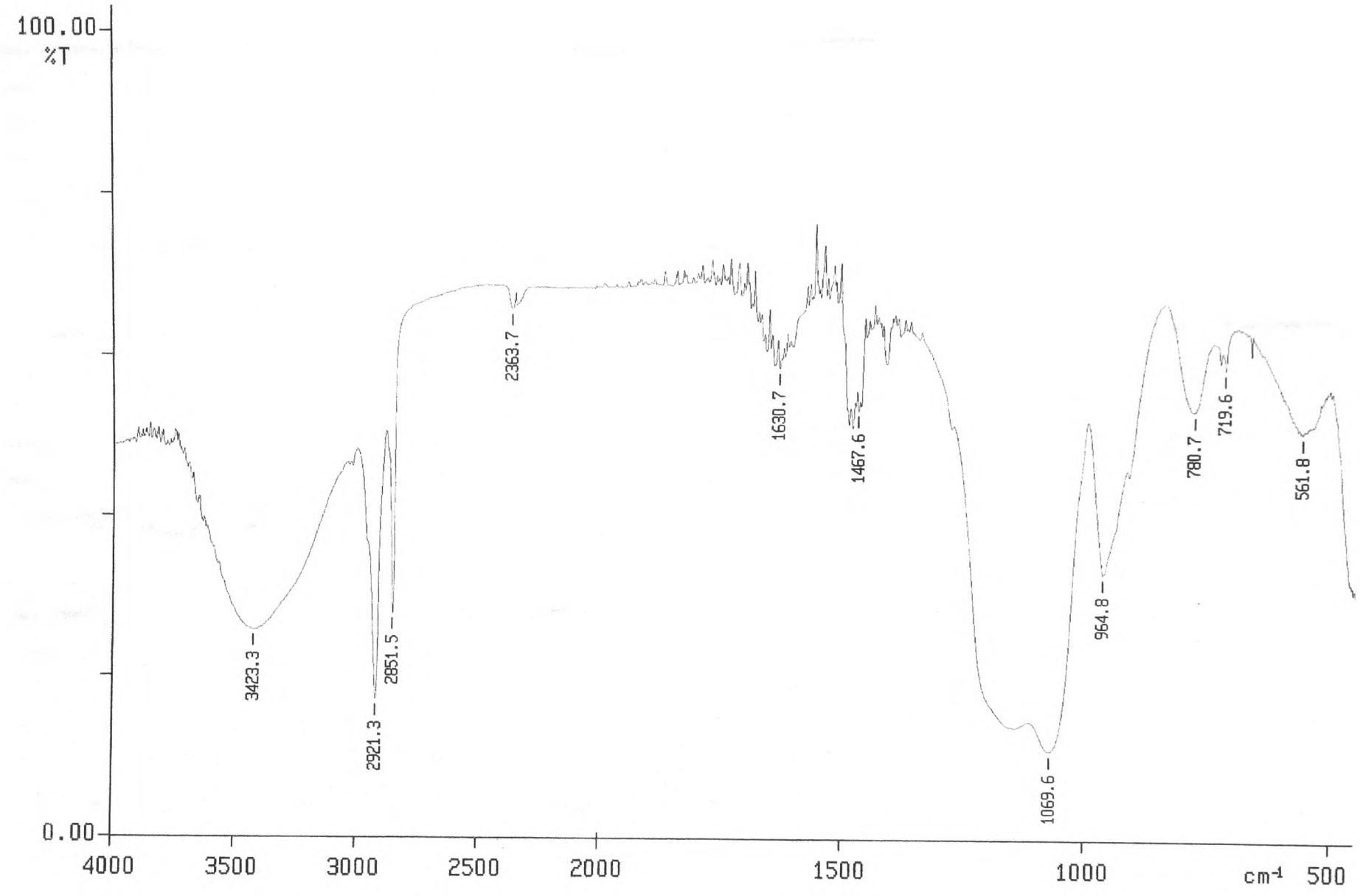

Infrared spectrum of EK85

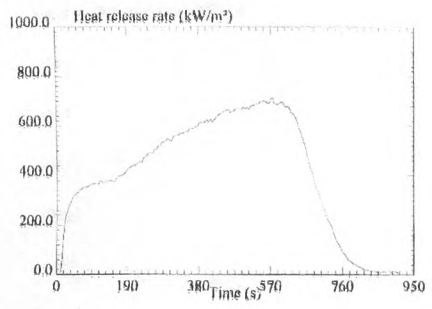

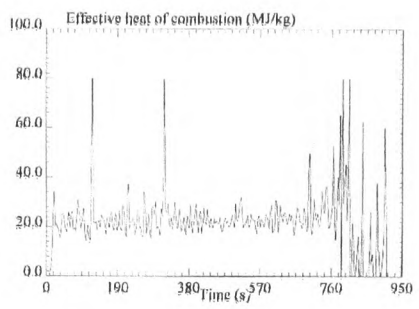

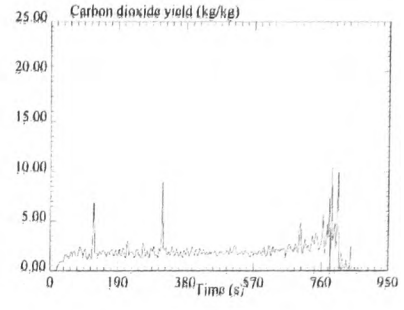

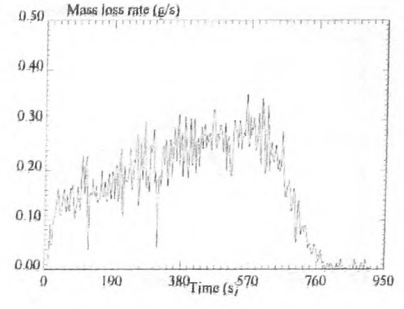

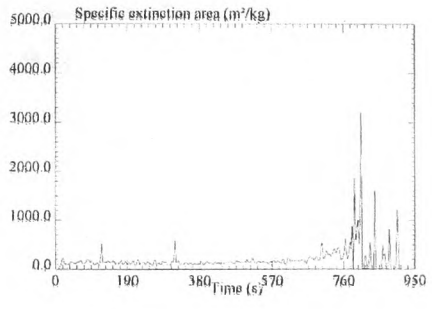

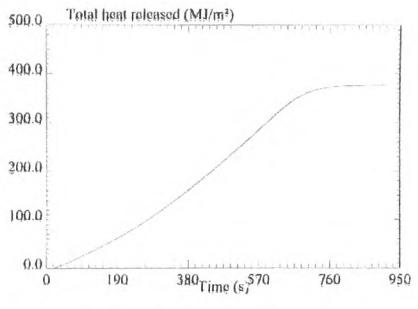

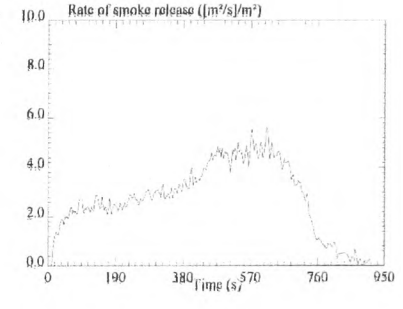

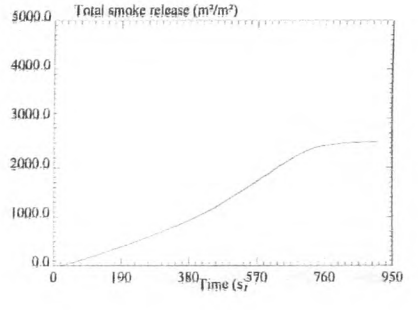

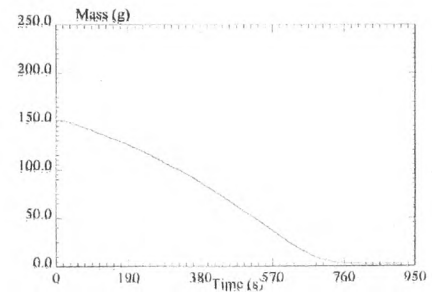

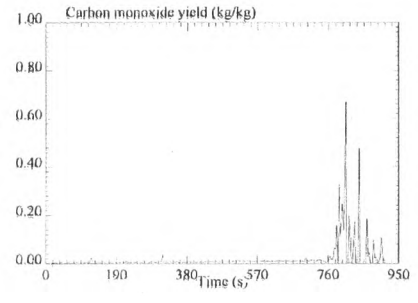

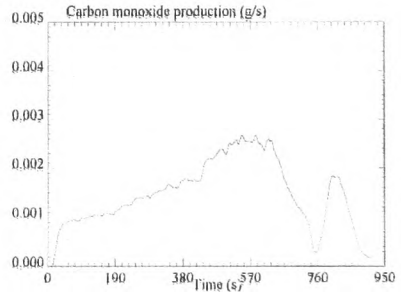

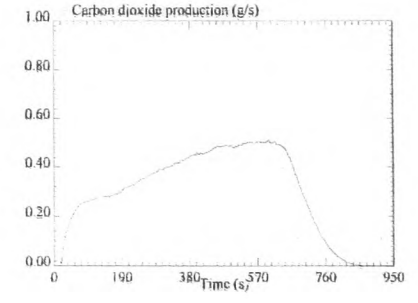

Cone Calorimeter single run data for 1D

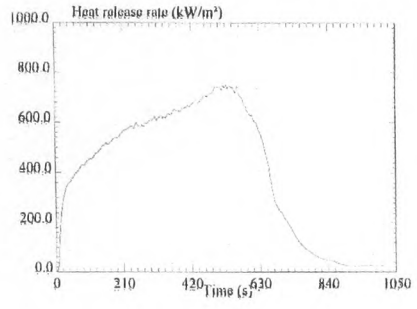

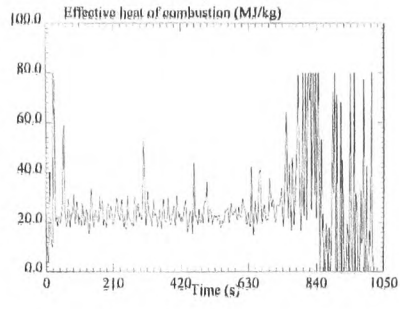

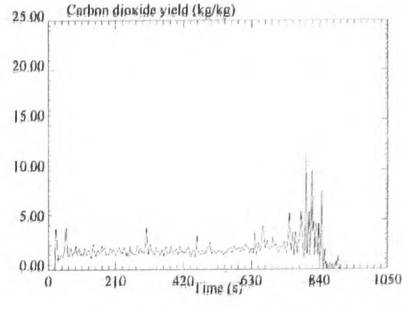

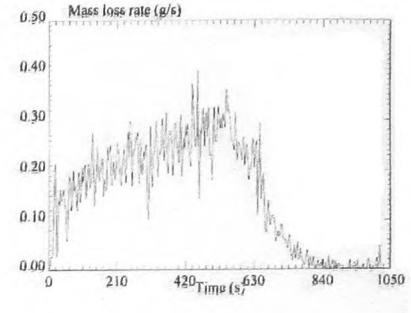

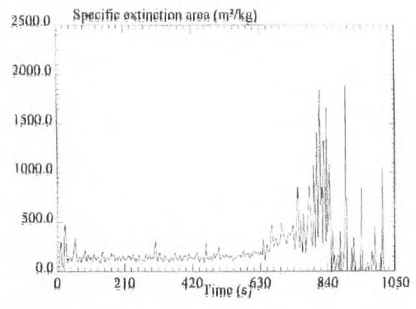

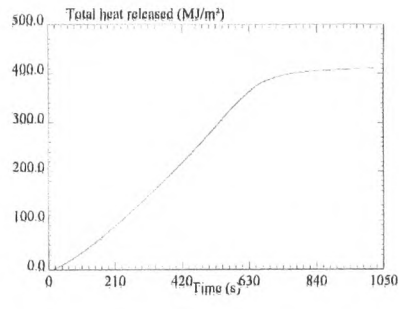

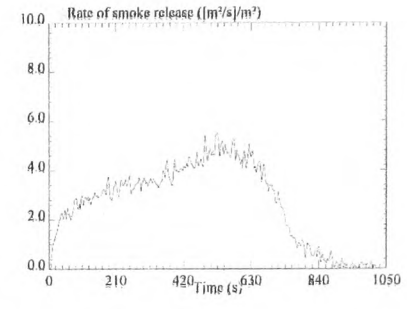

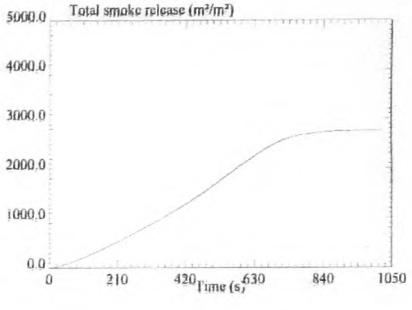

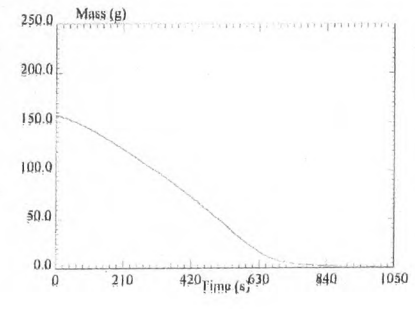

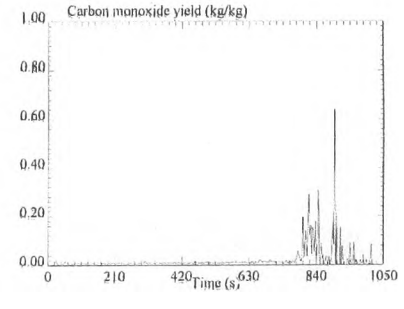

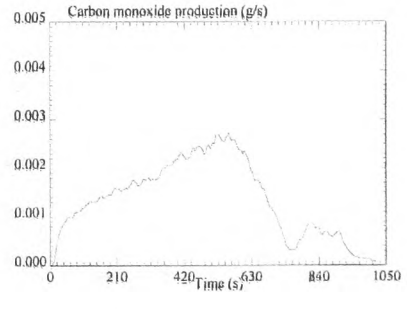

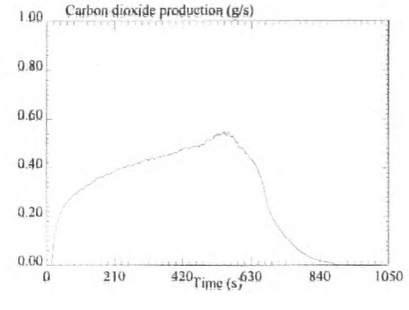

Cone Calorimeter single run data for 1B

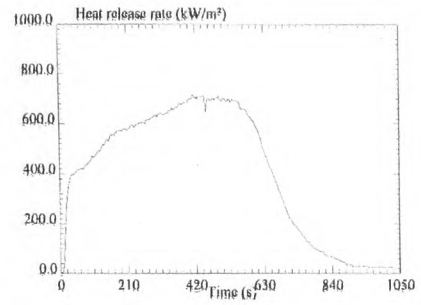

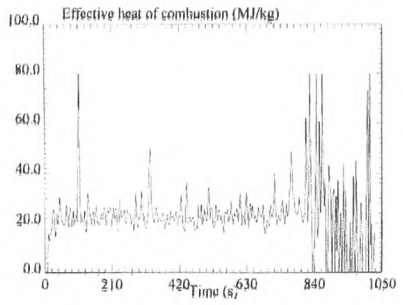

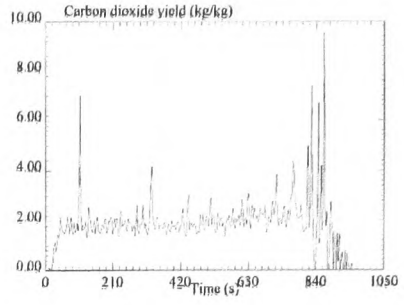

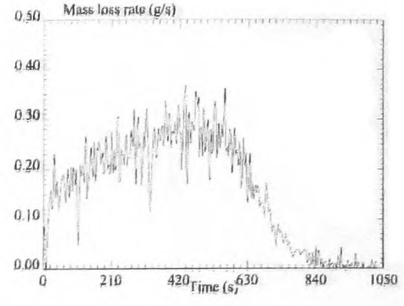

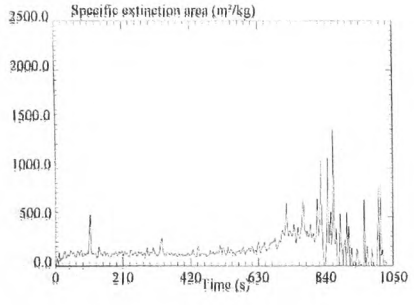

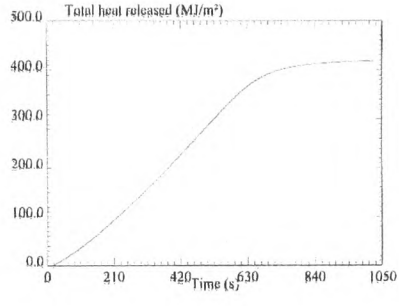

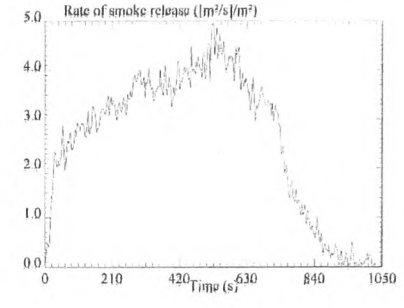

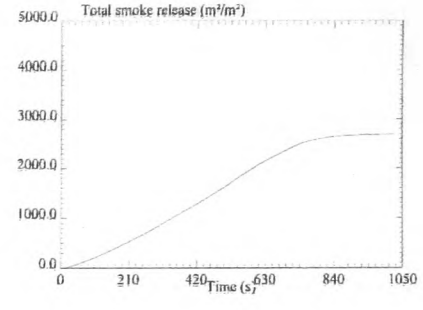

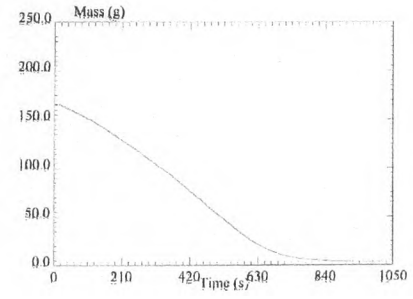

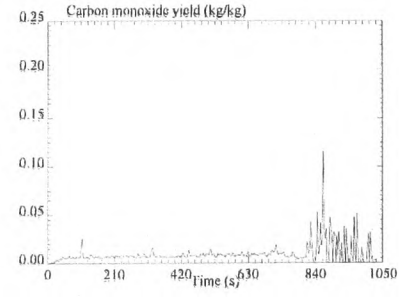

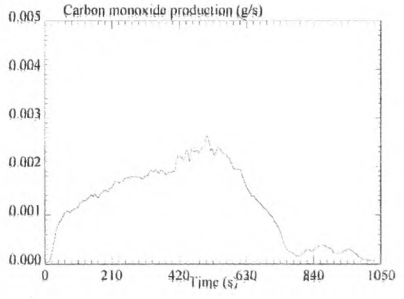

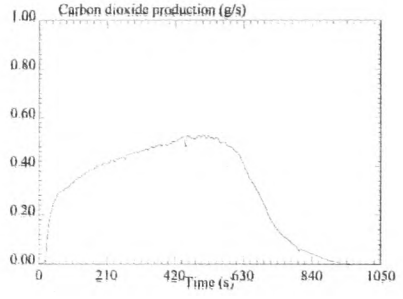

Cone Calorimeter single run data for 2D

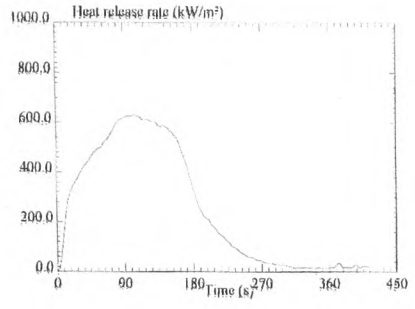

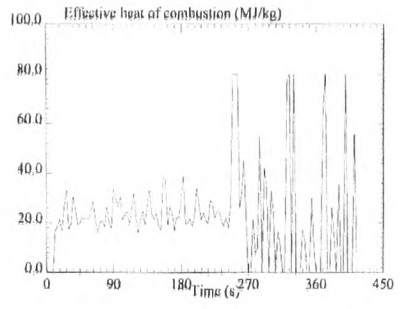

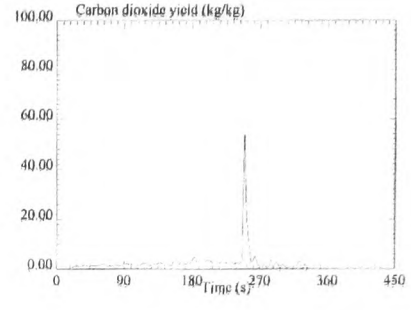

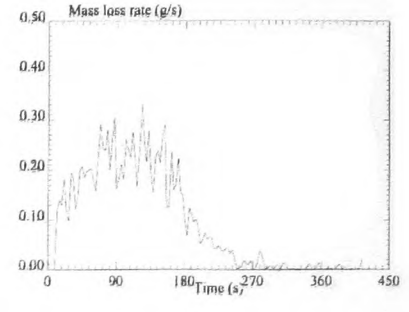

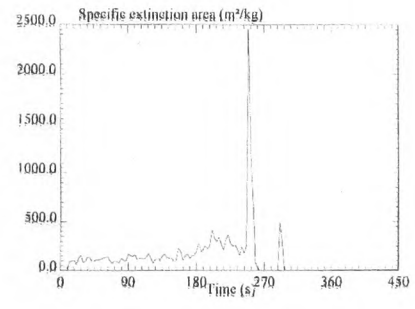

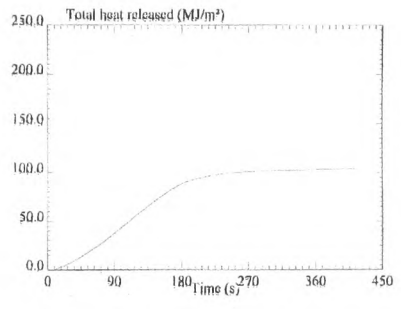

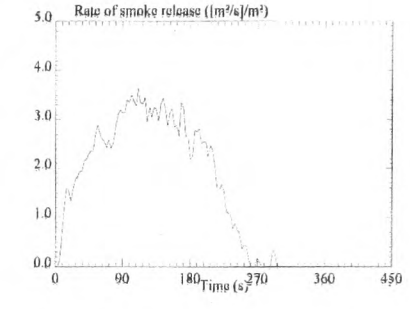

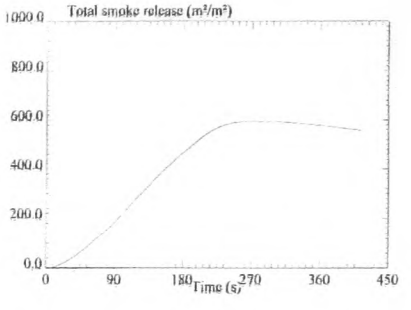

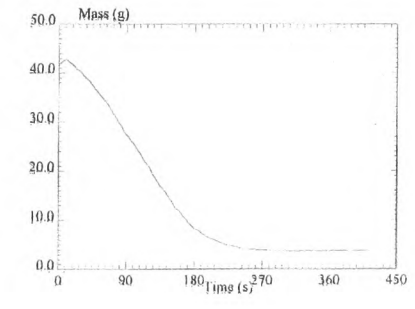

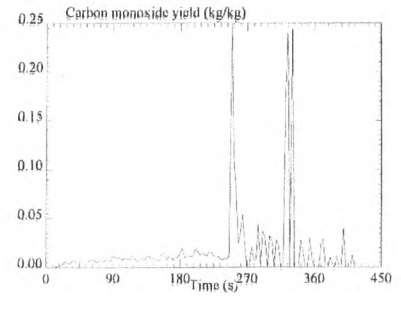

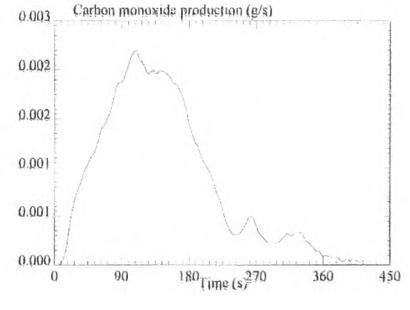

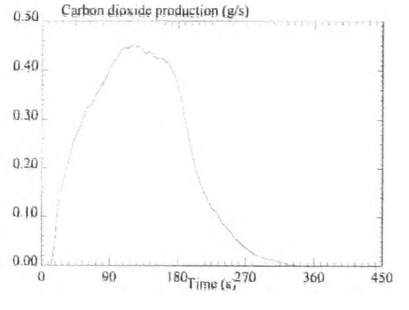

Cone Calorimeter single run data for 2AB

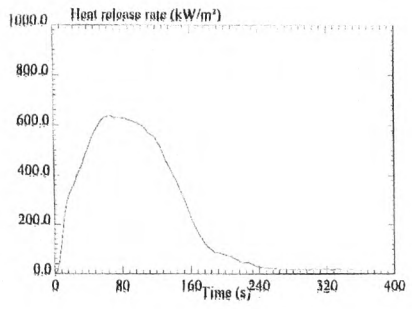

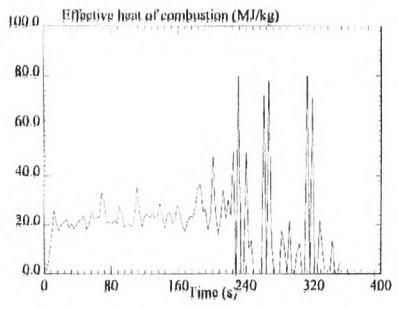

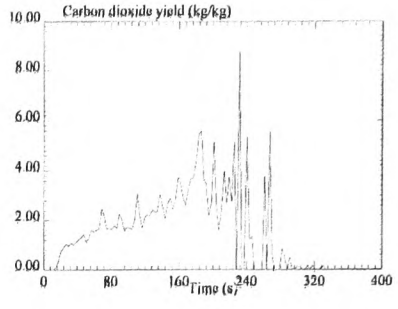

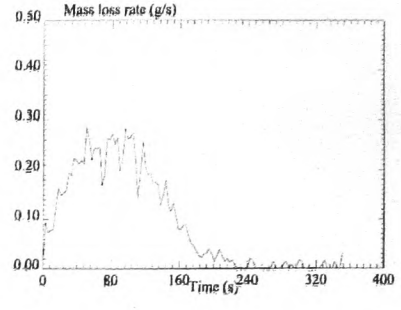

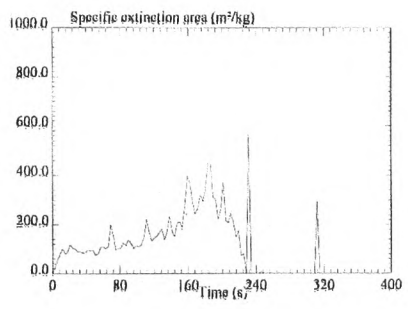

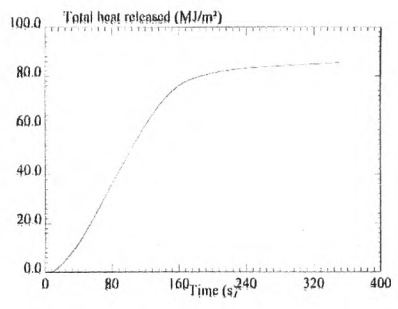

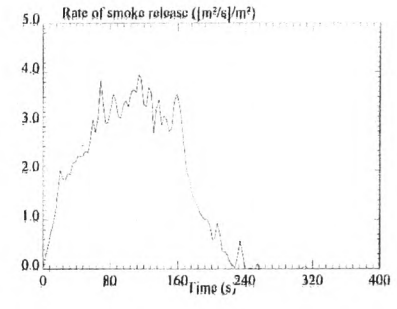

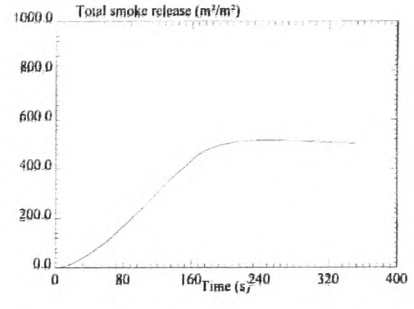

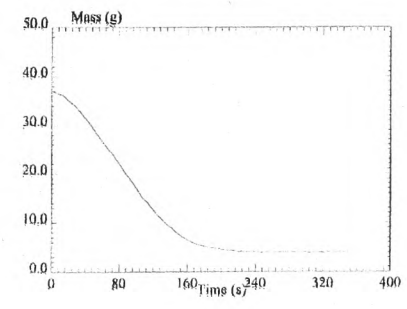

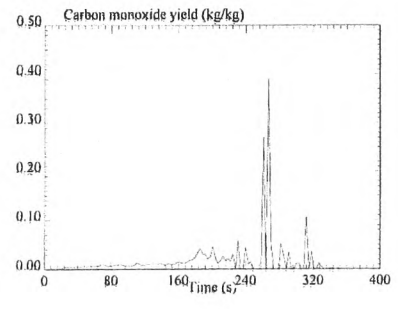

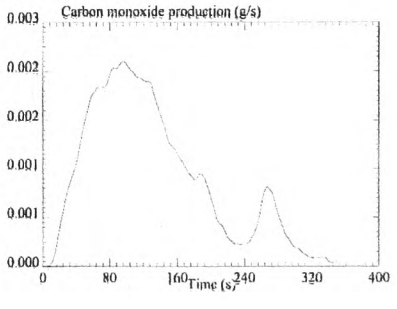

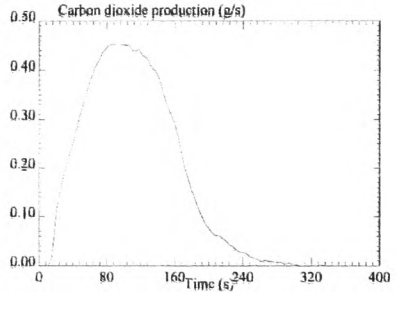

Cone Calorimeter single run data for 2BB